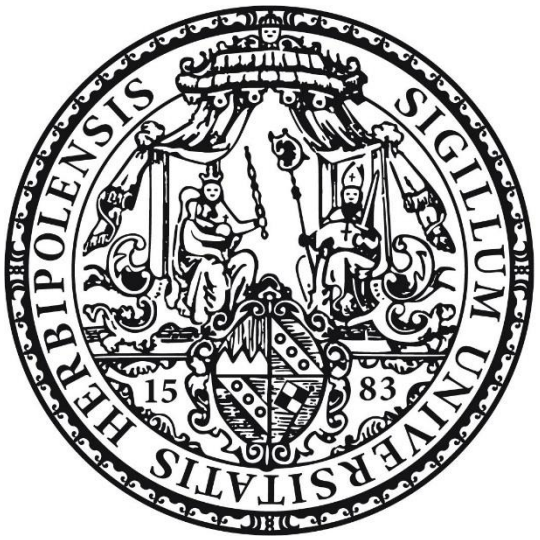

Development of functionalized electrospun fibers as biomimetic artificial basement membranes

***

Entwicklung funktionalisierter elektrogesponnener Fasern als biomimetische künstliche Basalmembranen

Doctoral thesis for a doctoral degree
at the Graduate School of Life Sciences,
Julius-Maximilians-Universität Würzburg,
Section Biomedicine

submitted by

Angela Francesca Rossi
from Ulm

Würzburg 2016

Submitted on: ……..……..

Members of the Promotionskomitee:

Chairperson: Prof. Dr. Ulrike Holzgrabe

Primary Supervisor: Prof. Dr. Heike Walles

Supervisor (Second): Prof. Dr. Jürgen Groll

Supervisor (Third): Prof. Dr. Dr. Lorenz Meinel

Date of Public Defence: ……

Date of Receipt of Certificates: ……..

"Wer über sich selbst lachen kann,

wird am ehesten ernst genommen."

Albert Einstein, 1879 – 1955

Table of contents

List of figures

List of tables

Abbreviations

Table 1: List of abbreviations

abbreviation	long term
%	percent
®	registered
°C	degree celsius
Ø	average
µg	microgram
µl	microliter
µm	micrometer
2D	two-dimensional
3D	three-dimensional
AFM	atomic force microscopy
ALI	air-liquid interface
Asc-P	L-ascorbic acid 2-phosphate
ATR-FTIR	attenuated total reflectance fourier transform infrared spectroscopy
AUT	Austria
BSA	bovine serum albumin
CDI	carbonyl diimidazole
CGEFYFDLRLKGDK	cysteine-glycine-glutamic acid-phenylalanine-tyrosine-phenylalanine-aspartic acid-leucine-arginine-leucine-lysine-glycine-aspartic acid-lysine
CGIKVAV	cysteine-glycine-isoleucine-lysine-valine-alanine-valine
CGRGDS	cysteine-glycine-arginine-glycine-aspartic acid-serine
CGYIGSR	cysteine-glycine-tyrosine-isoleucine-glycine-serine-arginine
CH	Confederation Helvetica (Switzerland)
CK 5/6	cytokeratin 5/6
CK 10	cytokeratin 10
CK 13	cytokeratin 13
CK 14	cytokeratin 14
cm	centimeter

abbreviation	long term
CO_2	carbon dioxide
Coll I	collagen type I
Coll III	collagen type III
Coll IV	collagen type IV
DAB	3,3'-diaminobenzidine
DAPI	4',6-Diamidino-2-phenylindole
DCC	dicyclohexylcarbodiimide
DCM	dichloromethane
DMEM	dulbecco's modified eagle medium
DMF	dimethylformamide
DMSO	dimethyl sulfoxide
DNA	deoxyribonucleic acid
DSC	differential scanning calorimetry
ECM	extracellular matrix
EDC	N-(3-dimethylaminopropyl)-carbodiimide
EDTA	ethylenediaminetetraacetic acid
EGF	epidermal growth factor
ELISA	enzyme-linked immunosorbent assay
ET-50	concentration that reduces the viability to 50 %
EtOH	ethanol
Et al.	et alii
EURL-ECVAM	european union reference laboratory for alternatives to animal testing
FCS	fetal calf serum
FDA	fluorescein diacetate
FGF	fibroblast growth factor
Fib	fibronectin binding sequence
FITC	fluorescein-isocyanate
g	gram
GER	Germany
GNL	gel neutralization solution
h	hour

abbreviation	long term
HaCaT	human keratinocyte cell line
HCl	hydrogen chloride
hDF	human dermal fibroblasts
H&E	haematoxylin and eosin
hEK	human epidermal keratinocytes
HKGS	human keratinocyte growth supplement
HRP	horseradish-peroxidase
HSPGs	heparin-sulfate proteoglycans
I	Italy
IHC	immunohistochemistry
IND	India
iPS	induced pluripotent stem cells
JaCVAM	Japanese Center for Validation of Alternative Methods
kDa	kilo Dalton
KGF	keratinocyte growth factor
KH_2PO_4	potassium dihydrogen phosphate
kV	kilo Volt
l	liter
Lam	laminin derived binding sequence
M	molar
MSC	mesenchymal stem cells
mg	milligram
min	minute
ml	milliliter
mm	millimeter
mol	unit of the amount of substance n
MTT	3-(4,5-dimethylthiazol-2-yl)-2,5-diphenyltetrazolium bromide
Mw	weight average molecular weight
N_2	nitrogen
NaCl	sodium chloride

abbreviation	long term
NAD(H)/NADP(H)	nicotinamide adenine dinucleotide/ nicotinamide adenine dinucleotide phosphate
NCO	isocyanate group
NCO-sP(EO-*stat*-PO)	six-armed star-shaped poly(ethylene oxide-*stat*-propylene oxide) in the ratio 4:1 with isocyanate end groups
O_2	oxygen
OD	optical density
OECD	organization for Economic Co-operation and Development
PBS^-	phosphate buffered saline without calcium and magnesium ions
PBS^+	phosphate buffered saline containing calcium and magnesium ions
PBS-T	phosphate buffered saline with Tween®-20
PC	polycarbonate
PCL	poly(ε-caprolactone)
PEG	poly (ethylene glycol)
PEO	poly (ethylene oxide)
Pen/Strep	penicillin/streptomycin
PFA	paraformaldehyde
PGA	poly (glycolic acid)
PI	propidium iodide
PLA	poly(lactic acid)
PLLA	poly(L-lactic acid)
PLGA	poly(lactic-*co*-glycolic acid)
PPTA	poly(p-phenylene terephthalamide)
PU	polyurethane
PVA	polyvinyl alcohol
PVB	polyvinyl butyral
QCM	quartz crystal microbalance
rpm	revolutions per minute
RT	room temperature
s	seconds

abbreviation	long term
SAW	surface acoustic wave
SB	stratum basale
SC	stratum corneum
SD	standard deviation
SDS	sodium dodecyl sulfate
SEM	scanning electron microscopy
SG	stratum granulosum
SIS	small intestine mucosa
SOP	standard operation procedure
sP(EO-*stat*-PO)	six-armed star-shaped poly(ethylene oxide-*stat*-propylene oxide) in the ratio 4:1
SPR	surface plasmon resonance
SS	stratum spinosum
TCEP	tris (2-carboxyethyl) phosphine
TEER	transepithelial resistance
TEM	transmission electron microscopy
TFA	trifluoroacetic acid
Tg	glass transition temperature
TM	trade mark
TOF-SIMS	time of flight secondary ion mass spectrometry
U	units
UK	United Kingdom
USA	United States of America
UV	ultraviolet
wt%	weight percent
XPS	x-ray photoelectron spectroscopy

Summary

The basement membrane separates the epithelium from the stroma of any given barrier tissue and is essential in regulating cellular behavior, as mechanical barrier and as structural support. It further plays an important role for new tissue formation, homeostasis, and pathological processes, such as diabetes or cancer. Breakdown of the basement membrane is believed to be essential for tumor invasion and metastasization. Since the basement membrane is crucial for many body functions, the development of artificial basement membranes is indispensable for the ultimate formation of engineered functional tissue, however, challenging due to their complex structure.

Electrospinning enables the production of fibers in the nano- or microscale range with morphological similarities to the randomly orientated collagen and elastic fibers in the basement membrane. However, electrospun fibers often lack the functional similarity to guide cells and maintain tissue-specific functions. Hence, their possible applications as matrix structure for tissue engineering are limited.

Herein, the potential of polyester meshes, modified with six armed star-shaped pre-polymers and cell-adhesion-mediating peptides, was evaluated to act as functional isotropic and bipolar artificial basement membranes. Thereby, the meshes were shown to be biocompatible and stable including under dynamic conditions, and the degradation profile to correlate with the rate of new tissue formation. The different peptide sequences did not influence the morphology and integrity of the fibers. The modified membranes exhibited protein-repellent properties over 12 months, indicating the long-term stability of the cross-linked star-polymer surfaces.

Cell culture experiments with primary fibroblasts and a human keratinocyte cell line (HaCaT) revealed that cell adhesion and growth strongly depends on the peptide sequences and their combinations employed. HaCaT cells grew to confluence on membranes modified with a combination of laminin/collagen type IV derived binding sequences and with a combination of fibronectin/laminin/collagen type IV derived peptide sequences. Fibroblasts strongly adhered to the fibronectin derived

binding sequence and to membranes containing a combination of fibronectin/laminin/collagen type IV derived peptide sequences. The adhesion and growth of fibroblasts and HaCaT cells were significantly reduced on membranes modified with laminin, as well as collagen IV derived peptide sequences. HaCaT cells and fibroblasts barely adhered onto meshes without peptide sequences.

Co-culture experiments at the air-liquid interface with fibroblasts and HaCaT cells confirmed the possibility of creating biocompatible, biofunctional and biomimetic isotropic and bipolar basement membranes, based on the functionalized fibers. HaCaT cells grew in several layers, differentiating towards the surface and expressing cytokeratin 10 in the suprabasal and cytokeratin 14 in the basal layers. Migration of fibroblasts into the electrospun membrane was shown by vimentin staining. Moreover, specific staining against laminin type V, collagen type I, III, IV and fibronectin illustrated that cells started to remodel the electrospun membrane and produced new extracellular matrix proteins following the adhesion to the synthetic surface structures.

The culturing of primary human skin keratinocytes proved to be difficult on electrospun fibers. Cells attached to the membrane, but failed to form a multilayered, well-stratified, and keratinized epidermal layer. Changing the fiber composition and fixation methods did not promote tissue development. Further investigations of the membrane demonstrated the tremendous influence of the pore size of the membrane on epithelial formation. Furthermore, primary keratinocytes reacted more sensitive to pH changes in the medium than HaCaT cells did.

Since primary keratinocytes did not adequately develop on the functionalized meshes, polycarbonate membranes were used instead of electrospun meshes to establish oral mucosa models. The tissue-engineered models represented important features of native human oral mucosa. They consisted of a multilayered epithelium with stratum basale, stratum spinosum, stratum granulosum, and stratum corneum. The models formed a physical barrier and the expression of characteristic cell markers was comparable with that in native human oral mucosa. The results from the ET-50 assay and the irritation study reflected the reproducibility of the tissue equivalents.

Altogether, electrospinning enables the production of fibers with structural similarity to the basement membrane. Incorporating extracellular matrix components to mimic the functional composition offers a safe and promising way to modify the fibers so that they can be used for different tissue engineering applications. The resultant biomimetic membranes that can be functionalized with binding sequences derived from widely varying proteins can be used as a toolbox to study the influence of isotropic and bipolar basement membranes on tissue formation and matrix remodeling systematically, with regards to the biochemical composition and the influence and importance of mono- and co-culture. The oral mucosa models may be useful for toxicity and permeation studies, to monitor the irritation potential of oral health care products and biomaterials or as a disease model.

Zusammenfassung

Die Basalmembran trennt das Epithel vom Stroma eines jeden Wandgewebes und ist entscheidend bei der Regulierung des Zellverhaltens, als mechanische Barriere, und als strukturelle Unterstützung. Darüber hinaus spielt sie eine wichtige Rolle sowohl bei der Neubildung von Gewebe und der Homöostase, als auch bei pathologischen Prozessen, wie Diabetes mellitus oder Krebs. Es wird angenommen, dass die Überquerung der Basalmembran eine entscheidende Rolle bei der Tumorinvasion und Metastasierung spielt. Wegen der großen Bedeutung der Membran für eine Vielzahl an Körperfunktionen, ist die Entwicklung von strukturierten und funktionalen künstlichen Basalmembranen für den Aufbau von im Labor entwickeltem funktionalem Gewebe unerlässlich; nichtsdestotrotz stellt die Herstellung aufgrund der komplexen Struktur eine Herausforderung dar.

Das elektrostatische Verspinnen ermöglicht es, Fasern im Nano- oder Mikrometer-Maßstab mit morphologischen Ähnlichkeiten zu den zufällig orientierten Kollagen- und elastischen Fasern in der Basalmembran herzustellen. Allerdings fehlt den elektrogesponnenen Fasern häufig die funktionale Ähnlichkeit um die Zellbewegung innerhalb des Gewebes zu regulieren und gewebespezifische Funktionen aufrecht zu erhalten. Daher sind ihre Anwendungsmöglichkeiten als Membranen für das Tissue Engineering begrenzt.

In dieser Arbeit wurde das Potential eines Polyestergerüsts beurteilt, das mit einem sechsarmigen sternförmigen Additiv und Zelladhäsion vermittelnden Peptiden modifiziert worden war, als isotrope und bipolare künstliche Basalmembran. Zunächst wurden die Materialeigenschaften der Faservliese untersucht. Dabei konnte gezeigt werden, dass die Vliese biokompatibel, und auch unter dynamischen Bedingungen stabil sind. Zudem korrelierte der Abbau der Vliese mit dem Aufbau von neuem Gewebe. Die Modifizierung der Faseroberfläche mit Peptidsequenzen beeinflusste nicht die Morphologie und die Integrität der Fasern. Die funktionalisierten Gerüste zeigten proteinabweisende Eigenschaften über 12 Monate, was die langfristige Stabilität der quervernetzten Stern-Polymer Oberflächen bestätigte.

Zellkulturversuche mit primären Fibroblasten und einer humanen Keratinozyten-Zelllinie (HaCaT) ergaben, dass die Zelladhäsion und das Wachstum stark von den Peptidsequenzen und deren Kombinationen abhängig sind. HaCaT Zellen wuchsen zur Konfluenz auf Vliesen, die mit einer Kombination aus Laminin/Kollagen Typ IV stammenden Peptidsequenzen und mit einer Kombination aus Fibronektin/Laminin/Kollagen Typ IV stammenden Peptidsequenzen funktionalisiert worden waren. Fibroblasten dagegen adhärierten und proliferierten stark auf Vliesen, die mit Fibronektin, und einer Kombination aus Fibronektin/Laminin/Kollagen Typ IV stammenden Bindungssequenzen modifiziert worden waren. Die Adhäsion und das Wachstum von Fibroblasten und HaCaT Zellen waren dagegen auf mit Laminin sowie mit Kollagen Typ IV funktionalisierten Membranen deutlich geringer. Fibroblasten und HaCaT Zellen adhärierten kaum auf Vliesen ohne Peptidsequenzen.

Ko-Kultur Versuche an der Luft-Flüssigkeits-Grenzfläche mit Fibroblasten und HaCaT Zellen bestätigten, dass es möglich ist, basierend auf funktionalisierten Fasern, biokompatible, biofunktionale und biomimetische isotrope und anisotrope Basalmembranen aufzubauen. HaCaT Zellen wuchsen mehrschichtig, differenzierten und polarisierten, dies wurde belegt durch den Nachweis von Zytokeratin 14 in den basalen und Zytokeratin 10 in den oberen Schichten des Epithels. Die Vimentin-Färbung zeigte, dass die Fibroblasten in das Vlies einwandern. Durch spezifische Färbung von Laminin V, Kollagen I, III, IV und Fibronektin konnte gezeigt werden, dass die Zellen beginnen das Vlies umzubauen und extrazelluläre Matrix-Proteine zu produzieren.

Die Kultivierung von primären Keratinozyten, sowohl aus der humanen Haut als auch aus der humanen Mundschleimhaut, erwies sich als komplex auf elektrogesponnenen Fasern. Die Zellen adhärierten auf der Membran, bildeten aber weder mit noch ohne Fibroblasten ein mehrschichtiges, verhorntes Epithel aus. Die Anpassung der Faserzusammensetzung und der Fixierungsmethoden begünstigte die Entwicklung des Epithels nicht. Weiterführende experimentelle Studien belegten, dass der Porendurchmesser des Vlieses eine wichtige Rolle für die

Entwicklung des Epithels spielt und dass primäre Keratinozyten stärker auf pH Veränderungen reagieren als HaCaT Zellen.

Da die funktionalisierten Fasern sich nicht als geeignete Struktur für primäre Keratinozyten erwiesen, wurden Polycarbonat-Membranen anstelle von elektrogesponnenen Strukturen als Träger für den Aufbau von Mundschleimhautmodellen verwendet. Die Modelle zeigten wichtige Eigenschaften der nativen Mundschleimhaut. Es bildete sich ein mehrschichtiges, polarisiertes Epithel aus basalen Zellen, einer Stachelzellschicht, Körnerzellschicht und Hornschicht. Die Modelle entwickelten eine physikalische Barriere und exprimierten Zellmarker ähnlich der nativen Mundschleimhaut. Die Ergebnisse des ET-50 Assays und der Irritationsstudie legten dar, dass die Modelle reproduzierbar hergestellt werden können.

Das elektrostatische Spinnen ermöglicht es, fibrilläre Strukturen, die der Basalmembran sehr ähnlich sind, herzustellen. Die Funktionalisierung der Fasern mit Zelladhäsionssignalen stellt eine vielversprechende Möglichkeit dar, diese Fasern so zu modifizieren, dass sie als Basalmembranen für verschiedene Anwendungen des Tissue Engineerings geeignet sind. Die biomimetischen Membranen können mit Bindungssequenzen von sehr unterschiedlichen Proteinen modifiziert werden. Darüber hinaus können sie genutzt werden, den Einfluss von isotropen und anisotropen Basalmembranen auf die Gewebebildung und den Matrixumbau systematisch in Bezug auf die biochemische Zusammensetzung und den Einfluss sowie die Bedeutung von Mono- und Ko-Kultur zu untersuchen. Die Mundschleimhautmodelle können für toxikologische Untersuchungen, Permeationsstudien, sowie als Krankheitsmodelle eingesetzt werden. Außerdem können sie verwendet werden, um das Irritationspotenzial von Mundhygieneprodukten und Biomaterialien einzuschätzen.

1 Introduction

1.1 Tissue engineering – principles and applications

The idea of replacing tissue goes back until the 16th century, A professor of Surgery and Anatomy at the University of Bologna described a nose replacement that was constructed from a forearm flap [1]. However, it was only in 1997 that tissue engineering gained much attention. The laboratory of Charles Vacanti implanted an ear-shaped cartilage structure under the skin of a mouse [2]. This achievement helped to transfer the idea and vision of generating new tissues and organs from the imaginary to reality. Since then, tissue engineering is considered as one of the most promising biomedical technologies [3].

Due to the increasing life expectancy of humans, the demand for replacement material to repair defective tissues or diseased organs is a major health problem all over the world. Treatment options such as surgical reconstruction, artificial prosthesis, mechanical devices, and drug therapy have saved and improved countless lives [4]. However, severely damaged tissue and organs can often not be repaired or recovered, and transplantation represents the only satisfactory way to restore the physiological function [5].

Transplantation is the most effective form of treatment for the final degenerative stages of organ failure [6]. Currently, about 65 000 patients are on the organs' waiting list in the European Union [7]. Therefore, it is obvious that the demand for tissues and organs is higher than the current supply.

In the 1970s and 1980s, researchers began developing tissues and organs. Initial efforts have concentrated on the development of skin equivalents for treating burns. However, quickly an increasing number of tissue types were engineered [5]. Organs such as skin grafts [8] and even a full trachea were successfully implanted in patients [9], while more complex organs like heart, lung, and liver were indeed successfully recreated in the lab, however not implanted into a patient yet [5].

Although not all organs can be employed in the clinic thus far, the tissues can be extremely useful in research, particularly to elucidate biological functions in healthy

and diseased tissue, for toxicity screening, and for drug development [5]. There is an increasing demand for *in vitro* organ-like tissue models as an alternative to certain types of animal testing.

New drug formulations are usually tested on animals, before clinical trials with humans, and finally commercialization of the drugs. However, these experiments are ethically doubtable, costly, and often not transferable to humans. More than 90 % of the drugs that have passed preclinical studies failed to meet the desired efficacy or safety margins in subsequent clinical trials [10]. One of the reasons is the difference between animals and humans [11].

Therefore, tissue models are needed that better reflect the physiology of the human body, help to investigate specificity and efficacy of pharmacological substances, and to reduce the high failure rates in clinical trials. Using organ-like tissue models has a positive impact on the development of new pharmaceuticals and provides, moreover, key tools for facilitating personalized medicine while saving money. Besides drug screening, these models can be used to mimic diseases and hence, to analyze molecular principles in healthy, as well as in pathologically altered tissues, as well as for toxicology testing of chemicals, cosmetics and household products.

Tissue engineering is an interdisciplinary field of material scientists, chemical engineers, physicians, geneticists, and related professions of engineering and the life sciences that aim to develop adequate three dimensional (3D) tissues mimicking original tissue functions [12]. The term "tissue engineering" originated from a workshop of the National Science Foundation in 1988 designating "the application of principles and methods of engineering and life sciences toward fundamental understanding of structure-function relationships in normal and pathological mammalian tissues and the development of biological substitutes to restore, maintain or improve tissue function" [13].

The principles of tissue engineering rely on membranes, which are seeded with cells and occasionally regulating molecules, to act as a template for tissue formation [14]. Figure 1 illustrates the fundamental principle approach of tissue engineering. Cells are isolated from either the patient himself (autologous) or from a donor (allogenic). Instead of freshly isolated primary cells, cell lines can also be used for

the synthesis of *in vitro* tissues. After isolation, the cells are expanded in two-dimensional (2D) environments, and afterward, seeded on membranes. By adding regulating molecules as growth and differentiation factors, as well as physical or mechanical stimuli, conditions can be created that are ideal for cell proliferation, differentiation, extracellular matrix (ECM) synthesis, and tissue formation. Finally, tissue-engineered models can either be implanted into the patient or employed for *in vitro* applications.

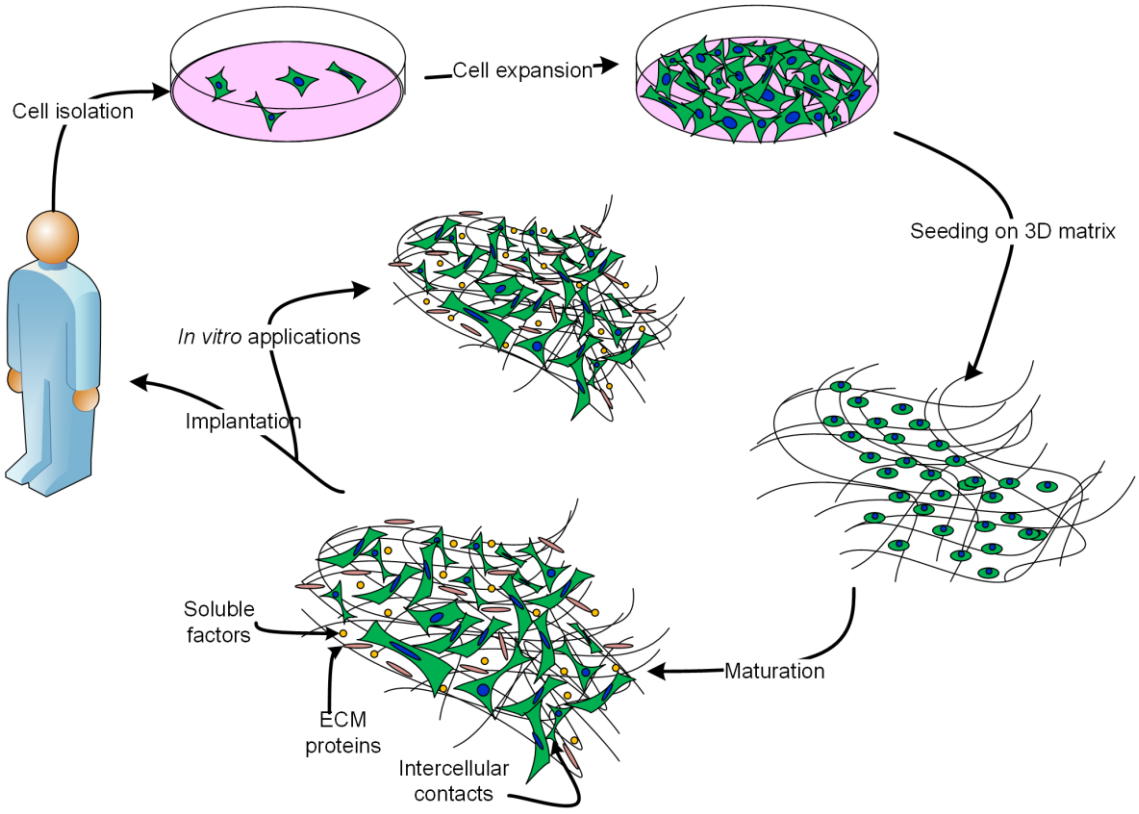

Figure 1: Schematic of the fundamental principles of tissue engineering.
Cells are isolated from human biopsies, expanded in 2D cell culture and seeded on 3D matrices. The tissue maturates, forms intercellular contacts, and produces ECM proteins, as well as soluble factors. Subsequently, the models can be used for implantation or for *in vitro* applications.

Models are either cultured under static conditions in plastic dishes or under dynamic conditions in bioreactor systems. Bioreactors are sealed mechanical chambers providing suitable environment conditions for cellular activity [15]. A basic bioreactor system includes a perfusion reservoir, a pump for perfusion, and a tissue chamber. Dynamic culture conditions are necessary to allow the simulation

of physical parameters such as mechanic shear stress, fluid pressure, and medium flow.

1.2 Skin and oral mucosa tissue engineering

The first reports on skin tissue engineering were published in the 1980s [16, 17]. Since then, tremendous effort has been undertaken to develop biomimetic human skin and oral mucosa models. The approaches are different depending on whether the models are used in clinical applications or as *in vitro* models. For clinical applications, optimal mechanical properties are desired. Additionally, the membrane should be biodegradable and biocompatible. Transmission of infection and tissue rejection often represent major problems in the clinic. Virally transformed and tumor-derived cell lines are excluded from use.

On the other hand, skin and oral mucosa equivalents can serve as an alternative to animal use in drug and cosmetic testing, as well as to elucidate biological processes as wound healing and pathogenesis of diseases. For many years, *in vitro* cell culture experiments have been performed on flat surfaces. However, 2D cultures do not properly model the *in vivo* environment in terms of cellular communication, gene and protein expression, and diffusion of soluble factors [4]. In the context of using tissue-engineered skin and oral mucosa models for *in vitro* applications, characteristics such as reproducibility and costs play a more prominent role than in the context of clinically applied models. Therefore, the use of tumor or virally transduced cell lines may be an alternative to the use of primary cells. Well studied biological endpoints such as inflammation, mutation, chromosomal aberrations, oncogenic transformation, and apoptosis [18] are defined to facilitate the reliable and systematic analysis of skin and oral mucosa models.

1.2.1 Anatomy of the skin and the oral mucosa

The basic structure of the human skin and the oral mucosa is similar: they consist of (1) an outer epidermis and (2) an underlying connective tissue firmly connected by a basement membrane. Both tissues play a crucial role as anatomical barriers, protecting the body from loss of water, electrolytes, and other body constituents,

while preventing the entry of exogenous substances such as pathogens, as well as microorganisms.

1.2.1.1 Skin

The skin, the largest organ of the human body, is 0.5 mm to 4 mm thick and has protective, immunologic, thermoregulatory, and sensory functions [19]. Healthy human skin consists of three layers, the stratified epidermis, the underlying dermis and the subcutis, composed of mainly fat and loose connective tissue (Figure 2). Besides its function as an anatomical barrier, the skin has several other tasks: with its sweat glands, it plays a major role in the temperature regulation of the body [20]. The melanocytes of the skin produce melanin and are responsible for pigmentation and protection against UV-light [21, 22]. Hair follicles and various receptors act as sensory organs [23], nerve cells sense temperature, pain and pressure [24]. Antigen-presenting immune cells, the Langerhans cells, and anti-microbial substances support the immune system. The embedded blood vessels supply the skin with nutrients and are involved in thermoregulation [25, 26].

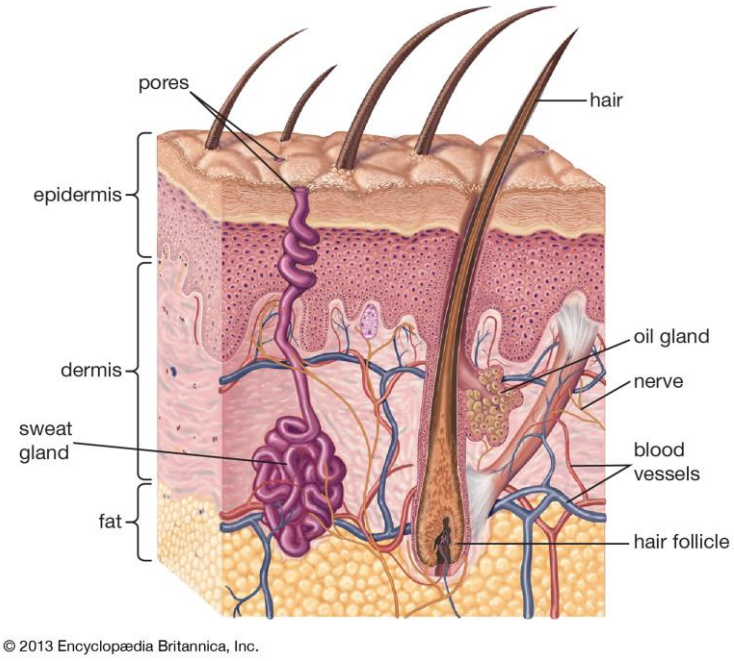

Figure 2: Schematic of the anatomy of the human skin.
The human skin consists of the outer epidermis, the dermis and the subcutis, composed of fat and loose connective tissue. Appendages such as sweat and oil glands, as well as hair shafts are embedded in the skin. The image was used with permission by the courtesy of Encyclopaedia Britannica, Inc., copyright 2013 [27].

Epidermis

The epidermis is the outermost layer of the skin and has a polarized structure, where the apical surface is facing the external environment and the basal surface is connected to the basement membrane. Most of the cells in the epidermis are keratinocytes. They originate from the deepest layers, the stratum basale (SB), which is connected to the basement membrane by hemidesmosomes. As the keratinocytes proliferate, part of the cells differentiate and migrate superficially, forming successively the stratum spinosum (SS), stratum granulosum (SG), and stratum corneum (SC). The process is called desquamation and takes about 14-30 days in healthy skin [28]. In the thick skin on the soles of the feet and the palms of the hands, additionally a stratum lucidum (SL) can be found [29]. The SC is part of the non-viable epidermis whereas SG, SS, SB, and SL are part of the viable epidermis [30]. The SC, being the superficial region of the skin, primarily provides the protective function of the skin to the body from external influences, as well as from water loss. It is 10-40 µm thick and has been proposed to possess a "bricks and mortar" structure. Whereby the keratinocytes present the "bricks" and the intercellular lamellar lipid bilayers represent the "mortar" [31]. Since the epidermis lacks blood vessels, small molecules and gases derived from the blood pass the basement membrane and supply the cells with nutrients.

Dermis

The dermis nourishes the epithelium and is the connection between the skin and the underlying subcutis. It is 2-3 mm thick and contains blood vessels, glands, nerves, hair follicles, smooth muscles, and lymphatic tissue [32, 33]. It can structurally be divided into a superficial papillary region composed of loose connective tissue and a reticular region made up of a dense irregular connective tissue. The reticular layer provides the overall strength and elasticity of the skin. Fibroblasts embedded in the reticular layer are responsible for secreting extracellular matrix proteins, including collagen, elastin and proteoglycans, which provide the skin support and elasticity [34, 35]. The subcutis presents the lowest layer of the skin and is responsible for functions, such as thermoregulation and serves as nutrient reservoir [36].

1.2.1.2 Oral mucosa

Similarly to the skin, the oral mucosa is composed of an epithelium and an underlying fibroblast containing connective tissue, called lamina propria (Figure 3). Both tissues are connected by a basement membrane. In comparison to the skin, keratinized and non-keratinized epithelial layers exist in the oral cavity. Regions which are subject to mechanical forces, such as the gingiva and the hard palate, are mostly stratified (orthokeratinized) and resemble the epidermis in the skin. Parts of the mouth are parakeratinized, meaning that the nuclei of the cornified layer are still recognizable. Buccal regions and the floor of the mouth, which require flexibility, are covered with a non-keratinizing epithelium [37]. The turnover time for the oral mucosa epithelium has been estimated between 5-6 days [38]. The underlying lamina propria is composed of a dense collagen network formed mostly by fibroblasts, but consists also of macrophages, plasma cells, mast cells, and lymphocytes [39]. Loose fatty or glandular connective tissue underlies the lamina propria in many regions of the oral cavity [40].

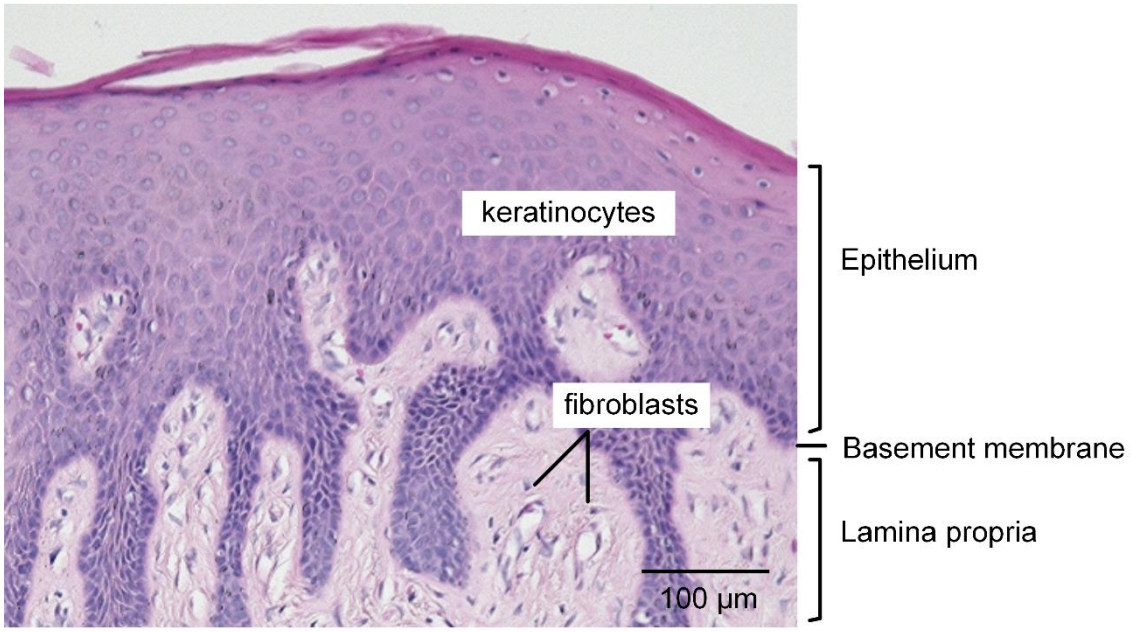

Figure 3: Histology of the human oral mucosa.
Haematoxylin and eosin staining of the oral mucosa consisting of a multilayered epithelium, as well as the underlying lamina propria. Both tissues are connected by a basement membrane.

1.2.2 Skin equivalents

In recent years, significant progress has been made in the development of tissue-engineered skin equivalents that mimic the human skin. These skin models can either be employed for clinical applications or as organ-like *in vitro* tissue models to study cell biology and diseases, for the assessment of chemical toxicity and for testing of pharmaceutical products [41].

1.2.2.1 Skin equivalents for clinical applications

For clinical applications, autografts are known as gold standard for skin regeneration, because rejection is not feared. However, availability is limited and patients sometimes suffer from donor site morbidity and scar formation after transplantation [42]. Allografts and xenografts as alternatives are more abundantly available, but inherently harbor the risk of disease transmission and immunological rejection [43]. These reasons stimulated the development of transplantable tissue-engineered skin substitutes. Besides burn and wound treatments, these skin grafts can be applied in reconstructive surgery, scar revision, scar preventions, and the correction of pigmentation defects [32]. Skin substitutes for clinical applications are mostly based on biodegradable, biocompatible polymers cultured with either allogenic or autologous human cells. Several products are approved for use by the Food and Drug Administration [29]. Therefore, the substitutes can be classified into epidermal, dermal, and composite substitutes according to their structure and their functional resemblance. In addition to these skin substitutes, current research projects integrate induced pluripotent stem cells (iPS), mesenchymal stem cells (MSC) or adipose tissue-derived stem cells (ASC) in cell-based skin therapies [44].

Epidermal skin equivalents

The product EpiCel™ (Genzyme Tissue Repair, USA) represents an example of an epidermal skin graft for clinical applications. The integrated sheet of autologous keratinocytes is enzymatically detached for the delivery to the patient and placed cell surface down onto the wound bed [45]. The ReCell™ (Avita Medical, UK) device employs autologous keratinocytes as a suspension in a fibrin spray directly to the wound [46].

Dermal skin equivalents

Currently three types of biomaterials are employed to reconstruct the dermis for clinical applications: natural collagen, either obtained from human allodermis or from porcine dermis, extracted bovine collagen, and synthetic membranes [41]. Integra™ (Integra LifeSciences Corp., USA) is a classical cell-free dermal graft. The bi-layered membrane is designed to heal major burns and consists of bovine collagen and shark chondroitin-sulfate with a silicone membrane as temporary barrier [47]. Dermagraft™ (Advanced Tissue Sciences, Inc., USA) is a dermal substitute generated by the culture of neonatal dermal fibroblasts onto a bioresorbable polyglactin mesh membrane [48]. TransCyte™ (Advanced Tissue Sciences, Inc., USA) is composed of human newborn fibroblasts, which are cultured on a nylon mesh [49].

Composite skin equivalents

Composite skin substitutes combine allogenic keratinocytes and fibroblasts, and thus resemble both layers of human skin. An example for an epidermal/dermal skin equivalent is Apligraf™ (Organogenisis, USA). It is composed of allogenic keratinocytes grown on a bovine collagen gel populated by fibroblasts [50]. Orcel™ (Forticell Bioscience, USA) is a fibroblast embedded collagen type I sponge with keratinocytes from the same donor on top of the gel [51]. The skin substitute is suitable to cover chronic wounds and acute surgical defects.

1.2.2.2 Skin equivalents for *in vitro* studies

Besides the use for clinical applications, tissue-engineered skin models enable the investigation and the reproduction of fundamental processes in the skin. Epidermal substitutes mimicking the epidermis only, or full-thickness substitutes, resembling the epidermal and dermal structure of the skin, are employed for *in vitro* studies. Depending on the application and the biological endpoint, both models may be applicable and useful.

Epidermal skin equivalents

Epidermal models for *in vitro* applications consist of keratinocytes seeded on synthetic or collagen carriers. Until now, five epidermis models are available which

have been adopted in the Organization for Economic Cooperation and Development (OECD) guidelines for toxicity screening models, these being SkinEthic™ (L'Oreal, France), EpiSkin™ (L'Oreal, France), Epiderm SIT™ (MatTek Corporation, USA), EST1000™ (CellSystems, Germany) and LabCyte™ (J-TEC Co, Japan). The two validated endpoints of the tests are corrosion (OECD Guideline TG 431) and irritation (OECD Guideline TG 439). Most of the epidermal models are grown on inert synthetic polycarbonate filters. EpiSkin™ uses a membrane material composed of collagen type I coated with a layer of collagen type IV [52].

Composite skin equivalents

Although the majority of the skin substitutes used in risk assessment and pharmaceutical research are composed of only an epidermal layer, full-thickness skin equivalents are of great value for the investigation of questions, where the molecular crosstalk between keratinocytes and fibroblasts is crucial [53]. Bell *et al.* first described the process for generating a skin model with a dermal and an epidermal component [16]. To date, different techniques for the formation of a dermal layer have been investigated. Fibroblasts are seeded in collagen gels [54], fibrin gels [55], and on membranes composed of collagen/chitosan/chondroitin-4-6-sulfates [56]. Moreover, small intestine submucosa (SIS) [57] has been utilized as membrane. Furthermore, the use of synthetic polymers such as PLGA [58], PCL [59], and a combination of both [60] have been described. Although no full-thickness skin equivalent is validated so far, there are two models commercially available as StrataTest™ (Stratatech Corporation, USA) and Epiderm-FT™ (MatTek Corporation, USA).

1.2.3 Oral mucosa equivalents

There is a high demand for tissue-engineered oral mucosa for clinical applications and as an *in vitro* test system. However, less research has been conducted on these models due to the limitations in manufacturing facilities, governmental regulatory issues and low profitability. One reason for this may be that demands for engineered oral mucosal grafts are not as urgent as for skin substitutes, which are indispensable in life-threatening situations, such as extensive burns.

1.2.3.1 Oral mucosa equivalents for clinical applications

Although there is a high demand for oral mucosa equivalents for patients with cleft palate or to replace diseased tissue due to trauma or cancer, tissue-engineered oral mucosa is not commercially available for clinical applications, in contrast to tissue-engineered skin, which has been commercialized for many years. Nevertheless, several research groups worked on the development of oral mucosa equivalents. Models based on a biodegradable collagen membrane have been used for the treatment of patients with inadequate attached gingival and for the regeneration of peri-implant gingival tissue [61]. Luitaud *et al.* developed a biodegradable collagen membrane as viable palatal mucosa-like tissue [62]. Oral mucosa keratinocytes were seeded on acellular cadaveric human dermis (AlloDerm™) and cultured for 4 days under submersed conditions and 7 days under air-liquid interface. The ex-vivo produced tissue-engineered oral mucosa equivalents (EVPOME) were then successfully implanted into five patients [63]. The only oral mucosa that was commercially available, is Bio-Seed®-M. Therefore, a small piece of mucosa was taken from the patient's mouth and mucosal cells were expanded for about three weeks. The cultured oral mucosa cells together with a carrier foil were placed directly onto the wound surface in the oral cavity. More than 70 patients have been treated with this type of construct [64]. However, since 2009, the product is exclusively distributed in modified form for urethral reconstructions.

1.2.3.2 Oral mucosa equivalents for *in vitro* studies

Advances in tissue engineering permit the reconstruction of oral mucosa equivalents for *in vitro* investigations. The models are valuable as disease models, to analyze the mucotoxicity of biomaterials and oral health care products, as well as to study penetration/permeation of agents into the oral mucosa [65].

Epidermal oral mucosa equivalents

Today, there are few epithelial oral mucosa models commercially available, although none of them has been validated yet. Two models are produced by SkinEthic Laboratories: an *in vitro* model of the oral epithelium derived from an oral squamous cell carcinoma cell line (TR146) [66] and a gingival epithelium model

with human gingival keratinocytes [67]. The TR146 based model has been used to study the effects of *Candida albicans* [68, 69] and of different surfactants [70]. MatTek Corporation has also two different epidermal models on the market: EpiOral™ with human-derived oral epithelial cells from buccal tissue, and EpiGingival™ with epithelial cells from gingival tissue [71]. The models have recently been used to investigate the influence of ethanol and ethanol-containing mouth rinses on permeability [72], and to study the effects of repeated cigarette smoke exposure on the buccal and gingival tissue [73].

Composite oral mucosa equivalents

The fibroblast component is critical for promoting growth and differentiation of keratinocytes into squamous epithelial cells. Several research groups have investigated full-thickness oral mucosa models. Odioso *et al.* developed an *in vitro* gingival model composed of oral epithelial cells and connective tissue fibroblasts on a nylon mesh [74]. Acellular cadaveric human dermis (AlloDerm™) was used for the *in vitro* tissue engineering of the oral mucosa [75] as for the reconstruction of human hard palate mucosal epithelium [76]. MatTek Corporation sells three different composite oral mucosa equivalents: ORL-300-FT, a model with cells isolated from buccal tissue; ORL-300-FT-LC, a model with buccal and Langerhans cells; and GIN-300-FT, a model based on cells isolated from gingival tissue. Oral mucosa equivalents have already been utilized for *in vitro* studies to investigate the effects of dentifrices on the tissue structure [77] and to study the mucosal irritation potential of metals used in dentistry [78]. Moreover, oral candidiasis [79], HIV type 1 [80], human cytomegalovirus [81], and oral cancer cell invasion [82] were investigated.

1.3 The role of the basement membrane in the skin and oral mucosa

The basement membrane, a specialized form of the ECM, constitutes the boundary between the epidermis and the dermis. It was identified by transmission electron microscopy as a 50-100 nm amorphous, dense, sheet-like structure [83] and can be divided into basal lamina and reticular lamina. In addition to dividing tissues into compartments, it acts as structural support, and regulates cellular behavior. Apart

from epithelia tissues, basement membranes can be found basolateral to endothelia, fat and muscle cells, and peripheral nerve axons [84].

1.3.1 Basement membrane composition

About 50 proteins build up the natural basement membrane. Thus, its composition is extremely diverse, tissue-specific, and dynamic. Different isoforms of the basement membrane components, as well as variations in their relative amounts, provide tissue-specificity. The main constituents are laminin, nidogen/entactin, perlecan and collagen type IV [85], which accounts for more than 50 %. In contrast to collagen type I, II, and III, collagen type IV is non-fibrillar and has the capacity to self-assemble into organized networks. So far, seven different collagen type IV units have been identified. Their interaction with cellular receptors is important for cell adhesion, migration, differentiation, and proliferation [86]. In addition to collagen type IV, laminin plays a vital role in the basement membrane. Each laminin molecule consists of a-, β- and γ-chains. To date, five different α-chains, three different β-chains, and two γ-chains have been identified at the molecular level [87]. The combination of different chains determines the individual laminin form. Laminin-5 and laminin-1 seem to be most abundant in the basement membrane of the skin, though different forms may also be present [88]. Nidogen, also named entactin, makes up 2-3 % of all basement membrane proteins. Two different isoforms are known, which are ubiquitously expressed in all basement membranes throughout the body and are able to bind to collagen type IV, perlecan, laminin, fibrinogen and fibronectin [89]. Perlecan, a heparan sulfate proteoglycan (HSPG), is another constituent of the basement membrane [90]. It has various binding sites for nidogen/entactin, collagen type IV, integrins, and heparin, and its overall structure resembles that of “pearls on a string” [91, 92]. Several other components are included in the basement membrane as agrin, collagen type XV, collagen type XVIII, osteonectin, and fibulin [91]. However, their biological significance and function remains unknown.

1.3.2 Basement membrane assembly

The cellular origin of the basement membrane constituents and their regulation is still not completely understood [88]. Cell culture experiments in monolayer cultures on plastic substrates suggest that both epithelial and mesenchymal cells are capable of synthesizing basement membrane components [93, 94]. It seems as if collagens and perlecan are produced by epidermal and mesenchymal cells, while fibroblasts are the main source for nidogen and keratinocytes for laminin [95]. As indicated in Figure 4, basement membrane components are synthesized and secreted from the cells to form a sheet-like structure. It is believed that laminin polymerization triggers the formation of the basement membrane and functions as the primary organizer [96]. The laminin network is anchored to the cell by receptor proteins. The collagen type IV fibrils interact with the laminin network and give the basement membrane its tensile strength [91, 97]. Nidogen/entactin and perlecan are not capable of forming sheet-like structures by themselves, but bridge and stabilize the collagen type IV and laminin fibrils [90]. The membrane provides specific interaction sites for other constituents to generate a fully functional, tissue-specific basement membrane.

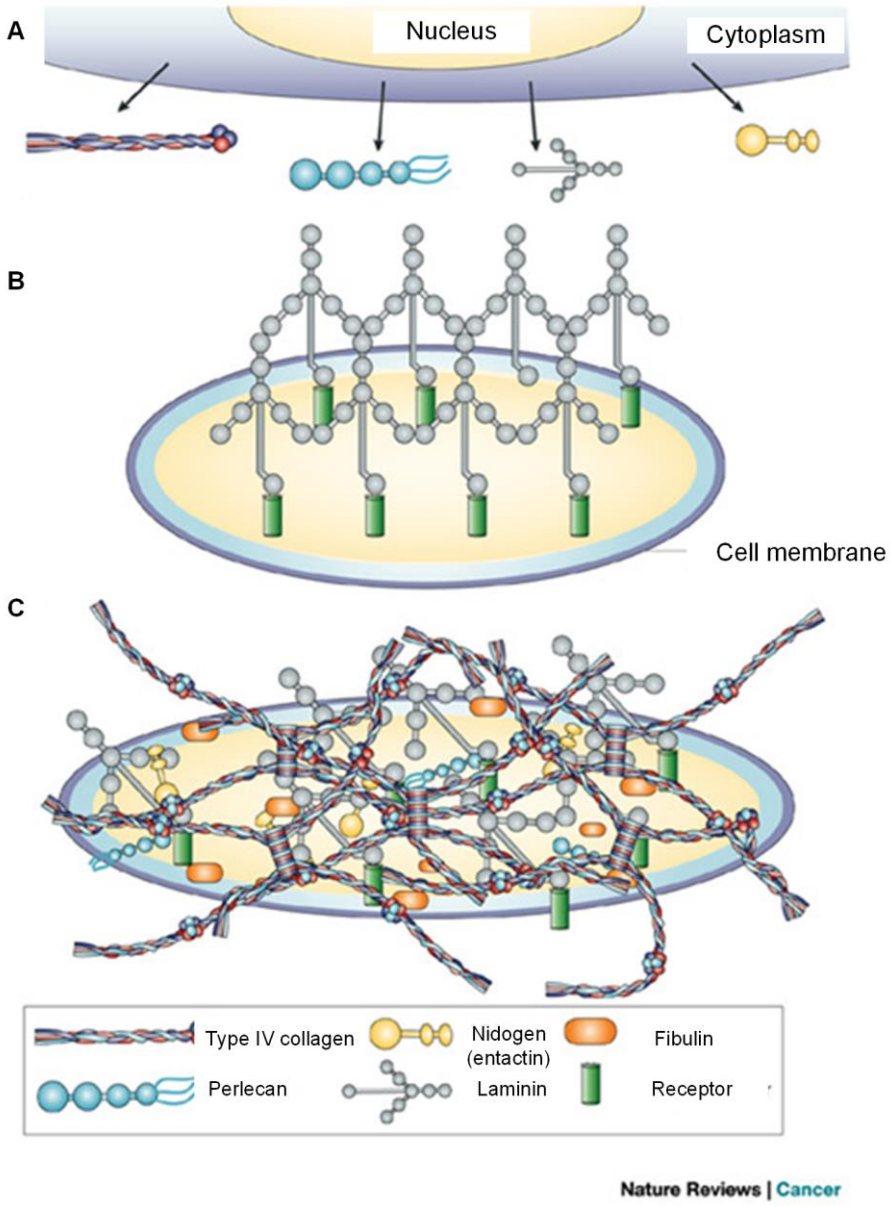

Figure 4: Molecular composition of the basement membrane.
(A) Cells produce basement membrane components and secrete them. (B) Laminin polymerization is believed to initiate the basement membrane formation. The laminin network is anchored to the cell surface by integrin receptors and dystroglycans. (C) The laminin network is associated to the collagen type IV network. Other components interact with the laminin and collagen type IV network to organize a functional basement membrane. Adapted from [92] with permission from the Nature Publishing Group.

1.3.3 Basement membrane function

Apart from providing structural support to the adherent cells, individual basement membrane components serve as regulators for many biological activities, such as

cell migration, proliferation, differentiation, gene expression, and secretion of various hormones and growth factors [98]. Basement membrane proteins possess multiple binding sites which serve as ligands for cell surface receptors. The attachment of the cells to the basement membrane initiates intracellular signaling pathways, which in turn influence cellular behavior. In addition, the basement membrane binds various cytokines and growth factors, acting as a reservoir for their controlled release [99]. Furthermore, it divides tissues into compartments and acts as a mechanical barrier, all the while being essential for angiogenesis and the prevention of malignant cells infiltrating the tissue. It plays, for example, an important role in pathological processes such as diabetes mellitus or cancer. Breakdown of the basement membrane is believed to be an essential step for tumor invasion and metastases [100]. If the basement membrane is damaged through injury or pathogenesis, the membrane is remodeled, consisting of *de novo* deposition of basement membrane proteins, self-assembly, and network formation. The altered basement membrane composition, in turn, changes cellular behavior and guides the cells to promote tissue repair [85, 91].

1.4 Development of artificial basement membranes

In the natural environment, cells grow in an organized 3D environment, communicating with each other by cell-cell and cell-matrix interactions. These interactions determine cellular behavior as proliferation, differentiation, apoptosis or invasion. However, for a long time, cell biology was investigated in 2D geometries by growing cells on flat surfaces. Although 2D models are still applied in many cell culture studies, there is an increasing agreement that co-culture models with several cell types in a 3D environment can provide a more physiologically relevant mimic of tissue morphology and function in the body [101, 102]. Indeed, many pathological, physiological, and cellular processes have been demonstrated to exclusively occur in 3D. Cells can respond to the 3D environment and remodel the local ECM by synthesizing new ECM elements. This cell-triggered ECM remodeling is a unique feature of 3D cell culture contributing to its superiority to conventional 2D cell culture.

One of the most critical aspects of *in vitro* 3D cell culture and tissue engineering is to establish a support structure that presents important cues for cells and guides them to maintain tissue-specific functions. In the natural environment, the basement membrane plays an important role in these tasks. Therefore, for the development of tissue-engineered models, artificial membranes should be engineered that ideally emulate the composition, structure, and topography. They should be highly porous to trigger cellular adhesion, infiltration, proliferation, differentiation, and tissue development in three dimensions and to allow transport of nutrients and metabolic waste. Furthermore, the material should be biocompatible and bioresorbable to avoid immunoreactions. In addition, the surface chemistry should be suitable for cell attachment, proliferation and differentiation, while permitting cellular remodeling and tissue regeneration. The mechanical properties of the biomaterial should further match those of the native tissue at the site of implantation and should be retained until the tissue is fully remodeled.

1.4.1 Electrospinning

In the last two decades, electrospinning has been recognized as an efficient technique to produce ultra-fine fibers with diameters in the range of nanometers and micrometers [103]. The fibrillar structure of the electrospun membranes, as well as the high porosity, the large surface to volume ratio, and their mechanical properties, resemble the interwoven fiber meshwork of collagen and elastic fibers in the basement membrane [104].

In 1934, the electrostatic spinning technique was first patented [105]. Since the 1980s and especially in recent years, the electrospinning process has regained more attention, since nanofibers can be easily and cost effectively fabricated with this process. Electrospinning can be applied in the manufacture of encompassing filtration devices, textiles, electrical and optical components, as well as biomedical materials such as medical implants, antimicrobial materials, wound dressings, dental materials, drug delivery vehicles, and enzyme immobilized membranes [9, 106]. Electrospun fibers have also been extensively investigated for tissue engineering applications, including cartilage [107, 108], bone [108, 109], neural

[110, 111], skin [112, 113], corneal [114], cardiovascular [113, 115], tendon [113, 116], and stem cell [117] tissues.

For a basic electrospinning setup, three components are essential: a high voltage power supply, a syringe with a needle of small diameter in a syringe pump, and a conductive collector (Figure 5). One electrode is either attached to the collector or, in most cases the collector is grounded. The other electrode induces charging of the polymer solution. The surface tension of the solution counteracts the electrostatic repulsion. As the intensity of the electric field increases, the liquid stretches. At a critical point, a stream of liquid erupts from the surface. This point is known as the "Taylor cone". The polymer solution jet undergoes an instability and elongation process caused by electrostatic repulsion. On the way to the collector, the solvent evaporates. Finally, the fibers are deposited on the target [118]. By these means, electrospinning produces 3D nonwoven, porous, and nano-scale fiber based matrices.

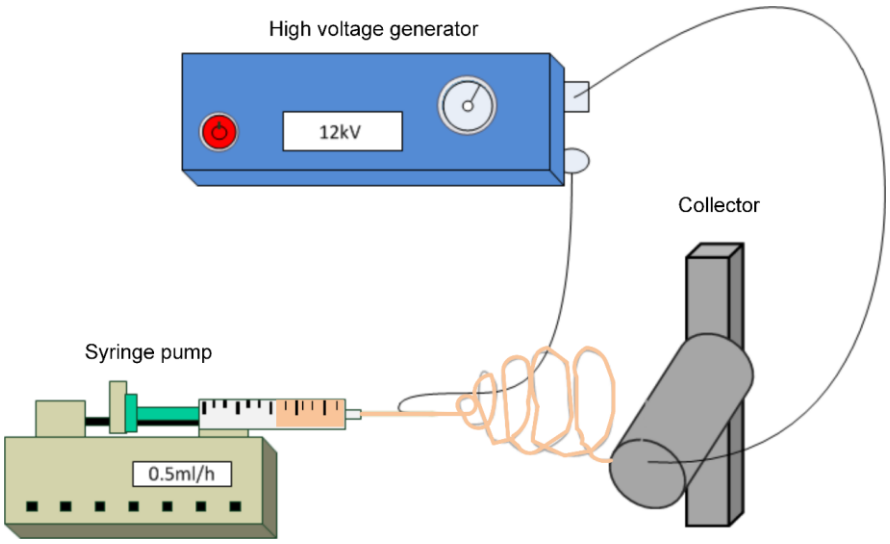

Figure 5: Electrospinning setup.
Electrospinning setup consisting of a syringe pump, a high voltage generator and a metal collector.

Prior to the use of electrospun matrices in cell-culture experiments, the materials must be sterilized. Several techniques exist to sterilize medical devices. Each of them has advantages, limitations and effects on the material. Steam sterilization, dry heat sterilization, ultraviolet (UV)-radiation, ethylene oxide, γ-sterilization, and ethanol

treatment are only some of the procedures applied to sterilize electrospun fibers [119].

1.4.1.1 Parameters influencing electrospinning

The parameters influencing electrospinning can be divided into three categories: firstly, solution parameters, such as concentration, molecular weight, viscosity, surface tension, conductivity, dipole moment, and dielectric strength affect the electrospinning characteristics. Moreover, there are process parameters which are of significance for the electrospinning process, such as the electric field strength, needle and collector geometry, tip-to-collector distance, as well as the flow rate. Ambient parameters, such as solution temperature, humidity, and air velocity in the electrospinning chamber also alter the behavior of electrospinning.

Solution parameters

The polymer concentration is one of the crucial properties to maintain a stable jet and to induce homogeneous fiber formation during the electrospinning process. When the concentration of the polymer in the solution increases, higher chain entanglement occurs, and thus the viscosity increases. If the viscosity is too low, the liquid jet breaks up into droplets, known as electrospraying. Therefore, minimum concentrations are defined for different polymers. With higher polymer concentration, the diameter of the fibers increases [120, 121]. If the concentration is too high, helix-shaped micro-ribbons can be observed [122]. The molecular weight of the polymer is another parameter that affects the electrospinning process. It modifies the entanglement of the polymer chains in the solution. Lowering the molecular weight and keeping the concentration constant results in droplets rather than smooth fibers. The influence of the molecular weight of polyvinyl alcohol (PVA) was investigated by Tao *et al.* [123]. They found that at a constant concentration, the structure observed changed from beads to beaded fibers to complete fibers and flat ribbons respectively, by increasing the molecular weight only. Along with polymer concentration and molecular weight, viscosities play an important role in fiber size and morphology. The viscosity can be tuned by adapting the concentration of the polymer solution and the molecular weight of the polymer. Thus, viscosity, concentration and molecular weight are closely related to each other.

The surface tension is another property that affects the morphology of the elctrospun fibers. Yang *et al.* analyzed the influence of the surface tension on electrospun polyvinyl butyral (PVP) fibers with ethanol, dimethylformamide (DMF), and dichloromethane (DCM) as solvents [122]. Their data show that different solvents result in different surface tensions. Reducing the surface tension, leaving polymer concentrations constant, converted beaded fibers into smooth fibers. The type of polymer and solvent used, as well as any addition of a salt, determines the solution conductivity. The formation of thinner fibers is favored when the solution conductivity is increased. By adding ionic salts like KH_2PO_4 or NaCl, the electrical conductivity can be fine-tuned, resulting in nanofibers with smaller diameters [124]. Liu *et al.* used formic acid as a solvent to dissolve nylon and obtained electrospun nylon-beaded fibers with 3 nm diameters. By adding small amounts of pyridine into the solution, the conductivity of the solution was increased and the beads were eliminated [125].

Process parameters

The applied voltage has a crucial impact on the morphology and diameter of the fibers. A critical voltage is needed to form a "Taylor cone". If a certain voltage is applied, there is a corresponding flow rate required. If the two parameters do not match, instabilities in the fiber formation occur. In general, lower flow rates are favorable, as it increases the time for polarization. However, only a few studies have investigated the influence of the flow rate on the fiber size and morphology. Zong *et al.* observed that a reduction in flow rate resulted in fibers with smaller diameters, while beading occurred if flow rates were too high [126]. During electrospinning, collectors usually act as a conductive substrate to collect the charged fibers. If the distance between capillary and collector is too low, the fibers do not have sufficient time to solidify completely before reaching the collector, leading to flattened nanofibers. Beaded fibers can be obtained if the distance is too high, due to instabilities of the polymer jet. An increase of the distance between capillary and collector leads to a decrease in fiber diameters. In the literature, the influence of the collector distance on fiber morphology is controversially discussed. Doshi *et al.* [103] as well as Yuan *et al.* [127] reported a decrease in nanofiber diameter with an

increase in collector distance. However, if the distance between capillary and collector was too far, the fiber jet became too small and unstable. Megelski and coworkers stated that the distance between the capillary and the collector did not have a significant influence on the diameter [128].

Ambient parameters

Ambient parameters such as temperature and humidity can affect the morphology and the diameter of the fibers. The humidity has an influence on the solvent evaporation. Low humidity leads to an increased velocity of solvent evaporation. High humidity in contrast can neutralize the charge so that the stretching forces decrease. Casper *et al.* showed that humidity has also an influence on the morphology of the fibers. As humidity increases, pores on the surface of the fibers increase due to the evaporation of water on the surface [129]. Mit-uppatham *et al.* investigated the influence of temperatures ranging from 25 to 60 °C on the diameter of electrospun polyamide-6 fibers. They showed a decrease in fiber diameters with respect to an increase in temperature, probably resulting from the lower viscosities at higher temperatures [130].

1.4.1.2 Polymers for electrospinning

So far, more than 50 different polymers have been electrospun successfully [131]. Natural polymers including proteins such as gelatin, collagen, and silk fibrinogen, as well as polysaccharides such as chitosan, hyaluronic acid, and cellulose have been used. Extensive literature about electrospinning of natural polymers can be found elsewhere [132, 133]. Natural polymers are typically intrinsically bioactive, and thus promote excellent cell adhesion and growth, while allowing the host cells to remodel the matrix and to replace the membrane. However, they are usually not very well characterized with significant batch-to-batch variations and often yield mechanically weak scaffolds. Moreover, a systematic biochemical tailoring of natural polymers is difficult [134]. In contrast, synthetic polymers represent a more reliable source of raw material. They are economically advantageous, possess good mechanical properties, excellent processability and can be individually tailored for specific functions and properties, by altering chemical composition, crystallinity, molecular weight, and copolymerization. Synthetic polymers that are often

investigated for tissue engineering applications, include polyurethane (PU) [135, 136], poly(ε-caprolactone) (PCL) [137, 138], polyethylene oxide (PEO) [139, 140], and poly(p-phenylene terephthalamide) (PPTA) [141]. The most widely applied synthetic polymers are polyesters based on lactic and glycolic acid. Many research groups work with poly-L-lactic acid (PLLA), polyglycolic acid (PGA) and poly-lactic-*co*-glycolic acid (PLGA). PLGA is the most popular biodegradable synthetic polymer due to its excellent biocompatibility and adjustable degradation rates [142, 143]. Depending on the ratio of lactide and glycolide used for polymerization, different forms of PLGA can be obtained. In the literature, PLGA 85/15, PLGA 75/25, and PLGA 50/50 are most commonly described for tissue engineering applications. PLGA 85/15, for instance, is a copolymer with a composition of 85 % lactide and 15 % glycolide. Copolymer composition affects the mechanical properties of the membrane. Increasing the content of the less hydrophobic glycolide unit in the copolymer facilitates the absorption and diffusion of water, thus aiding in hydrolysis [144], which accompanies a drop in glass transition temperature (Tg) and a decrease in mechanical properties. Blackwood *et al.* investigated different PLGA mats in terms of biodegradability. PLGA 85/15, PLGA 75/25, and PLGA 50/50 lost half of their mass within 4 months, 3 months and 2 weeks, respectively [145]. Degradation of PLGA occurs mainly through chemical hydrolysis of the hydrolytically instable ester bonds into lactic acid and glycolic acid, which are both nontoxic and can be metabolized from the body [146].

1.4.2 Modification of electrospun membranes

A large number of biocompatible synthetic polymers with different mechanical stabilities and elasticities are available for electrospinning. However, nowadays biomaterials should not only be incorporated into the host without causing harm, but also be able to integrate and interact with surrounding tissue and ideally, promote regeneration [147, 148]. Therefore, efforts have focused on modifying the surface of materials to control protein-material interactions and selective adhesion of the surrounding cells [149].

1.4.2.1 Protein/membrane interactions

Protein adsorption is expected to play a key role in determining the acceptance of a biomaterial. As soon as a biomaterial is exposed to body fluids, proteins rapidly adsorb onto the surface of the material, occupying the surface within seconds to minutes. When cells approach the surface of the biomaterial, they rather interact with the adsorbed proteins than with the surface of the material. The resulting signal cascades are neither controlled nor intended. Inflammation, fibrous capsule formation, implant loosening, and implant failure are provoked [150]. To prevent immune reactions and to promote selective cell adhesion, the amount and types of proteins that are adsorbed on the surface of the biomaterial and their orientation, conformation, and packing arrangement need to be controlled [151].

The interaction and adhesion of proteins is based on hydrophobic interactions. Various types of surface chemistries have been studied to give biomaterials a non-fouling surface, such as coating with poly(acrylamide), poly(hydroxyethyl methacrylate), poly(N,N-dimethyl acrylamide), dextran and poly(oxazoline), as well as other hydrophilic materials [152]. However, poly(ethylene)glycol (PEG) has received the greatest attention. The hydrophilic and uncharged polymer is known to resist unspecific protein adsorption [153]. It is non-immunogenic, non-toxic and is approved for biomedical applications [154]. Oligo(ethylene)glycol (OEG) terminated alkanethiol self-assembled monolayers have been coupled on gold by the Whitesides group [155, 156] and others [157, 158]. PEG films were anchored to glass or other oxide terminated surfaces by silane coupling chemistry [159, 160]. The grafting density and the chain length are two essential control parameters by which the resistance is governed, although the reasons for the non-fouling property of PEG are still not yet fully understood [161, 162]. Due to instabilities and steric hindrance of linear PEG chains on the surface, higher grafting densities are difficult to achieve. Therefore, star-shaped PEG (sP(EO-*stat*-PO)) macromers were developed that are able to graft surfaces at higher densities [163].

In Figure 6, the chemical composition of the sP(EO-*stat*-PO) system is illustrated. It consists of a six armed, star-shaped sorbitol core with 80 % ethylene oxide and 20 % propylene oxide statistically copolymerized into the backbone, and reactive

isocyanate (NCO) endgroups (NCO-sP(EO-*stat*-PO)). Dissolution of NCO-sP(EO-*stat*-PO) in water results in hydrolysis of the isocyanate groups to carbamide acid, which leads to the release of carbon dioxide and the formation of amine groups at neutral pH. The amine groups react with other NCO-groups and form urea bridges between different NCO-sP(EO-*stat*-PO) molecules. It was shown, that after complete hydrolysis and aminolysis of the isocyanate groups, a dense surface layer that minimizes adsorption of proteins, was formed. A detailed overview of the different star-shaped PEG pre-polymers and their properties is given in a review by Gasteier *et al.* [163]. Comparison between sP(EO-*stat*-PO) and linear PEG has shown that the suppression of unspecific protein binding of sP(EO-*stat*-PO) is superior to linear PEG coatings and that the intermolecular crosslinking reaction of the sP(EO-*stat*-PO) system is indispensable to obtain densely packed polymer networks [164].

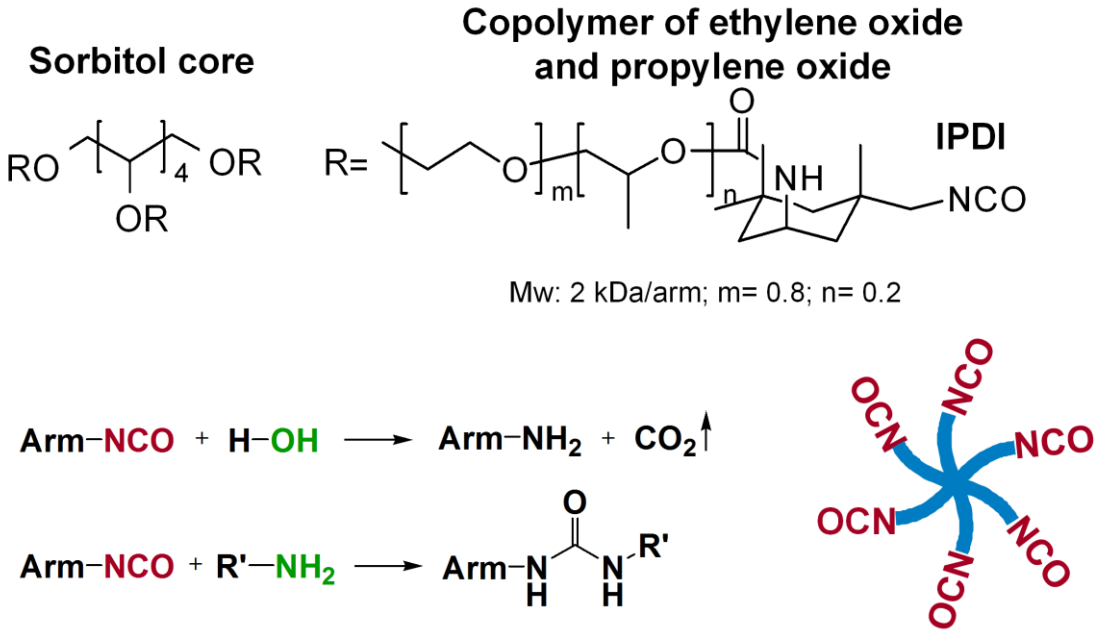

Figure 6: Chemical composition of NCO-sP(EO-*stat*-PO) pre-polymers.
The system consists of a star-shaped sorbitol core with 80 % ethylene oxide and 20 % propylene oxide statistically copolymerized in the backbone and reactive isocyanate (NCO) endgroups. Isocyanate groups react with water and form primary amines. These amines react with other isocyanate groups to form carbamid bridges. The graphic was adapted from [163].

1.4.2.2 Cell/membrane interactions

To restore tissue function and stimulate new tissue formation, a membrane should support cell proliferation, and extracellular matrix remodeling [165]. However, the surfaces of synthetic biomaterials do not promote cell interactions by themselves. The bioactivity is rather triggered by the adsorbed proteins. By coating materials that cause minimal protein adsorption with cell adhesive proteins like collagen, fibronectin, and laminin, specific cell-material interactions can be provoked [166]. However, modifying biomaterials with natural polymers often results in problems such as batch-to-batch variations, low stability, high costs, and immunogenicity. Linking bioactive peptide sequences to synthetic membranes is advantageous in many cases, because they are inexpensive, easier to produce and uncomplicated to control than large heterogeneous ECM molecules. Due to their smaller sizes, peptide sequences can be packed with higher densities on the surface and offer greater flexibility for surface modification.

Stable linkage of the peptide sequences to a surface is essential to promote cell adhesion and function. Biomolecules can either be physically adsorbed [167] or covalently attached [168, 169] on the surface. Chemical immobilization is often favored over physical immobilization, because covalently attached bioactive molecules cannot easily be leached out from the surface when incubated for extended periods. Functional groups to bind the sequences can be generated by plasma treatment, partial surface hydrolysis under acidic or basic conditions, surface graft polymerization or blending with other polymers that contain functional groups [170]. Peptide sequences can then be attached to the polymer via these functional groups.

By directly conjugating bioactive molecules to the surface of the biomaterial, cells have difficulties recognizing the ligands, due to the cell-adhesion binding sites not being fully exposed to the surface, but instead probably being hidden within the fibrillar structure. Thus, hydrophilic linkers between the polymer surface and the bioactive molecules were introduced to promote cellular recognition and in addition, to suppress protein adsorption. Kim *et al.* synthesized di-block copolymers of PLGA-PEG-NH_2 and used them for electrospinning. GRGDY was covalently grafted

onto the aminated surface of the electrospun mesh under hydrating conditions. The surface conjugation of GRGDY enhanced cell attachment and proliferation [168]. This approach, however, is time consuming, involves several steps of activation and functionalization, and the activated carboxyl groups can be deactivated quickly by hydrolysis.

Recently, the use of sP(EO-*stat*-PO) system with isocyanate functional groups at the distal ends, with its cell and plasma protein-repellent properties, was described to form a dense surface layer that minimizes protein adsorption and enables the covalent binding of cell-adhesion-mediating peptide sequences [171]. The crosslinking process, and hence the formation of a hydrogel layer of NCO-sP(EO-*stat*-PO) described in Figure 6 is relatively slow. This fact can be used to covalently attach protic groups such as amines and thiols so that cell-adhesion-mediating peptide sequences can be immobilized to the isocyanate groups positioned at the end of the star-shaped additive without any further activation of the surface to trigger cell adhesion (Figure 7). Hence, each immobilized peptide is automatically positioned on the surface of the fiber with a PEG-spacer of a molecular weight of 2 kDa/arm accessible to the cells. The mechanisms by which the hydrophilic star-shaped molecules are enriched at the fiber surface are not completely understood. We hypothesize that the molecules surface segregates during the spinning process as an effect of solvent evaporation. Electrostatic forces may also contribute to the surface segregation.

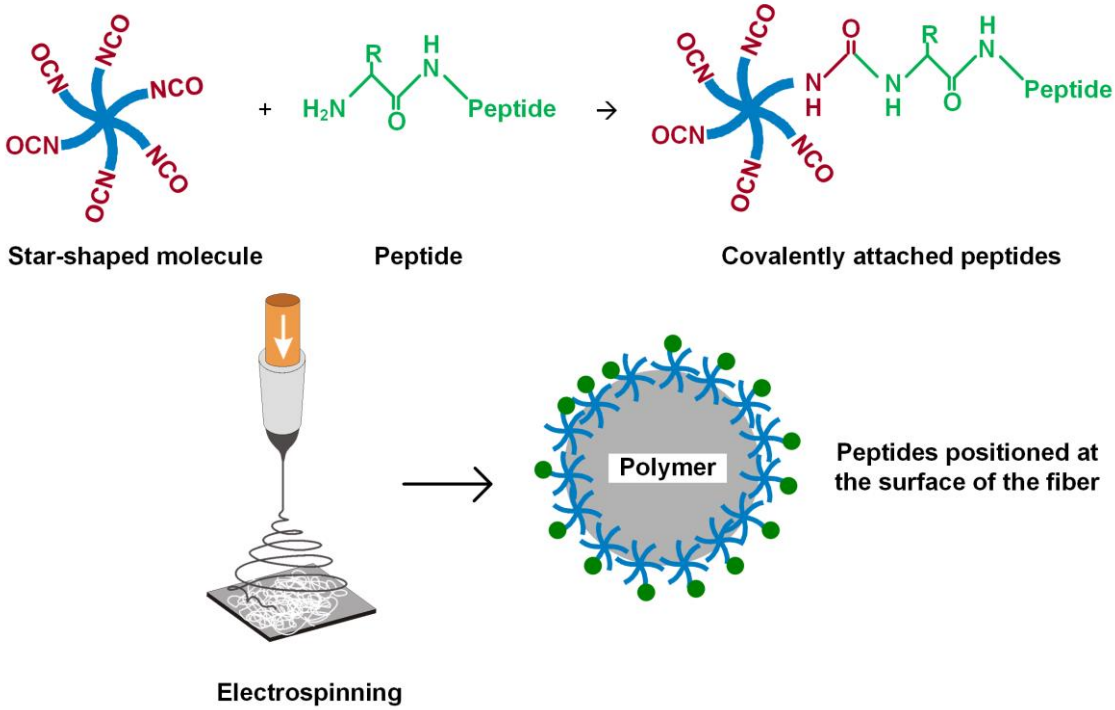

Figure 7: Covalent attachment of peptides to NCO-sP(EO-*stat*-PO).
N-terminal peptides can be covalently linked to the star-shaped molecules. After electrospinning, the peptide sequences are automatically positioned on the surface of the fibers. The arms of the NCO-sP(EO-*stat*-PO) molecule act furthermore as a spacer to promote cellular recognition.

To develop artificial basement membranes, meshes were functionalized with four different peptide sequences. The fibronectin derived binding site CGRGDS, the laminin derived binding sites CGYIGSR and CGIKVAV, and the collagen type IV derived binding site CGEFYFDLRLKGDK (Table 2).

Table 2: List of bioactive peptide sequences

Chemical composition	Biological origin	Description
CGRGDS	fibronectin, laminin, collagen, vitronectin	Fibronectin derived binding sequence
CGYIGSR	laminin β1 of laminin-111	laminin β1 derived binding sequence
CGIKVAV	laminin a1 of laminin-111	laminin a1 derived binding sequence
CGEFYFDLRLKGDK	collagen type IV residues 531-543	collagen type IV derived binding sequence

The integrin-binding sequence cysteine-glycine-arginine-glycine-aspartic acid-serine (CGRGDS) is the most widely studied adhesive peptide in the biomaterials field. It is found in many ECM proteins such as fibronectin, laminin, collagen, and vitronectin [172, 173]. RGD containing peptide sequences have been attached to different surfaces to enhance cell adhesion, migration, and differentiation [174, 175]. Laminins are heterodimeric proteins with three distinct units, α-, β-, and γ- chains [176]. The amino acid sequence cysteine-glycine-tyrosine-isoleucine-glycine-serine-arginine (CGYIGSR) from the β1 chain of laminin-111, also called laminin 1, has been identified as a major binding site for laminin receptors [177, 178]. The sequence is involved in cell adhesion, neural crest migration, and cell signaling [179, 180]. When combined with the fibroblast growth factor (FGF), the YIGSR peptide sequence enhances proliferation and motility of aortic endothelial cells [181]. The peptide sequence cysteine-glycine-isoleucine-lysine-valine-alanine-valine (CGIKVAV), which is found on the α1-chain of laminin-111, supports cell adhesion, cell migration, cell spreading, and neurite outgrowth [182]. Both of the laminin-derived peptide sequences have a number of protein-binding partners, the detailed nature of the cell surface receptors recognizing them, however, has to be investigated. The peptide sequence cysteine-glycine-glutamic acid-phenylalanine-tyrosine-phenylalanine-leucine-arginine-leucine-lysine-glycine-aspartic acid-lysine (CGEFYFDLRLKGDK) represents the isolated type IV collagen residues 531-543 from the amino terminus of the α1-chain [183]. The synthetic peptide sequence was found to be a potent promoter of cell adhesion and spreading for many cell types. It was investigated for keratinocyte cell culture [184, 185] and for cellular behavior of pre-osteoblasts, chondrocytes, and pre-adipocyte cell lines [186].

1.4.2.3 Quantification of bioactive peptides on electrospun membranes

Although a considerable amount of electrospun membranes have been functionalized with cell-adhesion-mediating peptides, the quantification of peptides is often disregarded. However, for the function of a biomaterial and to improve coupling conditions, it is pivotal to determine whether and how many bioactive groups are attached to the surface [187, 188]. There are some methods, which were

used to evaluate the amount of peptide sequences on the surface. In doing so, it is important to distinguish whether the method is surface sensitive or also measures the bulk material and whether the method is fully quantitative. Atomic force microscopy (AFM), transmission electron microscopy (TEM), and scanning electron microscopy (SEM) are powerful techniques to understand surface morphology and topography [189], however, they do not give any quantitative information. Methods that use radiolabelled ligands detect peptides throughout the bulk of the coating [187]. X-ray photoelectron spectroscopy (XPS) and time-of-flight secondary ion mass spectrometry (TOF-SIMS) measure surface-near regions of materials [190, 191]. For both setups, the penetration depth depends on the experimental set-up and the material characteristics. The chemical analysis obtained with attenuated total reflection (ATR) gives information on both, the surface and the deeper layers of the substrate [192]. Enzyme linked immunosorbent assay (ELISA) and colorimetric assays are semi-quantitative methods often used in combination with other methods to describe the material's surface [193]. Surface plasmon resonance (SPR), quartz crystal microbalance (QCM), and surface acoustic waves (SAW) are methods that are surface sensitive, but cannot be applied to fibrillar structures [194]. To our knowledge, however, there is no method which is surface sensitive, applicable to electrospun fibers, and fully quantitative. One reason for this is the experimentally difficult determination of surface ligand densities on textile structures.

1.5 Scope and structure of the thesis

In the human body, basement membranes divide tissues into compartments, are crucial as cell substrates and regulate cellular behavior. Thus, for tissue engineering applications, it is pivotal to establish a support structure that presents similar cues to the cells and guides them to maintain tissue-specific functions. Electrospinning has been recognized as an efficient technique to produce membranes structurally resembling native basement membranes. By modifying the electrospun fibers with star-shaped additives and cell-adhesion-mediating peptide sequences, meshes can

be produced mimicking the topography and the functional composition of natural basement membranes.

Due to the hydrophobic nature of polyesters, electrospinning of PLGA results in protein adsorption that mediates cell adhesion unspecifically (Figure 8A). In order to generate fibers that are non-adhesive for proteins, but can easily be biofunctionalized, PLGA was modified with an amphiphilic macromolecule based on six armed star-shaped polyether prepolymers, with 80 % ethylene glycol and 20 % propylene glycol (sP(EO-*stat*-PO)) having been statistically copolymerized with reactive isocyanate (NCO) endgroups. This leads to a hydrophilic surface of the membrane, associated with reduced protein adsorption and cell adhesion (Figure 8B). The free isocyanate groups of the star-shaped additive are very reactive and due to the slow hydrolysis, amine groups, as well as alcohols and thiols, can be covalently attached by reaction between the N-terminus of the peptide chain and the isocyanate groups. By incorporating cell-active peptides derived from the major constituents of the basement membrane, artificial membranes can be created with cues familiar to the cells (Figure 8C). Therefore, not only are the morphology and pore size similar to the native basement membrane, but also the biochemical specificity.

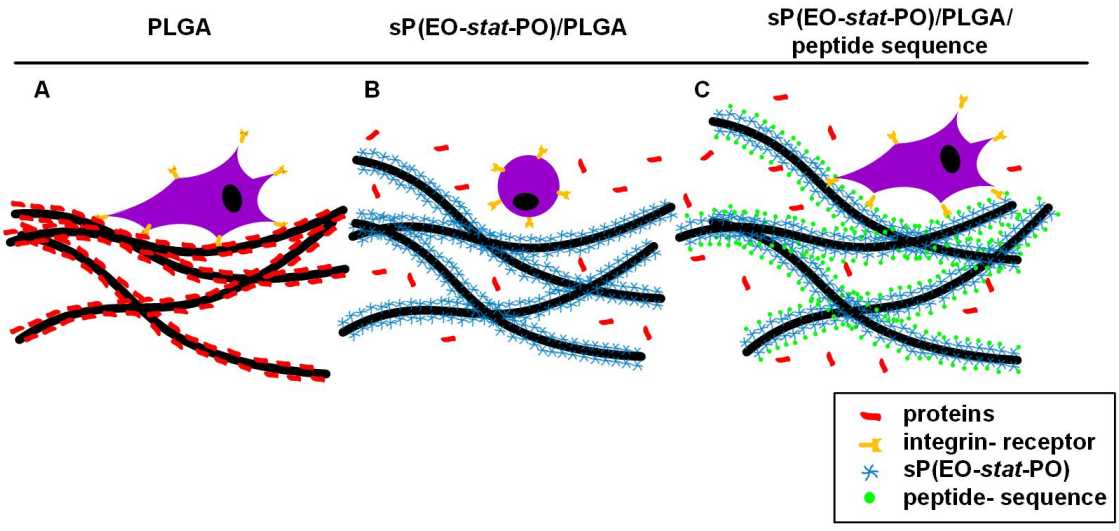

Figure 8: Specific biofunctionalization of PLGA fibers.
(A) Unmodified PLGA fibers lead to protein adsorption and unspecific cell adhesion. (B) Modification with sP(EO-*stat*-PO) suppresses protein adsorption. (C) By adding peptide sequences, cells selectively adhere to the fibers.

Aim of this study was to exploit the spinning technology and develop biomimetic, fully synthetic meshes that reflect the bioactivity of the natural basement membrane. Therefore, PLGA polymers, modified in a one-step preparation with NCO-sP(EO-*stat*-PO) and biologically active peptide binding sequences from fibronectin (CGRGDS), laminin (CGYIGSR, CGIKVAV), and collagen type IV (CGEFYFDLRLKGDK) were electrospun. As biological proof-of-concept model system, the human skin and oral mucosa were used as basement membrane containing tissue.

Chapter 4.1 focuses on the characterization and optimization of the electrospun membranes towards the development of tissue-specific synthetic basement membranes. Therefore, the influence of different peptide sequences on fiber morphology and integrity is studied. Different techniques to increase the pore size are explored, as well as degradation studies are performed. Moreover, sterilization techniques for electrospun fibers are investigated. To culture the functionalized membranes also under dynamic conditions, meshes with increased mechanical stability and reduced degradation rates are evaluated.

Chapter 4.2 addresses the quantification of immobilized peptide sequences on the surface of the functionalized membranes. For the function of the electrospun matrix, it is pivotal to determine the surface ligand densities.

In Chapter 4.3 biological interactions of the functionalized membranes in mono-culture are investigated. Protein adsorption studies are performed and the influence of covalently bound basement membrane derived peptides is studied on cell adhesion and proliferation of HaCaT cells and human dermal fibroblasts.

Chapter 4.4 and Chapter 4.5 focus on the development of skin tissue, based on the artificial basement membranes. Therefore, biodegradable electrospun polyester meshes exhibiting isotropic and bipolar bioactivation are prepared, co-cultured with HaCaT cells, primary human keratinocytes, and primary human fibroblasts and new tissue formation and extracellular matrix remodeling are investigated

In the last part of the thesis, in Chapter 4.6 oral mucosa models are developed based on the functionalized electrospun membranes and on polycarbonate membranes.

2 Materials

Biological materials, equipment, disposable and laboratory material, chemicals, buffers and solutions, as well as antibodies, peptides, and software used for this study are listed in the following tables.

2.1 Cell sources

A keratinocyte cell line (HaCaT cells), as well as primary keratinocytes and fibroblasts derived from human skin and from human oral mucosa, were used for the experiments. Cell culture supernatants were regularly checked for mycoplasma contamination, because they are known to alter cellular behavior.

2.1.1 Cell line

The aneuploid immortal keratinocyte line from adult human skin (HaCaT) was kindly provided by the DKFZ in Heidelberg (DSMZ No. ACC 771).

2.1.2 Primary skin cells

Human juvenile foreskin biopsies and skin biopsies were obtained with approval of the local ethics committee (local ethics committee approval 182/10, April 4th 2011) from clinically healthy donors undergoing routine surgical exposures in local hospitals.

2.1.3 Primary oral mucosa cells

Biopsies from the buccal and gingival mucosa were kindly made available with approval of the local ethics committee (local ethics committee approval 182/10, April 4th 2011) by the Dental Clinics of the University Hospital Würzburg.

2.2 Equipment

Table 3: List of equipment

Equipment/device	Producer
Accu-jet® pro pipettor	Brand, Wertheim (GER)
Analytical balance	Kern, Balingen-Frommern (GER) Sartorius, Göttingen (GER)
Aspiration device	Integra Biosciences, Fernwald (GER)
Autoclaves: Tecnoclav Table-top autoclave Varioclav	 Biomedis, Giessen (GER) Systec, Wettenberg (GER) H+P, Hackermoos (GER)
Bioreactor	Weckert Labortechnik, Kitzingen (GER)
Blocking station: EG1150H	Leica, Wetzlar (GER)
Cassette printer: VCP5001	Vogel Medizintechnik, Gießen (GER)
Cell incubator Haraeus: BBD6220 37 °C, 5 % CO_2	Thermo Fisher Scientific, Dreieich (GER)
Centrifuges: Multifuge X3R Centrifuge 5417R Centrifuge 5424	 Thermo Fisher Scientific, Dreieich (GER) Eppendorf, Hamburg (GER) Eppendorf, Hamburg (GER)
Cold-storage room, 4 °C	Genheimer, Höchberg (GER)
Cryostat: CM 1850 UV	Leica, Wezlar (GER)
Digital camera	Canon, Krefeld (GER)
Digital hand counter	NeoLab, Heidelberg (GER)
Dish washer	Miele, Gütersloh (GER)
Drying oven	Memmert, Schwabach (GER)
DSC differential thermal analysis: DSC 204 F1	Netzsch, Selb (GER)
Electrospinning apparatus	Department of Functional Materials, Würzburg (GER)
Embedding station: Microm STP120	Thermo Fisher Scientific, Dreieich (GER)
Freezer: -80 °C -20 °C	 Kendro, München (GER) Liebherr, Biberach a.d. Riss (GER)
Freezing container “Mr. Frosty”	VWR, Darmstadt (GER)
Fume hood	Prutscher Laboratory Systems, Neudörfl (AUT)

Equipment/device	Producer
High voltage generator: PS-2403D, Voltcraft PPS-11815, Voltcraft Harvard apparatus 11 Plus	Conrad, Hirschau (GER)
Hot air sterilizer	Memmert, Schwabach (GER)
Ice machine: AF-80	Scotsman, Milan (I)
Imaging station: FluorChem Q	Biozym Scientific GmbH, Hessisch Oldendorf (GER)
Immersion thermostat for water bath	Lauda, Lauda-Königshofen (GER)
Laminar air flow cabinet: Safe 2020	Thermo Fisher Scientific, Dreieich (GER)
Liquid nitrogen storage tank: MVE 815 P-190	German-cryo, Jüchen (GER)
Magnetic stirrer: 720-HPS	VWR, Darmstadt (GER)
Micro-plate reader: Tecan Infinite M200	Tecan, Crailsheim (GER)
Microscopes: Axiovert 40C Biorevo BZ-9000 Evos AMG Scanning electron microscope Zeiss DSM 940A	 Zeiss, Oberkochen (GER) KEYENCE, Neu-Isenburg (GER) Life technologies, Darmstadt (GER) Zeiss, Oberkochen (GER)
Multi-Channel Pipette Plus	Eppendorf, Hamburg (GER)
Multistep pipette: Multipipette M4	Brand, Wertheim (GER)
Neubauer cell counting chamber	Hartenstein, Würzburg (GER)
Orbital shaker	NeoLab, Heidelberg (GER)
Paraffinized tissue floating bath 1052	Medax, Kiel (GER)
pH meter	Mettler Toledo, Giessen (GER)
Pipette tamping machine	BellCo Glass Dunn, Asbach (GER)
Pipettes: 0.5–10 µl, 10–100 µl, 100–1000 µl	Eppendorf, Hamburg (GER)
Power supplies: EV202, EV243	PeqLab Biotechnology, Erlangen (GER)
Rocking platform shaker	NeoLab, Heidelberg (GER)
Roller mixer	Hartenstein, Würzburg (GER)
Safety cabinet: Safe 2020	Thermo Fisher Scientific, Dreieich (GER)
Slide printer: VSP 5001	Vogel Medizintechnik, Gießen (GER)
Sliding microtome: SM 2010R	Leica, Wetzlar (GER)

Equipment/device	Producer
Sputter coater gold: Emitek K550	Quorum Technologies, East Sussex (GB)
Steamer "Multi Gourmet"	Braun, Kronberg (GER)
Syringe pump Aladdin	World precision instruments, Sarasota, FL (USA)
TEER electrode millicell epithelial volt-ohmmeter	World precision instruments, Sarasota, FL (USA)
Thermomixer comfort	Eppendorf, Hamburg (GER)
Vortex Genie 2	Scientific Industries, INc., NY (USA)
Water bath	Memmert, Schwabach (GER)
Water purification system	Millipore, Schwalbach (GER)

2.3 Disposable material

Table 4: List of disposable material

Disposable Material	Producer
Aluminum foil	Carl Roth GmBH, Karlsruhe (GER)
Biopsy punch 8 mm	Kai medical, Solingen (GER)
Brandplates® insert system: 0.4 µm, 4.0 µm, 8.0 µm	Brand, Wertheim (GER)
Cannula	Baun, Melsungen (GER)
Cell culture flasks: 25 cm^2, 75 cm^2, 150 cm^2	TPP, Trasadingen (CH)
Cell culture plates: 6 well, 12 well, 24 well, 96 well	TPP, Trasadingen (CH)
Cell strainer: 100 µm	Greiner Bio-One, Frickenhausen (GER)
Centrifuge tubes: 15 ml, 50 ml	Greiner Bio-One, Frickenhausen (GER)
Chamber slides: 8 well, glass	Nunc, Wiesbaden (GER)
Combitips Plus: 0.5 ml, 1.0 ml, 2.5 ml, 5.0 ml	Eppendorf, Hamburg (GER)
Cover slips for object slides: 24 x 60 mm	Menzel-Glaser, Braunschweig (GER)
Cryo tubes: 1.8 ml	Nunc, Wiesbaden (GER)
Disposable pipettes: 5 ml, 10 ml, 25 ml, 50 ml	Greiner Bio-One, Frickenhausen (GER)
Disposal bags	Hartenstein, Würzburg (GER)

Disposable Material	Producer
Embedding cassettes	Klinipath, Duiven (NET)
Embedding filter paper	Labonord, Mönchenglattbach (GER)
Glass vials	Hartenstein, Würzburg (GER)
Gloves: Latex Nitrile	 Cardinal Health, Kleve (GER) Kimberly-Clark, Koblenz (GER)
Microtome disposable blades A35	pfm Medical, Köln (GER)
Object slides: uncoated Polysine® Superfrost®	 Menzel, Braunschweig (GER) Thermo Fisher Scientific, Dreieich (GER) Langenbrinck, Emmendingen (GER)
Parafilm®	Carl Roth, Karlsruhe (GER)
Pasteur pipettes	Brand, Wertheim (GER)
Petri dishes: 145 x 20mm	Greiner Bio-One, Frickenhausen (GER)
Pipette tips: 0.5–10 µl, 10–100 µl, 100–1000 µl	 Eppendorf, Hamburg (GER)
Reaction tubes: 1.5 ml, 2.0 ml	Sarstedt, Numbrecht (GER)
Scalpel blades, rounded	Bayha, Tuttlingen (GER)
Sterile filter: 0.2 µm	Sartorius Stedium Biotech, Göttingen (GER)
Syringes: 1 ml, 2 ml, 5 ml, 10 ml, 20 ml	BD Biosciences, Heidelberg (GER)
Weighing dish	Hartenstein, Würzburg (GER)
Whatman filter paper	Hartenstein, Würzburg (GER)

2.4 Laboratory material

Table 5: List of laboratory material

Laboratory Material	Producer
Beakers: 250 ml, 1 L	Schott, Mainz (GER)
Cell crowns: Metal Plastic	 TERM Würzburg (GER) Minucells, Bad Abbach (GER)
Centrifuge tube racks	neoLab, Heidelberg (GER)
Cold protection gloves	VWR, Darmstadt (GER)

Laboratory Material	Producer
Funnel	Hartenstein, Würzburg (GER)
Glass cuvette with lid: 110 x 90 x 80 mm	Mercateo, Munich (GER)
Glass pipettes: 5 ml, 10 ml, 25 ml	Brand, Wertheim (GER)
Grease pencil	Dako, Hamburg (GER)
Humidity chamber	TERM, Würzburg (GER)
Laboratory bottles: 50 ml, 100 ml, 250 ml, 1 L	Schott, Mainz (GER)
Magnetic stirring bar	Hartenstein, Würzburg (GER)
Magnetic stirring bar retriever	Hartenstein, Würzburg (GER)
Object slide racks: glass, stainless steel	Mercateo, Munich (GER)
Protective goggles	NeoLab, Heidelberg (GER)
Reaction tube rack	NeoLab, Heidelberg (GER)
Scalpel	Bayha, Tuttlingen (GER)
Screws, stainless steel, A2-70	Viray, Maharashtra (IND)
Spatula	VWR, Darmstadt (GER)
Spoon spatula	Hartenstein, Würzburg (GER)
Spray flask (Ethanol 70 % (v/v), Descosept)	Hartenstein, Würzburg (GER)
Stainless steel casting moulds for embedding tissue	Labonord, Mönchengladbach (GER)
Sterile filter	Hartenstein, Würzburg (GER)
Tweezers	Assistent, Sondheim (GER)
Volumetric flasks with plug: 1 L, 2 L	Schott, Mainz (GER)

2.5 Chemicals and solutions

Table 6: List of chemicals and solutions

Chemical/solution	Producer	Catalog No
3-(4,5-Dimethylthiazol-2-yl)-2,5 diphenyltetrazoliumbromide (MTT)	Serva, Heidelberg (GER)	20395
Accutase	Life technologies, Darmstadt (GER)	A1110501

Chemical/solution	Producer	Catalog No
Acetic acid	Sigma-Aldrich, Munich (GER)	A6283
Acetone (≥ 99.5 % (v/v))	Sigma-Aldrich, Munich (GER)	48358
Acetone Chromasolv	Sigma-Aldrich, Munich (GER)	34850
Albumine fraction V (BSA)	Sigma-Aldrich, Munich (GER)	85040C
Albumine from bovine serum, tetramethylrhodamine conjugate	Life technologies, Darmstadt (GER)	A23016
Antibody diluent	DCS Innovative Diagnostik-Systeme, Hamburg (GER)	AL120R500
Benzyltriethylammonium chloride	Sigma-Aldrich, Munich (GER)	146552
Bouin`s solution	Sigma-Aldrich, Munich (GER)	HT101128
Calcium chloride dihydrate ($CaCl_2$*2 H_2O)	Sigma-Aldrich, Munich (GER)	C3306
5(6)-Carboxyfluorescein	Sigma-Aldrich, Munich (GER)	21877
Chondroitin-6-sulfat shark cartilage	Sigma-Aldrich, Munich (GER)	27043
Citric acid	Sigma-Aldrich, Munich (GER)	251275
4',6-Diamidino-2-phenylindole dihydrochloride (DAPI)	Sigma-Aldrich, Munich (GER)	D9542
Collagenase	Serva, Heidelberg (GER)	17454
Descosept	Dr. Schumacher, Malsfeld (GER)	00311-100
Dimethyl sulfoxide (DMSO)	Sigma-Aldrich, Munich (GER)	472301
Dispase II powder	Life technologies, Darmstadt (GER)	17105-041
Donkey serum	Sigma-Aldrich, Munich (GER)	D9663
Dulbecco's Modified Eagle Medium (DMEM)	Life technologies, Darmstadt (GER)	61965-026
Eosin B	Sigma-Aldrich, Munich (GER)	861006
Epilife	Life technologies, Darmstadt (GER)	M-EPI-500-CA
Ethanol, absolute	Sigma-Aldrich, Munich (GER)	24102
Ethanol, denatured (96 % (v/v))	Carl Roth, Karlsruhe (GER)	T171.2
Ethylenediaminetetraacetic acid (EDTA-Na_2*2 H_2O)	Sigma-Aldrich, Munich (GER)	E5134
Experion electrode cleaner	BioRad, Munich (GER)	700-7251
Fetal Calf Serum (FCS)	Bio&SELL, Feucht (GER)	FCS.ADD.0500

Chemical/solution	Producer	Catalog No
Fibronectin	Life technologies, Darmstadt (GER)	33016-015
Fluorescein Diacetate (FDA)	Sigma-Aldrich, Munich (GER)	F-7378
Fluorescein isothiocyanate–dextran (FITC-dextran)	Sigma-Aldrich, Munich (GER)	46944
Gentamycin (50 mg/ml)	Sigma-Aldrich, Munich (GER)	G1397-
H_2O_2, 30 %	Sigma-Aldrich, Munich (GER)	216763
Haematoxylin	Sigma-Aldrich, Munich (GER)	9627
HEPES	Sigma-Aldrich, Munich (GER)	H4034
Human keratinocyte growth supplement (HKGS), (100 x concentrated)	Life technologies, Darmstadt (GER)	S-001-5
Hydrochloric acid (HCl; 37 %)	Sigma-Aldrich, Munich (GER)	258148
Isopropyl alcohol	Sigma-Aldrich, Munich (GER)	278475
Keratinocyte basal medium (KBMr)	PromoCell, Heidelberg (GER)	C-20211
Keratinocyte growth factor (KGF)	Sigma-Aldrich, Munich (GER)	K1757
L-ascorbyl-2-phosphate	Sigma-Aldrich, Munich (GER)	A8960
Magnesium Chloride hexahydrate ($MgCl_2$ *6 H_2O)	Sigma-Aldrich, Munich (GER)	M9272
2-Mercaptopyridine	Sigma-Aldrich, Munich (GER)	M5852
Mounting Medium: Entellan Mowiol 488	 Merck, Darmstadt (GER) Carl Roth, Karlsruhe (GER)	 107961 0713
Paraffin	Carl Roth, Karlsruhe (GER)	6642
Paraformaldehyde (PFA)	AppliChem, Darmstadt (GER)	A3813
Penicillin/Streptomycin (100 x concentrated)	Sigma-Aldrich, Munich (GER)	P4333
Phosphate Buffered Saline (PBS) Tablets	Invitrogen, Darmstadt (GER)	18912-014
Phosphate-buffered saline with calcium and magnesium (PBS^+)	Sigma-Aldrich, Munich (GER)	D8662
Phosphate-buffered saline without calcium and magnesium (PBS^-)	Sigma-Aldrich, Munich (GER)	D8537
PLGA 50/50 (RG 504)	Sigma-Aldrich, Munich (GER)	739944
PLGA 85/15 (RG 858 S)	Sigma-Aldrich, Munich (GER)	739979
Propidiumiodid (PI)	Sigma-Aldrich, Munich (GER)	P4170

Chemical/solution	Producer	Catalog No
Rat-tail collagen type I, 10 mg/ml	TERM, Würzburg (GER)	
Roti®-Histofix 4 %	Carl Roth, Karlsruhe (GER)	P087
Sodium chloride	Sigma-Aldrich, Munich (GER)	S7653
Sodium hydroxide pellets	Sigma-Aldrich, Munich (GER)	S8045
Tissue-Tek OCTTM compound	Sakura, Leiden (NL)	4583
Trifluoroacetic acid (TFA)	Sigma-Aldrich, Munich (GER)	302031
Tris	Carl Roth, Karlsruhe (GER)	4855.1
Triton-X 100	Carl Roth, Karlsruhe (GER)	3051
Trypan blue, 0.4 %	Sigma-Aldrich, Munich (GER)	T8154
Trypsin-EDTA stock solution (10 x)	Life technologies, Darmstadt (GER)	15400-054
Tween®-20	Sigma-Aldrich, Munich (GER)	P2287
Weigert's haematoxylin, stock solution A	Morphisto, Frankfurt (GER)	10225A.02500
Weigert's haematoxylin, stock solution B	Morphisto, Frankfurt (GER)	10225B.02500
Versene	Life technologies, Darmstadt (GER)	15040-066
Xylene	Sigma-Aldrich, Munich (GER)	16446

2.6 General buffers and working solutions

Table 7: List of general buffers and working solutions

Buffer/Solution	Composition	
BSA tetramethylrhodamine solution	50 µg/ml	BSA tetramethylrhodamine in PBS^{+} Stored at -20 °C under exclusion of light
Carboxyfluorescein solution	0.25 mg/ml	Carboxyfluorescein in E1 medium Prepared immediately before use Sterile filtered
FITC-dextran solution	0.25 mg/ml	FITC-dextran in E1 medium Prepared immediately before use Sterile filtered

Buffer/Solution	Composition	
1 M Tris-HCl	121.14 g ad 1000 ml	Tris demineralized water pH was adjusted as needed (between 7.4 and 8)
1 x TCEP solution	98 mg ad 11.15 ml	TCEP 0.1 N NaOH
2 x TCEP solution	196 mg ad 11.15 ml	TCEP 0.2 N NaOH

2.7 Buffers and solutions for cell culture

Table 8: List of buffers and solutions for cell culture

Medium/Solution	Composition	
0.05 % Trypsin/EDTA working solution	10 % (v/v)	Trypsin/EDTA stock solution in PBS^-/EDTA solution
Ascorbyl-2-phosphate solution	73 mg/l	Ascorbyl-2-phosphate in E1 medium sterile-filtered before use stored at -20 °C
$CaCl_2$-solution (300 mM)	22.1 g 500 ml	$CaCl_2$ Ultrapure water sterile-filtered before use stored at 4 °C
Collagenase (500 U/ml)	1.0 g 436 ml	Collagenase DMEM sterile-filtered before use stored at -20 °C
Chondroitin-6-sulfate solution	25 mg 5 ml	Chondroitin-6-sulfate PBS^+ sterile-filtered before use stored at 4 °C
DAPI staining solution	0.1 µg/ml	DAPI in PBS^- prepared immediately before use
Dispase (2 U/ml)	400 mg 100 ml	Dispase PBS^- sterile-filtered before use stored at -20 °C
2 x DMEM	6.65 g 1.85 g 250 ml	DMEM powder $NaHCO_3$ Ultrapure water

Medium/Solution	Composition	
Fluorescein diacetate (FDA) solution	5 mg/ml	FDA in acetone stored at -20 °C
Fibronectin stock solution	0.5 mg/ml	Fibronectin lyophilisate in ultrapure water sterile-filtered
Fibronectin working solution (50 µg/ml)	10 % (v/v)	Fibronectin stock solution in PBS^+
Gel neutralization solution (GNL)	7.5 ml 2.5 ml 7.5 ml 232.5 ml	3 M HEPES Chondroitin-6-sulfat-solution FCS 2 x DMEM sterile-filtered stored at 4 °C
3M HEPES solution	7.15 g 10 ml	HEPES PBS^-, sterile-filtered
KGF solution	10 µg/ml	KGF in EpiLife
MTT reagent	3 mg/ml	MTT in PBS^+ sterile-filtered Stored at -20 °C
MTT solution	1 mg/ml	MTT reagent in PBS^+ Prepared immediately before use
PBS^-/EDTA solution	0.5 ml 500 ml	EDTA PBS^-
Propidiumiodid (PI) solution	2 mg/ml 1 ml	PI in PBS^+ Stored at -20 °C
PI/FDA solution	1 µl 9 µl 990 µl	FDA solution PI solution PBS^+

2.8 Media for cell culture

Table 9: List of media for cell culture

Medium/Solution	Composition	
E1 medium	500 ml 5,0 ml 1 % (v/v)	Epilife® Medium HKGS Pen/Strep

Medium/Solution	Composition	
E2 medium	500 ml	Epilife® Medium
	5.0 ml	HKGS
	2.4 ml	0.3 M $CaCl_2$
	1 % (v/v)	Pen/Strep
ALI medium	500 ml	Epilife® Medium
	5.0 ml	HKGS
	2.4 ml	0.3 M $CaCl_2$
	500 µl	L-ascorbic acid 2-phosphate
	500 µl	KGF
	1 % (v/v)	Pen/Strep
Fibroblast/HaCaT culture medium	500 ml	DMEM
	10 % (v/v)	FCS
	1 % (v/v)	Pen/Strep
HaCaT airlift medium	500 ml	DMEM
	10 % (v/v)	FCS
	1 % (v/v)	Pen/Strep
	2.4 ml	0.3 M $CaCl_2$
	500 µl	L-ascorbic acid 2-phosphate

2.9 Chemicals and solutions for histology and immunohistochemistry

Table 10: List of chemicals/solutions for histology and immunohistochemistry

Chemical/Solution	Composition	
Antibody diluent	5 % (w/v)	BSA in PBS^- sterile-filtered before use stored at 4 °C
Blocking solution	0.5 % (v/v)	BSA in PBS^- sterile-filtered before use stored at 4 °C
Citrate buffer solution (10 x stock solution)	42.0 g 17.6 g ad 1000 ml	Citric acid NaOH pellets demineralized water pH 6.0 stored at RT
Citrate buffer working solution	10 % (v/v)	Citrate buffer stock solution in demineralized water stored at RT
Eosin	10 mg/ml	Eosin in demineralized water stored at RT

Chemical/Solution	Composition	
H_2O_2 3 %	10 % (v/v)	H_2O_2 30 % in demineralized water Prepared immediately before use
Haemalaun	1.2 g 0.2 g 20 g 20 g 1 g ad 1000 ml	Haematoxylin Sodium iodate Potassium alum Chloral hydrate Citric acid in demineralized water used after 4 weeks of maturation stored at RT
HCl /EtOH	6.85 % (v/v)	HCl, 1M in Ethanol (50 % v/v)
PFA 4 %	40 g/L	Paraformaldehyde in PBS- solution (solved at 60 °C) pH 7.4
Washing buffer (PBS-T) 0.05 M	10 % (v/v) 0.5 % (v/v)	PBS stock 0.5 M Tween®-20 in demineralized water stored at RT
Triton-X Permeabilizing Solution	0.2 % (v/v)	Triton-X 100 in PBS-T (0.05 M) stored at RT
Weigert's haematoxylin	50 % (v/v) 50 % (v/v)	Stock solution A Stock solution B stored at RT

2.10 Kits for immunohistochemistry

Table 11: List of kits for immunohistochemistry

Kit	Description	Producer
Super Vision 2 HRP-Polymer-Kit	Kit containing secondary mouse- and rabbit-antibody, a polymer conjugated with HRP against secondary antibody, DAB concentrate, DAB substrate buffer	DCS Innovative Diagnostik-Systeme, Hamburg (GER) Cat. No PD000KIT
Live/Dead staining kit	Calcein AM and Ethidium homodimer-1	Life Technologies, Darmstadt (GER) Cat. No L3224

Kit	Description	Producer
CellTiter-Fluor™ Cell Viability Assay	Kit for the determination of cell viability	Promega, Mannheim (GER) Cat. No G6080

2.11 Antibodies for immunohistochemistry

Table 12: List of antibodies

Antibody	Concentration	Host	Producer	Catalog No
Cytokeratin 10	1:2000	mouse	Dako Cytomation, Hamburg (GER)	M7002
Cytokeratin 14	1:50	mouse	Santa Cruz Biotechnology, Heidelberg (GER)	sc-53253
Fibronectin	1:100	rabbit	Abcam, Cambridge (UK)	ab23750
Filaggrin	1:2000	rabbit	Abcam, Cambridge (UK)	ab81468
Ki 67	1:100	rabbit	Abcam, Cambridge (UK)	ab16667
Laminin I	1:250	rabbit	Acris Antibodies, Herford (GER)	BP8037
Laminin V	1:2000	rabbit	Sigma-Aldrich, Heidelberg (GER)	HPA008069
Vimentin	1:1000	mouse	Abcam, Cambridge (UK)	ab8069
Collagen I	1:2000	rabbit	Acris Antibodies, Herford (GER)	BP8028
Collagen III	1:200	rabbit	Sigma-Aldrich, Heidelberg (GER)	HPA007583
Collagen IV	1:2000	rabbit	Abcam, Cambridge (UK)	ab6586

2.12 Peptide sequences for electrospinning

Table 13: List of peptide sequences

Peptide Sequence	Producer
CGRGDS	JPT Peptide Technologies GmbH, Berlin (GER)

Peptide Sequence	Producer
CGYIGSR	JPT Peptide Technologies GmbH, Berlin (GER)
CGIKVAV	JPT Peptide Technologies GmbH, Berlin (GER)
CGEFYFDLRLKGDK	JPT Peptide Technologies GmbH, Berlin (GER)
SGRGDS-Cys(2-Thiopyridin)-OH	JPT Peptide Technologies GmbH, Berlin (GER)

2.13 Software

Table 14: List of software

Software	Manufacturer
ImageJ	NIH (USA)
Keyence BZ-II Viewer Keyence BZ-II Analyzer	KEYENCE Deutschland GmbH, Neu-Isenburg (GER)
Office Excel 2013 Office PowerPoint 2013 Office Visio 2013 Office Word 2013	Microsoft Deutschland GmbH, Unterschleißheim (GER)
Endnote X7	Thomson Reuters, Philadelphia, PA (USA)
Graphpad Prism 5	GraphPad Software, La Jolla, CA (USA)
Tecan-i-control™ 1.7	Tecan, Crailsheim (GER)

3 Methods

The Department for Tissue Engineering and Regenerative Medicine works in the research and development segment with a Standard Operating Procedure (SOP) system (see Appendix). The standardized methods for the isolation of skin cells, standard cell culture methods, and the construction of skin models based on polycarbonate membranes and collagen I hydrogels were conducted according to these guidelines. Methods for the isolation of oral mucosa cells, the development of oral mucosa models, and the construction of 3D models based on electrospun membranes were newly developed and are described in more detail in the methods section.

3.1 Preparation of membranes for tissue models

The membranes for the tissue models were based on collagen type I hydrogels, functionalized electrospun PLGA membranes, and polycarbonate membranes (Table 15).

Table 15: List of membranes for tissue models

3D biomaterial	Species	Description
Collagen I hydrogel	rat	Collagen type I with GNL
Polycarbonate (PC) insert	synthetic	Purchased PC membrane
PLGA membrane	synthetic	Functionalized electrospun PLGA fibers

3.1.1 Collagen type I hydrogel

After incubating the rat tails for 2 minutes in 70 % (v/v) EtOH to avoid contamination, the skin of the tails was peeled off, tendons were excerpted and washed 3 times with PBS^- and twice with 70 % (v/v) EtOH for disinfection, followed by 3 washing steps with PBS^- to remove the remaining EtOH. Tendons were weighted and incubated in 0.1 % (v/v) acetic acid in a spinner flask under constant agitation at 4 °C for 2 to 3 weeks. During this time, remaining tendon rests should

be dissolved. The collagen solution was centrifuged at 1750 x g for 1 hour at 4 °C and afterward, stirred on a magnet stirrer for 20 minutes. Having determined the collagen content, the solution was diluted to a concentration of 10 mg/ml collagen I with 0.1 % (v/v) acetic acid. The SOP "Collagen type I isolation from rate tail" is attached in 7.1.

3.1.2 Solution for electrospinning

The fibronectin (CGRGDS), laminin (CGYIGSR, CGIKVAV) and collagen type IV (CGEFYFDLRLKGDK) derived binding sequences were dissolved in 10 µl diluted trifluoroacetic acid (TFA) (20 µl/ml H_2O). After adding 50 µl dry dimethylsulfoxide (DMSO) and 30 mg sP(EO-*stat*-PO), the solution was stirred for 10 minutes. 450 µl dry acetone and 143 mg PLGA 50/50 were added, the dispersion mixed and immediately used for electrospinning. sP(EO-*stat*-PO)/PLGA fibers without peptide sequences served as control membranes. For this, 30 mg sP(EO-*stat*-PO) were dissolved in 10 µl TFA (20 µl/ml H_2O) and 50 µl DMSO and stirred for 10 minutes. 450 µl acetone and 143 mg PLGA 50/50 were added, dissolved and used for electrospinning. PLGA membranes were prepared by simply mixing 50 µl DMSO with 450 µl acetone and 143 mg PLGA 50/50.

3.1.3 Electrospinning of PLGA membranes

The solution was electrospun at a feed rate of 0.5 ml/hour through a flat-tip stainless steel spinneret (Ø = 0.4 x 25 mm) assisted by a programmable syringe pump. A high voltage generator was utilized to charge the solution to 13 kV. Fibrous mats were collected at a distance of 16 cm on a grounded rotating drum. Spinning duration was 45 minutes. Membranes with a thickness of approximately 20 µm were produced.

3.2 Cell culture methods

All cell culture experiments were performed under sterile conditions using a class II laminar airflow safety cabinet. Before and after use, the surface of the laminar airflow was thoroughly cleaned with Descosept®. All disposable materials,

laboratory material, as well as all solutions were sterile, sterilized by autoclaving or by sterile-filtering. Gloves reduced the risk of contamination. Cells were cultured in cell culture flasks in a humidified atmosphere at 37° C and 5 % CO_2 unless mentioned otherwise. Cells were observed daily to monitor cell growth, cell density and characteristic cell morphology. Cell culture supernatants were checked regularly for mycoplasma contamination. The corresponding SOP "Sterile working station" is attached in 7.1.

3.2.1 Isolation of primary cells from human skin biopsies

Biopsies should be processed as early as possible, ideally on the same day after removal, owing to a gradual loss of yield. A sterile control from the transport medium was taken and incubated to investigate possible contaminations. To avoid contaminations of freshly isolated primary cells, the cell culture medium was supplemented with 100 U/ml penicillin and 0.1 mg/ml streptomycin.

Samples were placed with the epidermis side down in 10 cm bacterial petri dishes and rinsed 3 times with PBS^+. Subcutaneous fat and loose connective tissue were removed using a scalpel, scissors, and fine tweezers while the biopsy was kept moist with PBS^+. The biopsy had to be cut into strips of approximately 2-3 mm in width to ensure proper digestion. After placing the pieces in a 6 cm petri dish containing 7-8 ml 2 U/ml dispase, the dish was wrapped with parafilm® and incubated at 4 °C for 16-18 hours. The next day, 2 petri dishes with PBS^+ were prepared: one for the dermis and one for the epidermis. Following aspiration of the dispase solution, 10 ml of PBS^+ was added. The epidermis was slowly peeled off with tweezers from the dermis. The dermal part was stored in the petri dish until the isolation of the fibroblasts.

3.2.1.1 Isolation of skin keratinocytes

The epidermis was placed in a petri dish and washed first with PBS^+, afterward with PBS^- to remove residues of enzymes. The epidermal part was cut into small pieces of 1 mm^2 and placed in a 50 ml centrifuge tube together with 5 ml 37 °C pre-warmed 0.05 % trypsin/EDTA. The petri dish was washed with another 5 ml pre-warmed trypsin solution. The trypsin solution was added to the pieces of epidermis in the

centrifuge tube and the tube was placed for 6 minutes in a water bath at 37 °C under gentle blending. After adding 1 ml FCS to the tube, the cell suspension was vigorously pipetted up and down for 5 minutes to detach the cells from their cell bonds. The suspension was passed through a cell strainer with a pore size of 100 µm to remove undigested pieces of tissue into a new centrifuge tube. To avoid loss of cells, the filter and the tube were washed twice with 5 ml PBS^+ followed by a centrifugation step at 270 x g for 5 minutes. The supernatant was removed and the pellet re-suspended in 5 ml E1 medium. Cells were seeded at a density of 5 x 10^3 cells/cm^2. To remove dead cells and cell fragments, the media was changed the following day. The corresponding SOP "Isolation dermal keratinocytes" is attached in 7.1.

3.2.1.2 Isolation of skin fibroblasts

After removing the epidermis, the dermis was cut into 0.5-1.0 mm^2 pieces and incubated in a centrifuge tube at 37 °C for 45 minutes with 5 ml of collagenase A solution (500 U/ml). The suspension was centrifuged at 270 x g for 5 minutes, the collagenase aspirated, and the dermal pieces washed 3 times with 10 ml fibroblast medium followed by a subsequent centrifugation step to remove collagenase residues. The dermal parts were placed in a T75 flask with 3-4 ml fibroblast medium. To ensure sufficient medium supply, 2 ml of medium was added the next day. It is important that tissue pieces rest on the surface of the culture flask to enable outgrowth of the human dermal fibroblasts. The corresponding SOP "Isolation dermal fibroblasts" is attached in 7.1.

3.2.2 Isolation of primary cells from human oral mucosa biopsies

As described for the isolation of cell from human skin samples, human oral mucosa biopsies should be processed as early as possible, ideally the same day after removal owing to a gradual loss of yield. A sterile control from the transport medium was taken and incubated overnight to investigate possible contaminations. Human oral mucosa keratinocytes were isolated from buccal and gingival biopsies in cell type-specific medium. To avoid contaminations of freshly isolated primary cells, the

cell culture medium was supplemented with 100 U/ml penicillin and 0.1 mg/ml streptomycin.

3.2.2.1 Isolation of oral mucosa keratinocytes

The cells were isolated as described for human skin biopsies with some modifications. In most cases, it was not necessary to remove subcutaneous fat and loose connective tissue since the oral mucosa biopsies are much smaller and do not contain a lot of connective tissue after surgery. Moreover, it was not necessary to cut the biopsy into strips before dispase digestion to isolate the keratinocytes since the biopsies were very small. To avoid a loss of cells, the cell suspension was not filtered with a cell strainer after detachment. Oral mucosa keratinocytes were seeded at a density of 5 x 10^3 cells/cm^2. To remove dead cells and cell fragment, media was changed as soon as the cells attached.

3.2.2.2 Isolation of oral mucosa fibroblasts

After removal of the epidermis, the dermis was cut into 0.5-1.0 mm^2 pieces and placed in T25 flasks with 2 ml fibroblast culture medium until pieces attached. The next day, 2 ml medium was added. After 1 week, the cells grew to confluence and were passaged.

3.2.3 Culture conditions of cells

HaCaT cells were cultured in fibroblast culture medium in T150 flasks. They were seeded at a density of 3 x 10^3/cm^2 and reached cell numbers of 2-3 x 10^4 cells/cm^2 at a confluence of 80-90 %. The medium was changed every 2-3 days.

Primary human dermal and oral fibroblasts were cultured in fibroblast culture medium in T150 flasks. They were seeded at a density of 3 x 10^3 cells/cm^2 and reached cell numbers of 1-2 x 10^4/cm^2 at a confluence of 80-90 %. The medium was changed every 2-3 days.

Primary human dermal and oral keratinocytes were cultured in E1 medium, if not described differently herein. They were seeded at a density of 5 x 10^3 cells/cm^2. After 1 week they grew to 70-80 % confluence. The medium was changed every 2-3 days.

3.2.4 Passaging of cells

To passage cells, the medium was aspirated and the cells were washed with PBS^-/EDTA to remove dead cells, serum residues and divalent ions such as Mg^{2+} and Ca^{2+}, which are essential for cell adherence [195].

After rinsing, keratinocytes were treated with 0.06 ml accutase solution/cm^2 and incubated for 15-20 minutes at 37 °C and 5 % CO_2. Gentle tapping supported the dissolution of the cells. The detachment of the cells could be observed and controlled microscopically. The cell suspension was transferred into a 50 ml tube and the flask washed with PBS^-. After centrifuging the tube at 270 x g for 5 minutes, the supernatant was aspirated, the cells re-suspended in E1 medium, and the cell number determined.

Fibroblasts were incubated with 0.06 ml pre-heated 0.05 % trypsin/EDTA solution/cm^2 at 37 °C and 5 % CO_2 for 3-5 minutes followed by the addition of 1 ml FCS to stop the reaction. The detachment of the cells could be microscopically confirmed. The cells were transferred to a 50 ml centrifuge tube and the empty cell flasks rinsed with PBS^-/EDTA to detach single remaining cells. The solution was added to the same centrifuge tube followed by centrifugation at 270 x g for 5 minutes. The supernatant was aspirated, the cell pellet re-suspended in an appropriate amount of cell culture medium and the cell number determined. The corresponding SOP “Passaging of cells” is attached in 7.1.

3.2.5 Determination of cell number and viability

The Neubauer counting chamber and trypan blue staining served to determine cell vitality. Trypan blue penetrates damaged cell membranes resulting in a blue staining of dead cells [196]. Cells were detached and an aliquot of the cell suspension was mixed 1:2 with 0.4 % trypan blue solution. 10 µl of the mixture were applied to the Neubauer counting chamber. The number of viable cells and dead cells could be counted in all four big quadrants by light microscopy.

Cell number calculated as follows:

The absolute number of viable and dead cells was calculated by multiplication of its number with the volume of the cell suspension as follows:

$$Viable\ or\ dead\ cells/ml = mean\ cells/square \times 2 \times 10^4$$

The cell viability could be determined as a quotient of living cell number to total cell count.

$$cell\ viability\ [\%] = \frac{number\ of\ viable\ cells}{total\ number\ of\ cells} \times 100$$

The corresponding SOP "Cell number and viability" is attached in 7.1

3.2.6 Freezing and thawing of cells

To freeze cells, the cell number should be adjusted to 1 x 10^6 cells/ml in cell specific culture medium supplemented with 10 % (v/v) FCS and 10 % (v/v) DMSO. Primary keratinocytes were frozen without FCS. Because of the hypertonic environment and possible cell damage by DMSO at room temperature, 1 ml of the cell suspension was instantly added to each cryo-tube and the tube was immediately placed into a "Mr. Frosty" freezing container. The container was stored at -80 °C for at least 24 hours to ensure a slow freezing process of 1 °C per minute. For long-term storage, frozen cells had to be transferred to a liquid nitrogen tank at -180 °C.

To thaw cells, cryo-tubes were placed shortly in a water bath at 37 °C until a small piece of ice remained in the tube. The cell suspension was then immediately transferred to a 50 ml centrifuge tube containing 9 ml pre-warmed cell type-specific medium followed by a centrifugation step at 270 x g for 5 minutes. The supernatant was aspirated, the cell pellet re-suspended in a fresh pre-warmed cell type-specific medium and the cells seeded in a cell culture flask. After 24 hours, the medium was changed. Thawed cells were passaged at least once before being used for experiments. The corresponding SOP "Freezing and thawing of cells" is attached in 7.1.

3.2.7 Cell culture on chamber slides

For 8-well glass chamber slides, 2×10^4 cells were seeded in 400 µl of the corresponding medium per chamber. When cells reached a confluence of 50-70 %, they were fixed with 4 % paraformaldehyde (PFA) for 10 minutes and subsequently used for immunohistochemical staining. The corresponding SOP "Cells on chamber slides" is attached in 7.1.

3.2.8 Cell culture on cytospots

A glass slide was placed together with filter paper and a funnel on top into a cytocentrifuge. A cell suspension of 5.0×10^4 cells/ml in a cell type-specific medium was prepared with 50 µl of the cell suspension placed into each funnel, followed by a centrifugation step of 120 x g for 5 minutes to spin the cells on the glass slide. The object slides were dried at room temperature, then stored at -80 °C. Before immunohistochemical staining, cytospots were fixed for 10 minutes with 4 % PFA. The corresponding SOP "Cells on cytospots" is attached in 7.1.

3.2.9 Fixation of membranes for static cell culture

If not described otherwise, electrospun membranes were fixed in cell crowns for cell culture experiments. Each cell crown was composed of two plastic rings; a smaller inner ring and a larger outer ring to prevent the matrix from touching the cell culture plate. A piece of electrospun matrix was pulled over the inner ring of the cell crown (Figure 9A; B) and fixed with the outer ring (Figure 9C). The cell crown was turned around (Figure 9D) and the remaining ends were cut to provide equal culture areas (Figure 9E). The cell crowns were transferred to 24-well plates (Figure 9F) and seeded with cells in cell-type specific medium.

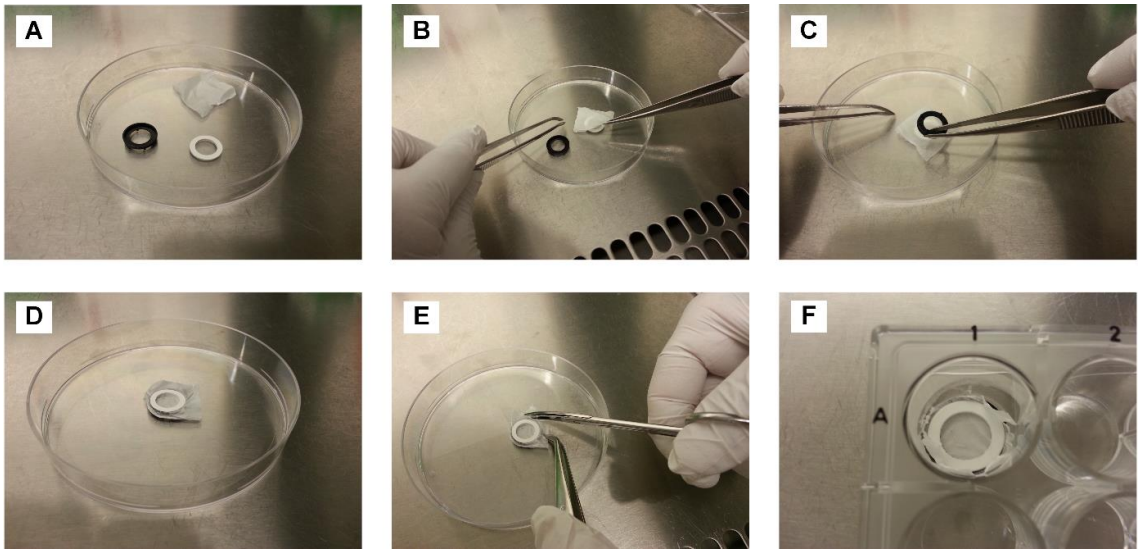

Figure 9: Fixation of functionalized membranes.
(A) The electrospun membrane is visible, as well as the outer (black) and inner (white) ring of the cell crown. (B) The membrane is placed on top of the inner white ring and (C) fixed with the outer black ring. (D) The cell crown is inverted and (E) the remaining ends are cut off. (F) The membrane is placed into a 24-well plate.

3.2.10 Dynamic culture of membranes in flow-bioreactor

For dynamic cell culture experiments, the electrospun matrix was inserted into a flow-bioreactor system. The reactor system was composed of a reactor body consisting of two parts and a medium reservoir bottle connected to the reactor body via silicone tubes. After autoclaving all parts, the matrix was fixed in the reactor system and fibroblast culture medium was filled in the medium reservoir bottle. The reactor system was placed into the incubator and attached to the peristaltic pump. Medium was pumped through the tubes with a constant pumping speed of 5 rpm which corresponds to a medium flow of 3.8 ml/minute. Membranes were cultured for 14 days and medium was exchanged after 7 days of dynamic culture.

3.3 Construction of tissue models

Skin tissue models were constructed on functionalized electrospun membranes, on polycarbonate membranes and on collagen I hydrogels. Electrospun membranes and polycarbonate membranes served as matrix structure for oral mucosa equivalents.

3.3.1 Mono-culture of cells on functionalized membranes

Matrices were fixed in cell crowns, placed in 24-well plates, treated with 70 % (v/v) EtOH for 10 minutes, dried under the laminar airflow safety cabinet and seeded after detachment of cells and cell counting with different cell densities in 100 µl cell specific medium. After 2 hours at 37 °C, 1.5 ml additional medium was added to ensure sufficient nutrient supply.

3.3.2 Co-culture of cells on functionalized membranes

Electrospun membranes were fixed in cell crowns, placed in 24-well plates, treated with 70 % (v/v) EtOH for 10 minutes and dried under the laminar airflow safety cabinet. Fibroblasts were detached, counted, and seeded with a cell density of 5×10^4 cells per sample in 100 µl fibroblast culture medium. After 2 hours at 37 °C and 5 % CO_2, 1.5 ml DMEM medium was added and samples incubated for 1 week. Afterward, the membranes were turned around with HaCaT cells and primary keratinocytes being seeded respectively, at a cell density of 3×10^5 cells in 100 µl cell specific medium on the other side of the membrane. After incubation for 7 days under submersed conditions, the medium was changed to airlift medium followed by a culture under air-liquid interface. The culture medium was changed 3 times a week.

3.3.3 Mono-culture of cells on polycarbonate membranes

Epidermis models were prepared in 24-well format on polycarbonate membranes with 0.4 µm pore size. Two of these inserts were placed in each column of the culture plate. This ensured sufficient nutrient supply. Primary keratinocytes were detached and cell number was determined. The cell concentration was adjusted to 2.06×10^6 cells/ml in E2 medium. 150 µl of the cell suspension containing 3.12×10^5 cells were seeded on each insert. Incubation for 2 hours at 37 °C enabled the cells to adhere. Subsequently, 3.7 ml E2 medium was added to the lower compartment. After 1 day of incubation, the medium was discarded and the models were further cultured at the air-liquid interface in ALI-medium. Medium was changed 3 times a week.

3.3.4 Co-culture of cells on collagen I hydrogels

Full thickness skin models were prepared in 24-well format on polycarbonate membranes with 8 µm pore size. Placing two of the inserts in each column of the culture plate ensures an optimal supply of nutrients for the models. 500 µl cell/GNL/collagen suspension and 5 x 10^4 fibroblasts were needed per insert. Since there is a certain loss of suspension during preparation, 10 ml cell/GNL/collagen suspension was prepared for 12 inserts. 3.33 ml collagen (6mg/ml) was placed in a 50 ml tube and stored on ice. 1 x 10^6 fibroblasts were detached, counted, and re-suspended in 6.66 ml cooled gel neutralization solution (GNL) without producing bubbles. The suspension was added to the prepared 50 ml tube containing 3.33 ml collagen and then re-suspended carefully. 500 µl of the suspension was filled with a multistep-pipette in each insert. Incubation for 20 minutes in an incubator at 37 °C, 5 % CO_2 enables the gels to cure. Afterward, the gels were submerged in 2 ml fibroblast medium per well and incubated for 24 hours in an incubator at 37 °C, 5 % CO_2. The corresponding SOP "Full thickness skin equivalents" is attached in 7.1.

3.4 Characterization of functionalized membranes and tissue models

Characterization of functionalized membranes was achieved by microscopic techniques and protein adsorption studies. Cell viability and proliferation could be analyzed with Live/Dead staining, MTT viability assay, and CellTiter-Fluor™ assay. TEER, FITC-dextran, carboxyfluorescein and ET-50 measurements served as methods to determine the barrier formation of the tissue models.

3.4.1 Scanning electron microscopy

The structure morphology of electrospun fibers was analyzed using scanning electron microscopy (SEM). Therefore, the electrospun membranes were cut in pieces of 0.4 mm x 0.4 mm and adhered to a stainless steel sample holder with two-component adhesive and sputter-coated with gold. The specimens were then examined using a field-emission scanning electron microscope at 5 kV.

3.4.2 Qualitative protein adsorption studies

Prior to incubation with proteins, the membranes were fixed in cell crowns in 24-well plates and pre-wetted with deionized water for 60 minutes. 500 µl bovine serum albumin (BSA) tetramethylrhodamine conjugate (50 µg/ml) was incubated for 180 minutes at room temperature. Samples were subsequently immersed 5 times for 20 minutes with PBS buffer and washed thoroughly with deionized water. After drying the samples in a stream of nitrogen, they were immediately used for optical/fluorescence microscopy.

3.4.3 Quantification of peptide sequences

Quantification of the peptide sequences was performed by linking the UV-detectable group 2-mercaptopyridine to the cysteine flanked fibronectin derived cell binding sequence SGRGDSC via disulfide formation with the thiol group of the cysteine.

3.4.3.1 SGRGDSC-2-mercaptopyridine solution

Different amounts of the model peptide were dissolved in 3.4 x 10^{-5} mol/ml tris (2-carboxyethyl) phosphine (TCEP) in 0.1 N NaOH and assessed by UV-spectroscopy at 270 nm to obtain the calibration curve. TCEP was used as a reducing agent to break the disulfide bond within the peptide. The pH was kept neutral (pH = 7.4) and controlled regularly as the UV-absorption of mercaptopyridine is pH-dependent. With the obtained calibration curve, the concentration of the peptide on the surface of the membrane could be determined by measuring the absorbance.

3.4.3.2 2-mercaptopyridine reference solution

Different amounts of 2-mercaptopyridine with a purity of 99 % were dissolved in 3.4 x 10^{-5} mol/ml TCEP in 0.1 N NaOH TCEP (pH = 7.4) and used as a reference for the standard curve obtained from the solution containing the model peptide in aqueous TCEP solution.

3.4.3.3 Electrospinning of quantifiable membranes

Membranes for peptide quantification were electrospun as mentioned in 3.1.3, but without TFA to avoid any pH-influence. Afterward, the membranes were incubated

for 96 hours under ambient conditions to enable crosslinking of NCO-sP(EO-*stat*-PO) and to remove remaining solvents which could manipulate the results.

3.4.3.4 Quantification of non-covalently attached peptide

For peptide quantification, electrospun membranes were cut into 4 cm x 6 cm pieces and weighted. Afterward, the membranes were placed in 6 cm bacterial dishes and incubated for 24 hours in 2 ml 3.4 x 10^{-5} mol/ml TCEP in 0.1 N NaOH (pH = 7.4) on a rocket-shaker. The supernatant was used for UV-measurements at 270 nm. Afterward, the membrane was freeze-dried, placed in a 2 ml tube, and treated with 1.15 ml 1 N NaOH to dissolve the meshes. After 24 hours, 3.4 x 10^{-4} mol/ml TCEP was added to the solution. Thus, the solution had a pH of 7.4. The suspension was incubated for 24 hours on a thermo-shaker. The amount of 2-mercaptopyridine, which was embedded in the fibers, was determined UV-metrically at 270 nm.

3.4.3.5 Quantification of covalently attached peptide

For quantification of the covalently attached peptide, electrospun membranes were cut into 4 cm x 6 cm pieces and weighted, placed in 6 cm bacterial dishes and treated with 2 ml deionized water for 24 hours. The non-covalently bound peptide remained in the water washings. 1 ml of the water washings was mixed with 1 ml of 6.8 x 10^{-5} mol/ml in 0.2 N NaOH, producing a solution with a pH of 7.4. 2-mercaptopyridine was released and could be determined UV-metrically at 270 nm. Analysis of the amount of peptide non-covalently attached and embedded in the fibers was completed as described in 3.4.3.4. Briefly, membranes were incubated 24 hours in 2 ml 3.4 x 10^{-5} mol/ml TCEP in 0.1 N NaOH (pH = 7.4) before freeze-drying and placing them in 1 N NaOH.

3.4.4 Live/Dead staining

The use of the fluorescent dyes propidium iodide (PI) and fluorescein diacetate (FDA) allowed the discrimination of living cells from dead cells by microscopy. FDA is taken up by viable cells, which convert the dye into green fluorescein. PI passes only damaged cell membranes and intercalates into the DNA. As a result, nuclei of dead cells are stained in red. Samples were fixed in cell crowns, placed in 24-well

plates and rinsed 3 times with PBS^+. Afterward, they were incubated in PI/FDA solution for 1 minute. The amount of staining solution was chosen so that the entire sample was covered. The solution was aspirated, and then the samples were washed twice with PBS^+ to remove residues of PI/FDA and kept in PBS^+ until investigation. During experiments, all solutions and samples were handled in darkness to avoid premature bleaching. It was important to work fast and to examine the samples under the microscope immediately due to the cytotoxicity of the staining solution, which could influence the results. The corresponding SOP "Live/Dead staining" is attached in 7.1.

3.4.5 Invasive cell viability assay (MTT-assay)

The MTT assay is an invasive colorimetric cell viability assay which measures the metabolic activity of the mitochondrial reductase in cells. The yellow tetrazolium dye 3-(4,5-Diamethylthiazol-2-yl)-2,5-diphenyltetrazolium bromide (MTT) is reduced by NAD(P)H-dependent cellular oxidoreductase enzymes to a purple insoluble formazan which is accumulated in the cells. The amount of formazan can be correlated to the cell viability [197]. After aspirating the medium, models were washed with PBS^+, dried on adsorbent tissue and incubated in 1 ml MTT reagent (1mg/ml) in 24-well plates for 3 hours at 37 °C in an incubator. Afterward, the blue precipitated formazan dye, which has been deposited inside the living cells, was extracted with 2 ml 2-propanol. The inserts were removed from the MTT solution, placed for a few seconds on an adsorbent tissue in order to remove droplets of MTT, placed in a second 24-well plate, and incubated overnight on a shaker at 4 °C. The following day, 100 µl of formazan extract was quantified in triplicates in a 96-well plate by measuring the optical density (OD) at 570 nm with a micro-plate reader. The average of the measured blanks had to be subtracted from the mean of the triplicates. For irritation studies, the tissue viability was determined by normalizing the OD for treated tissues as a percentage of unexposed control tissues as illustrated in the equation:

$$\% \text{ viability} = OD \text{ (treated tissue)} / OD \text{ (untreated tissue)}$$

The corresponding SOP "MTT viability assay" is attached in 7.1.

3.4.6 Non-invasive cell viability assay (CellTiter-Fluor™)

In comparison to the cytotoxic MTT assay, the CellTiter-Fluor™ assay allows the determination of the cell viability non-invasively so that models could be measured after different time points. The substrate glycylphenylalanyl-aminofluorocoumarin enters intact cells where it is cleaved to a fluorescent signal proportional to the number of living cells. The assay was used according to the manufacturer´s protocol. Briefly, after 2, 4, 6, 8 and 10 days in culture, electrospun membranes seeded with cells were washed with PBS^+, dried, and placed in 24-well plates. 500 µl of CellTiter-Fluor™ was pipetted on top of the models and incubated for 30 minutes at 37 °C. The fluorescence of the supernatant was determined at an excitation wavelength of 400 nm and an emission wavelength of 525 nm in a micro-plate reader. The average of the measured background values had to be subtracted from the mean of the triplicates. The generated fluorescent signal is proportional to the number of living cells.

3.4.7 Transepithelial electrical resistance

Transepithelial electrical resistance (TEER) is a quantitative technique to measure the integrity of tight junction in cell culture models. The TEER apparatus contains a pair of circular electrodes specifically designed for the use in 24-well inserts. Prior to TEER measurements, tissues were filled with cell-type specific medium so that the medium in the basolateral compartment had the same height as in the apical compartment. After equilibration for 25 minutes, TEER measurements were determined following Ohm's law. The electrical resistance R was recorded and TEER calculated according to:

$$TEER = (R_{(insert\ with\ cells)} - R_{(insert\ without\ cells)}) \times A$$

with A as the growth surface area (cm^2).

3.4.8 Permeation studies

To study the permeation of peptides and proteins through the oral mucosa, FITC-labeled dextran and carboxyfluorescein were used as model compounds.

3.4.8.1 FITC-dextran measurement

Fluorescein-isothyocyanate (FITC) can be covalently attached to dextran molecules. Hence, the FITC label allows fluorometric detection of dextrans in permeation studies. Models were washed with PBS^+ and placed in 24-well plates containing 1700 µl cell-type specific medium in the basolateral compartment. 500 µl FITC-dextran solution (0.25 mg/ml) with an average molecular weight of 4 kDa was added to the apical compartment of each insert so that the apical chamber was filled equally to the level in the basolateral chamber. The models were incubated for 60 minutes on a shaker at 37 °C, 5 % CO_2. After incubation, 100 µl of the medium in the basolateral compartment were quantified in triplicates in a black 96-well plate by measuring the fluorescence at an excitation wavelength of 490 nm and an emission wavelength of 525 nm in a micro-plate reader. Cell-type specific medium and FITC-dextran solution served as references. The corresponding SOP "FITC-dextran" is attached in 7.1.

3.4.8.2 Carboxyfluorescein measurement

Carboxyfluorescein measurement allowed the analysis of the barrier development of oral mucosa models after 3, 7, 10 and 14 days of culturing. The models were placed in 24-well plates containing 1700 µl cell-type specific medium in the basolateral compartment. 500 µl of carboxyfluorescein solution (0.25 mg/ml) was added to each of the apical compartments of the inserts, so that both compartments were filled equally. The models were incubated for 35 minutes on a shaker at 37 °C, 5 % CO_2 in an incubator. Afterward, 100µl of the medium in the basolateral compartment had to be quantified in triplicates in a black 96-well plate by measuring the fluorescence at an excitation wavelength of 492 nm and an emission wavelength of 517 nm in a micro-plate reader. Cell-type specific medium and carboxyfluorescein solution served as references. To analyze how long oral mucosa models resist carboxyfluorescein permeation, models were incubated with carboxyfluorescein for 30, 120, 240, and 360 minutes, and compared with empty inserts and reconstructed skin models.

3.4.9 ET-50 measurement

The ET-50 value is defined as the effective time after which the viability of the treated model decreased to 50 % of the control model. Usually Triton X-100 is applied in order to test how long the tissue can resist the damaging impact of a detergent. Depending on the barrier function, Triton X-100 can more or less penetrate and damage the cells underneath the stratum corneum. Placing two of these inserts in each column of the culture plate ensures an optimal supply of nutrients to the models. After adding 3.7 ml ALI medium in the basolateral chamber, 25 µl of Triton X-100 solution were applied to the surface of each model. Untreated models served as a control. Models were incubated for 0, 20, 50, 80, 110, 150, 200, and 300 minutes at 37 °C, 5 % CO_2 in an incubator. Subsequently, Triton X-100 was decanted and the models rinsed with PBS^+ to remove residues. The insert were placed on sterile blotting paper in order to remove adhering liquid, transferred to 24-well plates containing 200 µl MTT (1mg/ml) solution each and incubated for 3 hours in MTT to determine tissue viability. The equation $V = a + b * log\ (t)$, where V = % viability, t = time in minutes and "a" and "b" are constants, allows the calculation of the time in which the reduction of the tissue viability reaches 50 % (ET-50). The constants could be determined using the mean viability data from 3 exposure times. The equation was solved for t by setting V = 50 %. In general, a lower "ET-50" corresponds to reduced resistance of the barrier.

3.4.10 Irritation study

Before applying the test substances to the models, the substances had to be investigated for interactions with MTT reagent. Therefore, 25 µl of the test substances were incubated for 3 hours at 37 °C, 5 % CO_2 with 200 µl MTT (1mg/ml) reagent. If the substance did not convert MTT, they could be used for irritation studies. Oral mucosa models were placed in a 24-well plate containing 1 ml ALI medium per well. A volume of 23.6 µl of the test substances was applied on top of the models and incubated for 35 minutes in an incubator at 37 °C, 5 % CO_2. 5 % sodium dodecyl sulfate (SDS) served as positive control and PBS^+ as negative control. After the indicated period of time, the test substances were aspirated, the tissues thoroughly washed 8 times with 600 µl PBS^+ with a multi-pipette and

afterward dipped 5 times in a beaker containing 10 ml PBS^+. To ensure appropriate results for every test substance, a new beaker had to be used. After plunging, the remaining buffer was aspirated and the models transferred in fresh 24-well plates containing 3.7 ml pre-warmed ALI medium. After 42 hours of incubation at 37 °C, 5 % CO_2, the tissue viability was analyzed using MTT. Substances reducing the relative viability of 3 individual tissues below or equal to the 50 % threshold of the mean viability of the negative control were described as irritants.

3.5 Histology

Tissue structures as well as cellular and matrix components were investigated by histologically stained sections. If not indicated otherwise, stained sections were mounted in entellan® and covered with glass slips.

3.5.1 Fixation

If necessary, medium was aspirated and tissues washed once with PBS^- to remove medium and serum residues. Tissues and matrices with cells, as well as cells cultured on chamber slides and cytospots, had to be fixed with 4 % PFA at room temperature for histological and immunohistochemical staining. Because of the different tissue depth, chamber slides and cytospots were fixed for 10 minutes, insert membranes and electrospun matrices for 1 hour, and collagen hydrogels for 2 hours. To ensure that the tissue was sufficiently fixed, the tissue remained in cell crowns and inserts respectively, whenever possible. The corresponding SOP “PFA-fixation” is attached in 7.1.

3.5.2 Plunge freezing and cryo-sectioning

After fixation and careful dissection, tissues were embedded in Tissue-Tek® and frozen in liquid nitrogen. Afterward, the frozen tissue block was fixed with Tissue-Tek® to the tissue holder. Slices of 3-5 µm thickness were cut, placed on super-frost object slides, air-dried for 30 minutes and kept in the freezer. Before staining, they were stored for 2 hours at room temperature.

3.5.3 Paraffin embedding and microtome sectioning

After fixation, tissues were removed from cell crowns, transferred onto the embedding filter paper and placed together with the filter into a plastic embedding cassette. The embedding cassettes were transferred into a beaker with tap water for at least 1 hour to remove PFA remnants and then placed in the water compartment of the embedding station and embedded according to the program in Table 16.

Table 16: Paraffin embedding program of embedding station

Time in hours	Solution	Purpose
1	Tap water	Washing out fixative
1	50 % (v/v) Ethanol	Ascending alcohol chain for dehydration
1	70 % (v/v) Ethanol	
1	90 % (v/v) Ethanol	
1	96 % (v/v) Ethanol	
1	Isopropyl alcohol I	
1	Isopropyl alcohol II	
1	Isopropyl alcohol/Xylene 1:2	Removing alcohol from tissue
1	Xylene I	
1	Xylene II	
1.5	Paraffin I	Infiltration with paraffin
1.5	Paraffin II	

After embedding, the samples were removed from the embedding cassette, cut into 2-3 equal pieces and blocked with the cutting edges facing downwards in a stainless steel casting mold in paraffin. After hardening, tissue sections of 5 µm thickness could be prepared, placed on polysine coated object slides and dried at 37 °C overnight. The corresponding SOP “Paraffin embedding” is attached in 7.1.

3.5.4 Deparaffinization and rehydration of tissue sections

Prior to staining, paraffinized tissue sections had to be deparaffinized and rehydrated. Therefore, sections were incubated at 60 °C for 1 hour to melt paraffin and afterward deparaffinized and rehydrated, as described in Table 17.

Table 17: Deparaffinization and rehydration of tissue sections

Time in minutes	Solution	Purpose
10	Xylene I	Deparaffinization
10	Xylene II	
Dip 3 times	Ethanol 96 % (v/v) I	Rehydration
Dip 3 times	Ethanol 96 % (v/v) II	
Dip 3 times	Ethanol 70 % (v/v)	
Dip 3 times	Ethanol 50 % (v/v)	
Slew until cords clear	Demineralized water	

3.5.5 Haematoxylin-eosin staining

Haematoxylin-eosin (H&E) staining provides an excellent overview for the analysis of cell and tissue morphology. Haematoxylin attaches to basophilic structures such as the nucleus staining them blue, while eosin stains acidophilic structures such as cytoplasmatic proteins and are stained red. After deparaffinization and rehydration, staining could be performed according to the protocol in Table 18. To preserve slides, sections had to be mounted with entellan® for preservation. The corresponding SOP "Haematoxylin&Eosin staining" is attached in 7.1.

Table 18: H&E staining procedure

Time in minutes	Solution	Purpose
8	Haemalaun	Staining basophilic structures
Until solution is clear	Demineralized water	Rinsing off haemalaun
Dip twice	HCl/Ethanol	Differentiation of haematoxylin
Dip once	Demineralized water	Rinsing
5	Tap water	Blueing

Time in minutes	Solution	Purpose
1	Eosin	Staining acidophilic structures
Until solution is clear	Demineralized water	Rinsing off eosin
Dip 3 times	Ethanol 70 % (v/v)	Dehydration
2	Ethanol 96 % (v/v)	
5	Isopropyl alcohol I	
5	Isopropyl alcohol II	
5	Xylene I	
5	Xylene II	

3.5.6 Immunohistochemistry

Immunohistochemistry (IHC) is a powerful method to localize specific antigens in tissue sections. Tissues were analyzed by DAB-based staining performed with DCS Super Vision 2 Kit. The antigen is recognized by a specific primary antibody. The Fc region of the primary antibody is detected by a secondary antibody or amplifier, which in turn is conjugated to a micropolymer that binds horseradish peroxidase (HRP). HRP can than mediate the oxidation of the substrate 3,3'-diaminobencidine (DAB) and the generation of a brown-colored oxidation product. The brown-colored reaction product is exactly located at the antigen site of the primary antibody binding. DAB-based immunohistochemical staining was performed on tissue sections, as well as on cytospots. Tissue sections were deparaffinized and rehydrated. For heat-induced antigen retrieval, slides had to be heated for 20 minutes at 100 °C in citrate buffer (pH = 6). Subsequently, slides were placed in washing buffer and circled with a liquid-repellent slide marker pen. All incubation steps were carried out at room temperature in a humidity chamber, whereas washing steps were performed in a cuvette on a rocking platform shaker. The primary antibodies were diluted as described in Table 12 and the DAB staining performed as illustrated in Table 19. For a better overview, nuclei were stained with haemalaun. After transferring the samples to demineralized water, sections were hydrated by ascending ethanol series and embedded in entellan®. The

corresponding SOP "Immunohistochemical staining with HRP-based detection system" is attached in 7.1.

Table 19: DAB staining procedure

Step	Solution	Time (minutes)
Blocking of endogenous peroxidase	3 % (v/v) H_2O_2	10
Washing	PBS-Tween®	5
Primary antibody	Primary antibody/Isotype	60
Washing (3 times)	PBS-Tween®	5
Amplifying I	DCS Enhancer solution	10
Washing (3 times)	PBS-Tween®	5
Amplifying II	DCS Polymer solution	20
Washing (3 times)	PBS-Tween®	5
Detection step	DAB solution	5
Washing	PBS-Tween®	Slewed
Nucleus staining	Haemalaun	0.5-0.75
Blueing	Tap water	1-1.5
Preparation for embedding	Demineralized water	Infinite

3.6 Degradation studies

Morphological changes of the membranes were examined under physiological conditions. Therefore, mesh pieces were fixed in cell crowns and incubated with 15 ml PBS solution at a pH 7.4 on a rocket shaker at 37 °C, 5 % CO_2 with a rotation speed of 150 $seconds^{-1}$. The buffer was exchanged 3 times a week. After 1, 7, 14, and 28 days, samples were washed with deionized water to extract remaining PBS, freeze-dried for 24 hours, and investigated using SEM.

3.7 Differential scanning calorimetry

The differential scanning calorimetry (DSC) equipment was programmed to heat samples in two distinct runs. The first run was intended to erase the thermal history

of the material. The second run determined the glass transition temperature (Tg) of the samples. Therefore, membranes with a mass of 10 ± 1 mg were placed on a sample holder and heated in a first run from -50 °C up to 210 °C at a heating rate of 1 °C/minute. The equipment was cooled with liquid nitrogen. Afterward, the second run was achieved by heating the samples again from -50 °C up to 210 °C, at a rate of 1 °C/minute. Nitrogen at a rate of 20 ml/minute served as the flow gas. The protective gas was used at a flow rate of 70 ml/minute.

3.8 Lyophilization

For morphological characterization and for quantification experiments, samples were placed in 15 ml tubes and frozen at – 80 °C overnight. Afterward, the freeze-drying procedure was performed for 24 hours in a lyophilization apparatus.

3.9 Statistical analysis

Statistical significance of fibroblast and HaCaT proliferation on differently functionalized membranes was determined with two-way ANOVA by GraphPad® Prism 5.

4 Results

4.1 Characterization of functionalized membranes

By electrospinning the synthetic, degradable polymer PLGA with NCO-sP(EO-*stat*-PO) additives and cell-adhesion-mediating peptide sequences in one solution, fibers with controlled surface chemistry and functionality can be produced. However, to use the functionalized fibrous membranes for tissue engineering applications and as artificial basement membranes, the meshes must fulfill certain requirements: systematic variation of the peptide sequences used for bioactivation should be enabled; the integrity of the membrane should not be influenced by the peptides; the fibrous structure of the mesh should be maintained also under cell culture conditions; cellular infiltration and tissue ingrowth should be promoted by a large void volume; the degradation profile should correlate with new tissue formation; the membrane should tolerate sterilization and should be able to be cultured under dynamic culture conditions.

4.1.1 Electrospinning of functionalized membranes

Aim of the study was to develop biomimetic artificial basement membranes that reflect the bioactivity of the natural structure. To achieve this, we included NCO-sP(EO-*stat*-PO) for the electrospinning of poly(D,L-lactide-*co*-glycolide) PLGA. Functionalization was performed by adding sequences from major basement membrane proteins, including the fibronectin derived binding sequence CGRGDS, the laminin derived binding sequences CGYIGSR and CGIKVAV, as well as the collagen IV derived binding sequence CGEFYFDLRLKGDK. The principle of the one-step preparation of fully synthetic, bioactive and degradable membranes by electrospinning is depicted in Figure 10.

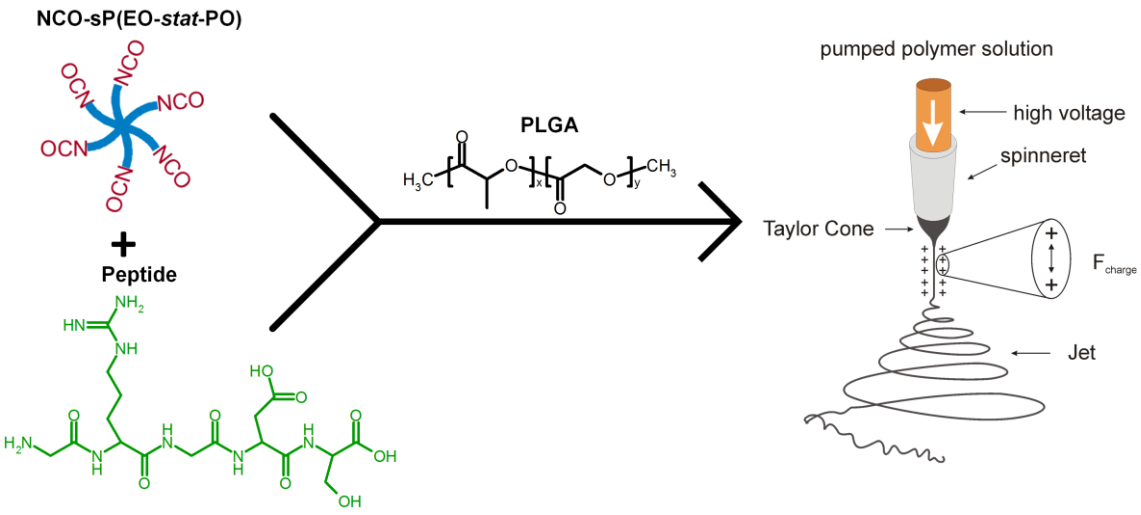

Figure 10: Electrospinning NCO-sP(EO-*stat*-PO) with PLGA and peptides.
One-step functionalization method that combines the synthetic polymer (PLGA), the functional additive (NCO-sP(EO-*stat*-PO)) and bioactive peptide sequences in a co-electrospinning setup.

Electrospinning of 25 wt% PLGA and 5 wt% NCO-sP(EO-*stat*-PO) with a solvent composition of 88/10/2 v/v% acetone/DMSO/TFA in water resulted in high quality fibers that were used for further investigations. Electrospun membranes were stored at ambient conditions overnight to allow evaporation of solvent residues before the experiments.

4.1.2 Influence of peptides on fiber morphology and integrity

To use the electrospun membranes as artificial basement membrane, it was important to ensure that peptide sequences do not have an influence on the fiber morphology, integrity and diameter. Therefore, membranes with different peptide sequences were electrospun and investigated. Scanning electron microscopy (SEM) analysis showed that the integrity and morphology was not affected by adding peptide sequences (Figure 11). Modification with fibronectin, laminin and collagen IV derived peptide sequences generated uniform fibers. Moreover, combining different peptides did not influence fiber integrity and appearance.

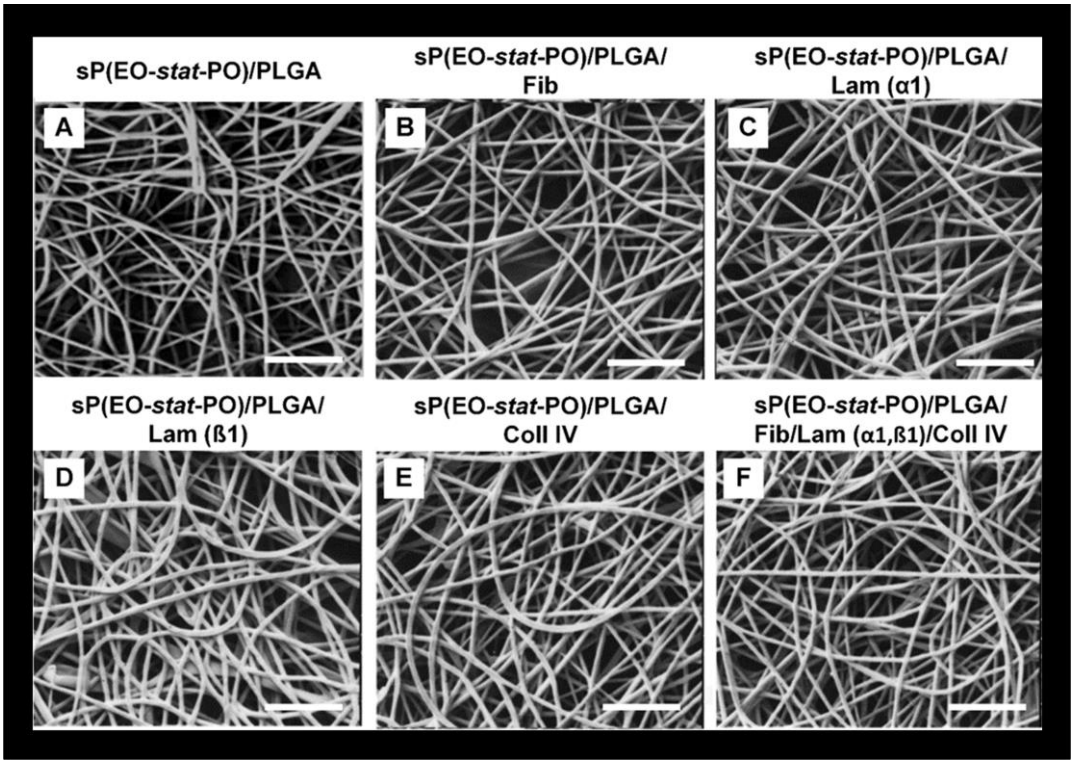

Figure 11: Influence of peptides on fiber morphology and integrity.
(A) sP(EO-*stat*-PO)/PLGA membranes were electrospun, and in combination with different peptide sequences, (B) sP(EO-*stat*-PO)/PLGA/fibronectin, (C) sP(EO-*stat*-PO)/PLGA/laminin α1, (D) sP(EO-*stat*-PO)/PLGA/laminin β1, (E) sP(EO-*stat*-PO)/PLGA/collagen IV and
(F) sP(EO-*stat*-PO)/PLGA/fibronectin/laminin α1/laminin β1/collagen IV.
Fib = fibronectin, Lam = laminin, Coll IV = collagen IV. Scale bars = 5 µm.

The diameter of the electrospun fibers, biofunctionalized with different peptide sequences, was quantified. The peptides did not have an influence on the fiber diameter (Figure 12). Independent of the peptide sequence, electrospun fibers revealed fiber diameters of 300 $\pm$ 34 nm.

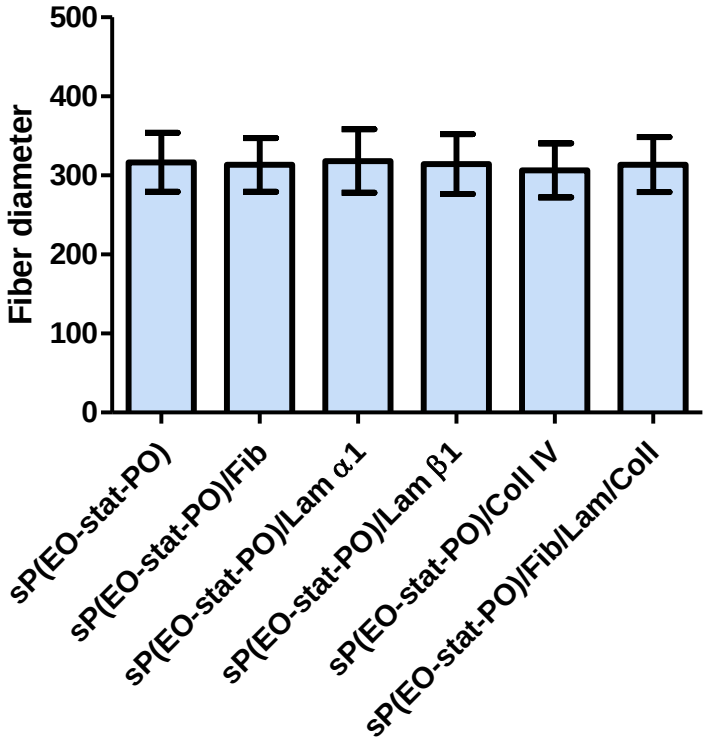

Figure 12: Influence of peptides on fiber diameter.
Fibers with different peptide sequences were electrospun and the influence of the peptide sequences on the fiber diameter was analyzed. Fib = fibronectin, Lam = laminin, Coll IV = collagen IV. Error bar represent SD (n = 100).

4.1.3 Influence of fixation mode on fiber morphology

To investigate the influence of the fixation mode on fiber morphology, sP(EO-*stat*-PO)/PLGA fibers were electrospun and afterward incubated in PBS, either fixed in cell crowns (Figure 13B) or without fixation (Figure 13C), for 24 hours at 37 °C, 5 % CO_2. As reference, membranes were incubated at room temperature under dry conditions (Figure 13A). In SEM micrographs, it could be observed that fibers fixed in cell crowns were stable and did not shrink due to local fiber fixation. The morphology was comparable to dry fibers. Fibers incubated in PBS for 24 hours at 37 °C, 5 % CO_2 without fixation shrank and lost their shape.

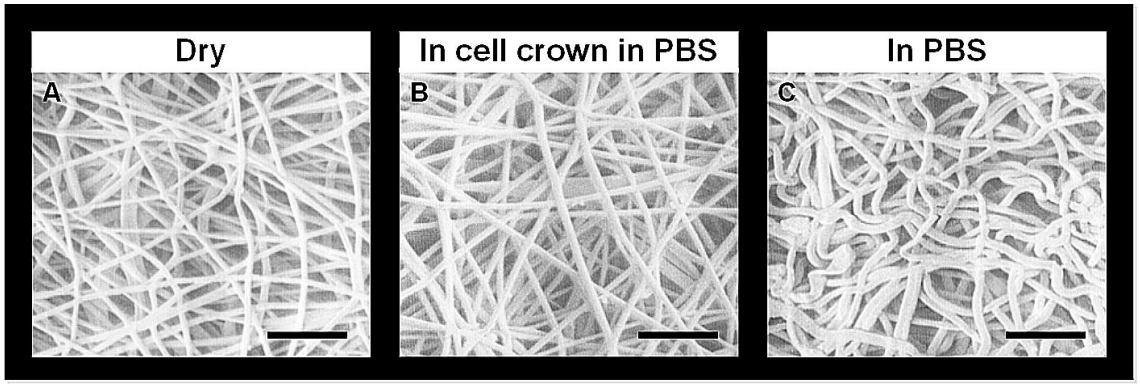

Figure 13: Influence of fixation mode on fiber morphology.
Electrospun membranes were incubated for 24 hours under (A) dry conditions at room temperature, (B) fixed in cell crowns in PBS at 37 °C, 5 % CO_2 (C) without fixation in PBS at 37 °C, 5 % CO_2. Scale bars = 5 µm.

Fibers stored at ambient conditions revealed fiber diameters of 296 ± 45 nm. The diameter of fibers fixed in cell crowns in PBS was 450 nm ± 101 nm after 24 hours. Without fixation, the fiber diameter increased in PBS to 604 nm ± 186 nm, whereas the pore size decreased. Consequently, as soon as fibers were in contact with liquid, swelling of fibers occurred, independent of the fixation technique. Nevertheless, this effect could be kept to a low level. Therefore, for further experiments membranes were used with cell crowns to ensure sufficient pore size and ultra-thin fiber diameters.

4.1.4 Modifying pore size of functionalized membranes

Membranes with small pores that avoid cell infiltration are advantageous for applications in which the membrane serves as a barrier. However, for the development of artificial basement membranes, porosity is viewed as a crucial parameter enabling cellular infiltration and tissue ingrowth. It is challenging to create well-defined pore sizes by the solution electrospinning technique due to the random deposition of fibers onto the collector. Nevertheless, several techniques have been investigated previously to modify the pore size, either by modifying the electrospinning setup or by post-electrospinning modifications.

4.1.4.1 Low temperature electrospinning

For low temperature electrospinning, the collector is cooled to -20 °C so that ice crystals start to form on the fibers as they deposit. The ice crystals work as spacers between the fibers. When melting, they leave behind pores. To evaluate whether the temperature of the collector has an influence on the pore size of sP(EO-*stat*-PO)/PLGA membranes, fibers were electrospun on a frozen collector and on a collector at room temperature. SEM analysis revealed that both membranes were comparable. Pore sizes of membranes electrospun on a collector with room temperature (Figure 14A) and on a frozen collector (Figure 14B) ranged from 0.1 to 2.5 µm and 0.4 to 2.4 µm, respectively.

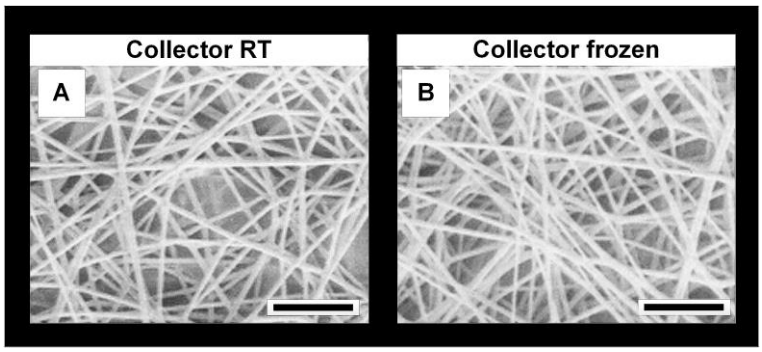

Figure 14: Influence of low temperature electrospinning on pore size.
sP(EO-*stat*-PO)/PLGA fibers were electrospun on (A) a collector stored at room temperature and on (B) a collector stored at -20 °C. RT = room temperature. Scale bars = 5 µm.

4.1.4.2 Fiber leaching

A simple technique to increase the pore size is electrospinning of sacrificial material, which is dissolved afterward. PEG is a common sacrificial polymer due to its aqueous solubility. Hence, a solution containing NCO-sP(EO-*stat*-PO) and PLGA was electrospun from one side on a rotating collector and a 5 wt% PEG solution from the other; both solutions at a flow rate of 0.5 ml/hour. Membranes were incubated in water for 15 minutes after electrospinning so that PEG fibers dissolved. However, the pore size did not increase by fiber leaching (Figure 15).

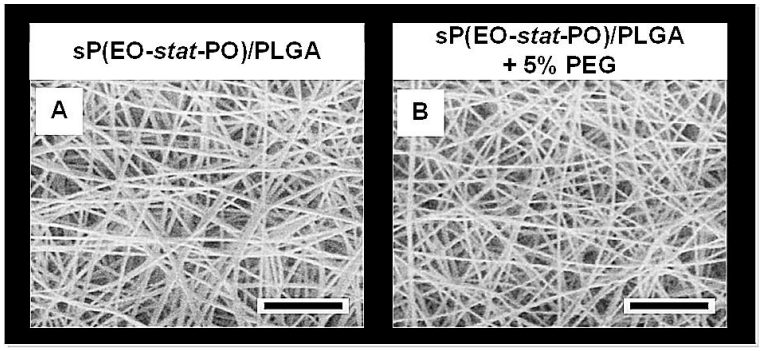

Figure 15: Influence of fiber leaching on pore size.
(A) Electrospun sP(EO-*stat*-PO)/PLGA membranes in comparison to (B) sP(EO-*stat*-PO)/PLGA fibers co-electrospun with a 5 wt% PEG solution. Scale bars = 5 µm.

4.1.4.3 Ultrasonic treatment

Another method to increase the pore size is ultrasonic treatment. Therefore, ultrasound (100 W) was applied for 1 x 30 seconds, 2 x 30 seconds, 4 x 30 seconds and 8 x 30 seconds to the electrospun sP(EO-*stat*-PO)/PLGA membranes. The resulting pore size of the treated membranes was compared to the untreated controls (Figure 16). The SEM images showed no visible differences in pore size.

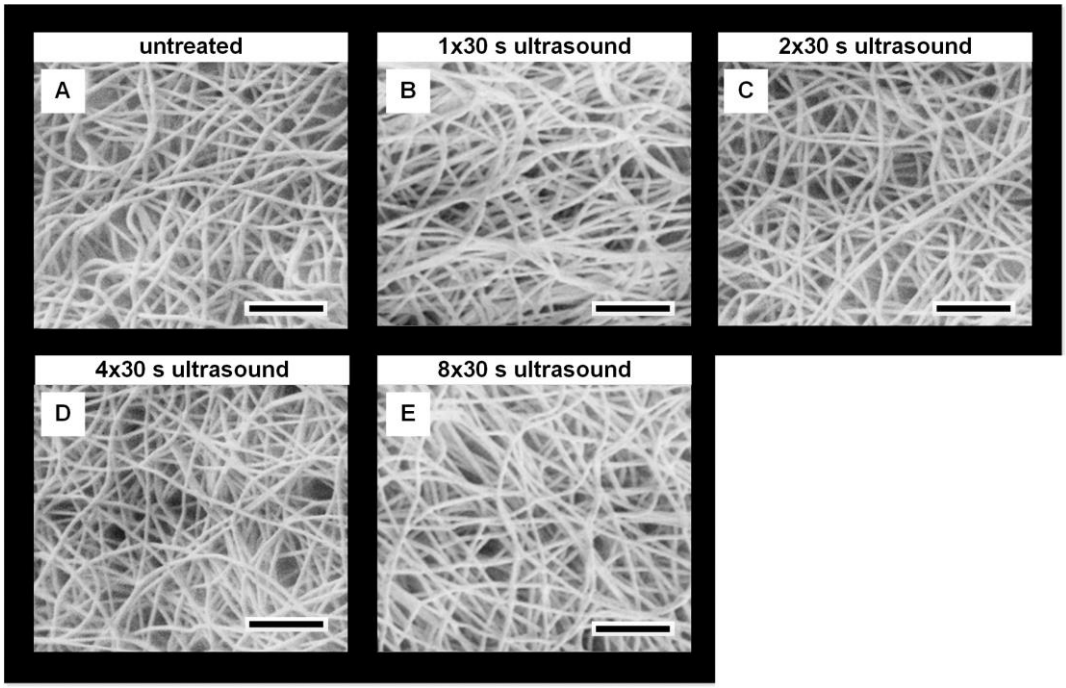

Figure 16: Influence of ultrasonic treatment on pore size.
sP(EO-*stat*-PO)/PLGA fibers were treated for (B) 1 x 30 s, (C) 2 x 30 s, (D) 4 x 30 s and (E) 8 x 30 s with ultrasound. (A) Untreated control. s = seconds. Scale bars = 5 µm.

4.1.5 Degradation of functionalized membranes

As the target application of the electrospun membrane is to serve as a temporary substitute of the native basement membrane, degradation and bioresorption of the membrane over a defined time frame and excretion from the body are key issues. Skin cells need about 2-3 months to produce their own extracellular matrix proteins and to develop a basement membrane, so it would be advantageous for the functionalized PLGA membrane to degrade within that time frame.

4.1.5.1 Morphological characterization

To investigate the influence of the bioinert, non-degradable, hydrophilic additive on the degradation rate, PLGA and sP(EO-*stat*-PO)/PLGA membranes were incubated in PBS over 28 days at 37 °C, 5 % CO_2. It was observed that better wetting and penetration of water into the more hydrophilic sP(EO-*stat*-PO)/PLGA fibers did not control the degradation, but the additive retarded the disintegration of the fibers.

PLGA samples exhibited swelling and fiber merging within the first two weeks of degradation. Addition of NCO-sP(EO-*stat*-PO) led to stable fibers without any morphological changes over the entire incubation period (Figure 17). After one month, PLGA membranes resembled more a film (see black arrows in B, C, D) than fibers, whereas electrospun sP(EO-*stat*-PO)/PLGA membranes appeared to be unchanged.

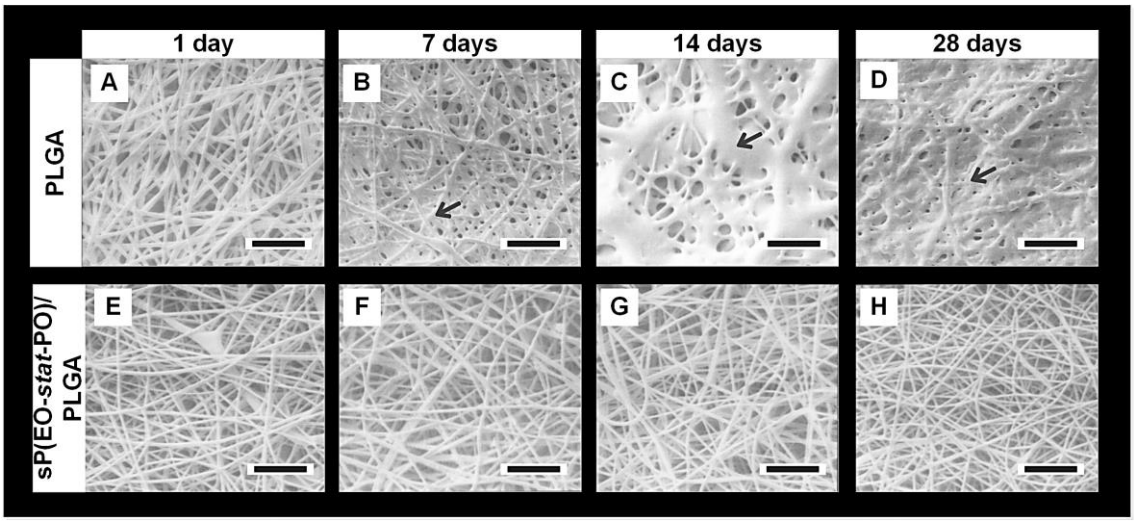

Figure 17: Influence of degradation on fiber morphology.
PLGA and sP(EO-*stat*-PO)/PLGA membranes were incubated for 28 days in physiological buffer (PBS) at 37 °C, 5 % CO_2. Morphological changes were observed after (A; E) 1 day, (B; F) 7 days, (C; G) 14 days and (D; H) 28 days. Black arrows show morphological changes of the fibers. Scale bars = 5 µm.

4.1.5.2 Investigation of glass transition temperature

Copolymer composition affects important properties, such as glass transition temperature (Tg) and crystallinity, which have an indirect effect on the degradation rate. The change in Tg was studied using differential scanning calorimetry (DSC). Samples were incubated for 1, 7, 14, and 21 days at 37 °C, 5 % CO_2 in DMEM + 10 % FCS, thoroughly washed, freeze-dried, and characterized for changes to the Tg. Comparison of the Tg of PLGA and sP(EO-*stat*-PO)/PLGA meshes showed that there was a shift of Tg for PLGA membranes, whereas negligible changes were observed for sP(EO-*stat*-PO)/PLGA membranes (Figure 18).

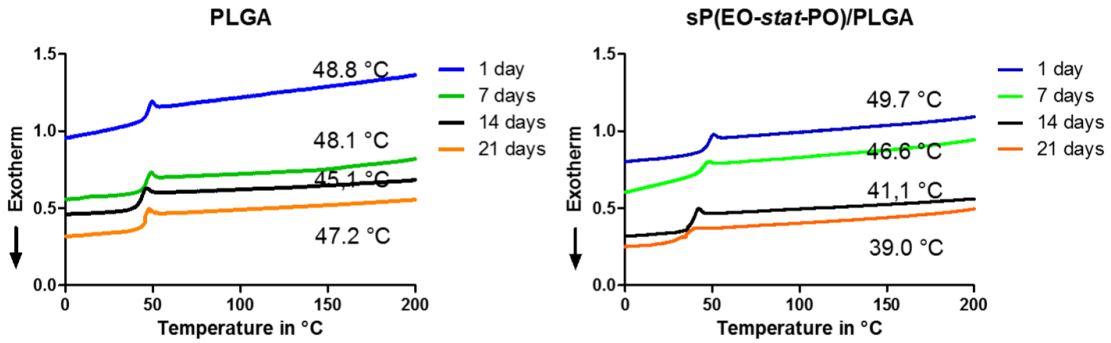

Figure 18: Influence of degradation on glass transition temperature.
PLGA and sP(EO-*stat*-PO)/PLGA were incubated in physiological buffer at 37 °C, 5 % CO_2. The Tg of PLGA fibers was measured at day 1, 7, 14, and 21 and compared with the Tg of sP(EO-*stat*-PO)/PLGA membranes (n = 3).

At day 1, PLGA and sP(EO-*stat*-PO)/PLGA samples presented a Tg of 48.8 °C and 49.7 °C, respectively. During the degradation process, there was a significant decrease of the Tg for sP(EO-*stat*-PO)/PLGA membranes, which changed from 49.7 °C at day 1 to 39.0 °C after 21 days, whereas the Tg of PLGA membranes dropped from 48.8 °C to 47.2 °C and therefore remained almost constant over 21 days.

4.1.6 Influence of sterilization on membrane morphology

Developing an artificial basement membrane requires the mesh to be completely eliminated from pathogens. Therefore, sterilization effectiveness and potential structural damage of 70 % (v/v) ethanol treatment and γ-sterilization was analyzed for sP(EO-*stat*-PO)/PLGA membranes. Sterilization efficacy was determined qualitatively by the absence of signs of infection after a 48 hour culture period at 37 °C, 5 % CO_2 in DMEM + 10 % FCS. Signs of infection are opacity of the culture medium, a change of the indicator color in the medium, and findings in the microscopic analysis. Structural damages were visualized by SEM. Non-sterilized membranes were used as controls.

4.1.6.1 γ-sterilization

Membranes were treated with a standard 2.5 Mrad sterilization dose and incubated for 48 hours in medium at 37 °C. Whereas, the non-sterilized controls showed

infection after 24 hours, all γ-sterilized membranes did not display contamination. Figure 19 shows details about the morphological changes of γ-sterilized membranes after 1, 7, and 30 days of incubation in culture medium at 37 °C, 5 % CO_2. Both γ-sterilized and non-sterilized membranes retained their fibrillar structure over 30 days. However, structural irregularities of the γ-sterilized fibers were observed. The fibers lost their homogeneous shape and some parts of the fibers appeared thinner than others (see arrows in Figure 19F). The morphological structure of non-sterilized membranes did not change over the incubation period.

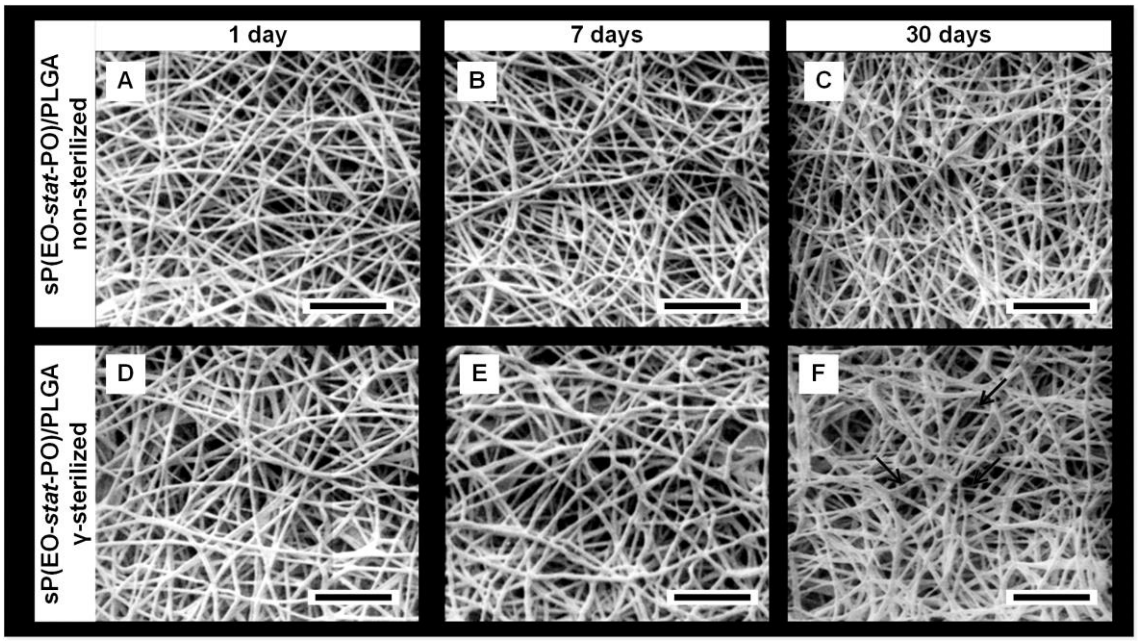

Figure 19: Influence of γ-sterilization on fiber morphology.
Morphology of γ-sterilized fibers was investigated followed by a (A; D) 1 day (B; E) 7 days and (C; F) 30 days culture in cell culture medium at 37 °C, 5 % CO_2. As control, non-sterilized membranes were analyzed. Black arrows present fiber defects after γ-sterilization. Scale bars = 5 µm.

4.1.6.2 Ethanol-disinfection

Ethanol at concentrations of 60–80 % (v/v) is classified as a disinfectant rather than a sterilization agent. Nevertheless, ethanol treatment is an easy and widely used tool to treat biomaterials for *in vitro* studies. Therefore, it was investigated whether ethanol treatment avoids contaminations and morphological changes of sP(EO-*stat*-PO)/PLGA fibers. Thus, samples were incubated for 10 minutes in 70 % (v/v) ethanol, dried under the laminar air flow, and cultured for different

periods of time in medium at 37 °C, 5 % CO_2. Ethanol treatment seemed to have negligible influence on the fiber morphology (Figure 20). After 30 days in culture, ethanol treated membranes looked comparable to the untreated controls. There were no contaminations detected in ethanol treated membranes. The untreated control samples, however, showed infection after 24 hours. Nevertheless, it has to be kept in mind that ethanol only works to disinfect rather than to sterilize and is therefore not suitable for clinical applications.

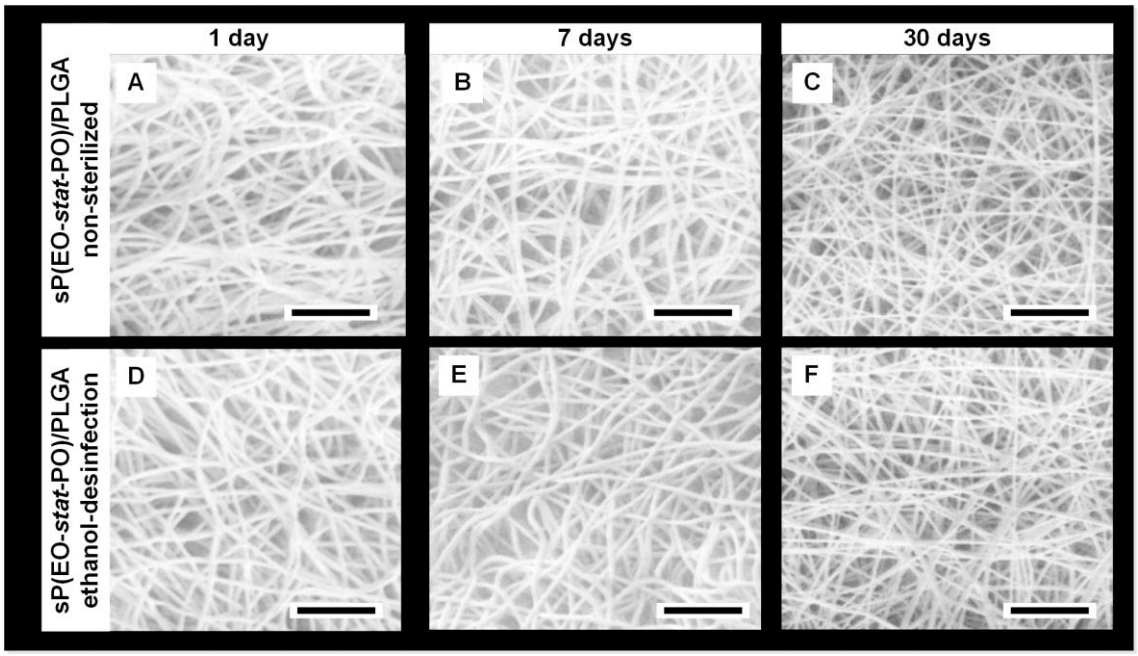

Figure 20: Influence of ethanol-disinfection on fiber morphology.
Morphology of fibers was investigated after 10 minutes of 70 % (v/v) ethanol treatment followed by a (A; D) 1 day (B; E) 7 days and (C; F) 30 days culture in cell culture medium at 37 °C, 5 % CO_2. As a control, non-sterilized membranes were analyzed. Scale bars = 5 µm.

4.1.7 Culture of functionalized membranes under dynamic conditions

Bioreactors are used in tissue engineering applications to provide a tissue-specific physiological environment during tissue maturation. Since the tissue is exposed to greater mechanical forces in the bioreactor system than under static culture conditions, a higher stability of the membrane is essential. Therefore, electrospun membranes were developed with sufficient mechanical stability to be cultured under dynamic culture conditions in a bioreactor system.

4.1.7.1 Electrospinning of PLGA 85/15 polymer

Depending on the application of the membrane, different stabilities and degradation times are needed. For tissues demanding high stabilities, PLGA with an increased amount of poly(D,L-lactide) provides more support due to its slower degradation rate. For dynamic cell culture experiments, PLGA membranes with higher mechanical stabilities are favorable, too. Therefore, a method was established that allows the electrospinning of PLGA 85/15, which has a higher percentage of poly(D,L-lactide) than PLGA 50/50 being used for the static cell culture experiments. Since the molecular weight of the polymer has an influence on viscosity and therefore on the electrospinning behavior, different concentrations of PLGA 85/15 are needed for successful electrospinning compared to PLGA 50/50.

Various concentrations of PLGA 85/15 were prepared for the electrospinning of high quality fibers. Concentrations of 6; 8; 10; 12; 14; 16; 18; 20; 22; 24 and 26 wt% PLGA 85/15 were dissolved in a mixture of acetone and DMSO. Fiber morphologies were observed by SEM (Figure 21). Electrospinning of PLGA 85/15 with concentrations lower than 8 wt% resulted in beaded fibers. Increasing the PLGA 85/15 concentration to 10 wt% led to the formation of defect free fibers. Further increasing the concentration to 16 wt% resulted in uniform fibers. Thus, increasing the concentration from 8 to 16 wt% significantly improved the fiber quality; beads were eliminated and homogeneous fibers were formed. A further increase from 18 wt% to 26 wt% did not improve fiber morphology, but resulted in an increase in fiber diameter due to the higher viscosity of the spinning solution and hence less stretching of the spinning jet.

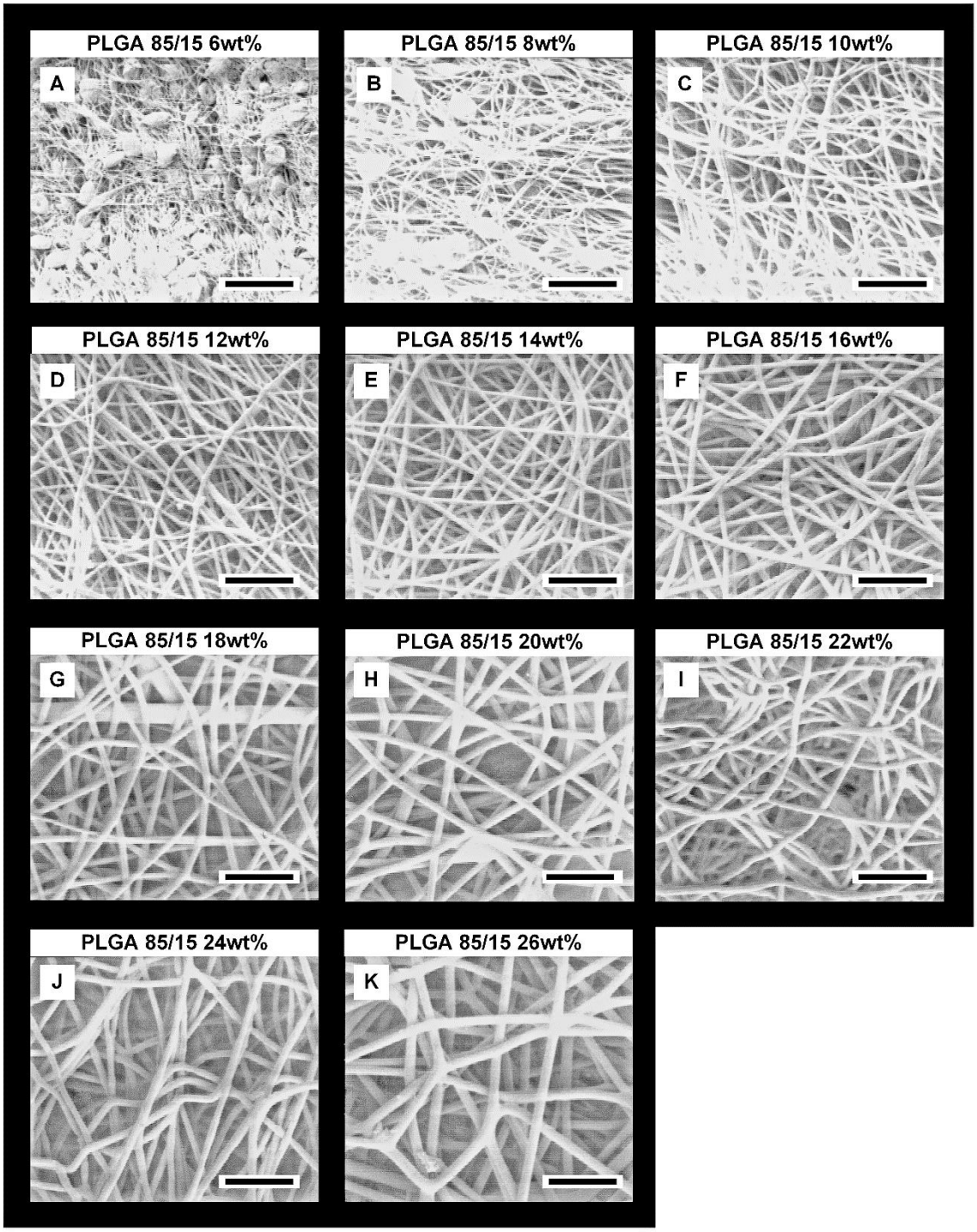

Figure 21: Influence of PLGA 85/15 concentration on fiber morphology.
(A) 6 wt% PLGA 85/15 (B) 8 wt% PLGA 85/15 (C) 10 wt% PLGA 85/15 (D) 12 wt% PLGA 85/15 (E) 14 wt% PLGA 85/15 and (F) 16 wt% PLGA 85/15 (G) 18 wt% PLGA 85/15 (H) 20 wt% PLGA 85/15 (I) 22 wt% PLGA 85/15 (J) 24 wt% PLGA 85/15 and (K) 26 wt% PLGA 85/15 were electrospun and the influence of the polymer concentration on fiber morphology was investigated. Scale bars = 5 µm.

Figure 22 illustrates the fiber diameter for different PLGA 85/15 concentrations. Beaded fibers from 6-8 wt% solutions were not quantified, as it was not possible to get reliable results. Fibers electrospun from a 10 wt% solution resulted in fiber diameters of 250 ± 86 nm. Fiber diameters increased to 732 ± 88 nm for fibers obtained from 26 wt% solutions, which is almost a threefold increase. The optimum concentration for electrospinning experiments was determined to be 16 wt%. Fibers with a diameter of 380 ± 46 nm were obtained and fiber distribution was very uniform. Increasing the concentration of PLGA 85/15 resulted in increased fiber diameters and a mixture of small and thick fibers.

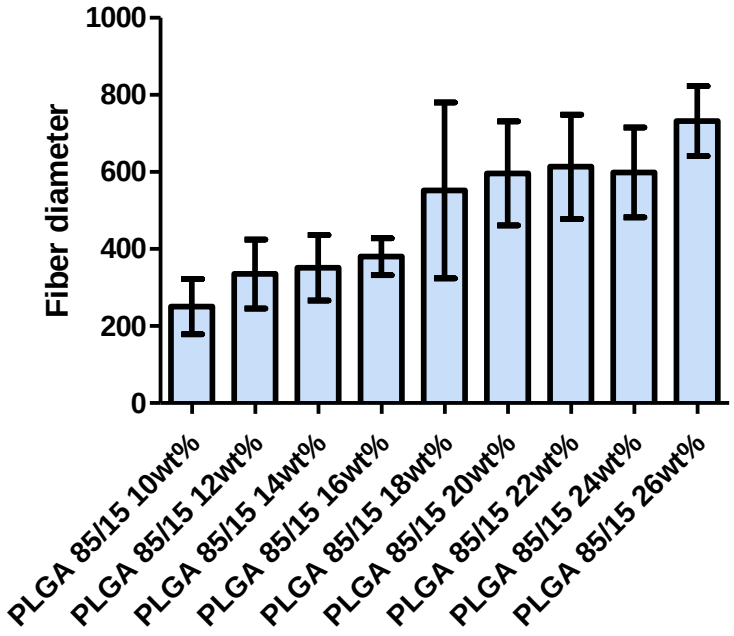

Figure 22: Influence of the PLGA 85/15 concentration on fiber diameter.
The diameter of electrospun fibers from different PLGA 85/15 polymer concentrations was measured. Error bars = SD (n = 100).

4.1.7.2 Influence of NCO-sP(EO-*stat*-PO) on PLGA 85/15 fiber morphology

To suppress protein adsorption and unspecific cell adhesion, NCO-sP(EO-*stat*-PO) was added to the electrospinning solution and the fiber morphology of different sP(EO-*stat*-PO)/PLGA 85/15 concentrations was investigated. Since experiments without NCO-sP(EO-*stat*-PO) demonstrated that concentrations below 8 wt% are unsuitable for electrospinning, these concentrations were not tested with

NCO-sP(EO-*stat*-PO). Figure 23 underlines that a concentration of 8 %wt was not appropriate to produce defect free fibers. Blurred fibers were observed. Increasing the concentration up to 14 wt% improved the fibrous structure. Concentrations of 16-18 wt% PLGA turned the overall structure into homogenous fibers.

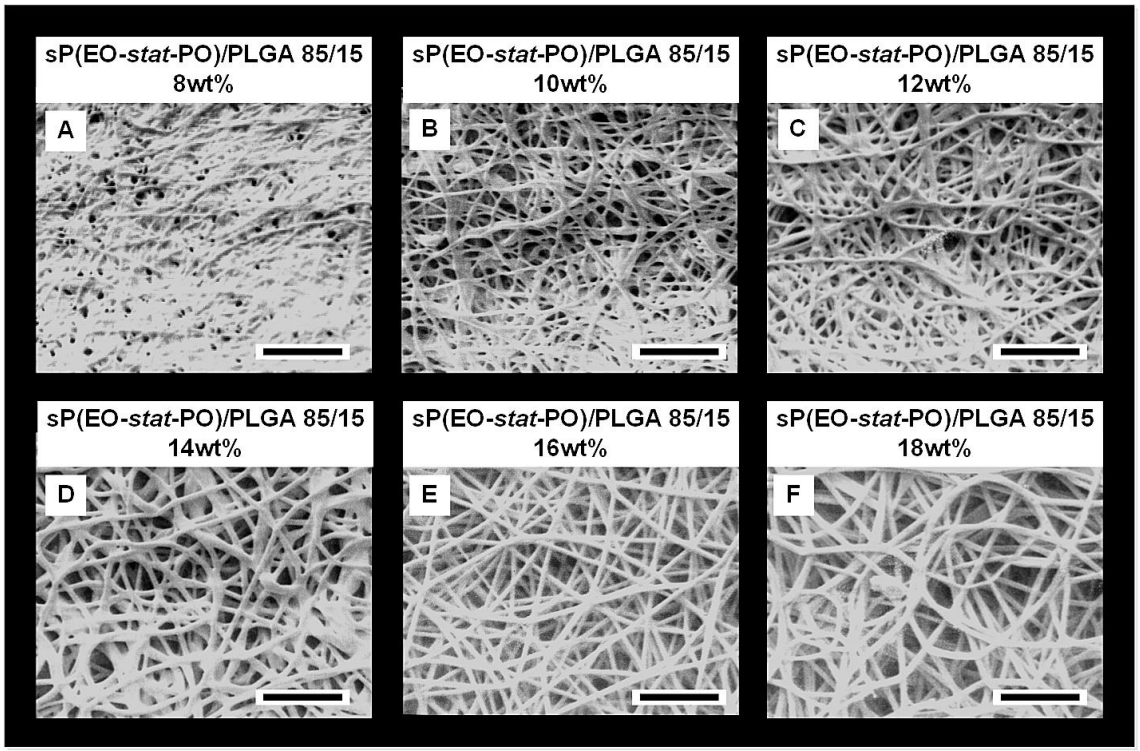

Figure 23: Influence of NCO-sP(EO-*stat*-PO) on PLGA 85/15 fiber morphology. (A) 8 wt% PLGA 85/15 (B) 10 wt% PLGA 85/15 (C) 12 wt% PLGA 85/15 (D) 14 wt% PLGA 85/15 (E) 16 wt% PLGA 85/15 and (F) 18 wt% PLGA 85/15 were electrospun with NCO-sP(EO-*stat*-PO) and the influence of the polymer concentration on fiber morphology was investigated. Scale bars = 5 µm.

Although NCO-sP(EO-*stat*-PO) increases the viscosity of the electrospinning polymer solution, it did not have an influence on the electrospinning characteristics of PLGA 85/15. 16 wt% polymer with and without the addition of NCO-sP(EO-*stat*-PO) was a suitable concentration for electrospinning defect free, homogenous fibers. Quantifying the fiber diameter makes evident that the average diameter of electrospun fibers using 16 wt% PLGA 85/15 decreased from 380 nm to 360 nm due to the addition of NCO-sP(EO-*stat*-PO) (Figure 24).

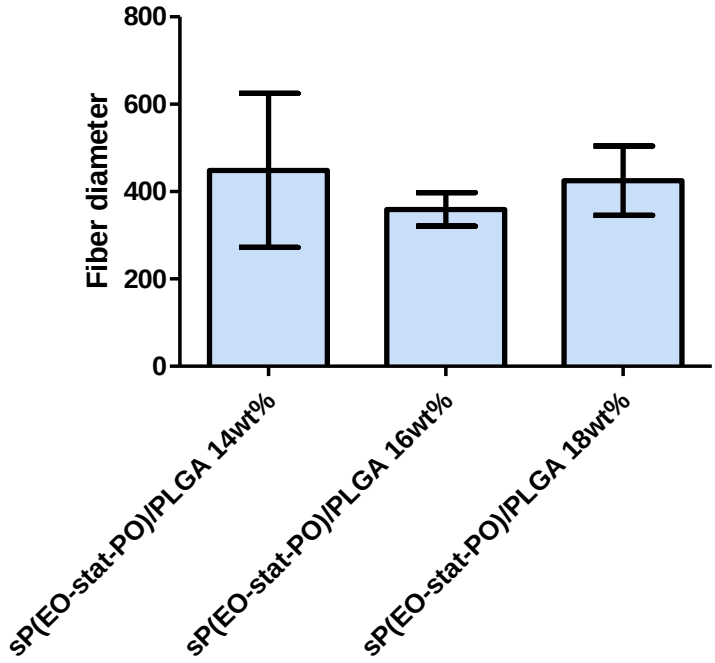

Figure 24: Influence of NCO-sP(EO-*stat*-PO) on PLGA 85/15 fiber diameter.
The fiber diameter of membranes, which were electrospun from polymer solutions containing sP(EO-*stat*-PO) and 14 wt%, 16 wt%, 18 wt% PLGA 85/15 was measured. Error bar represent SD (n = 100).

4.1.7.3 Functionalized membrane for bioreactor system

Two different PLGA polymers, PLGA 85/15 and PLGA 50/50 were electrospun with NCO-sP(EO-*stat*-PO) and cultured for 14 days in a bioreactor at a perfusion rate of 3.8 ml/minute. Moreover, a membrane composed of several layers, an inner layer of hydrophobic PLGA 85/15 and outer layers composed of hydrophilic sP(EO-*stat*-PO)/PLGA 85/15, was investigated under dynamic conditions. The membrane composed of sP(EO-*stat*-PO)/PLGA 50/50 appeared brittle with several holes after 14 days in dynamic culture (Figure 25). The sP(EO-*stat*-PO)/PLGA 85/15 membrane revealed small holes, and the layered membrane was stable over the entire incubation period. Thus, the mixture of hydrophilic and hydrophobic layers improved the mechanical properties and stability of the electrospun membrane.

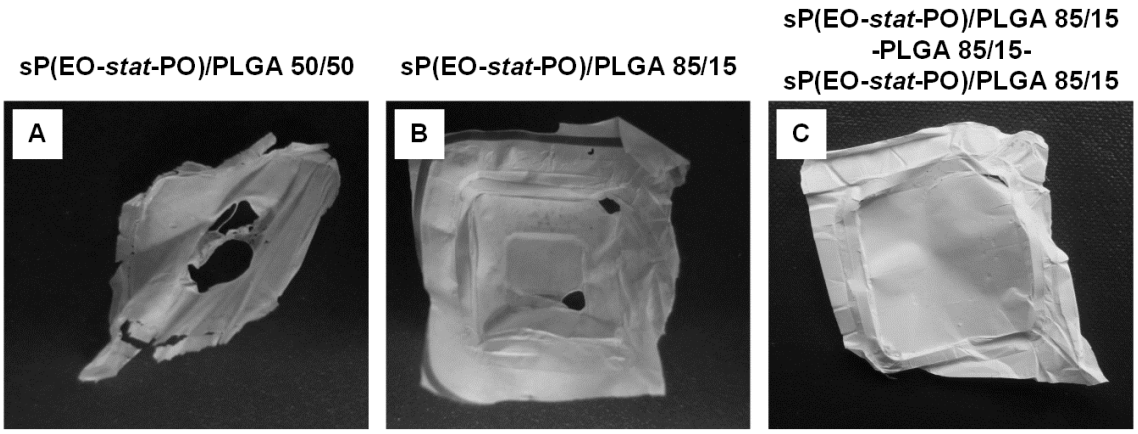

Figure 25: Influence of dynamic culture conditions on membranes.
(A) sP(EO-*stat*-PO)/PLGA 50/50 membrane after 14 days in culture in comparison to (B) a membrane composed of sP(EO-*stat*-PO)/PLGA 85/15 and (C) a membrane composed of an inner layer of hydrophobic PLGA 85/15 and outer hydrophilic layers of sP(EO-*stat*-PO)/PLGA (= sP(EO-*stat*-PO)/PLGA 85/15 - PLGA 85/15 - sP(EO-*stat*-PO) PLGA 85/15).

4.1.8 Summary

Ideally, fibrous meshes, which are used as artificial basement membranes, retain their fibrillar structure in culture, and provide a mechanically supportive environment with large surface to volume ratios. They should be bio-degradable and bio-compatible, and be cultured also under dynamic culture conditions. By fixing membranes in cell crowns, their fibrillar structure could be maintained also in contact with liquids. The membrane integrity and morphology was not affected by including peptide sequences. An inherent limitation of electrospun membranes is the relatively small pore size that does not promote cellular infiltration and tissue ingrowth. Techniques were developed to increase the pore size. These techniques include modification of electrospinning setup and post-electrospinning modifications. However, all methods tested did not result in an increased pore size. Degradation studies revealed that functionalization of the PLGA membranes improved the degradation characteristics. Treatment with 70 % (v/v) ethanol was suitable to avoid contaminations in cell culture experiments. To obtain membranes which can be cultured also under dynamic conditions, membranes containing hydrophobic and hydrophilic layers were established.

4.2 Quantification of immobilized peptides on functionalized membranes

Linking bioactive peptide sequences to the surface of fibers is important for improving their performance and function. However, it is challenging to precisely identify and quantify these functional groups on textile structures. For this purpose, a convenient, surface sensitive assay was developed to measure quantitatively small amounts of peptide sequences linked to complex surfaces like fibrillar membranes. Hence, the method can be used to figure out optimal concentrations of ligands regarding cell adhesion and proliferation. Moreover, coupling conditions can be adapted to improve the performance of the meshes.

4.2.1 Electrospinning of membranes with quantifiable peptides

To determine the amount of immobilized peptides on the surface of the fibers, the UV-detectable group 2-mercaptopyridine was linked to the cysteine flanked fibronectin derived binding sequence serin-glycin-arginine-glycine-aspartate-serin-cysteine (SGRGDSC) via disulfide formation with the thiol group of cysteine. Subsequently, the peptide sequence was dissolved in a mixture of 450 µl acetone, 50 µl DMSO, 30 mg NCO-sP(EO-*stat*-PO) and 143 mg PLGA and used for electrospinning. The peptide binds covalently to the isocyanate group of NCO-sP(EO-*stat*-PO) via the N-terminal serin and thus is present on the surface of the fiber after the electrospinning process.

The disulfide bridge within the peptide was cleaved with the reducing agent tris (2-carboxyethyl) phosphine (TCEP). Cleaving the disulfide bridge of one peptide yields one free 2-mercaptopyridine, which can rearrange to 2-thiopyridone (Figure 26). Both compounds can be measured quantitatively in solution by UV-spectroscopy showing UV-absorption maxima at 270 nm (2-mercaptopyridine) and 343 nm (2-thiopyridone), respectively.

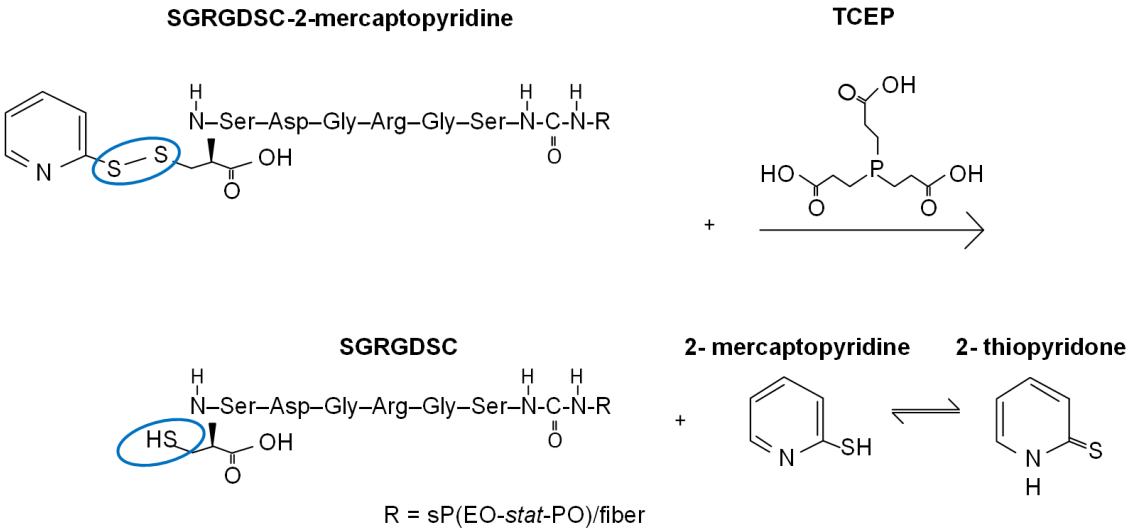

Figure 26: Mechanism of spectrophotometric quantification of peptides.
The peptide sequence SGRGDSC with 2-mercaptopyridine at the C-terminus binds to the isocyanate group of NCO-sP(EO-*stat*-PO) on the surface of the fiber. The disulfide bridge within the peptide is cleaved by aqueous TCEP solution. The released amount of 2-mercaptopyridine and 2-thiopyridone corresponds to the amount of peptide attached to the fiber.

4.2.1.1 UV-maxima of 2-mercaptopyridine

To measure the wavelength of maximum absorbance of 2-mercaptopyridine, the model compound SGRGDSC-2-mercaptopyridine was dissolved in aqueous TCEP solution (pH = 7.4). Thus, 2-mercaptopyridine was cleaved from the peptide and the absorption spectrum could be measured. As displayed in Figure 27, the UV-spectrum of SGRGDSC-2-mercaptopyridine showed two peaks, one at 270 nm corresponding to 2-mercaptopyridine, and one at 343 nm from the tautomer 2-thiopyridone.

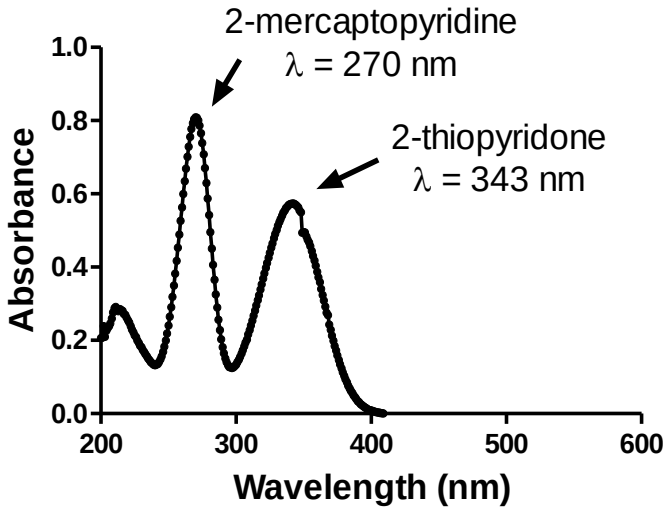

Figure 27: Absorption spectrum of 2-mercaptopyridine.
The absorption spectrum of a solution containing the peptide sequence SGRGDSC-2-mercaptopyridine in TCEP solution (pH = 7.4) was measured.

4.2.1.2 Correlation between peptide concentration and absorbance

To ensure that the splitting of the UV-sensitive group led to quantitative results, the absorbance of pure 2-mercaptopyridine was compared with that of 2-mercaptopyridine from the model peptide SGRGDSC-2-mercaptopyridine. Calibration curves were obtained by adding increasing amounts of peptide and pure 2-mercaptopyridine, respectively to aqueous TCEP solution (pH = 7.4). The results are summarized in Figure 28. The absorption of 2-mercaptopyridine from the peptide was in good agreement to that of pure 2-mercaptopyridine. Moreover, it was observed that there was a linear correlation between the UV-absorbance and the 2-mercaptopyridine cleaved from peptide concentration. The standard curve obtained from the model peptide in TCEP solution was used in further experiments to quantify the amount of peptide attached to the electrospun membranes by measuring the absorbance.

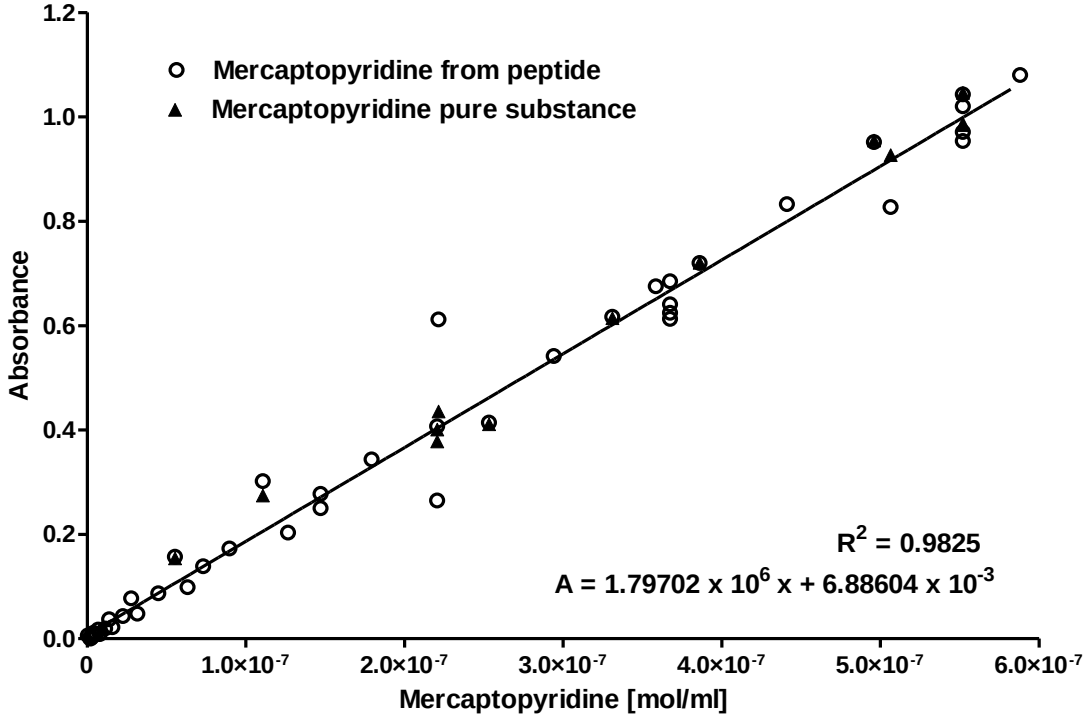

Figure 28: Calibration curve of 2-mercaptopyridine.
Different concentrations of pure 2-mercaptopyridine and SGRGDSC-2-mercaptopyridine were dissolved in TCEP solution. The absorbance of 2-mercaptopyridine was measured with a wavelength of 270 nm (pH = 7.4). The standard curve is used to quantify the amount of peptide in the membrane.

4.2.2 Quantification of peptide concentration

To evaluate the amount of peptides present on the surface of the electrospun membrane, fiber meshes were rinsed in a fixed volume of TCEP solution. Thus, the disulfide bridges within the peptide were reductively broken and 2-mercaptopyridine was measured UV-metrically in the supernatant (Figure 29). Afterward, the amount of peptide embedded in the fibers was analyzed. Therefore, the electrospun membrane was dissolved in 1N NaOH. To split off 2-mercaptopyridine from the peptide in suspension, TCEP was added. The amount of TCEP was chosen so that it was available in excess and neutralized the alkaline NaOH suspension to a pH of 7.4.

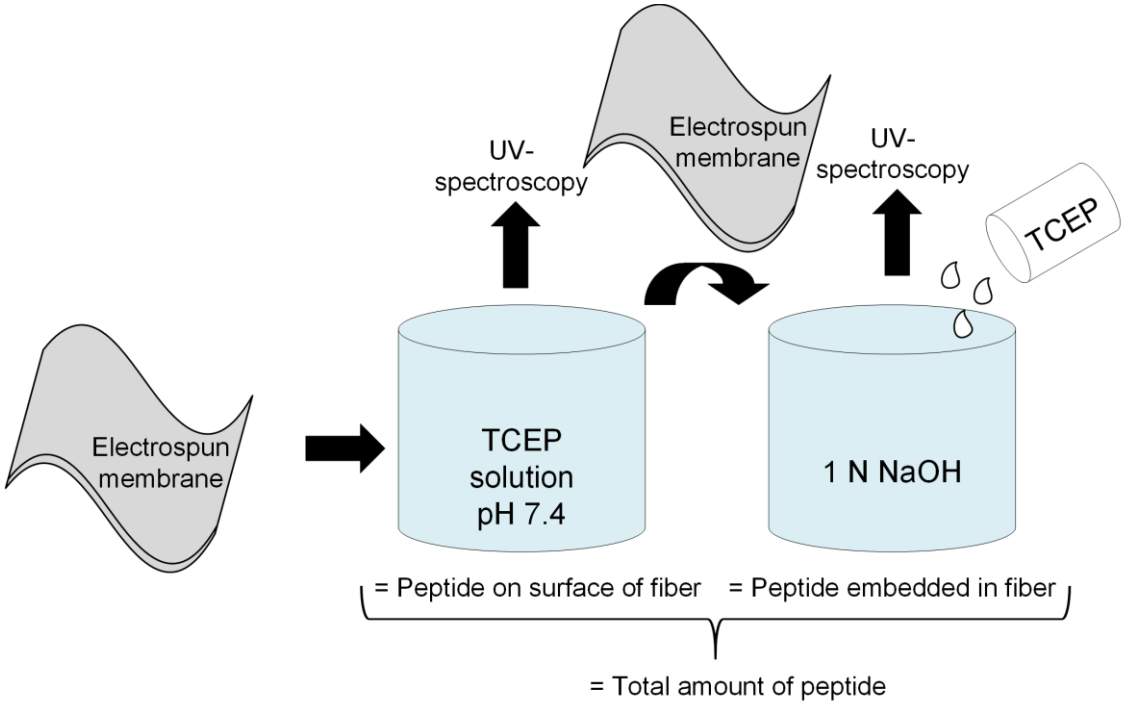

Figure 29: Schematic of quantification of peptide distribution.
To measure the amount of peptide in the membrane, the electrospun mesh was treated with aqueous TCEP solution (pH = 7.4). After 24 hours, the concentration of 2-mercaptopyridine in the solution was determined UV-metrically. To analyze the amount of peptide embedded in the fiber, the membrane was dissolved in 1 N NaOH. TCEP was added to the solution, incubated for 24 hours and the 2-mercaptopyridine concentration was determined by UV-spectroscopy.

Treatment of the electrospun membrane with TCEP solution and subsequently, the analysis of the solution illustrated that an average of 99 % of peptide was present on the surface of the fibers (Figure 30). After dissolving the membrane in 1N NaOH, 1 % of the peptide used for electrospinning was detected. Therefore, only a marginal amount of peptide was embedded in the fibers.

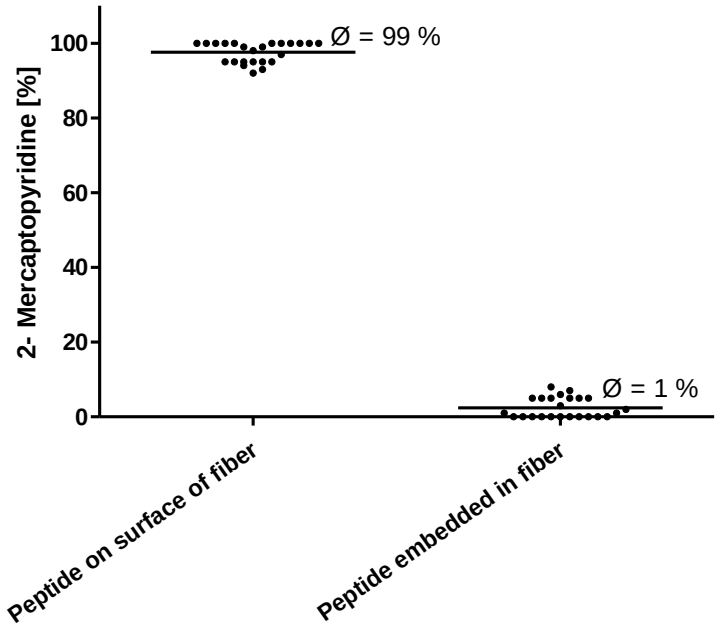

Figure 30: Quantification of peptide distribution.
The amount of peptides on the surface of the fiber was evaluated by treating the membrane with TCEP. Afterward, the membrane was dissolved in 1 N NaOH and the amount of peptide embedded in the fiber was analyzed.

4.2.3 Quantification of peptide binding mode

To quantify how much peptide is covalently attached, non-covalently attached, and embedded in the fibers, the membrane was incubated in deionized water for 24 hours to wash off non-covalently bound peptide. The amount of covalently attached peptide was evaluated by treating the washed membrane with TCEP solution and afterward, measuring the solution UV-metrically. The amount of peptide embedded in the fiber could be analyzed by dissolving the membrane in 1 N NaOH following the addition of TCEP to the suspension to cleave the disulfide bridge within the peptide (Figure 31).

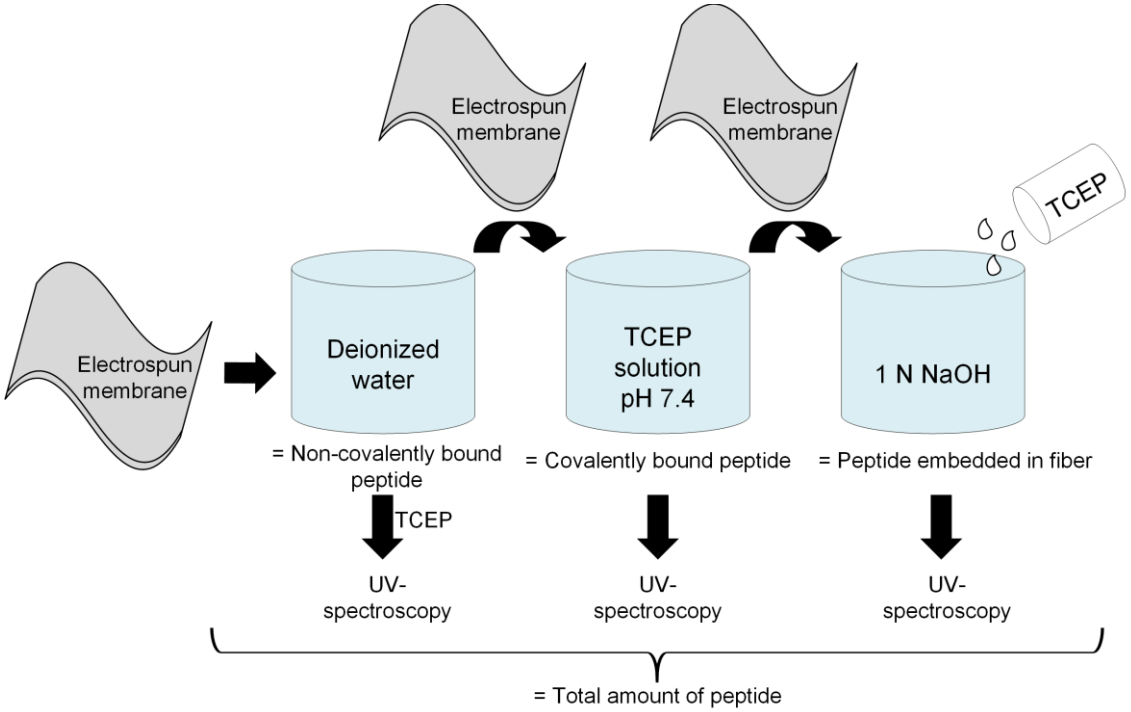

Figure 31: Schematic of quantification of peptide binding mode.
To quantify the amount of non-covalently attached peptide, the electrospun membrane was washed for 24 hours in deionized water. Then, TCEP was added to the washing water. To analyze the covalently attached peptide, the membrane was afterward incubated for 24 hours in TCEP solution (pH = 7.4) and the concentration of 2-mercaptopyridine in the solution was determined UV-metrically. The peptide embedded in the fiber was analyzed by dissolving the membrane in 1 N NaOH and afterward adding TCEP to the suspension.

After incubating the membrane in deionized water, an average of 80 % of the used peptide was measured in the water washings, and was thus non-covalently attached to the fibers. An average of 17 % with respect to the amount used for spinning could be determined as covalently attached to the electrospun membrane. 3 % of the used peptide was embedded in the fiber volume as analyzed by dissolving the complete membrane in 1 N NaOH and adding TCEP (Figure 32).

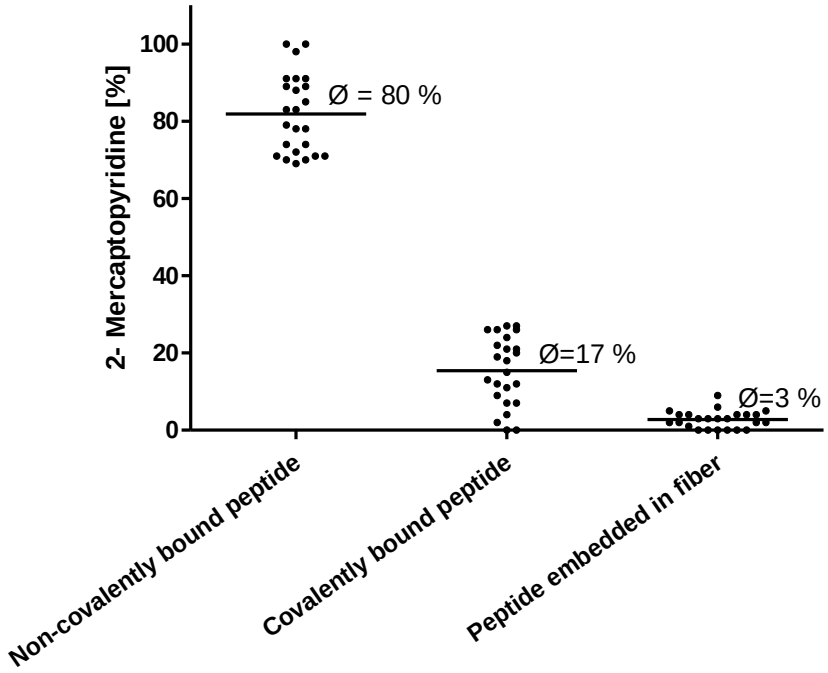

Figure 32: Quantification of peptide binding mode.
The amount of non-covalently bound peptide was determined by washing the membrane with water and adding TCEP to the washing solution. The amount of covalently attached peptide was evaluated by treating the washed membrane with TCEP solution. Afterward, the membrane was dissolved in 1 N NaOH to measure the amount of peptide embedded in the fiber.

4.2.4 Comparison of expected and measured peptide concentration

For quantification experiments, it is important to compare the expected peptide concentration, meaning the used peptide concentration for electrospinning, with the concentration measured in the membrane. Therefore, the measured peptide concentration attached to the fibers and embedded in the fibers were calculated and compared with the peptide concentration used for electrospinning. It is evident from Figure 33, that the majority of the peptide used for electrospinning could be detected in the quantification experiments. For membranes without washing, 98 % of the used peptide was measured and for membranes with washing, 99 % of the used peptide was measured, respectively.

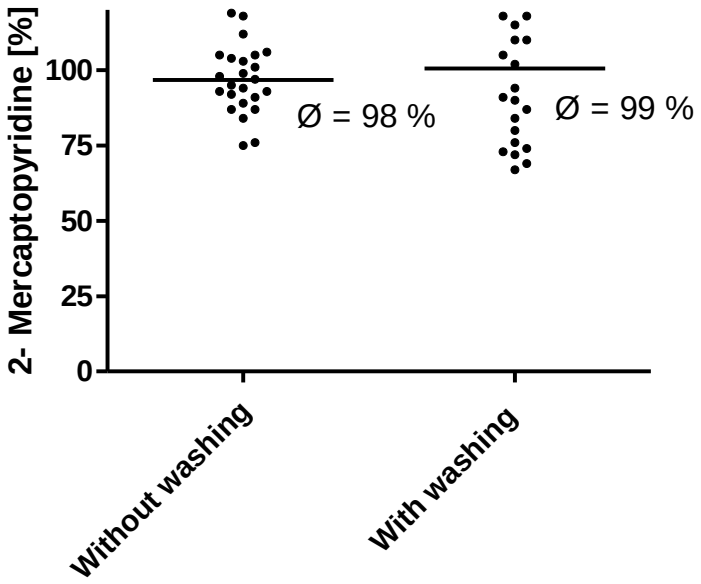

Figure 33: Comparison of expected and measured peptide concentration.
The expected peptide concentration was compared with the measured peptide concentration for membranes without washing and for membranes washed in water before quantification.

4.2.5 Influence of peptide concentration on binding

To evaluate if the amount of peptide used has an influence on peptide binding, membranes with different amounts of mercaptopyridine-modified model peptide sequences were electrospun and used for quantification. Plotting the amount of peptide used for electrospinning against the measured 2-mercaptopyridine concentration shows that the amount of covalently bound peptides increases with the amount used for spinning, while the amount embedded in the fiber volume remained unaffected (Figure 34).

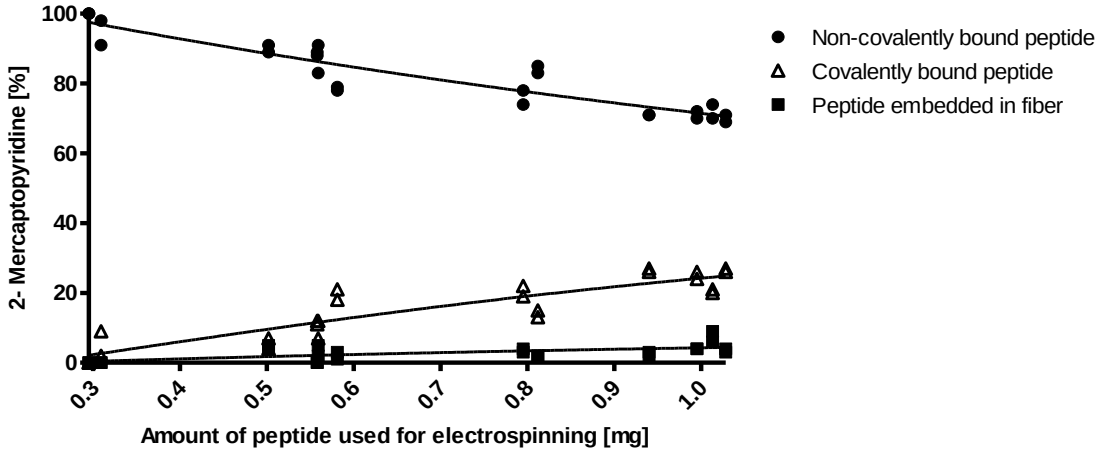

Figure 34: Influence of used peptide on binding.
Different amounts of peptides were used for electrospinning. The ratio of non-covalently bound peptide was compared with the amount of covalently bound peptide and the amount of peptide embedded in the fiber.

4.2.6 Influence of incubation on peptide binding

To analyze the influence of incubation on peptide binding, the ratio of covalently and non-covalently bound peptide was investigated directly after electrospinning without incubation and after 96 hours of incubation post-electrospinning. Comparison of the different membranes revealed that the incubation time after electrospinning had a significant influence on peptide binding (Figure 35). Measurements directly after electrospinning revealed that 94 % of the peptide sequences were non-covalently attached, 0 % covalently attached, and 6 % embedded in the fibers. Incubation of the membrane for 96 hours after electrospinning resulted in 80 % non-covalently attached peptides and 17 % covalently attached peptides, and 3 % of the peptides were embedded in the fiber.

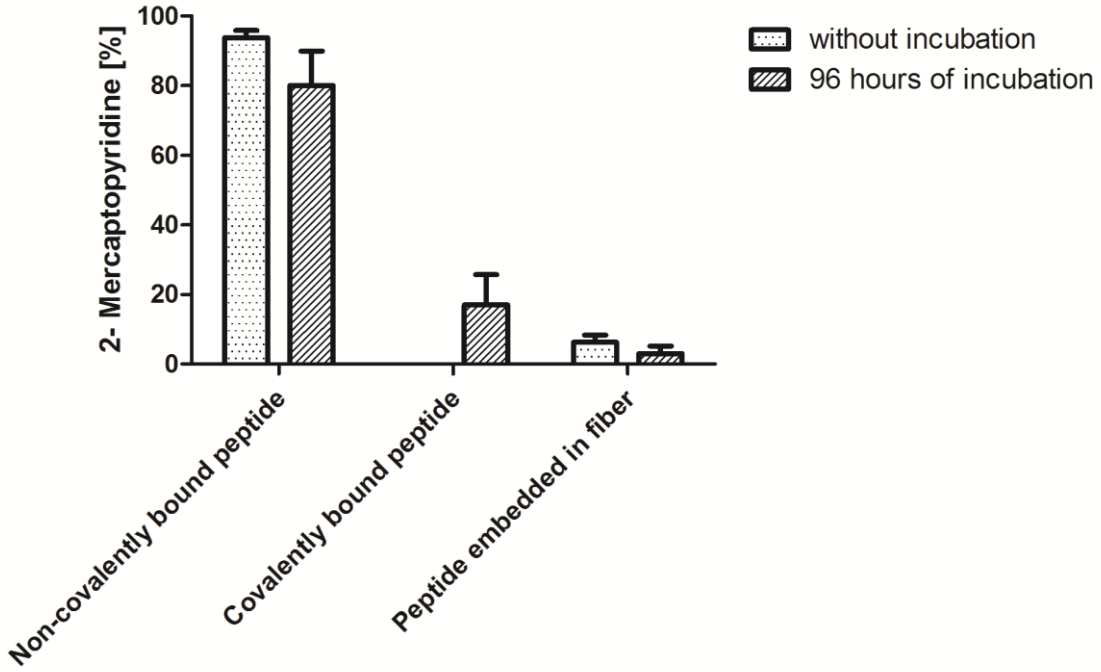

Figure 35: Influence of incubation after electrospinning on binding.
Peptide binding was quantified directly after electrospinning and after 96 hours of incubation at room temperature. The ratio of non-covalently attached peptides was compared with covalently attached peptides and peptides embedded in the electrospun fiber.

4.2.7 Summary

The quantification of peptides on the surface of fibers is both important for cell adhesion and to improve coupling conditions. By combining a peptide sequence with a cleavable and UV-metrically active group, a method was established to quantitatively describe the amount of peptide attached to the fibers. Quantification experiments showed that about 17 % of the peptides were covalently attached to the surface, whereas 80 % were non-covalently attached. Only a marginal amount of peptides were embedded in the fibers and thus not available for cell adhesion. The measured amount of peptides correlated closely to the used amount of mercaptopyridine-modified model peptide sequence. Incubation of the membranes after electrospinning was essential for covalent peptide binding.

4.3 Biological interactions of functionalized membranes in mono-culture

Fibrous membranes with controlled biological interactions are desirable and crucial for tissue engineering applications and for the development of artificial basement membranes. By using the star-shaped multifunctional amphiphilic additive NCO-sP(EO-*stat*-PO) and bioactive peptide sequences derived from extracellular matrix components for electrospinning, fibers with reduced protein adsorption and specific cell adhesion can be generated. To investigate whether the fibrous membranes composed of these functionalized fibers also show persistent protein adsorption, the adsorption of fluorescently labeled bovine serum albumin (BSA) as model protein was studied. In the context of the intended application as artificial basement membrane, the electrospun mesh should be able to support fibroblast adhesion and infiltration, as well as the capacity for keratinocyte adhesion, proliferation and differentiation. Thus, the cellular behavior of these cell types was analyzed on the functionalized membranes.

4.3.1 Protein adsorption on membranes

Protein adsorption studies were performed by incubating PLGA fibers and modified sP(EO-*stat*-PO)/PLGA fibers with BSA-tetramethylrhodamine (Figure 36). BSA is well known for its inherent tendency to deposit on surfaces and acts as a model compound to measure protein adsorption. It is coupled to tetramethylrhodamine to analyze the protein adsorption using fluorescence microscopy.

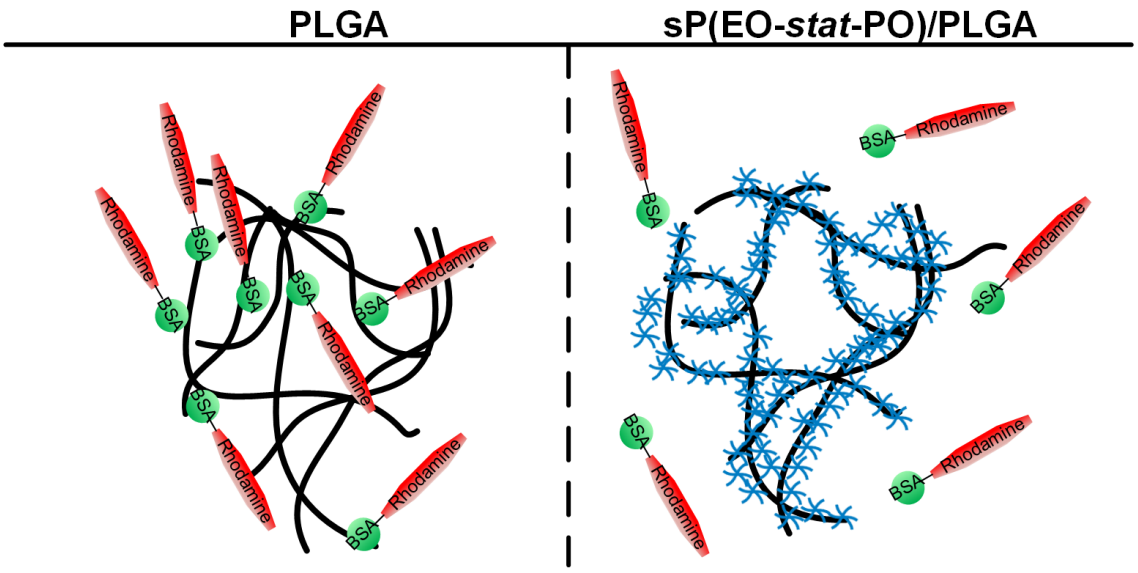

Figure 36: Schematic of protein adsorption studies.
PLGA and sP(EO-*stat*-PO)/PLGA fibers are incubated with fluorescently labeled BSA. Protein adsorption is monitored with fluorescence microscopy.

Fibers were electrospun and stored for 1, 8, 15, 22, 30 days and 2, 5, 9, 12 months in dry state at room temperature. After these time periods, protein adsorption of PLGA meshes was compared to sP(EO-*stat*-PO)/PLGA meshes. At all investigated time points, PLGA membranes showed red fluorescence on the fiber surface, which indicates a homogeneously adsorbed BSA protein layer (Figure 37). The hydrophilic sP(EO-*stat*-PO) minimized the amount of adsorbed BSA resulting in minimal fluorescence. Even after one year of storage at ambient conditions, sP(EO-*stat*-PO)/PLGA meshes retained their protein-repellent characteristics. All images were taken with the same exposure time of 500 ms. Therefore, a qualitative comparison between the samples based on the intensity of fluorescence was possible.

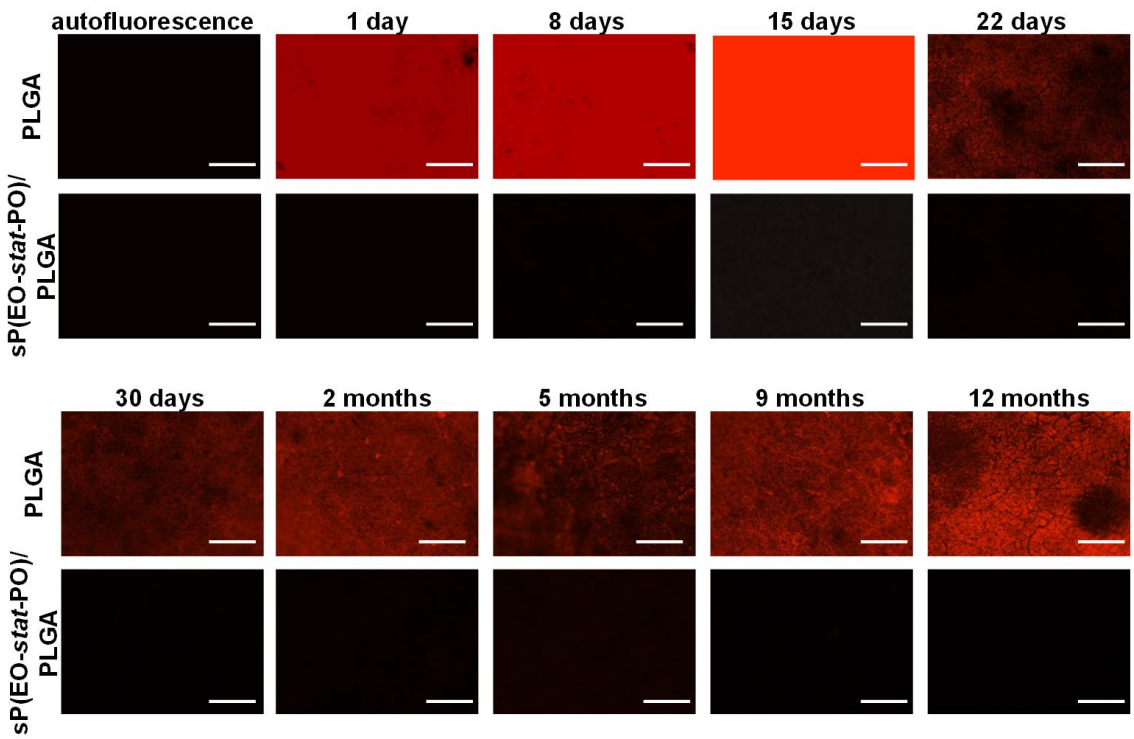

Figure 37: Protein adsorption on functionalized membranes.
Membranes were stored for different time points under ambient conditions and afterward incubated with fluorescently labelled BSA. Red fluorescence indicates protein adsorption. Scale bars = 5 µm.

4.3.2 Fibroblast adhesion and proliferation on membranes

To evaluate whether membranes modified with different peptide sequences can induce selective cell adhesion and whether they have an influence on cell adhesion and proliferation, membranes with peptides derived from major functional binding sequences of the basement membrane were electrospun. More precisely, membranes functionalized with peptide sequences derived from fibronectin (CGRGDS), laminin (CGYIGSR, CGIKVAV) and collagen IV (CGEFYFDLRLKGDK), also applied in the combinations laminin/collagen IV, and fibronectin/laminin/collagen IV were prepared and seeded with primary dermal fibroblasts. Cells were stained with fluorescein diacetate (FDA) and propidium iodide (PI) after 72 hours. To enable the comparison of the differently functionalized membranes, the overall peptide concentration used was the same for all presented surfaces. On membranes containing sP(EO-*stat*-PO)/PLGA/fibronectin (Figure 38A), as well a mixture of sP(EO-*stat*-PO)/PLGA/fibronectin/laminin/collagen IV

(Figure 38E), fibroblasts grew to confluence after 3 days, whereas a reduced amount of cells proliferated on sP(EO-*stat*-PO)/PLGA/laminin/collagen IV (Figure 38D). Fibroblast proliferation was considerably lower on membranes composed of sP(EO-*stat*-PO)/PLGA/laminin (Figure 38B) and sP(EO-*stat*-PO)/PLGA/collagen IV (Figure 38C). Cells barely adhered onto sP(EO-*stat*-PO)/PLGA (Figure 38F) modified fibers without peptide sequences. The well-elongated cell morphology on the functionalized fibers indicates the suitability of the nanostructured membrane for fibroblast proliferation.

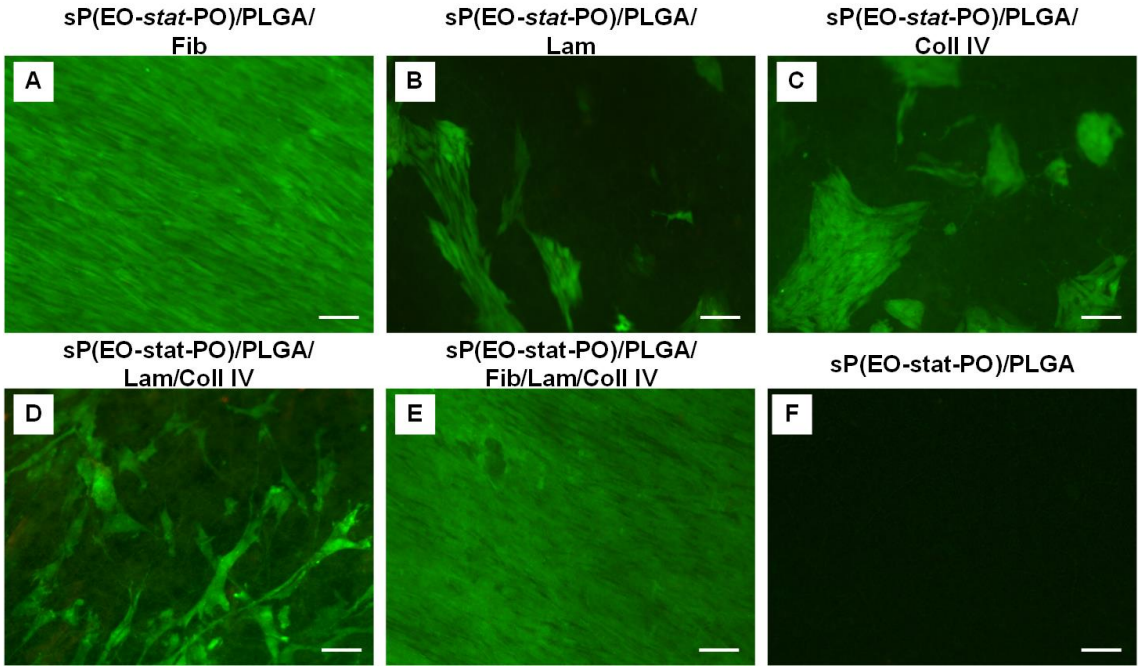

Figure 38: Effect of membranes on fibroblast adhesion.
Live/Dead assay of fibroblasts seeded on membranes modified with (A) sP(EO-*stat*-PO)/PLGA/fibronectin, (B) sP(EO-*stat*-PO)/PLGA/laminin, (C) sP(EO-*stat*-PO)/PLGA/collagen IV, (D) sP(EO-*stat*-PO)/PLGA/laminin/collagen IV and (E) sP(EO-*stat*-PO)/PLGA/fibronectin/laminin/collagen IV after 3 days in culture. Membranes modified with (F) sP(EO-*stat*-PO)/PLGA were used as negative control. The green staining indicates viable cells. Fib = fibronectin, Lam = laminin, Coll IV = collagen IV. Scale bars = 50 µm.

Fibroblast cell numbers, hence cell adhesion and proliferation, were analyzed on the differently functionalized scaffolds after 2, 4, 6, 8 and 10 days in culture using the CellTiter-Fluor™ assay. In contrast to the Live/Dead assay with FDA/PI or the widely used MTT assay, the dye is non-toxic and allows repeated monitoring of the

cell viability and proliferation. The change in color of the dye can be detected spectrometrically. Fibroblasts reached a relative cell number of 30 % on collagen IV and laminin modified membranes after 10 days. The combination of laminin and collagen derived sequences exhibited cell numbers of 57 %, whereas on fibronectin modified membranes, fibroblasts showed cell numbers of 82 %. Fibroblasts attained a cell number of 100 % on membranes functionalized with fibronectin/laminin/collagen IV derived peptide sequences (Figure 39). A marginal number of cells proliferated on sP(EO-*stat*-PO)/PLGA membranes without peptide sequences. The results show that both fibronectin modified and fibronectin/laminin/collagen IV modified membranes promoted fibroblast adhesion and proliferation relevantly.

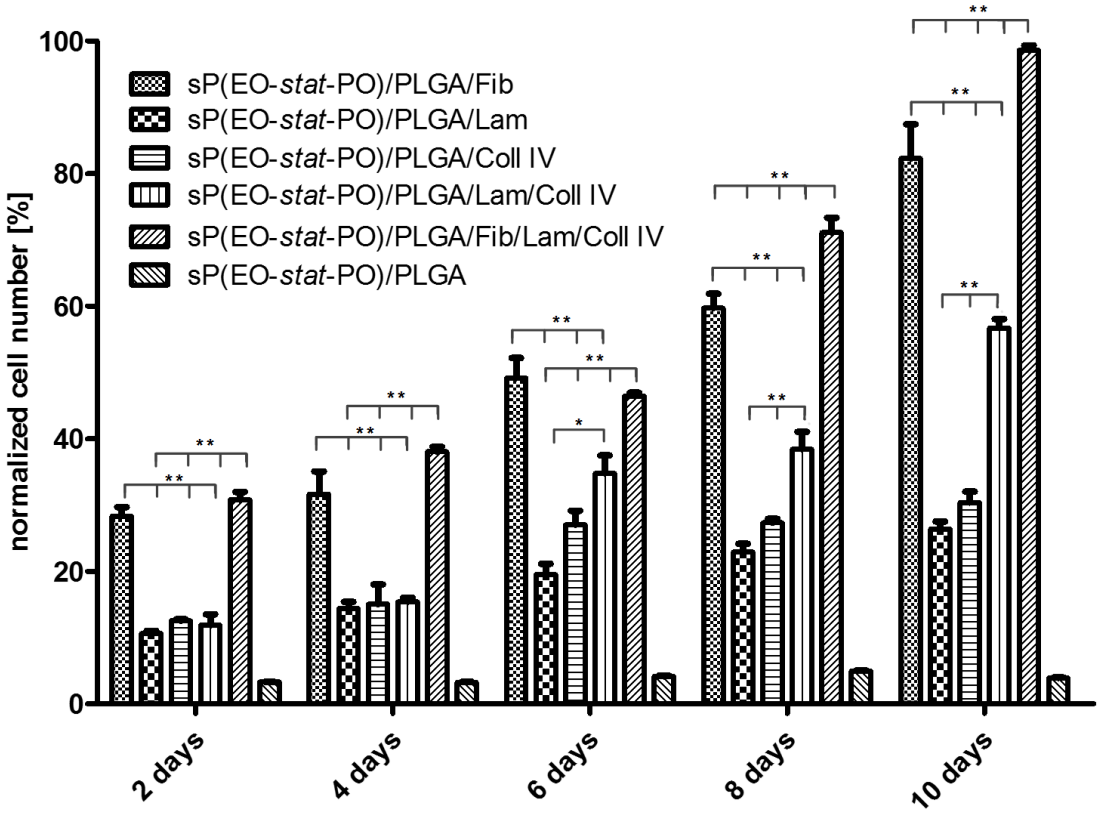

Figure 39: Quantification of fibroblast growth on functionalized membranes. Proliferation of fibroblasts was assessed by CellTiter-Fluor™ cell viability assay after 2, 4, 6, 8, and 10 days in culture. Fib = fibronectin, Lam = laminin, Coll IV = collagen IV. Error bars represent SD (n = 3). Statistical relevant differences are indicated with *$p < 0.05$, **$p < 0.01$.

SEM images on sP(EO-*stat*-PO)/PLGA/fibronectin/laminin/collagen IV membranes confirmed that fibroblasts adhered and spread on the substrate, indicating good interactions of the cells with the electrospun surface. A confluent cell layer of elongated fibroblasts was formed. It was also possible to observe the microvilli of the fibroblasts (Figure 40). Some cells showed a spherical morphology.

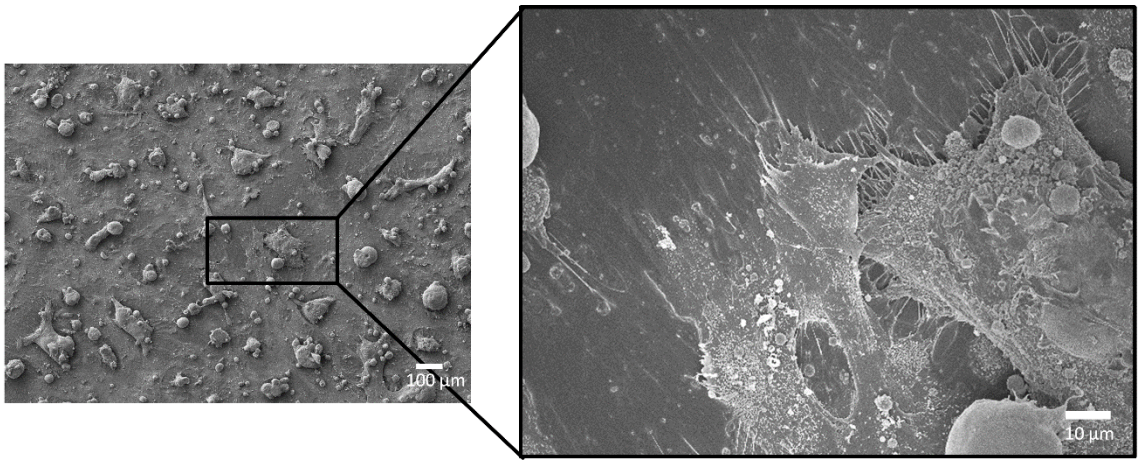

Figure 40: SEM micrographs of fibroblasts on functionalized membranes.
Fibroblasts were seeded on electrospun membranes modified with sP(EO-*stat*-PO)/PLGA/fibronectin/laminin/collagen IV derived peptide sequences. SEM images were performed after 24 hours in culture.

4.3.3 HaCaT adhesion and proliferation on membranes

The influence of differently functionalized membranes was also investigated for HaCaT cells. Meshes functionalized with peptide sequences derived from fibronectin (CGRGDS), laminin (CGYIGSR, CGIKVAV) and collagen IV (CGEFYFDLRLKGDK) were prepared. Moreover, peptide sequences were applied in the combination laminin/collagen IV, and fibronectin/laminin/collagen IV. As for fibroblast experiments, the overall amount of peptides used for the preparation of the different meshes was identical. The keratinocyte cell line was seeded on the membranes, and Live/Dead staining was performed after 72 hours. Cells adhered well to the membranes, showed typical cell morphology and grew to confluence on sP(EO-*stat*-PO)/PLGA/fibronectin membranes (Figure 41A), as well as on sP(EO-*stat*-PO)/PLGA/laminin/collagen IV membranes (Figure 41D) and sP(EO-*stat*-PO)/PLGA/fibronectin/laminin/collagen IV membranes (Figure 41E) after 3 days. On sP(EO-*stat*-PO)/PLGA/collagen IV membranes (Figure 41C) and

sP(EO-*stat*-PO)/PLGA/laminin membranes (Figure 41B), a significantly reduced number of HaCaT cells grew in clusters and proliferated. Only a marginal number of HaCaT cells adhered to sP(EO-*stat*-PO)/PLGA (Figure 41F) fibers without peptides. The cells maintained a normal phenotypic shape, suggesting that all functions of the cells are preserved as in their native environment.

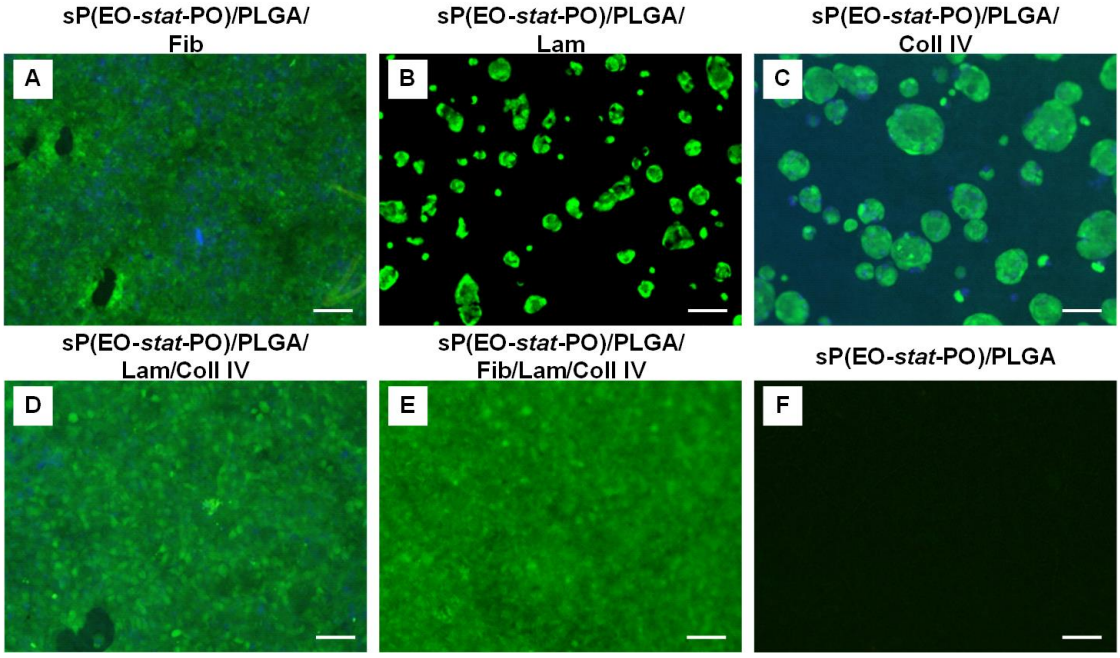

Figure 41: Effect of membranes on HaCaT adhesion.
Live/Dead staining of HaCaT cells after 3 days in culture on membranes modified with sP(EO-*stat*-PO) and different peptide sequences. The green staining indicates viable cells. HaCaT proliferation was investigated for (A) sP(EO-*stat*-PO)/PLGA/fibronectin, (B) sP(EO-*stat*-PO)/PLGA/laminin, (C) sP(EO-*stat*-PO)/PLGA/collagen IV (D) sP(EO-*stat*-PO)/PLGA/laminin/collagen IV and (E) sP(EO-*stat*-PO)/PLGA/fibronectin/laminin/collagen IV membranes. (F) sP(EO-*stat*-PO)/PLGA fibers were analyzed as negative control. Fib = fibronectin, Lam = laminin β1 and laminin α1, Coll IV = collagen IV. Scale bars = 50µm.

Determination of the cell numbers after 2, 4, 6, 8, and 10 days revealed that HaCaT cells proliferated strongly on sP(EO-*stat*-PO)/PLGA/fibronectin membranes and sP(EO-*stat*-PO)/PLGA/fibronectin/laminin/collagen IV membranes. In contrast to fibroblasts, HaCaT cells also grew to confluence on sP(EO-*stat*-PO)/PLGA/laminin/collagen IV membranes (Figure 42). Slight differences in cell proliferation were observed on sP(EO-*stat*-PO)/PLGA/laminin membranes and on sP(EO-*stat*-PO)/PLGA/collagen IV membranes. Both

membranes led to a reduction of over 60 % in cell number compared to membranes modified with a combination of laminin/collagen type IV derived binding sequences. A negligible number of cells proliferated on sP(EO-*stat*-PO)/PLGA membranes without peptide sequences.

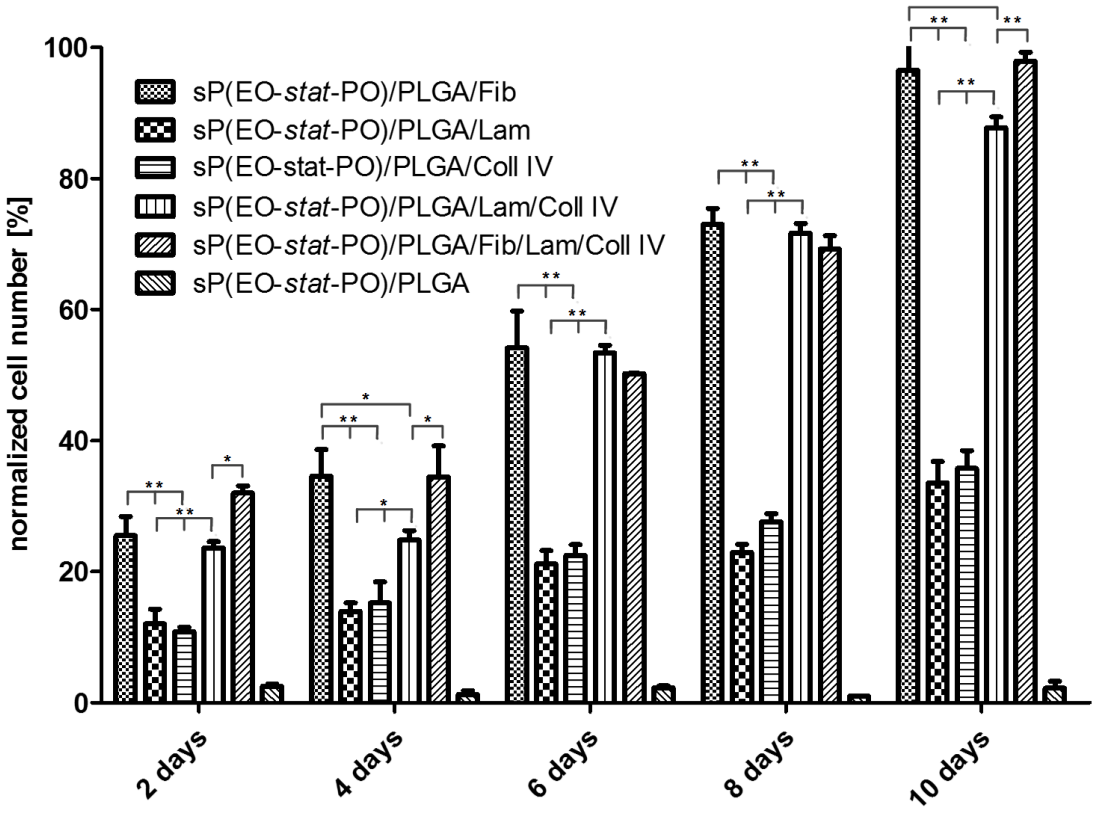

Figure 42: Quantification of HaCaT growth on functionalized membranes.
Proliferation of HaCaT cells was assessed by CellTiter-Fluor™ cell viability assay after 2, 4, 6, 8, and 10 days in culture. Fib = fibronectin, Lam = laminin, Coll IV = collagen IV. Error bars represent SD (n = 3). Statistical relevant differences are indicated with *$p < 0.05$, **$p < 0.01$.

SEM images on sP(EO-*stat*-PO)/PLGA/fibronectin/laminin/collagen IV membranes revealed that HaCaT cells grew to confluence similar to fibroblasts. Cells exhibited flattened morphologies. Characteristic microvilli were visible on the surface of the cells. HaCaT cells were more connected to each other and formed a denser network compared to fibroblasts (Figure 43).

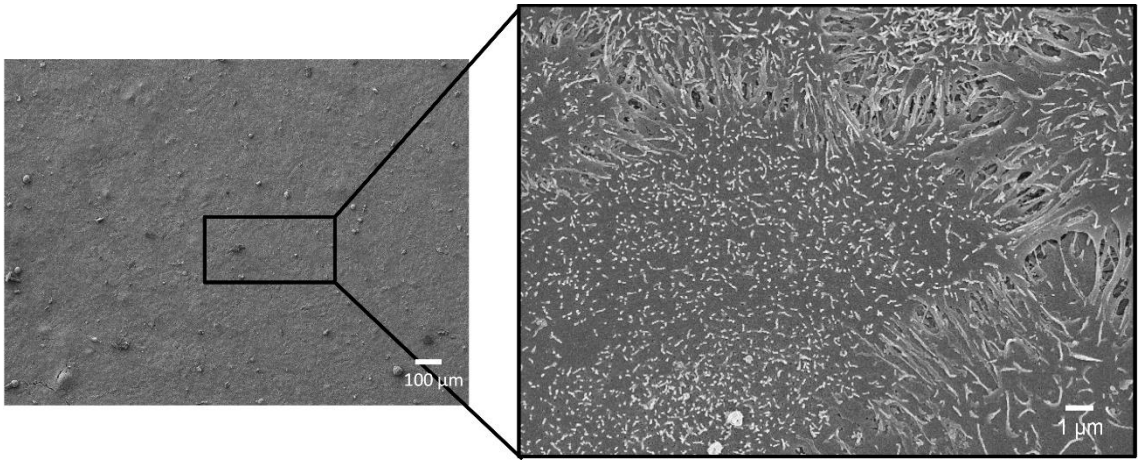

Figure 43: SEM micrographs of HaCaT cells on functionalized membranes.
HaCaT cells were seeded on electrospun membranes modified with sP(EO-*stat*-PO)/PLGA/fibronectin/laminin/collagen IV peptide sequences. SEM images were performed after 24 hours in culture.

4.3.4 Summary

To enable the use of the functionalized meshes as artificial basement membranes, minimal protein adsorption and specific cell adhesion are indispensable. Whereas electrospun PLGA membranes induced strong protein adsorption, addition of the NCO-sP(EO-*stat*-PO) resulted in a significant reduction of the fluorescently labeled model protein, indicating minimized nonspecific protein adsorption. The protein-repellent properties of the functionalized membrane were stable for up to one year when stored under ambient conditions. Cell culture experiments illustrated the ability of the meshes to induce specific cellular interactions in terms of cell adhesion, spreading and proliferation. Fibroblasts strongly adhered to membranes functionalized with fibronectin and fibronectin/laminin/collagen IV derived peptide sequences, while membranes modified with laminin/collagen IV and fibronectin/laminin/collagen IV derived peptide sequences were identified as a suitable substrate for HaCaT cells. sP(EO-*stat*-PO)/PLGA membranes without peptide sequences did not induce adhesion of fibroblasts and HaCaT cells.

4.4 Functionalized membranes for skin tissue engineering

Electrospinning has been recognized as an efficient technique to produce meshes that structurally mimic natural basement membranes. To provide not only the structural similarity, but also the functional analogy to the *in vivo* situation and to guide cells to maintain shape, orientation, migration and differentiation, electrospun membranes were modified with bioactive peptide sequences derived from fibronectin (CGRGDS), laminin (CGYIGSR, CGIKVAV), and collagen type IV (CGEFYFDLRLKGDK), all major constituents of the natural basement membrane. By combining different electrospinning solutions in one membrane, bipolar (bi-layered) membranes could be designed. Both the isotropic and bipolar membranes were exemplary used as membranes for the culture of skin cells. Thereby, the potential of the membranes to promote cellular adhesion, infiltration, tissue development and new extracellular matrix formation was investigated.

4.4.1 Isotropic membranes for skin tissue engineering

Mono-culture experiments showed that fibronectin, laminin, and collagen type IV functionalized membranes present suitable substrates for fibroblasts and for HaCaT cells. Therefore, isotropic PLGA membranes were electrospun with NCO-sP(EO-*stat*-PO), the fibronectin binding sequence CGRGDS, two laminin binding sequences CGYIGSR and CGIKVAV, as well as the collagen type IV binding sequence CGEFYFDLRLKGDK. The membrane was investigated for its functionality as artificial basement membrane in a co-culture model with HaCaT cells and fibroblasts.

Electrospinning of PLGA with NCO-sP(EO-*stat*-PO) and bioactive peptide sequences allowed the production of sheet-like membranes. In Figure 44A, the macroscopical and microscopical structure of the electrospun membranes is shown. The star-shaped NCO-sP(EO-*stat*-PO) macromers connected to the fibronectin, laminin, and collagen type IV derived peptide sequences arranged on the surface of the PLGA fibers and are therefore available for cell adhesion. In Figure 44B, the construction of the co-culture model is depicted. Cell crowns were used to fix the membrane in a

firm, adjustable position. At day 0, fibroblasts were seeded on top of the electrospun membrane. After 7 days under submerged culture conditions, the electrospun membrane was inverted and HaCaT cells were seeded on the other side of the matrix. The tissue equivalent was further cultured for 7 days under submerged conditions. Afterward, the amount of medium was reduced so that the upper side of the membrane was exposed to air (air-liquid interface culture). At day 28, the models were used for evaluation.

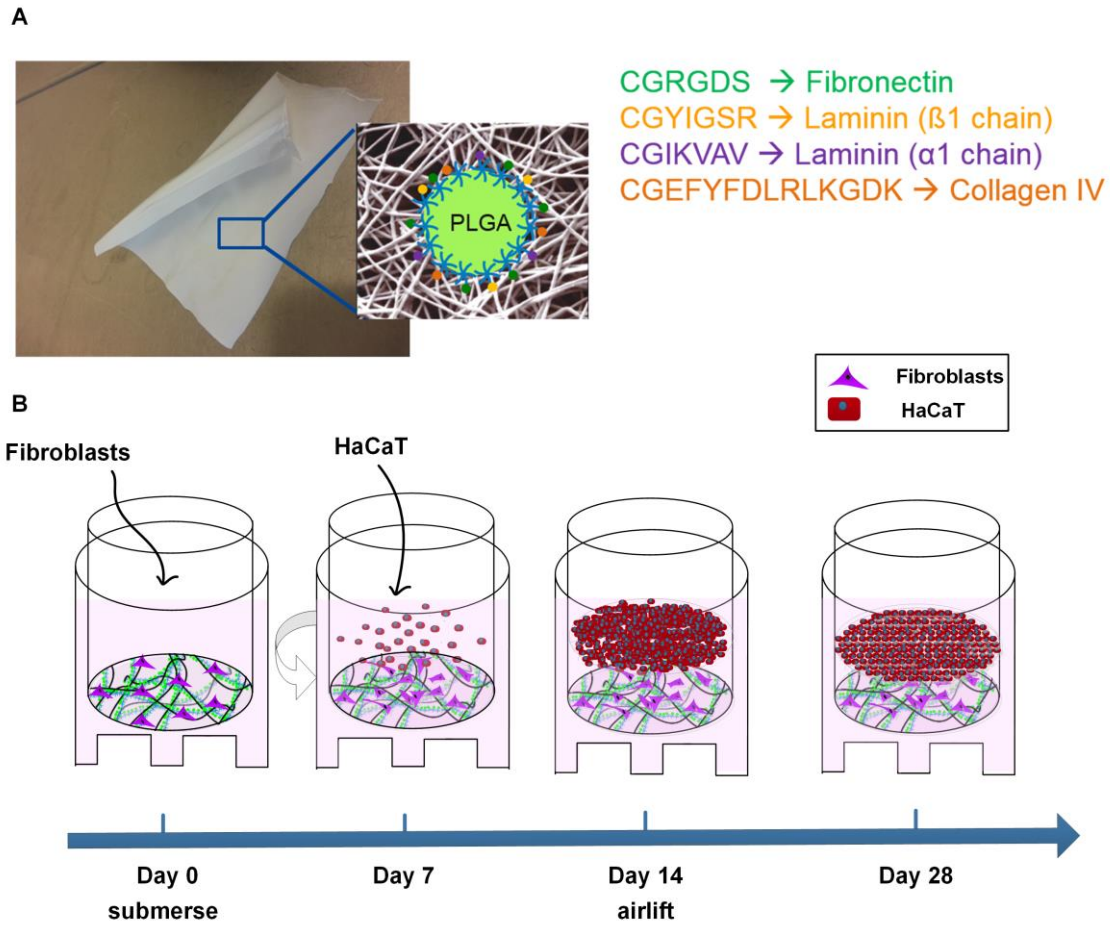

Figure 44: Engineering of co-culture model on isotropic membrane.
(A) Macroscopical and microscopical structure of the functionalized isotropic membranes. (B) Membranes containing the peptide sequences CGRGDS, CGYIGSR, CGIKVAV and CGEFYFDLRLKGDK were electrospun and fixed in cell crowns. At day 0, fibroblasts were seeded on the upper side of the electrospun matrix. At day 7, membranes were inverted and HaCaT cells were seeded on the other side of the membrane. At day 14, the medium was changed to air-liquid interface. At day 28, the models were used for evaluation.

To establish a membrane in close biomimicry to the natural basement membrane, cell infiltration and appropriate differentiation is desirable. Histological cross-section of the tissue model demonstrated that on the upper side of the membrane, HaCaT cells formed several layers consisting of basal cells with cuboid shape and of suprabasal cells showing a flattened appearance. Fibroblasts migrated in the membrane and formed a closed layer on the lower side of the membrane (Figure 45).

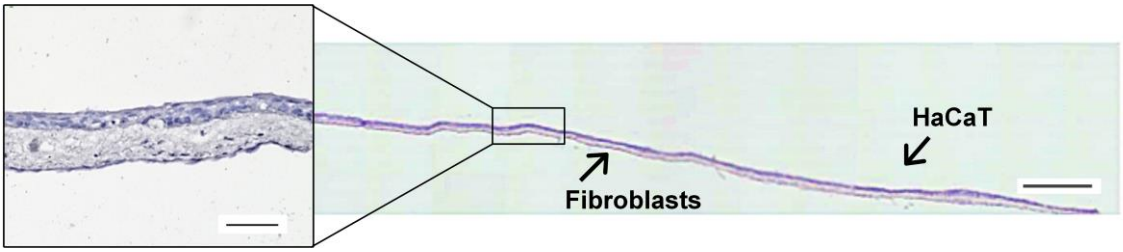

Figure 45: Histology of co-culture model on isotropic membrane.
After 28 days in culture, co-culture models of fibroblasts and HaCaT cells were fixed, cross-sectioned, and an overview staining was performed. Scale bar = 50 µm for magnified H&E staining and 500 µm for the cross-section of the entire model.

Cytokeratin 10 (CK 10), a marker for keratinized epithelium, was expressed in the suprabasal layers of the construct (Figure 46). Basal cells were positive for the early differentiation marker cytokeratin 14 (CK 14). Vimentin staining confirmed the ingrowth of fibroblasts in the membrane. The immunostaining of the co-culture model correlated with that of native skin with the markers in the model being expressed in the same regions.

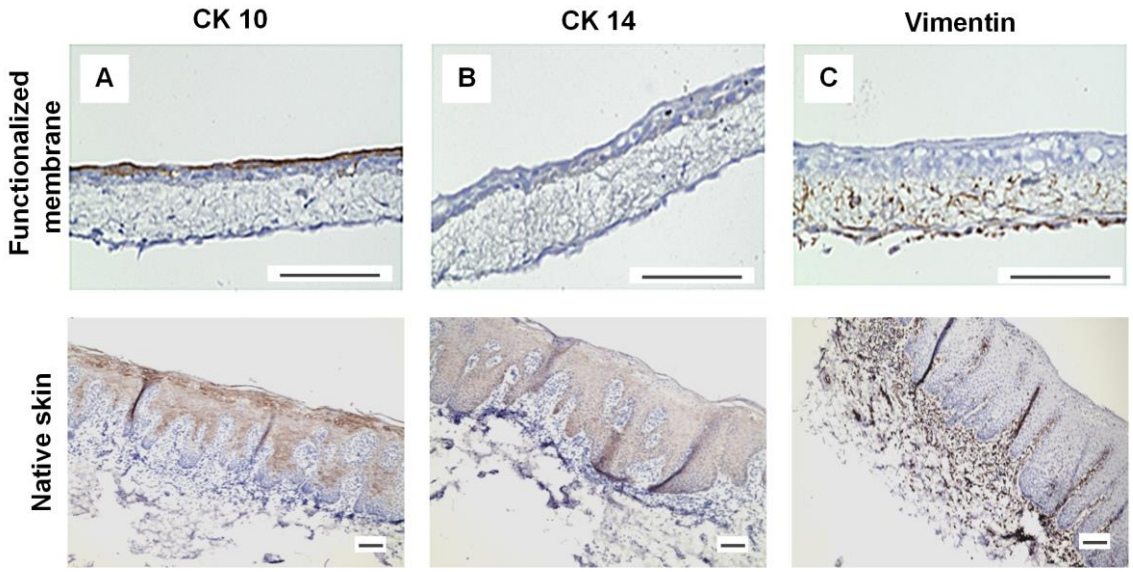

Figure 46: Immunohistochemistry of cell markers on isotropic membrane.
(A) CK 10, (B) CK 14 and (C) vimentin staining of reconstructed skin equivalents in comparison to native human skin. Scale bars indicate 100 µm for electrospun matrix and 200 µm for native skin.

For a reconstructed tissue model it is not only important that cells are positive for typical cell markers, but also that cells start to remodel their microenvironment by producing tissue-specific extracellular matrix proteins. As displayed in Figure 47, the most abundant extracellular matrix components collagen type IV (Coll IV) and laminin type V, as well as fibronectin, collagen type I (Coll I), and collagen type III (Coll III), were synthesized by HaCaT cells and fibroblasts. The expression of the extracellular matrix proteins was consistent with the stainings obtained in native human skin. To ensure that the antibodies did not stain the peptide sequences incorporated into the membrane, electrospun fibers without cells were stained with the same antibodies. No staining could be observed on the negative controls.

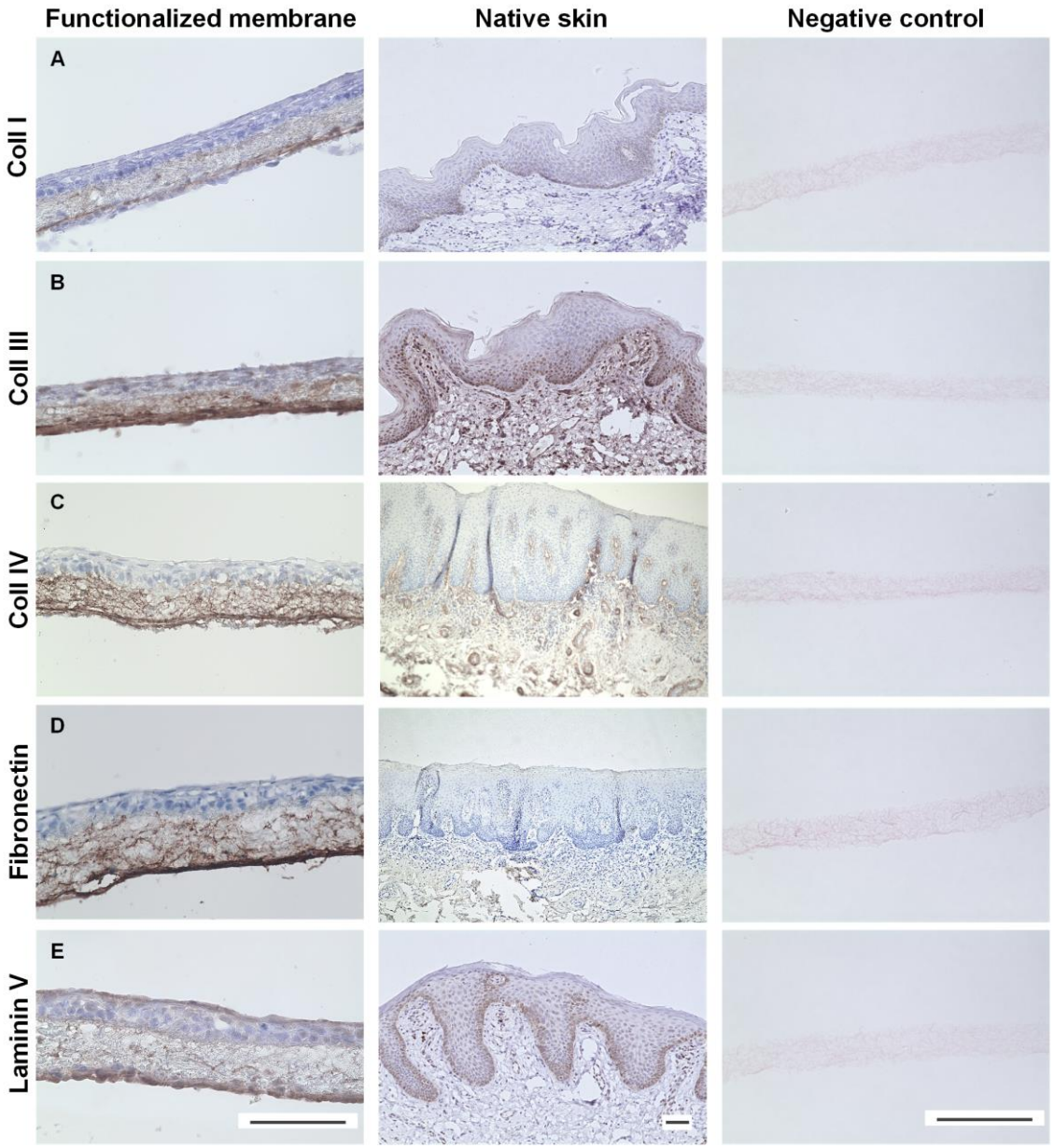

Figure 47: Immunohistochemistry of remodeling on isotropic membrane.
After 28 days in culture, models were stained for (A) Coll I, (B) Coll III, (C) Coll IV, (D) Fibronectin, and (E) Laminin V. Membranes without cells were analyzed to confirm that antibodies did not stain peptide sequences included in the membrane. Scale bars = 100 µm.

Extensive studies showed that fibroblast, as well as HaCaT cell adhesion, strongly depends on the peptide sequences. By combining different peptide sequences it was possible to build up a co-culture model of HaCaT keratinocytes and fibroblasts. The cells spatially organized in the membrane when cultured at an air-liquid interface,

produced tissue-specific extracellular matrix components and supported cellular in-growth.

4.4.2 Bipolar membranes for skin tissue engineering

Since natural basement membranes are a fusion of two laminae, the basal lamina and the reticular lamina, we intended to develop a bipolar (bi-layered) membrane which is able to mimic this situation *in vitro*. The one-step preparation of functionalized fibers allowed the production of a membrane with different bioactive substances on both sides. Since the collagen and laminin content in the basal lamina is increased in comparison to the reticular lamina with an increased amount of fibronectin, the intention was to model this situation in the electrospun matrix. Therefore, a solution containing fibronectin derived peptide sequences was electrospun on a rotating collector and on top a solution containing collagen type IV and laminin derived peptide sequences. The side containing fibronectin derived peptides later served for fibroblasts, the other side containing collagen type IV and laminin derived peptides for HaCaT cells.

The composition of the bi-layered membrane is indicated in Figure 48A. The upper side of the membrane was functionalized with the laminin β1 derived binding sequence CGYIGSR, shown in yellow, with the laminin α1 derived binding sequence CGIKVAV shown in purple, and with the collagen type IV derived binding sequence CGEFYFDLRLKGDK shown in orange. The lower side of the membrane was modified with the fibronectin peptide sequence CGRGDS, illustrated in green. The tissue model based on the bipolar membrane was built up as mentioned in Figure 48B. The membrane was fixed in a firm position and seeded with fibroblasts. After 7 days, the membrane was inverted and HaCaT cells were added to the other side. At day 14 of culture, submerged culture conditions were changed to air-liquid interface. The models were evaluated after 28 days in culture.

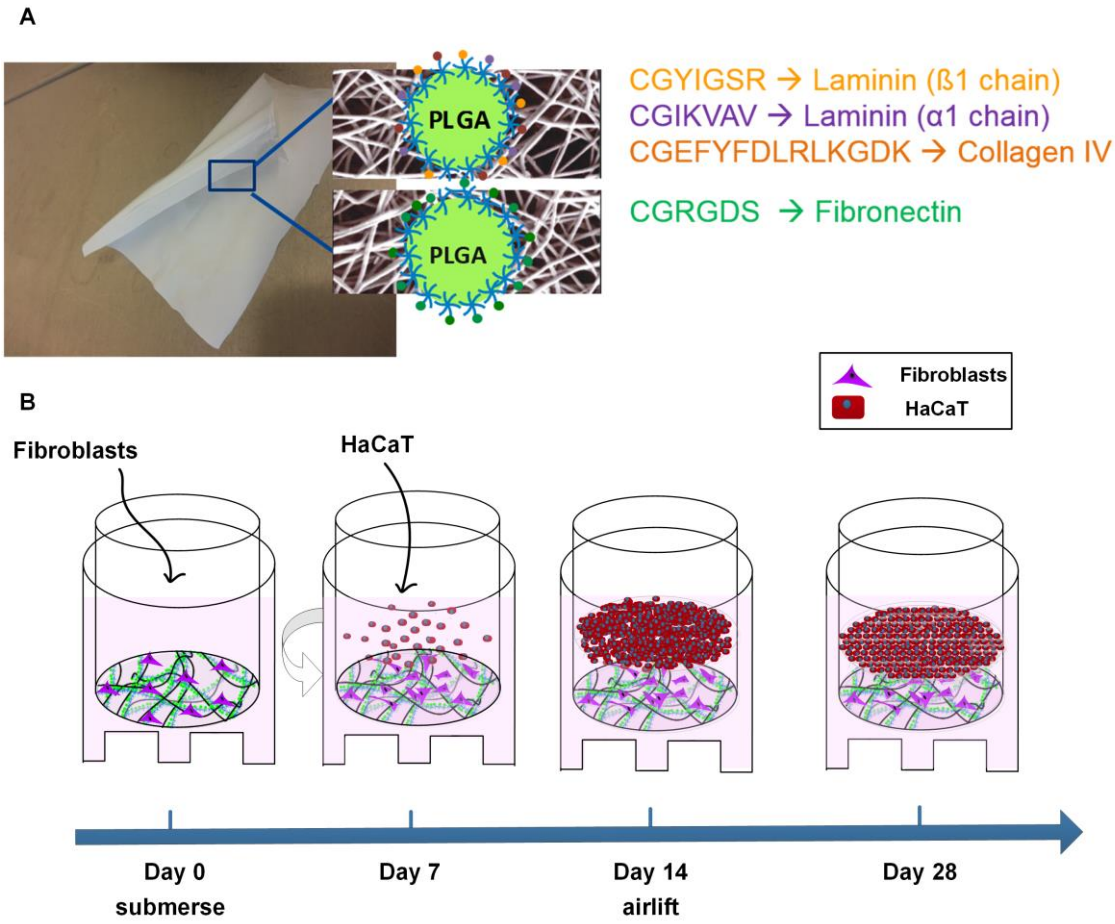

Figure 48: Engineering of co-culture model on bipolar membrane.
(A) Composition of the functionalized bipolar electrospun membrane. Membranes containing CGRGDS were electrospun as bottom layer, membranes containing CGYIGSR, CGIKVAV and CGEFYFDLRLKGDK as upper layer. (B) Membranes were fixed in cell crowns and fibroblasts were seeded on the electrospun matrix. At day 7 in culture, the electrospun membrane was inverted and HaCaT cells were seeded on the other side of the membrane. The model was cultured for further 7 days under submersed conditions until day 14, when the medium was changed to air-liquid interface. At day 28, the model was used for evaluation.

HaCaT cells and fibroblasts seeded on the upper and lower surfaces, respectively, proliferated over the culture period (Figure 49). Histological cross-sections revealed attachment of cells to both sides. Keratinocytes formed several epithelial layers covering the upper surface. The cells did not infiltrate the membrane confirming the successful cell segregation. The lower surface showed the presence of fibroblasts. Interestingly, the fibroblasts migrated into membrane containing CGRGDS peptides (M), and stopped to infiltrate at the border to membrane S,

containing collagen type IV and laminin derived peptide sequences. Moreover, it is remarkable that the membrane M appeared much thinner than membrane S, although the membranes were electrospun from the same volume.

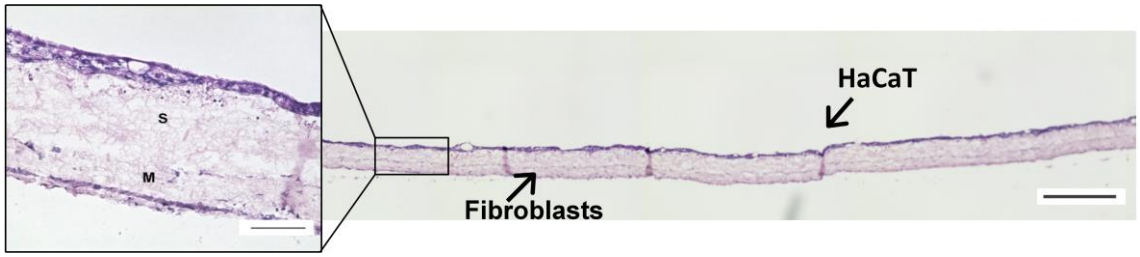

Figure 49: Histology of co-culture model on bipolar membrane.
After 28 days in culture, co-culture models with HaCaT cells on the top and fibroblasts on the bottom were fixed, cross-sectioned, and an overview staining was performed. (S) indicates the membrane containing laminin and collagen type IV derived peptide sequences. (M) displays the membrane modified with the fibronectin binding sequence. Scale bars equal 50 µm for magnified H&E staining and 500 µm for the cross-section of the entire model.

Cytokeratin 10 was expressed in the suprabasal layers of the construct (Figure 50A), cytokeratin 14 in the basal layers (Figure 50B), and vimentin by the fibroblasts (Figure 50C).

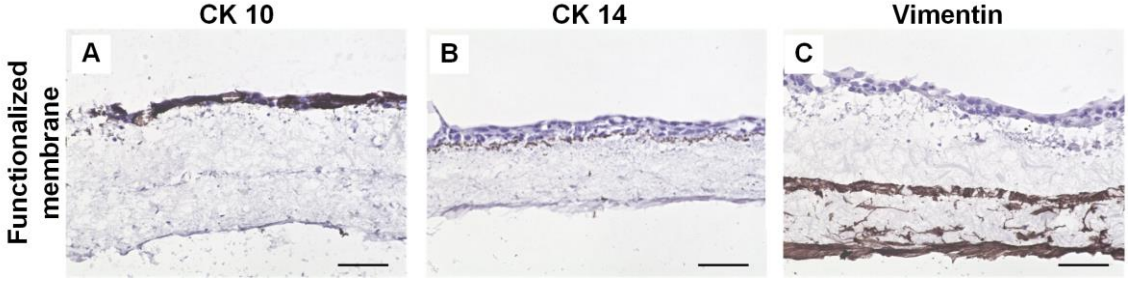

Figure 50: Immunohistochemistry of cell markers on bipolar membrane.
(A) CK 10, (B) CK 14, and (C) vimentin staining of reconstructed skin equivalents. CK = cytokeratin. Scale bars = 100 µm.

As shown in Figure 51, the most abundant extracellular matrix components collagen type I, collagen type III, collagen type IV, fibronectin and laminin type V were synthesized by HaCaT cells and fibroblasts. The immunohistochemical staining indicates that collagen type I, III, and fibronectin were produced by HaCaT cells and fibroblasts, collagen type IV was mainly synthesized by fibroblasts. The

expression of the extracellular matrix proteins was consistent with the results obtained for the isotropic membrane.

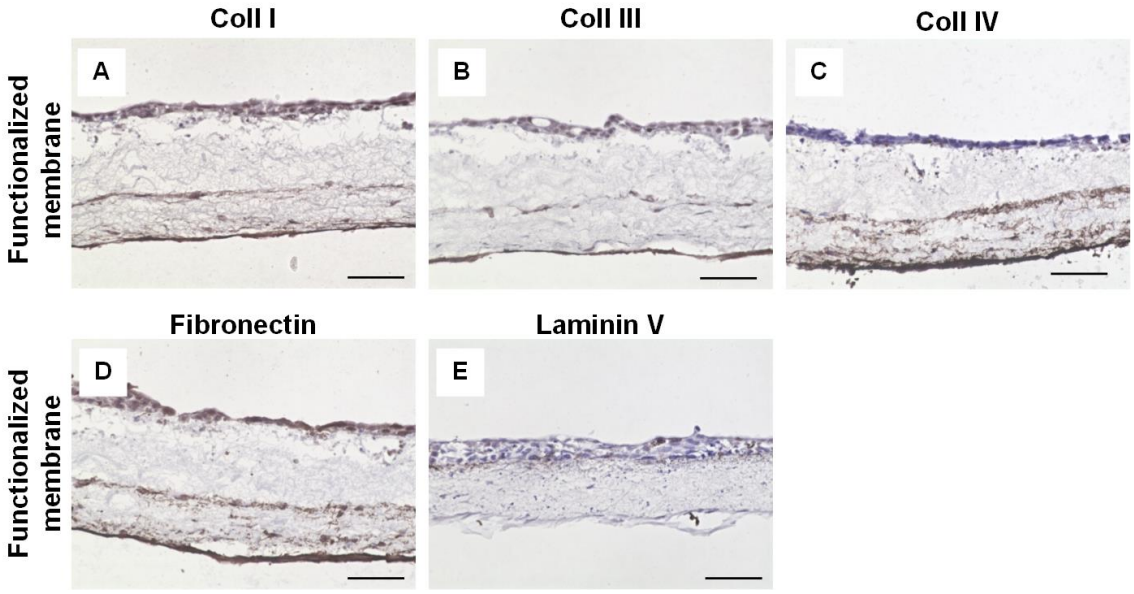

Figure 51: Immunohistochemistry of remodeling on bipolar membrane.
After 28 days in culture, models were stained for (A) Coll I, (B) Coll III, (C) Coll IV, (D) Fibronectin, and (E) Laminin V. Coll = collagen. Scale bars = 100 µm.

4.4.3 Summary

The potential of the functionalized isotropic and bipolar membrane as artificial basement membrane for skin tissue engineering was evaluated by observing the ability to support both the adhesion and proliferation of HaCaT cells and fibroblasts. Cells achieved spatial organization on both membranes, with fibroblasts penetrating into the membrane and epithelial cells forming a continuous barrier layer on the upper surface of the membrane. Cells were positive for typical cell markers and produced extracellular matrix proteins. Mimicking the fibrillar structure of the basement membrane by electrospinning and in addition incorporating extracellular matrix components to mimic their composition offers a safe and promising way to build up artificial basement membranes.

4.5 Functionalized membranes for primary skin cells

In contrast to HaCaT cells, an artificially immortalized cell line with altered metabolic function, proliferative capacities and differentiation characteristics, primary keratinocytes are taken directly from living tissue and are thus more representative to the *in vivo* state. To evaluate the potential of the functionalized membranes to act as artificial basement membrane for primary cells, primary keratinocytes isolated from skin biopsies were seeded on the membrane instead of HaCaT cells. Epithelial skin models and co-culture skin models with fibroblasts were developed. To favor tissue formation, the influence of the pore size and of the pH was investigated on keratinocyte viability and development.

4.5.1 Functionalized membranes for epithelial skin models

For the development of an epithelial skin model, primary keratinocytes were seeded on the functionalized electrospun membranes. As a reference, polycarbonate membranes were used. After 3, 7, 10, 15, and 19 days of air-liquid interface culture, the models were fixed and embedded. The polycarbonate inserts were either embedded in paraffin or cryo-stectioned. The models based on the electrospun matrices were only cryo-stectioned because the fibers would dissolve in xylol involved in the paraffin embedding protocol. Paraffin embedding is more suitable for the skin models (Figure 52). The cryo-sectioned models revealed holes in the epidermis. The insert models did not possess these holes, but exhibited a characteristic epidermal structure of 10-12 viable cell layers, including stratum basale, stratum spinosum, stratum granulosum, and stratum corneum. The models based on the electrospun membrane did not develop a multilayered epithelium. Whereas, on day 3, insert and electrospun models still appeared to be alike, but on day 7, the models based on polycarbonate membranes developed several layers of polarized epithelial layers, while the models based on functionalized membranes displayed a diffuse epithelium. Further culturing of the electrospun models resulted in a separation of the cells from the matrix. It appeared as if the epithelial cells on the surface decreased over culture time. After 19 days, there were only a few keratinocytes attached on the surface.

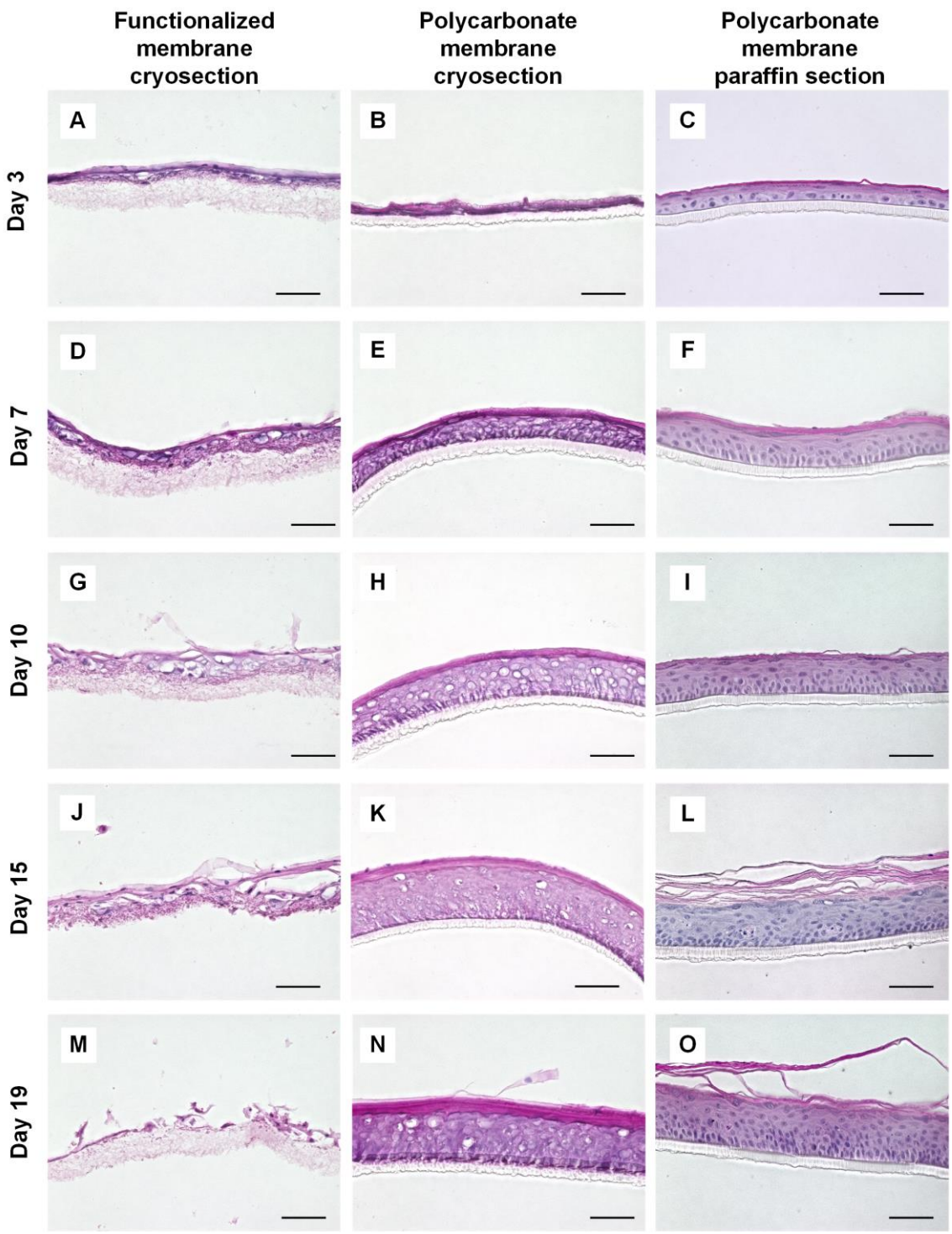

Figure 52: Histology of epithelial skin models.
Cryo-sectioned functionalized electrospun membranes seeded with keratinocytes were compared to cryo-sectioned and paraffin embedded polycarbonate membranes seeded with keratinocytes after 3, 7, 10, 15, and 19 days in culture. Scale bars = 100 µm.

Although the differences in histology between the cryo-sectioned models based on the electrospun fibers and the cryo-sectioned insert models was not as pronounced as for paraffin sectioned insert models, the insert models revealed a better developed epithelium. Increasing the cell seeding density from 3 x 10^5 to 1 x 10^6 keratinocytes per model and increasing the time of culturing the models under submerged conditions from 1 day to 7 days to allow cell attachment did not enhance tissue formation.

4.5.1.1 Analysis of cell viability

The viability of the models was measured after 3, 7, 10, 14, and 19 days using MTT. There was a steady increase in viability for the models based on polycarbonate membranes. The viability of the models based on functionalized membranes decreased after 10 days (Figure 53). The decrease in cellular viability is in line with the results obtained by histological analysis showing a separation of cells after 10 days in culture.

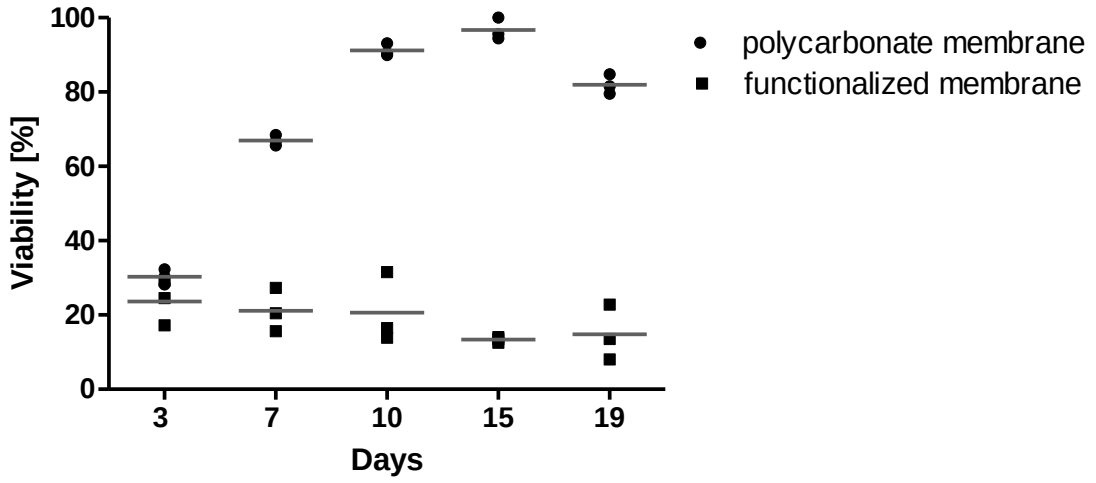

Figure 53: MTT viability assay of epithelial skin models.
The development of the cell viability of epithelial models based on functionalized electrospun membranes was compared to models based on polycarbonate membranes over 19 days. (n = 3).

4.5.1.2 Analysis of electrical resistance

To monitor the degree of barrier formation and the tightness of the cell layers, the transepithelial electrical resistance (TEER) was analyzed after 3, 7, 10, 15, and 19 days of culture. The values are indicated in Figure 54. The mean TEER value of the models based on polycarbonate membranes increased from 255 Ω cm^2 at day 3 to 5080 Ω cm^2 at day 14 in culture. At day 19, a mean TEER value of 4258 Ω cm^2 was measured. An electrical resistance on the functionalized electrospun membranes could not be measured.

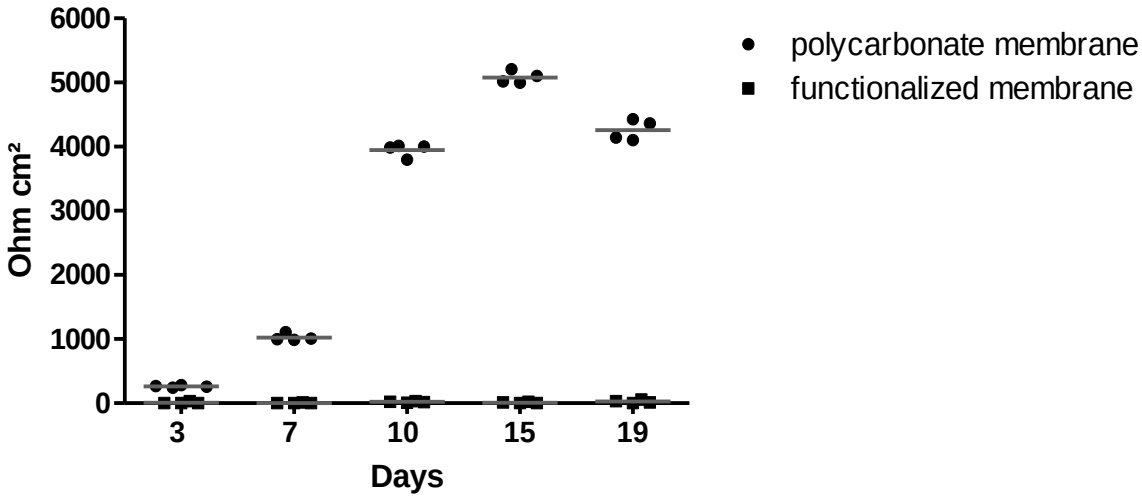

Figure 54: TEER of epithelial skin models.
TEER values of epithelial models based on electrospun fibers were compared to epithelial models on polycarbonate insert membranes over 19 days. (n = 4).

4.5.1.3 Scanning electron microscopy analysis

Primary keratinocytes were seeded on the electrospun membranes modified with fibronectin, laminin and collagen IV derived binding sequences and microscopically investigated after 24 hours in culture (Figure 55). SEM images revealed that primary keratinocytes adhered to the functionalized electrospun fibers. Characteristic microvilli were visible on the surface of the cells. Cells were connected to each other forming tight junctions. Parts of the membrane were sparsely populated.

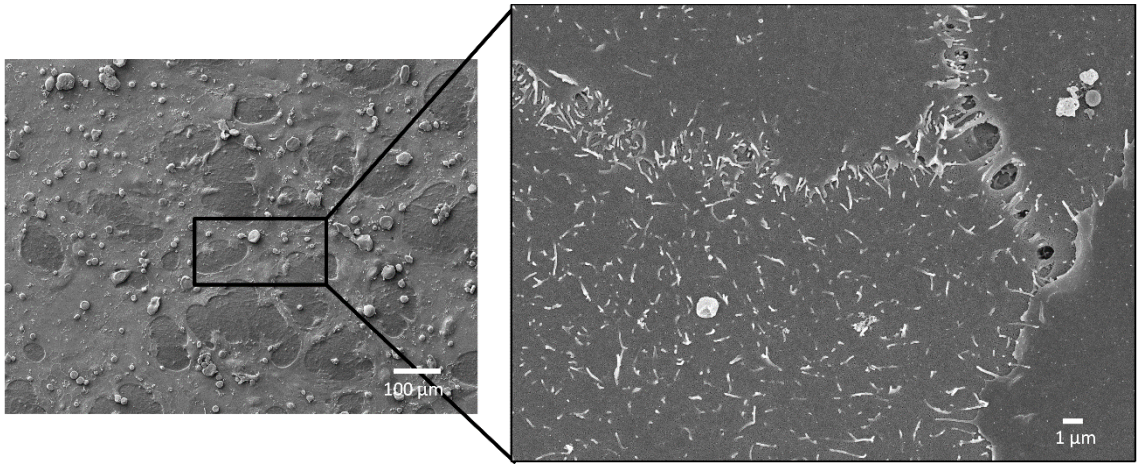

Figure 55: SEM micrographs of primary keratinocytes on membranes.
Primary keratinocytes were seeded on electrospun membranes modified with sP(EO-*stat*-PO)/PLGA/fibronectin/laminin/collagen IV peptide sequences. After 24 hours in culture, SEM images were performed.

4.5.1.4 Influence of membrane fixation

To improve the quality of the tissue models, several techniques to fix the electrospun membranes were compared. Membranes were laid in a petri dish and fixed with the inner part of a metal cell crown (Figure 56A). The small plastic cell crowns, which were employed for the development of the co-culture model based on HaCaT cells, were connected to a 12-well insert without a membrane to avoid overflowing when the cell suspension was pipetted on the membrane. The two parts were connected with a piece of tube (Figure 56E). As a control, membranes were fixed in small plastic cell crowns as in the experiments before (Figure 56I). Using metal cell crowns revealed not to be applicable, because the membranes could not be fixed properly in the crowns and slipped apart. 3 x 10^5/model HaCaT cells, primary fibroblasts and primary keratinocytes were applied on the differently fixed membranes and Live/Dead staining was performed after 72 hours. As indicated in Figure 56A-D, using the membrane without fixation was not suitable for cell seeding. A significantly reduced amount of HaCaT cells, fibroblasts and keratinocytes attached to the membranes compared to the other fixation methods. Fixing membranes in small plastic rings and afterward connecting them with inserts (Figure 56E-H) did not enhance cell adhesion in comparison to using the plastic rings without inserts (Figure 56I-L). It could also be seen from Figure 56 that HaCaT

cells and fibroblasts attached considerably stronger than primary keratinocytes did with all fixation techniques. HaCaT cells and fibroblasts grew to a confluent layer and showed typical cell morphologies. A marginal number of dead cells, appearing in red, were visible. In contrast, a lot of dead keratinocytes were detectable. The red staining was overlain by the blue staining of the nucleus and appeared purple in the images.

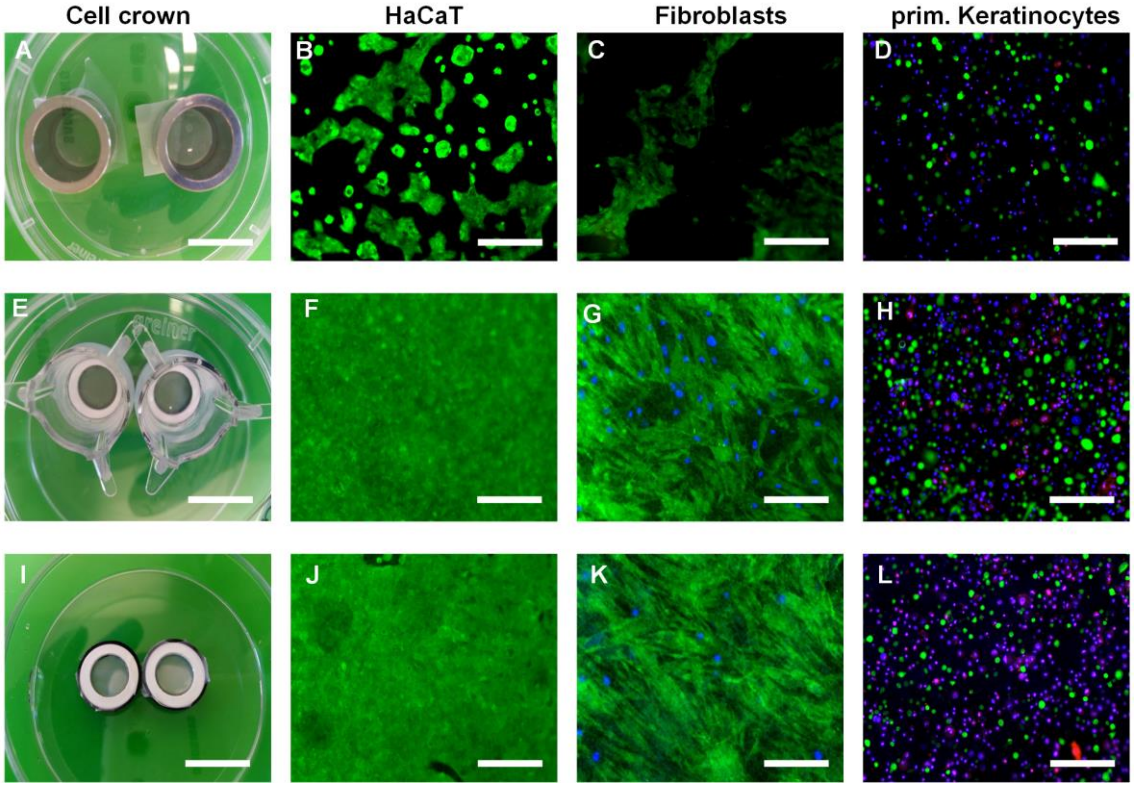

Figure 56: Comparison of different cell crowns.
Membranes were (A) weight down with metal rings, (E) fixed in plastic cell crowns and connected to 12-well inserts or (I) fixed in plastic cell crowns. HaCaT cells, fibroblasts and primary keratinocytes were seeded on the membranes and Live/Dead staining was performed after 72 hours. Scale bars = 50 µm.

To increase the number of keratinocytes attached to the membrane, parafilm® was placed under the electrospun membranes and fixed in cells crowns. However, the number of attaching cells did not increase.

4.5.1.5 Influence of fiber composition

To improve attachment and proliferation of primary keratinocytes, the fiber composition was changed. 1 % of benzyltriethylammoniumchlorid salt was added

to the electrospinning solution containing 0.6 mg fibronectin, 0.25 mg laminin β1, 0.25 mg laminin α1, and 0.5 mg collagen IV derived binding sequences. The addition of the salt to the solution influences the conductivity when spinning. The increased conductivity resulted in an increased stretching of the spinning jet, therefore producing thinner fibers. However, as indicated in the Live/Dead staining in Figure 57A, the addition of salt did not improve attachment and proliferation of keratinocytes after 72 hours. Decreasing the peptide concentration to 0.3 mg fibronectin, 0.15 mg laminin β1, 0.15 mg laminin α1, and 0.5 mg collagen IV derived peptide sequences (Figure 57B) and increasing the concentration to 0.75 mg fibronectin, 0.35 mg laminin β1, 0.35 mg laminin α1, and 1.5 mg collagen IV derived peptides (Figure 57C) did not promote keratinocyte attachment. Membranes containing 0.7 mg fibronectin derived peptide sequences had similar amounts of cells on the surface as the membranes containing a combination of peptide sequences (Figure 57D). Membranes modified with 0.5 mg fibronectin, and 1.0 mg collagen IV derived peptide sequences exhibited the lowest number of attached cells in the experiments (Figure 57E).

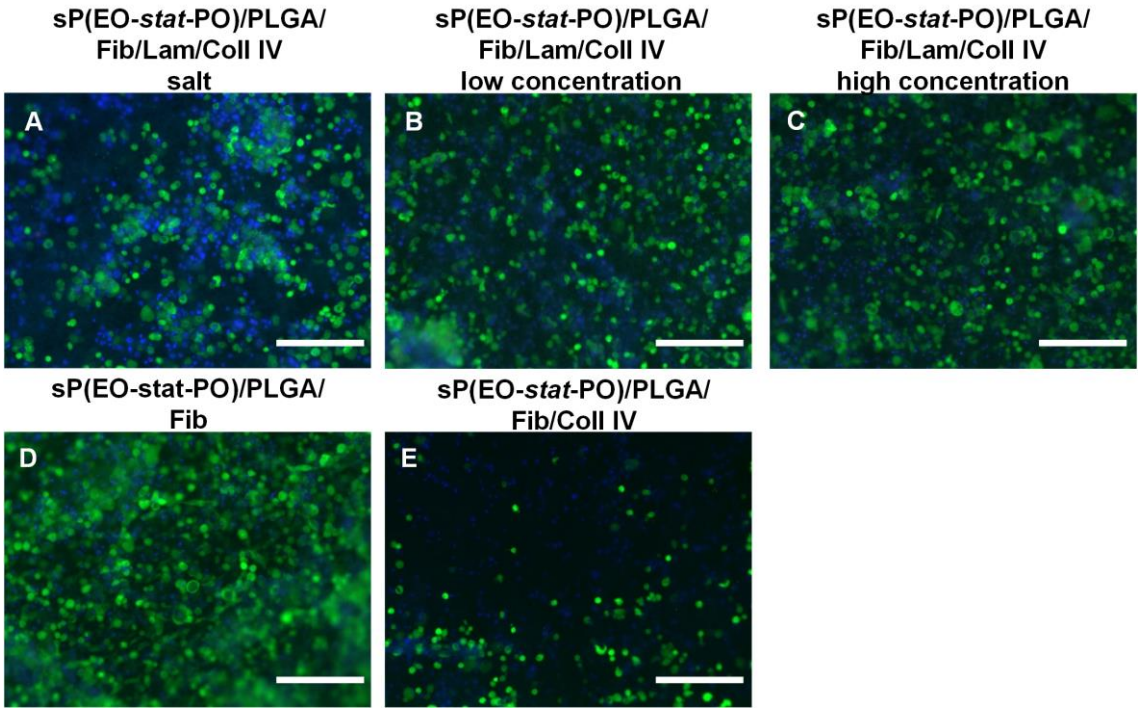

Figure 57: Influence of peptides on keratinocyte adhesion.
Fibers were electrospun with (A) benzyltriethylammoniumchlorid as a salt, (B) 0.3 mg fibronectin, 0.15 mg laminin β1, 0.15 mg laminin α1, 0.5 mg collagen IV, (C) 0.75 mg fibronectin, 0.35 mg laminin β1, 0.35 mg laminin α1, 1.5 mg collagen IV, (D) 0.7 mg fibronectin and (E) 0.5 mg fibronectin, 1.0 mg collagen IV derived peptide sequences. Primary keratinocytes were seeded on the membranes and Live/Dead staining was performed after 72 hours. Scale bars = 50 µm.

4.5.2 Functionalized membranes for co-culture skin models

The crosstalk of fibroblasts and keratinocytes is essential for adequate keratinocyte differentiation. To provide fibroblast associated stimuli to keratinocytes, a co-culture model was developed. Therefore, membranes containing the fibronectin binding sequence CGRGDS, two laminin derived sequences CGYIGSR and CGIKVAV and the collagen type IV derived binding sequence CGEFYFDLRLKGDK were fixed in plastic cell crowns and seeded with primary fibroblasts in DMEM medium at day 0. After 7 days, the membrane was turned around and primary keratinocytes were added to the construct. The next day, the models were set to an air-liquid interface and further cultured for 3, 7, 10, 15, and 19 days. The models were fixed and cryo-sectioned. As a control, fibroblasts were embedded in a collagen gel. After

24 hours, keratinocytes were seeded on the gel and cultured as described for the models based on electrospun membranes.

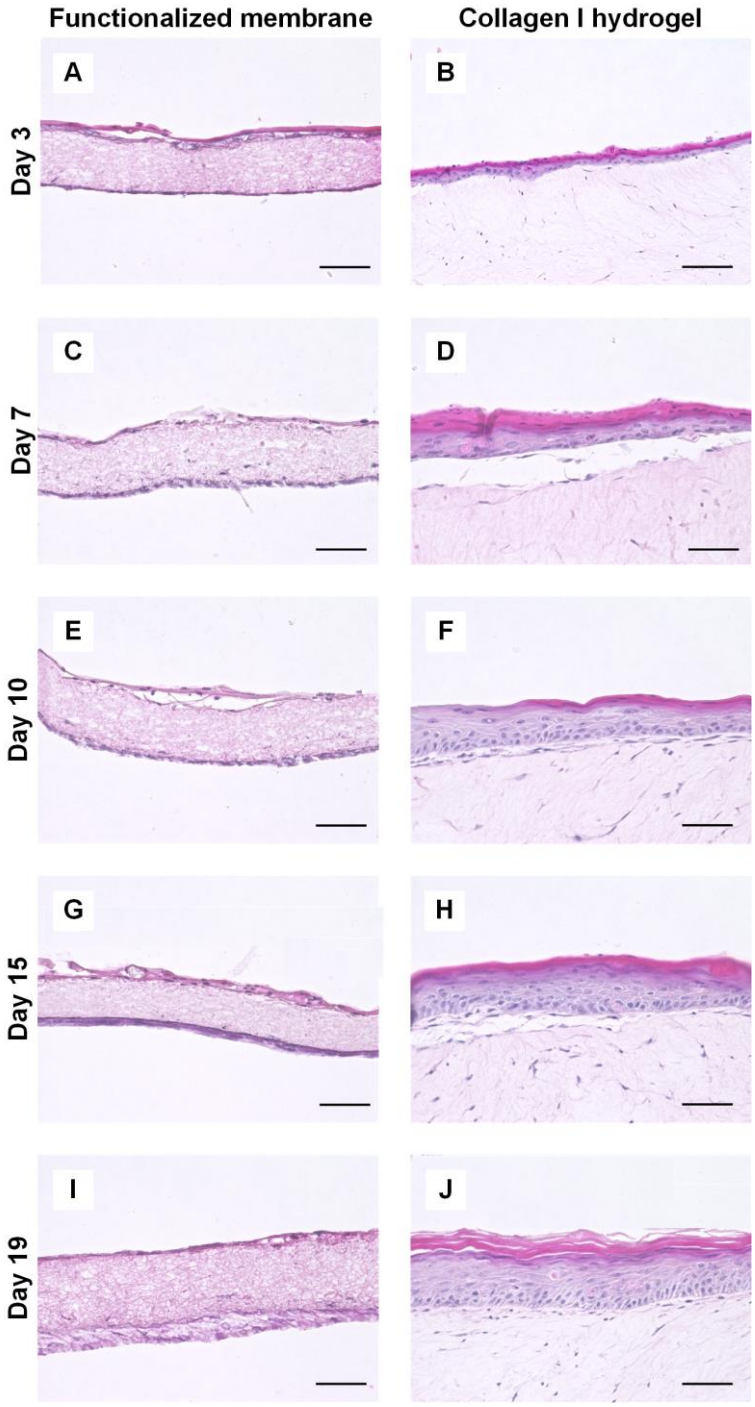

Figure 58: Histology of primary co-culture skin models.
Co-culture models of primary keratinocytes and fibroblasts based on functionalized electrospun membranes in comparison to collagen hydrogels seeded with fibroblasts and keratinocytes after 3, 7, 10, 15 and 19 days in culture. Scale bars = 50 µm.

In Figure 58, the models based on the electrospun membrane are compared with the collagen I hydrogel based skin models. The epithelium on the collagen gels developed within the culture period. At day 3, only 1-2 layers of epithelium were visible (Figure 58B). After 10 days, 7-8 cell layers (Figure 58F) and at day 19, 10-12 viable layers (Figure 58J) were detectable. The epithelium consisted of stratum basale, stratum spinosum, stratum granulosum, and stratum corneum. The fibroblasts proliferated within the collagen gel. In comparison, the models based on the electrospun matrix formed 1-2 layers of epithelium at day 3 (Figure 58A). However, the epithelium did not further proliferate over culture time (Figure 58C; E; G; I). The fibroblasts on the lower side formed a confluent layer. (Figure 58I).

4.5.3 Influence of pore size on keratinocyte development

Keratinocytes did not adequately attach and proliferate on the functionalized fibers. Comparing the properties of the polycarbonate membranes with the electrospun membranes, it becomes obvious that the electrospun membrane has a medium pore size of 4 µm. In contrast, the polycarbonate inserts, which were used as a control, reveal pore sizes of 0.4 µm. The larger pore size of the electrospun fibers might have a negative impact on the keratinocyte attachment and proliferation. Therefore, polycarbonate membranes with a pore size of 4 µm were seeded with keratinocytes and compared to the inserts that have been used before.

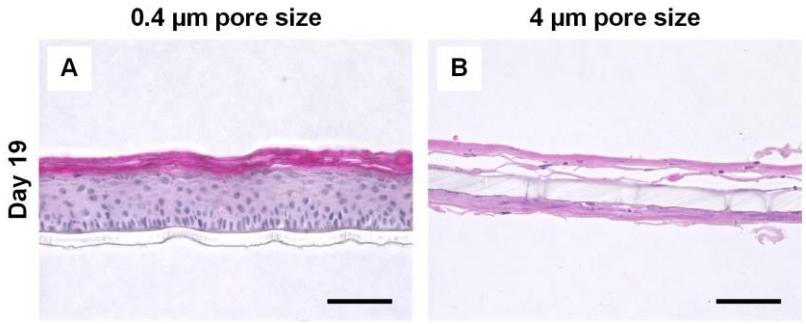

Figure 59: Influence of pore size on epithelial development.
Keratinocytes were seeded on polycarbonate membranes with (A) 0.4 µm pore size and (B) 4 µm pore size and the formation of the epithelium was investigated. Scale bars = 50 µm.

Figure 59 reveals the tremendous influence of the pore size on the tissue formation. The keratinocytes formed an epithelium consisting of 10-12 cell layers on the 0.4 µm pore size inserts (Figure 59A), in comparison to keratinocytes on the 4 µm pore size inserts, which fell through the membrane and grew in 1-2 layers on both sides (Figure 59B). There was no polarization of the epithelium detectable.

4.5.4 Influence of pH value on keratinocyte viability

When PLGA fibers degrade, lactic acid and glycolic acid are formed that cause a local decrease in the pH on the surface of the fibers. It was shown that HaCaT cells properly attached and proliferated on the fibers, keratinocytes did not. Therefore, it was investigated whether the cells behave differently regarding pH changes and how sensitive the cells react to a drop in pH. HaCaT cells and primary keratinocytes were seeded in a 6-well plate in medium (pH 7.7). After 3 hours, the medium was changed to a different pH (pH 7.7; pH 7.0; pH 6.5; pH 6.0; pH 5.5; pH 4.0). The cells were cultured for 24 hours in the medium and afterward viability was determined using MTT assay. As evident from Figure 60, the viability of HaCaT cells was reduced to 50 % at a pH of 5.4. Primary keratinocytes were more sensitive to changes in pH. A pH of 5.7 decreased the viability to 50 %. Cell viability of both cell types was again determined after 72 hours. The measurement confirmed the results investigated after 24 hours.

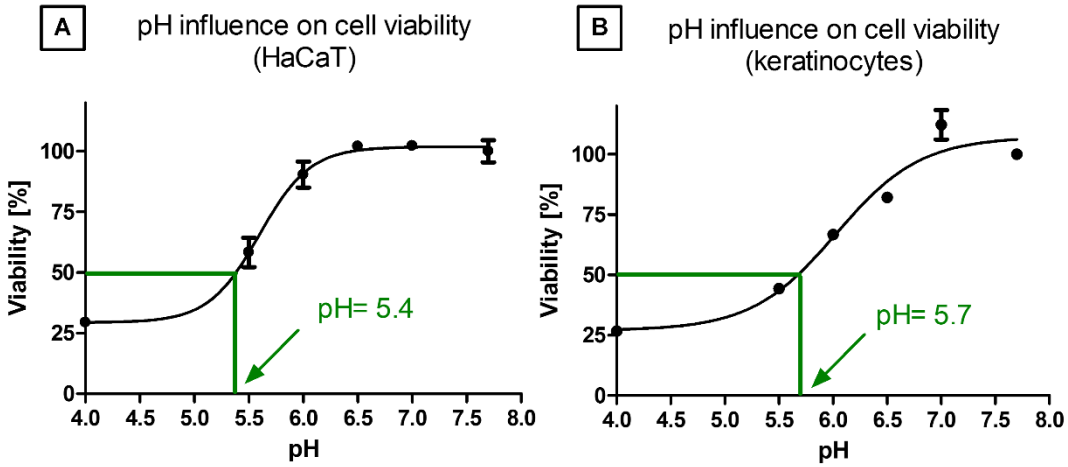

Figure 60: Influence of pH value on cell viability.
Cells cultured in media with different pH. Cell viability of (A) HaCaT and (B) primary keratinocytes was determined after 24 hours. (n = 2).

Besides the sensitivity of the keratinocytes to the pH change, we found that the keratinocyte medium (Epilife®) had a reduced buffer capacity compared to the HaCaT medium (DMEM).

4.5.5 Summary

Primary cells are isolated directly from living tissue, reveal normal morphology, cellular function and growth characteristics in culture and hence, represent the in *vivo* situation more closely than cell lines. To investigate if the functionalized membrane provides sufficient cues to support the organization of primary cells to functional tissue, cells isolated from skin biopsies were seeded on the membrane. As a reference, polycarbonate membranes were used for epithelial skin models and collagen I hydrogels for co-culture skin models. Both primary keratinocytes and fibroblasts attached to the functionalized membranes. However, in contrast to polycarbonate membranes, the electrospun membranes did not promote the formation of a polarized, multilayered, epithelium neither in epithelial skin models nor in co-culture skin models. Comparison of membranes with different pores showed that the pore size of the membrane had a tremendous influence on epithelial formation. Moreover, keratinocytes reacted very sensitively to pH changes in the medium.

4.6 Functionalized membranes for oral mucosa tissue engineering

Commonly, 2D cell culture and animal models are used for the assessment of the biocompatibility of restorative dental materials, pharmaceuticals, and oral health care products. Due to ethical concerns, limited reliability, and high costs of these models, there is a need for engineered human oral mucosa models. Therefore, a protocol was established to isolate primary oral mucosa cells from human buccal and gingival tissue. Two different membranes were investigated for their suitability as supporting structure for oral mucosa tissue engineering: electrospun functionalized membranes and polycarbonate membranes.

4.6.1 Isolation of oral mucosa cells

Primary human epithelial cells and fibroblasts were obtained from oral mucosa biopsies. The epithelial cells were isolated from the epidermis, while the fibroblasts from the connective tissue. As shown in Figure 61, isolated human oral mucosa keratinocytes exhibited a cobblestone shaped morphology. A few large and flat cells were visible, which had lost replicative potential. Fibroblasts showed an elongated, spindle shaped morphology.

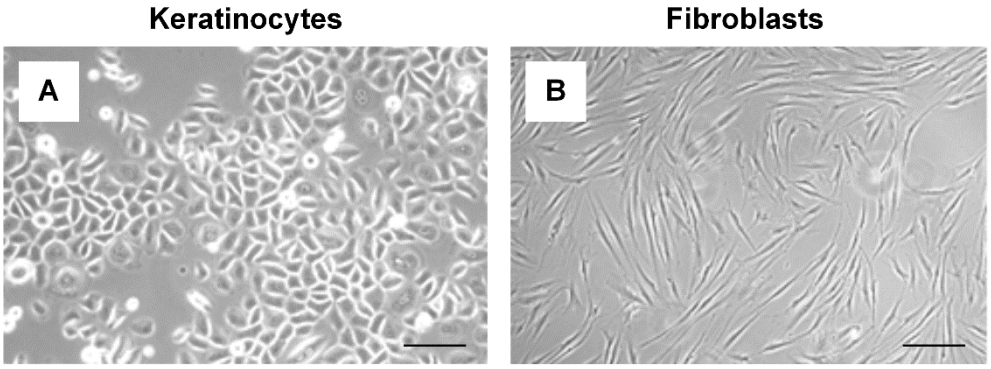

Figure 61: Light microscopy images of human oral mucosa cells.
(A) Primary keratinocytes and (B) fibroblasts in TCEP culture flasks. Scale bars = 100 µm.

4.6.2 Characterization of oral mucosa cells

Keratinocytes and fibroblasts were used after passage 2 to build up tissue models. Before the construction of oral mucosa equivalents, the cells were characterized. For this purpose, cytospots were prepared for keratinocytes and chamber slides for fibroblasts. The characterization was performed using immunohistochemistry. Keratinocytes expressed cytokeratin 14, a marker for basal epithelial cells. Cells were negative for cytokeratin 10, a marker for differentiated epithelial cells. Fibroblasts expressed vimentin, a mesenchymal cell marker (Figure 62).

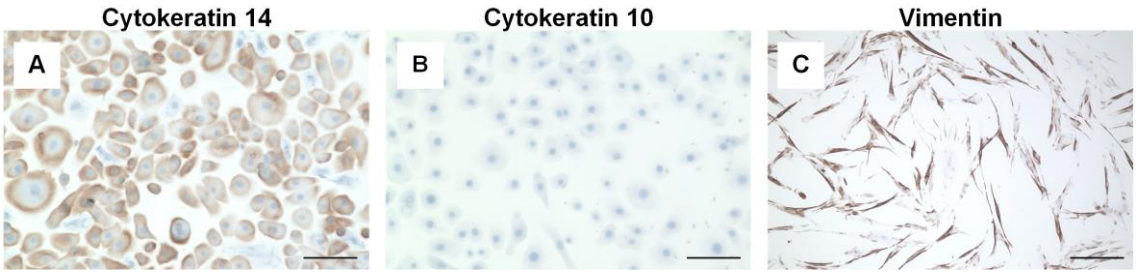

Figure 62: Immunohistochemistry of human oral keratinocytes and fibroblasts. (A) Keratinocytes are stained for cytokeratin 14 and (B) cytokeratin 10 expression, (C) fibroblasts for vimentin expression. Scale bars = 100 µm.

4.6.3 Functionalized membranes for oral mucosa models

Membranes containing the fibronectin derived binding sequence CGRGDS, two laminin derived sequences CGYIGSR and CGIKVAV, and the collagen type IV derived binding sequence CGEFYFDLRLKGDK were electrospun and seeded with primary oral keratinocytes as well as primary oral keratinocytes and fibroblasts respectively, as performed for skin models based on functionalized electrospun fibers. After 24 hours under submerged conditions, the models were cultured under air-liquid interface. For co-culture models, fibroblasts were pre-cultured for 7 days before the membrane was inverted and keratinocytes were added. The histology of oral mucosa equivalents based on electrospun fibers was performed after 14 days under air-liquid interface, using cross-sections stained with H&E. As illustrated in Figure 63A, modified PLGA membranes were biocompatible and biostable. Primary keratinocytes adhered to the fibers, but did not differentiate into typical polarized epithelial structure. Also in co-culture experiments, keratinocytes grew in 1-2 layers but did not form a well-developed epithelial layer (Figure 63B). Fibroblasts turned

into a confluent cell layer on the lower side of the electrospun membrane, but did not favor the formation of an epithelium.

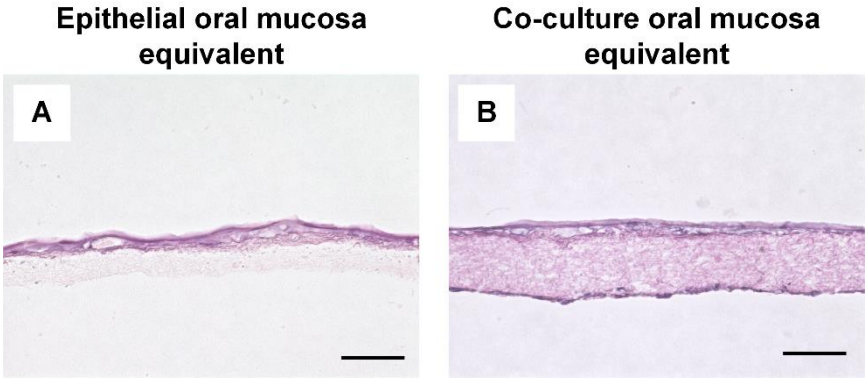

Figure 63: Histology of oral mucosa model on functionalized membranes. Membranes were seeded with (A) keratinocytes as well as (B) keratinocytes and fibroblasts and cultured for 14 days. Scale bars = 50 µm.

Since the electrospun fibers did not present an optimal membrane for engineered oral mucosa equivalents, polycarbonate cell culture membranes were used for the further development of an oral mucosa model.

4.6.4 Polycarbonate membranes for oral mucosa models

Closely following the protocol to build up skin equivalents and as already performed for oral mucosa equivalents based on functionalized electrospun fibers, 3 x 10^5 keratinocytes were seeded on each insert. After 24 hours of submerged conditions, the models were cultured for up to 14 days under air-liquid interface.

4.6.4.1 Morphological analysis

The histology of the reconstructed oral mucosa equivalents was evaluated using cross-sections stained with H&E. As indicated in Figure 64, models developed 2-3 viable cell layers and a relatively thin stratum corneum after 3 days. At day 7, the epidermis was composed of 5-6 cell layers. Further culture of the models resulted in a viable epidermis consisting of 7-8 cell layers and a distinct formation of the stratum corneum.

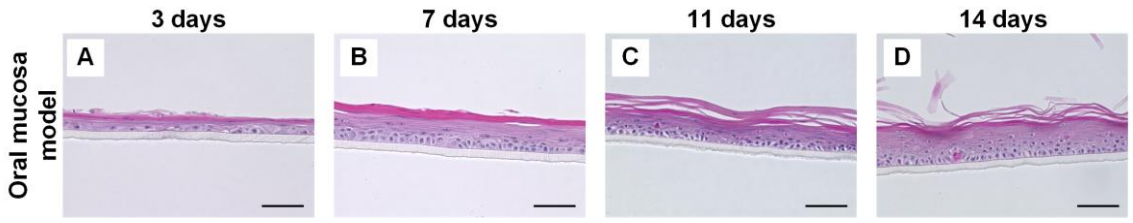

Figure 64: Histology of oral mucosa models on polycarbonate membranes.
Oral mucosa models were cultured for (A) 3 days, (B) 7 days, (C) 11 days and (D) 14 days. Scale bars = 100 µm.

Analysis of the oral mucosa equivalents after 14 days revealed a characteristic epidermal structure including 1-2 layers of columnar to round, regularly organized cells of the stratum basale, a relatively flattened stratum spinosum, cells of the stratum granulosum, and a keratinizing stratum corneum (Figure 65).

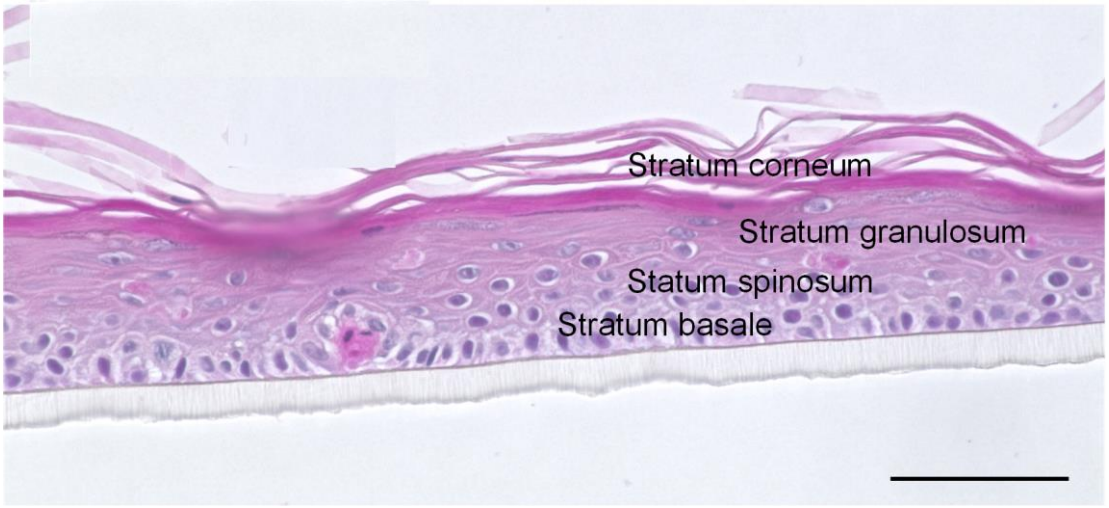

Figure 65: Histology of oral mucosa model.
The stratum basale differentiated into stratum spinosum, stratum granulosum und stratum corneum. Scale bars = 100 µm.

4.6.4.2 Immunohistochemical analysis

The cytokeratin profile reflects the cell type and the differentiation status in different types and different layers of the epithelium. The cytokeratin expression was investigated in the reconstructed oral mucosa equivalents after 14 days in culture and compared with the expression in native oral mucosa. Immunopositive staining against cytokeratin 5/6 (CK 5/6) was observed in the basal and upper

layers of the epithelium. Cytokeratin 10 (CK 10), a marker of keratinized epithelium, was strongly expressed in the suprabasal layers of the epithelium. Cytokeratin 13 (CK 13), a major differentiation associated marker of nonkeratinized oral mucosa, was visible in the basal and suprabasal layers of native oral mucosa. Basal cells in the oral mucosa model and in the native oral mucosa expressed cytokeratin 14 (CK14) and Ki67, a proliferation marker.

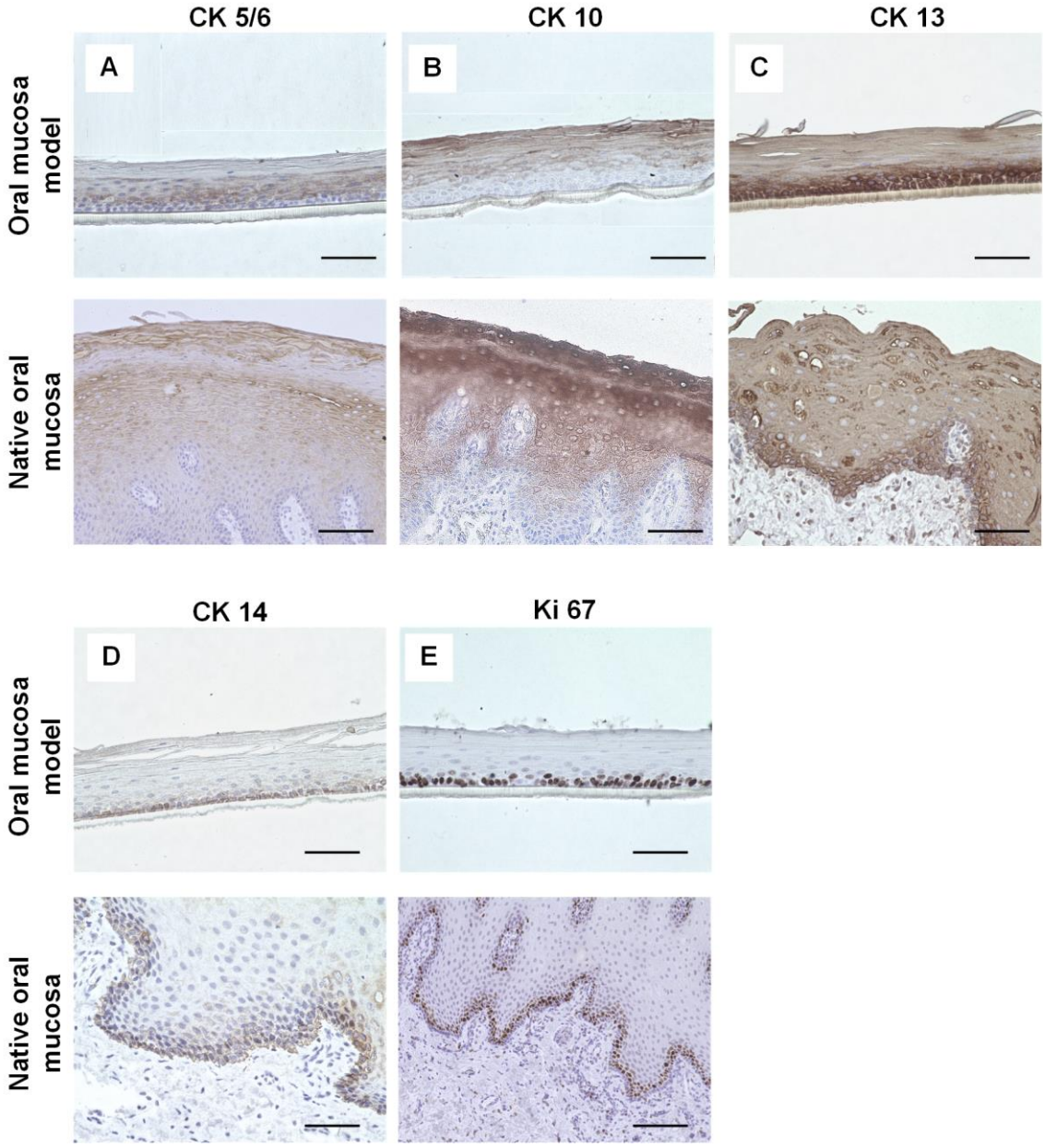

Figure 66: Immunohistochemistry of oral mucosa models.
(A) CK 5/6, (B) CK 10, (C) CK 13 and (D) CK 14 staining of the epithelium of oral mucosa models and native oral mucosa. (E) proliferative cells were stained with Ki67. CK = cytokeratin. Scale bars = 100 µm.

4.6.4.3 Functional characterization

To further investigate the reconstructed oral mucosa, the models were characterized using TEER measurements, Fluorescein isothiocyanate-dextran (FITC-dextran) and carboxyfluorescein permeation. An ET-50 assay and an irritation study helped to evaluate the functionality of the models.

Analysis of electrical resistance

To monitor the degree of barrier formation and the tightness of the cell layers, TEER was analyzed on day 3, 7, 10, and 14 of culture. The results are summarized in Figure 67. The mean TEER value increased more than 50 times from day 3 to day 14 in culture. The mean resistance of oral mucosa models after 14 days was 6219 Ω, which corresponds to a TEER value of 3669 Ω cm^2. The results indicate a steady increase of the integrity of the oral mucosa models and the formation of a permeability barrier.

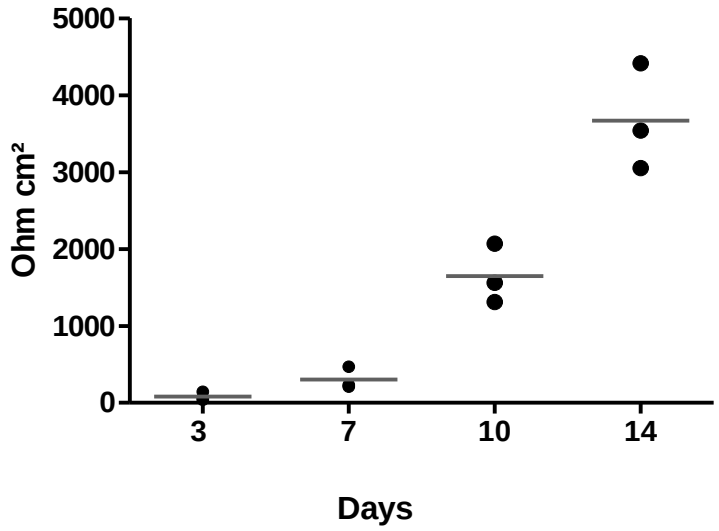

Figure 67: TEER of oral mucosa models.
Oral mucosa models were cultured for 3 days, 7 days, 10 days, and 14 days. At each point in time, TEER values were determined. (n = 3).

Analysis of FITC-dextran permeability

The convenience and reliability with which certain compounds can be absorbed across the oral mucosa has led to the development of pharmaceuticals for buccal

administration. In order to study the drug delivery of these macromolecular therapeutic agents with tissue-engineered oral mucosa models, these models must reveal a permeation barrier. To analyze the barrier properties of the oral mucosa equivalents, the flux of FITC-dextran as model compound was measured. FITC-dextran was applied for 60 minutes on the oral mucosa equivalents at day 14 of culture. As illustrated in Figure 68, 12.4 % FITC-dextran passed the inserts without cells after 60 minutes, whereas the molecule was unable to permeate the oral mucosa equivalents.

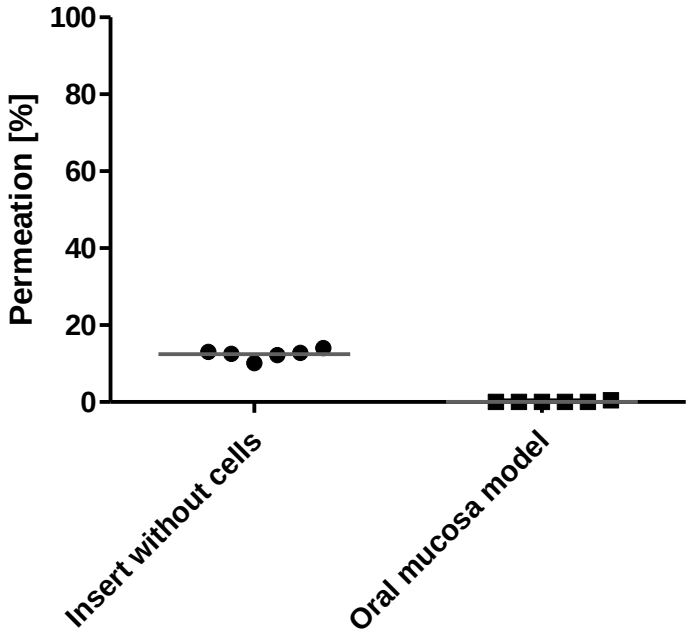

Figure 68: FITC-dextran permeability of oral mucosa models.
After 14 days in culture, the FITC-dextran permeability was determined and compared with the permeability of inserts without cells. (n = 6).

Analysis of carboxyfluorescein permeability

Considering that the molecular weight of FITC-dextran with 4 kDa is relatively high and that the permeation rate was relatively low both in inserts without cells and in oral mucosa equivalents, another model substance, namely 6(5)-carboxyfluorescein with a molecular weight of 376 Da, was utilized to assess the oral mucosa permeation. The permeation rate of carboxyfluorescein was fivefold higher in the cell free inserts compared to FITC-dextran, making it a more reliable compound for

investigation. Significantly more carboxyfluorescein permeated through the inserts without cells compared to oral mucosa models (Figure 69). The permeation rate of insert models without cells was 60 %. In oral mucosa models, 6.5 % of carboxyfluorescein permeated through the oral mucosa equivalents after 3 days in culture. At day 7, the models formed a tight barrier and there was no permeation of carboxyfluorescein detected. The models remained dense over the entire incubation period.

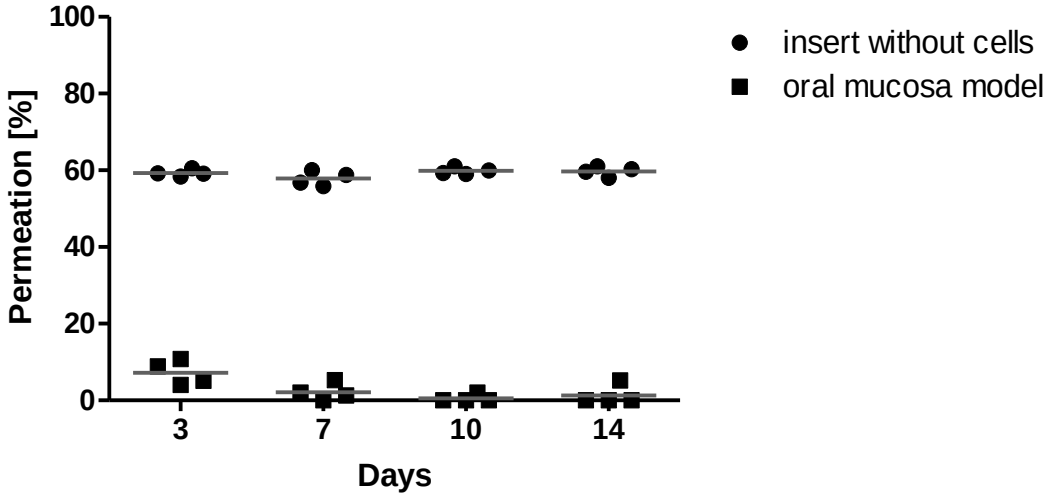

Figure 69: Carboxyfluorescein permeability of oral mucosa models.
Oral mucosa models were cultured for 3, 7, 10, and 14 days. At each mentioned point in time, carboxyfluorescein permeation was determined. (n = 4).

To analyze the retention time of carboxyfluorescein, carboxyfluorescein solution was incubated for 30, 120, 240, and 360 minutes on the oral mucosa equivalents. As a comparison, carboxyfluorescein permeation was measured in inserts without cells and in skin models. After 360 minutes of carboxyfluorescein incubation, skin models still formed a tight barrier, whereas there was a continuous increase in permeation rate detected in the oral mucosa models over time (Figure 70). After 30 minutes, the oral mucosa models formed a tight barrier, however, after 120 minutes and 240 minutes, 12.5 % and 21.5 % of carboxyfluorescein passed the models respectively, while after 360 minutes, a permeation rate of 31 % was measured. The results correlate with the *in vivo* situation where skin forms a much denser barrier than the oral mucosa, which is relatively permeable.

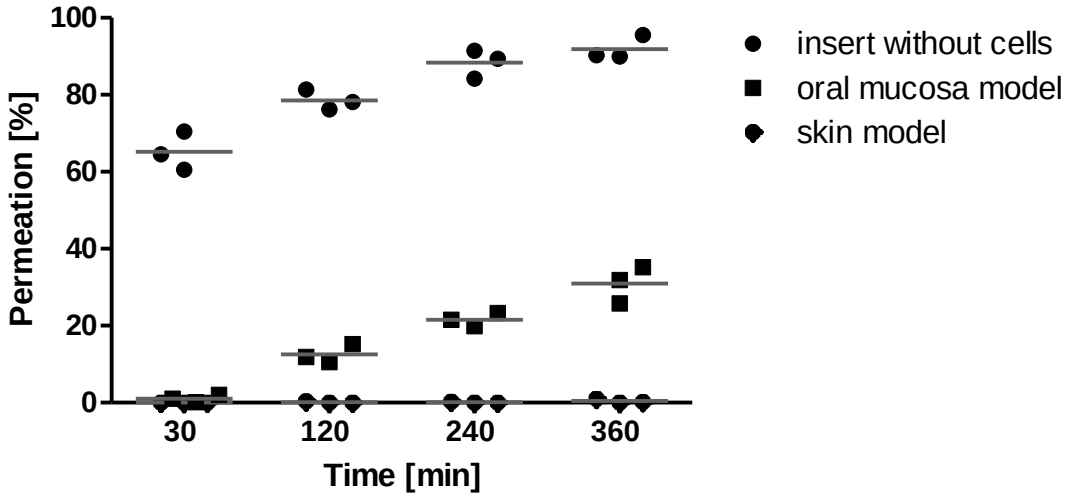

Figure 70: Time dependent permeability of oral mucosa models.
After 14 days in culture of oral mucosa models and skin models, carboxyfluorescein solution was incubated for 30, 120, 240 and 360 minutes on models. At each point in time, the amount of permeated carboxyfluorescein was determined. (n = 3).

Analysis of ET-50

In order to measure the resistance of the barrier of the oral mucosa models, an ET-50 assay was performed at day 14 of culture. Triton X-100 (1 %) was incubated for 8 different exposure times on the models. After exposure, tissue viability was determined with MTT and the ET-50 value was calculated. From Figure 71, it can be seen that 114 minutes of Triton X-100 exposure is required to decrease the tissue viability to 50 %.

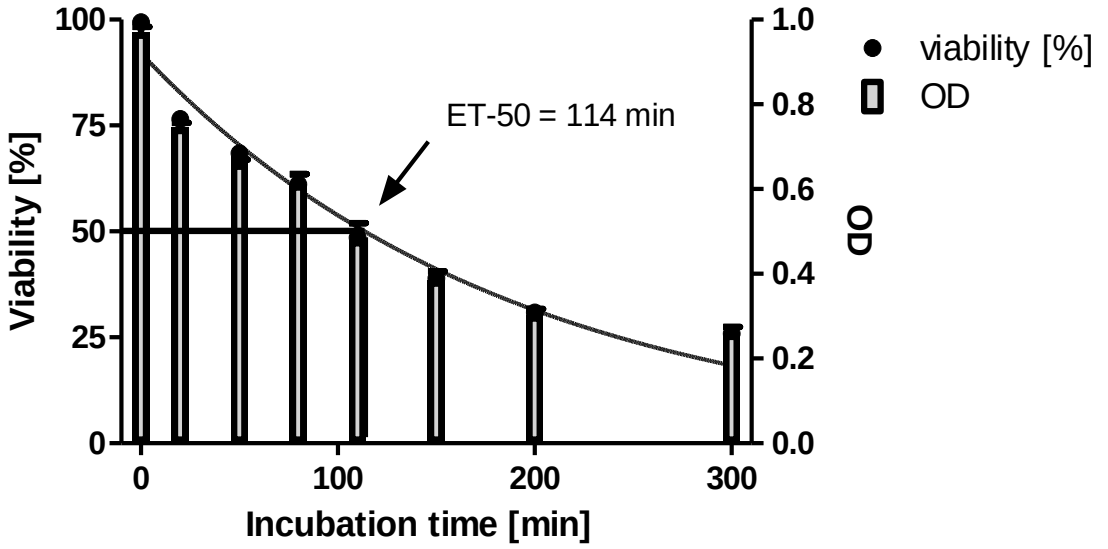

Figure 71: ET-50 of oral mucosa models.
The ET-50 represents the duration of treatment that results in half-maximal damage. Models were treated for different points in time with Triton X-100 (1 %). The time which reduces the viability to 50 % was determined. (n = 3).

Irritation study

In vitro methods play an important role in hazard identification and assessment of toxicology profile of compounds. The purpose of the irritation study was to evaluate the prediction potential of the oral mucosa equivalents. Therefore, two different oral health care products were applied on the models for 35 minutes (Table 20). Chlorhexamed®, an antimicrobial mouth rinse containing chlorhexidin and Salviathymol®, a solution for oral hygiene containing medicinal plants. Salviathymol® was applied in two different concentrations, a dissolution of 1:100 in water which is recommended by the producer and an undiluted solution.

Table 20: Test substances for irritation study

Test substance	Application recommended	Application in irritation study
Chlorhexamed®	Undiluted	Undiluted for 35 min
Salviathymol®	1g/100ml water	Undiluted for 35 min
		Diluted 1:100 for 35 min

The results for the two commercially available products are shown in Figure 72. Treatment with undiluted Salviathymol® resulted in cellular viability of 2 % as measured by MTT and is comparable with the viability after treatment with sodium dodecyl sulfate (SDS) as positive control. Diluted Salviathymol® and Chlorhexamed® did not reduce the viability. Values were normalized to the negative control PBS. Substances leading to tissue viability smaller than 50 % are defined as irritants. Substances resulting in viability greater than 50 % are classified as non-irritants. The results demonstrate that both undiluted Salviathymol® (tissue viability of 2 %) and SDS (tissue viability of 2 %) were irritating. Diluted Salviathymol® (tissue viability 98 %), Chlorhexamed® (tissue viability of 99 %) and PBS (tissue viability of 99 %) did not show any irritating potential.

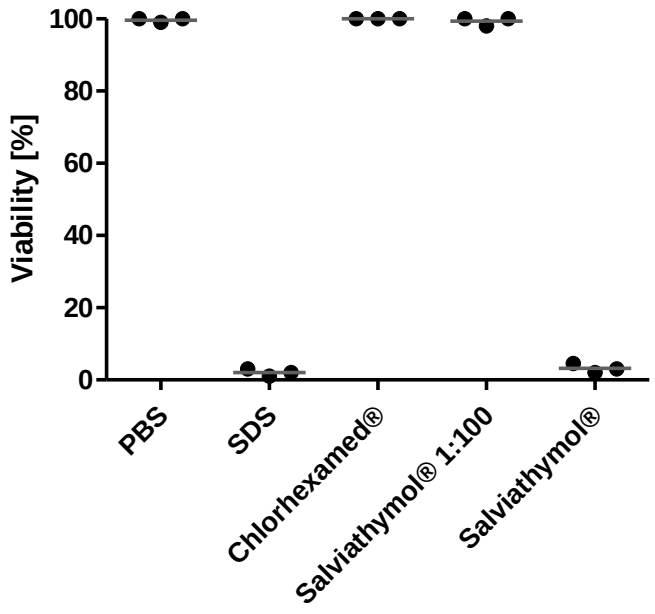

Figure 72: Irritation study of oral mucosa models.

The viability after treatment with Chlorhexamed®, diluted Salviathymol® and undiluted Salviathymol® was determined. As positive control, SDS was applied, as negative control PBS. Substances leading to a viability ≥ 50 % are defined as non-irritating, and to a viability ≤ 50 % as irritating. (n = 3).

The results are in accordance with the *in vivo* situation, where both oral care products do not show any irritation potential if applied properly. As soon as the concentration of Salviathymol® is increased 100 x, the solution causes irritation.

4.6.5 Summary

Functionalized electrospun membranes and polycarbonate membranes were evaluated for their suitability as membranes to produce tissue-engineered human oral mucosa models. On electrospun membranes, oral keratinocytes grew in several unstructured layers, but did not form a well-developed epithelial layer. Co-culture of epithelial cells with fibroblasts did not support the formation of a typical polarized epithelial structure. Polycarbonate membranes were revealed to be a suitable substrate for 3D equivalents of the oral mucosa. Primary oral mucosa epithelial cells grew in several layers with cells becoming increasingly squamous as the apical surface was approached. The expression of characteristic cell markers was consistent with the expression in native human oral mucosa. The barrier function of the models was confirmed measuring the electrical resistance, as well as FITC-dextran and carboxyfluorescein permeability. When exposed to the surfactant Triton X-100 (1 %), an exposure time of 114 minutes reduced the viability of the model to 50 % as determined by MTT. Undiluted Salviathymol® was irritative in comparison to diluted Salviathymol® and Chlorhexamed®, which did not show irritative properties.

5 Discussion

5.1 Characterization of functionalized membranes

A significant amount of research has focused on the development of tissue-engineered models which reflect the *in vivo* situation as closely as possible. For this purpose, a major challenge is the creation of a support structure that promotes adhesion, migration and, proliferation of the cells, while allowing the crosstalk between different cell types and the remodeling of the matrix. Thus, the overall aim of this thesis was the development of artificial basement membranes towards skin and oral mucosa tissue engineering.

Biodegradable functionalized electrospun PLGA membranes appear promising as surrogates of natural basement membranes. In a first step, the suitability of these membranes for tissue engineering applications and as an artificial basement membrane was demonstrated. Therefore, it was evaluated whether sP(EO-*stat*-PO)/PLGA membranes are biocompatible, offer suitable porosities and degradation characteristics, can be sterilized, and are stable under dynamic conditions.

PLGA is approved by the Food and Drug Administration for therapeutic devices and probably the most popular synthetic polymer because of its excellent biocompatibility. The star-shaped additive sP(EO-*stat*-PO) is bioinert. PEG is also approved as a material for biomedical and pharmaceutical applications and is considered non-toxic [24]. Therefore, it can be assumed that the functionalized electrospun membranes are biocompatible. Cell culture experiments confirmed this assumption.

Membranes made of sP(EO-*stat*-PO)/PLGA were stable at ambient conditions (20 °C, 50 % room humidity). This morphological stability changed by increasing the temperature. PLGA membranes shrank at 37 °C by up to 60 % of their original size. This can be explained by the fact that PLGA solidifies in an amorphous shape when membranes are electrospun at room temperature. As soon as the membranes are incubated at higher temperatures, the mobility of the polymer chains increases

significantly. At the glass transition point (Tg) of PLGA of around 45-50 °C, the oriented chains in the amorphous regions relax and heat shrinkage is observed with an increase in fiber thickness and a decrease in porosity [198]. Wetting accelerates the shrinkage because the medium penetrates the mesh accompanied by fiber swelling and allows direct heat transfer. To overcome this limitation, sP(EO-*stat*-PO)/PLGA membranes were fixed in cell crowns for further experiments to avoid membrane shrinkage and a decrease of the pore size.

The membrane porosity is another property, which is crucial for cells to produce their own ECM proteins and to form a natural basement membrane. Although electrospun membranes reveal high porosities of more than 90 %, the pores are relatively small compared to the size of the cells. This small pore size is a fundamental issue of electrospun membranes. It hinders cell infiltration *in vitro* and tissue ingrowth and vascularization *in vivo*. Thus, a nanofiber mesh will essentially behave as two-dimensional (2D) sheet, on which cells are able to migrate along the surface, rather than a three-dimensional (3D) membrane, in which cells are capable of infiltrating. Larger pores enhance the cell supporting capacity of the membrane by favoring cell migration and the diffusion of nutrients, metabolites and waste products. Several techniques were developed to introduce porosity into and between the fibers. Baker *et al.* first involved fiber leaching, i.e. including sacrificial fibers of PEG during electrospinning [199]. Other research groups confirmed the efficacy of this technique [200, 201]. It has also been shown that ultrasonication is able to loosen the electrospun fibers within the membrane and thus, to increase the pore size [151]. The methods of fiber leaching, low temperature electrospinning and ultrasonic treatment were evaluated for their capability to augment the pore size of sP(EO-*stat*-PO)/PLGA membranes and therefore to maximize the success of sP(EO-*stat*-PO)/PLGA fibers as artificial basement membrane. None of the approaches was found to be effective for increasing the pore size significantly. Future studies remain to be performed in order to improve the pore size. An approach would be to augment the diameter of the electrospun fibers resulting in larger inter-connective pores.

Since the fibers of the artificial basement membrane play an interim support role, they need to feature a degradation profile suitable for the targeted tissue and its related healing time. The degradation rate affects cell vitality, growth and host responses [202]. Membranes should maintain their structural integrity until the seeded cells adapt to the environment and remodel their microenvironment by producing tissue-specific extracellular matrix proteins. An ideal degradation rate might be similar to the tissue formation rate [203]. Morphological changes of degrading sP(EO-*stat*-PO)/PLGA and PLGA membranes were investigated using scanning electron microscopy (SEM). A few days of exposure to aqueous medium resulted in complete disintegration of pure PLGA membranes. Fibers already started to develop a film-like structure after 1 week at 37 °C. In contrast, sP(EO-*stat*-PO)/PLGA kept their fibrillar shape over 28 days. This gives cells enough time to start producing their own extracellular matrix proteins.

To elucidate the mechanism behind the change in morphology, the Tg of both PLGA and sP(EO-*stat*-PO)/PLGA membranes were measured by differential scanning calorimetry (DSC). A decrease in molecular weight lowers the Tg. For both sP(EO-*stat*-PO)/PLGA and PLGA membranes, a Tg of 48.8 $\pm$ 0.9 °C was measured at day 1 of incubation. These results are in line with published Tg of PLGA [204]. The Tg of sP(EO-*stat*-PO)/PLGA dropped from 49.7 °C to 39.0 °C within 3 weeks of incubation, whereas the Tg of PLGA fibers stayed almost constant over the investigated period. These results were unexpected at first glance. The SEM images of the degrading fibers suggested rather the opposite, namely that the Tg of PLGA dropped whereas the Tg of sP(EO-*stat*-PO)/PLGA remained constant.

Taking the morphological changes and the Tg into consideration, the degradation can be interpreted as follows: water can penetrate better into the more hydrophilic sP(EO-*stat*-PO)/PLGA fibers leading to increased hydrolytic chain scission. The hydrolytic chain scission of sP(EO-*stat*-PO)/PLGA may be even further accelerated by the hydrogel around the fibers. The acid degradation products having carboxylic acid end groups are retained within the matrix until the chains reach a critical molecular weight and become water-soluble. This results in an internal pH reduction which auto-catalyzes chemical hydrolysis. Due to this effect, several

research groups observed bulk materials with only a shell left around a completely dissolved core structure [205, 206]. Usually, the effect is minimized for electrospun fibrous membranes, because fiber dimensions prevent accumulation of large amounts of acid within the fibers [207, 208]. However, the hydrogel formed by sP(EO-*stat*-PO) acts as a cross-linker for PLGA and forms a dense hydrogel network around the fibers. This might overcome the positive effect of the electrospun fibers. The decrease of the molecular weight (M_w) results in a decreased Tg. In contrast, water does not penetrate to that extent into the hydrophobic PLGA fibers resulting in a constant Mw and therefore constant Tg.

Although the introduced sP(EO-*stat*-PO) increases hydrophilicity and water can penetrate better into the fibers and increase the degradation rate, which is confirmed by the drop in Tg, the fibers kept their morphology as investigated by SEM. This is probably due to the intermolecular bonds of sP(EO-*stat*-PO) forming a hydrogel network [32]. As the star molecules are mainly present on the fiber surface, the dense hydrogel network retards the disintegration of fibers through swelling. The changed degradation characteristics of the sP(EO-*stat*-PO)/PLGA fibers will allow cells to proliferate on the fibrillar structure, produce their own ECM proteins and form a natural basement membrane. Fibers need to feature a degradation profile suitable for the targeted tissue and its related healing time. Investigations have shown that after 2-3 month, sP(EO-*stat*-PO)/PLGA membranes also degraded [171]. The degradation profile of sP(EO-*stat*-PO)/PLGA fibers seems to resemble the cutaneous tissue repair [209].

Membranes which are used as artificial basement membrane must either be manufactured aseptically or sterilized after processing. For practical and economic reasons, materials intended for research are often sterilized post-processing. However, low polymer melting points, complex architectures and, hydrolytic degradation mechanisms result in membranes that may be easily damaged by sterilization [119]. Therefore, the goal was to establish a sterilization technique which preserves fiber structure, is easy to handle, accessible without long-hand planning and fast to perform. γ-sterilization, a technique widely used to sterilize medical equipment and PLGA [210], was compared to 70 % (v/v) ethanol

treatment, which is applied extensively in experimental studies, due to its convenience. Ethanol treated, as well as γ-sterilized samples, did not show signs of contaminations, whereas in untreated samples the media became cloudy and changed color from red to yellow after 24 hours. To avoid contamination, antibiotics were supplemented in untreated controls for further experiments. Morphological investigation revealed that after 1 day in medium, treated and untreated samples looked comparable. After one month, however, the morphological structure of the γ-sterilized fibers changed. Sterilization had negative effects on the fibers morphology, probably due to the ionizing nature. Ethanol treatment did not have a negative influence on fiber morphology. However, it is of limited use for the clinic, as it is classified as a disinfectant rather than as a sterilization agent due to its low penetration and the presence of resistant strains [211]. Although gram-positive, gram-negative, acid-fast bacteria, and lipophilic viruses react to concentrations of ethanol in water ranging from 60 % to 80 % (v/v), it has to be kept in mind that hydrophilic viruses and bacterial spores are resistant to the ethanol effects [210]. Furthermore, it is known from the literature that all methods of sterilization reduce the tensile strength of the membranes [211]. In our experiments, sP(EO-*stat*-PO)/PLGA fibers in cell crowns remained stable over the entire incubation period. Solely for PLGA fibers, tearing of fibers was often observed. An important question for further studies is to determine whether sterilization had an influence on fiber composition and properties, as for instance a loss of PEG, which in turn will influence protein adsorption and cell adhesion.

Meshes that are used as artificial basement membranes should have suitable mechanical properties. If not mentioned otherwise, PLGA 50/50 consisting of 50 % poly(glycolide) and 50 % poly(D,L-lactide) was used for experiments. It was shown before that electrospun sP(EO-*stat*-PO)/PLGA membranes have mechanical properties close to the skin. The ultimate tensile stress measured at fiber breakage was 6.20 $\pm$ 0.11 MPa for PLGA fibers and 5.48 $\pm$ 0.62 MPa for sP(EO-*stat*-PO)/PLGA fibers. The ultimate tensile strain was similar for both membrane types with 50.5 $\pm$ 13.5 % for PLGA and 53.4 $\pm$ 21.5 % for sP(EO-*stat*-PO)/PLGA membranes. As a comparison, the ultimate tensile stress of the skin was reported to be in the range of 5 to 30 MPa and the ultimate tensile strain between 35-115 % [212]. To better

mimic the physiological environment, sP(EO-*stat*-PO)/PLGA membranes should also be suitable to be cultured in bioreactors. Bioreactors provide a dynamic *in vitro* environment for tissue growth and maturation. The flow of medium provokes cell migration and differentiation by enhancing nutrient transport to the interior of the membrane and by providing mechanical stimulation in the form of shear stress. Experiments with sP(EO-*stat*-PO)/PLGA 50/50 membranes showed that their mechanical stability is not high enough to allow the culture under dynamic conditions. The membranes tore under the applied shear stress.

Therefore, PLGA 85/15 with an increased content of lactic acid compared to PLGA 50/50 was used as a polymer for electrospinning. For membranes demanding high stabilities, PLGA with an increased amount of poly(D,L-lactide) is supportive. The presence of the methyl side groups in poly(D,L-lactide) makes it more hydrophobic than poly(glycolide) and hence poly(D,L-lactide)-rich PLGA copolymers are less hydrophilic, hinder absorption and diffusion of water, and thus the chemical hydrolysis of the hydrolytically unstable ester bonds into D,L-lactic acid and glycolic acid. Consequently, membranes exhibit an increased tensile modulus, ultimate tensile stress, and ultimate tensile strain [213]. Different concentrations of the polymer were dissolved in the same solvents as for electrospinning of PLGA 50/50 membranes. Appropriate concentrations, with respect to solution viscosities, resulted in sufficient chain entanglements, which avoided the breaking up of the jet into droplets. 16 wt% PLGA 85/15 polymer revealed to be the optimal concentration to obtain uniform fibers. Concentrations below 16 wt% resulted in beaded fibers due to insufficient entanglement of polymer chains. Increasing the polymer concentration higher than 16 wt% increased the viscosity of the solution, leading to thicker fibers but did not improve the fiber quality. Transferring this knowledge to the electrospinning of PLGA 85/15 with NCO-sP(EO-*stat*-PO), solutions containing 8-18 wt% PLGA 85/15 and 5 wt% NCO-sP(EO-*stat*-PO) were prepared. Although NCO-sP(EO-*stat*-PO) increased the viscosity, 16 wt% polymer remained as the optimal concentration for homogeneous, defect free fibers. The fiber thickness of 380 ± 46 nm did not change significantly by adding NCO-sP(EO-*stat*-PO). In the native ECM, collagen fibrillar structures reveal a diameter in the range of 50-500 nm [214].

In bioreactor experiments, the electrospun sP(EO-*stat*-PO)/PLGA 85/15 membranes showed improved mechanical characteristics compared to sP(EO-*stat*-PO)/PLGA 50/50 membranes. However, small holes were visible after 14 days under dynamic culture conditions. One advantage of the one-step electrospinning approach is that it enables the production of membranes with several layers. Thus, hydrophobic fibers of PLGA 85/15 were combined with hydrophilic sP(EO-*stat*-PO)/PLGA 85/15 fibers by electrospinning a core of PLGA 85/15 and a shell of sP(EO-*stat*-PO)/PLGA 85/15 fibers. The layered membrane provided sufficient mechanical strength to be cultured under dynamic conditions for at least 14 days. With the intention of using the membranes as artificial basement membranes, further investigations should include cell culture experiments under dynamic conditions to observe if the layered sP(EO-*stat*-PO)/PLGA 85/15 membranes are stable, can be functionalized with peptide sequences, and if cell adhesion is promoted.

The simple preparation procedure, as well as the biocompatibility, degradation behavior, and stability recommended the use of the electrospun sP(EO-*stat*-PO)/PLGA membranes. Although the pore size of the membrane could certainly be increased, fixing membranes in cell crowns for experiments avoided fiber shrinkage going along with a decrease in pore size. Overall, the suitability of the functionalized electrospun membrane for the generation of artificial basement membranes was demonstrated, advocating the investigation of sP(EO-*stat*-PO)/PLGA membranes in continued work.

5.2 Quantification of immobilized peptides on functionalized membranes

Electrospun membranes serve as matrix structures for tissue engineering applications. Functionalization of the fibers with bioactive peptide sequences promotes specific cell-matrix interactions to induce tissue regeneration and cell adhesion. In order to understand the relationship between functionalization, surface properties of the membrane and their biological performance, it is essential to characterize the surface of the membrane.

There are numerous studies on the characterization of biomaterials such as microscopic techniques including fluorescence, confocal laser scanning, atomic force microscopy, scanning electron and transmission electron microscopy. Moreover, spectroscopic methods were used to characterize materials, including energy-dispersive x-ray, attenuated total reflectance fourier transform infrared, x-ray photoelectron, and time of flight secondary ion mass spectrometry. In addition, various non-spectral methods have been used, as water contact angle determination, dye assays, protein assays, biological activity assessment, radioassays, zeta potential, colorimetry, fluorometry, and x-ray photoelectron spectroscopy [215, 216].

Although the methods were successfully used for characterizing flat surfaces, it remains challenging to transfer these technologies to electrospun membranes due to their fibrillar structures, high porosities, and large surface to volume ratios. Moreover, it is hard to obtain precise quantitative results about surface ligand density and ligand distribution with these methods. Furthermore, the methods have limitations such as difficulties in detecting functional groups with concentrations in the nanometer and picometer range. Other disadvantages include their lack of robustness and they tend to measure bulk properties rather than surface properties. Therefore, some of the measured peptides may be embedded in the fiber and not available for adhesion. The development of a robust and surface-sensitive quantification method for functional groups on the surface of electrospun fibers presents a daunting challenge.

In this study, a method was established which allows to precisely quantify peptide sequences on the surface of electrospun membranes. In detail, a model compound was developed based on the extensively used cell-adhesion-mediating peptide sequence RGD. The cleavable, UV-metrically active group, 2-mercaptopyridine, was linked to the peptide via disulfide formation with the thiol group of cysteine. Due to this, the model peptide is able to bind with its N-terminus to the isocyanate groups of NCO-sP(EO-*stat*-PO) on the surface of the fibers. 2-mercaptopyridine can be liberated from the surface under reducing conditions once attached to the fibers. Thus, information can be obtained about peptide density on the surface of the

electrospun fibers, how much peptide is covalently bound, if their binding is influenced by the amount of peptide, and whether incubation after electrospinning has an influence on peptide binding using a conventional UV-spectrophotometer.

For quantification experiments, the wavelength of maximum absorbance of 2-mercaptopyridine derived from the model compound SGRGDSC-2-mercaptopyridine was determined. The measured UV-spectrum showed two peaks, one at 270 nm and the other at 343 nm due to the tautomerization of 2-mercaptopyridine to 2-thiopyridone. These two absorption maxima correlate with the UV-maxima described for 2-mercaptopyridine in the literature [217]. For quantification experiments, the peak at 270 nm was used. Under the conditions used in our study, which comprise a large excess of TCEP, the intensity ratio between the peaks in a given mixture did not change over time or other parameter variations used during the quantification procedure.

Different concentrations of the model peptide were dissolved in aqueous TCEP solution and absorption was measured at 270 nm to investigate whether the disulfide bridge between the peptide sequence and 2-mercaptopyridine is cleaved entirely by the reducing agent TCEP and whether the segregated 2-mercaptopyridine is UV-active. The correlation between absorbance and concentration of 2-mercaptopyridine from the peptide was compared with that of pure 2-mercaptopyridine. Both curves were almost identical and showed the same gradient. There was a linear correlation between the solution absorbance and the amount of peptide for concentrations up to at least of 6×10^{-7} mol/ml, higher concentrations were not tested. The R value close to 1 indicates good sensitivity of the assay. The similarity in the two curves, meaning pure 2-mercaptopyridine and 2-mercaptopyridine cleaved from peptide, suggests that 2-mercaptopyridine can be cleaved completely from the peptide and hence the method is directly applicable for quantification experiments. From the standard curve of 2-mercaptopyridine from the peptide, it was possible to deduce the amount of peptide included in the electrospun membrane by measuring the absorbance.

Since it was shown that treating membranes containing the RGD sequence without the UV-active 2-mercaptopyridine also results in minor UV-absorbance, these

membranes were used as controls. Absorbance of the control membranes was subtracted from the membranes used for quantification. The absorbance of 2-mercaptopyridine is pH dependent, hence it was kept at pH = 7.4 and controlled regularly.

To determine the peptide density within the electrospun membrane, the cleavable RGD derived model peptide sequence was electrospun with NCO-sP(EO-*stat*-PO) and PLGA. Quantification was performed by placing the electrospun membrane in aqueous TCEP solution. TCEP cleaves the disulfide bridge so that mercaptopyridine can be measured UV-metrically in solution. The amount of peptide embedded within the fiber and not exposed to the surface was analyzed by dissolving the membrane in NaOH. Afterward, the suspension was treated with TCEP and measured UV-metrically.

By treating the membrane directly with TCEP solution, information about the total amount of peptide on the surface of the fiber can be obtained. However, they do not provide predictions on peptide binding. Peptides can either be covalently attached or physically adsorbed to the surface. If peptides are physically adsorbed to the surface, they can be washed away as soon as the membrane is placed in cell culture medium and therefore not available for cell adhesion. To quantitatively evaluate the covalently attached content, a washing step was included before treating the membrane with TCEP. Hence, physically adsorbed peptide was removed with water. Covalently attached peptides remained on the surface of the membrane and were detected afterward by treating the membrane with TCEP solution.

The peptide concentration of the membrane was determined by measuring the absorbance and then calculating it from the standard curve obtained from the model peptide in aqueous TCEP solution. Quantification of peptides without an included washing step showed that 99 % of the peptide could be measured on the surface of the fibers. A marginal amount of peptide was embedded in the fiber and could not be measured until dissolving the membrane in NaOH. Including a washing step showed that 80 % of the peptides embedded in the fiber are non-covalently bound, whereas 17 % of the peptides are covalently bound to the surface. The amount of peptides embedded in the fibers and not detected until dissolution was not

influenced by the washing step. This unexpected small amount of covalent peptide binding may be attributed to the fact that the model peptide SGRGDSC-2-mercaptopyridine binds with its serin at the N-terminus to the free isocyanate groups of NCO-sP(EO-*stat*-PO). The cell-adhesion-mediating peptide sequences CGRGDS, CGYIGSR, CGIKVAV, CGEFYFDLRLKGDK used for cell culture experiments, however, bind to the isocyanate groups with their cysteine at the N-terminus. Due to the more nucleophilic nature of the thiol group in the cysteine molecule, it is assumed that cysteine-terminal peptides facilitate covalent binding compared to serine-terminal peptides. Hence, the results of the quantification experiments may underestimate the actual covalent binding of cell-adhesion-mediating peptide sequences on the surface of the fibers. Future studies remain to be performed in order to examine the assumption in more detail. The synthesis of a model peptide with an N-terminal cysteine was not possible, since the sulfur atom in the amino acid would react with the disulfide bridge within the peptide. An approach to overcome this limitation would be to design another UV-active model peptide for quantification, which does not include a disulfide bridge so that the peptide can be synthesized with a cysteine at the N-terminus, which is later used for attachment to NCO-sP(EO-*stat*-PO).

Comparing the expected peptide concentration, meaning the amount of peptide used for electrospinning, with the measured peptide concentration, calculated from the absorbance of 2-mercaptopyridine, it could be shown that the entire peptide content is detected in the membrane. These results suggest that the model peptide can be grafted to the surface of the fibers and that it is suitable for quantifying bioactive peptide sequences.

To analyze whether the peptide concentration has an influence on peptide binding, different amounts of peptides were used for electrospinning. UV-measurements of 2-mercaptopyridine showed that the used peptide concentration did not affect the peptide concentration on the surface of the fiber in comparison to the peptide concentration embedded within the fiber. However, the kind of peptide binding was influenced by the peptide concentration.

Covalent peptide binding increased with the amount of peptides used for electrospinning. This can be explained by the fact that the reaction between the isocyanate groups and the peptide is not finished in the time span between mixing of the components in the spinning solution and the spinning process as such. Moreover, as more peptides are included in the electrospinning solution, the probability to interact with the isocyanate groups is increased and therefore more peptides can covalently attach to NCO-sP(EO-*stat*-PO). The fact that at low peptide concentrations, no covalently attached peptide could be determined might be due to the minor absorbance of low amounts of peptides. We surmise that the peptide concentration was too low to obtain reliable absorption results by UV-spectroscopy. This might also be the reason why no peptide is embedded within the fiber with low peptide concentrations. For future research, it would be beneficial to include more model peptides in the electrospinning solution to overcome these inaccuracies.

Peptide binding is dependent on the crosslinking processes. Thus, we investigated the influence of storage after electrospinning on peptide binding. Therefore, peptide density was quantified directly after electrospinning and after 96 hours of incubation at room temperature. Whereas directly after electrospinning, the entire peptide was non-covalently bound and was washed away, 96 hours of incubation after electrospinning resulted in 17 % of covalently bound peptide. The results suggest that a certain period of time is needed for the reaction between the peptide and the isocyanate groups at the terminal end of NCO-sP(EO-*stat*-PO). These findings should be kept in mind for the production of functionalized sP(EO-*stat*-PO)/PLGA fibers.

Since surface properties of a biomaterial have an enormous impact on the success of a biomaterial, the application of adequate surface characterization and quantification is of paramount importance. The results underline the importance of characterizing and quantifying the surface of a biomaterial. It seems reasonable that the used amount of functional groups is later presented on the surface of the material. However, a key finding is that it cannot be assumed that the entire amount of peptide is covalently attached to the surface. Although we figured out that the covalent binding affinity is quite low, this does not present a serious problem. It is

rather important to know how much of the used peptide is presented to the surface in the end. By simply using an increased amount of peptides for electrospinning, adequate peptide concentrations can be obtained. Future work should further investigate whether covalent binding can be increased by improving coupling conditions, as for instance incubating the peptides for longer time points with NCO-sP(EO-*stat*-PO) before using them for electrospinning.

In summary, the presented method provides robust and reproducible results for the quantification of peptide sequences that are attached to the surface of biomaterials. The cleavable group allows quantification with a conventional UV-spectrometer with high sensitivity under aqueous conditions. The experimental approach may have advantages compared to other quantification techniques, as the present case is surface sensitive, low quantities of peptide can be measured, and no flat surfaces are required for quantification. Moreover, the approach is appropriate to determine whether the peptide is covalently attached or physically adsorbed to the surface. To obtain reliable results and information about homogeneous distribution of peptides, a combination of the described method with other established characterization and quantification techniques might be the best solution.

Analyzing the amount and distribution of functional groups on and within the fibers will enhance the fundamental understanding of the effects of functional groups on cellular behavior. Therefore, functionalization processes can be optimized for biological efficacy of the functional groups. By attaching the UV-active cleavable group to other peptide sequences, the quantification method may broadly be applied in successive work to monitor different peptides than the RGD peptide sequence. Besides using the method of surface quantification for quantifying modified fibers, it may also be applicable for hydrogels and nanoparticles.

5.3 Biological interactions of functionalized membranes in mono-culture

Electrospinning of synthetic polymers offers the possibility to produce membranes which are similar to the natural basement membrane in morphology and pore sizes. However, to offer biochemical similarity, membranes need to have by far more properties, e.g. biological analogy.

Synthetic biomaterials commonly do not contain bioactive binding sites. Rather, they gain bioactivity by proteins that adsorb to the biomaterials surface. Protein adsorption is believed to be the initial event when a material comes into contact with the biological environment. Proteins for example in blood or cell culture media rapidly adsorb to the surface of the biomaterial within seconds to minutes. The type and the amount of adsorbed protein determines the surface density of bioactive binding sites, which are later available for cell interactions [218]. When cells, which are moving much slower, approach the biomaterial, the surface is already covered with proteins. Therefore, cells interact with proteins on the surface, and not with the material. Overcoming protein adsorption and generating surfaces for specific cell adhesion at the same time remains a challenge in tissue engineering.

5.3.1 Protein adsorption on functionalized membranes

In the literature, there are various definitions for the word "biocompatible". Some define biocompatibility as the "quality of not having toxic or injurious effects on biological systems" [219]. Others have a more precise conception of biocompatibility and use it for "the ability to perform as a substrate that will support the appropriate tissue-specific cellular activity, including the facilitation of molecular and mechanical signaling systems, in order to optimize tissue regeneration, without eliciting any undesirable effects in those cells, or inducing any undesirable local or systemic responses in the eventual host" [220]. Despite the different views, there is widespread recognition that the surface chemistry and topography of the material is an important parameter which determines whether a material is biocompatible. Recently, a number of reviews have appeared covering the present challenges and future aspects of biocompatible materials [221-225]. The authors agree that protein adsorption is a key event which plays a major role whether a material is biocompatible or not. Protein adsorption can elicit adverse host responses such as blood clotting and complement activation. Therefore, controlling the protein-surface interactions is an important factor for the design of a biomaterial.

Over the last decades, various efforts have focused on suppressing non-specific protein adsorption [226, 227]. PEG has extensively been used for this purpose.

Several approaches to prepare PEG coatings have been reported including self-assembly [228, 229], polymer grafting on activated surfaces [230, 231], physical adsorption [232] and surface polymerization [233, 234]. However, often PEG does not permanently remain on the surface, multi-step reactions are needed and it is difficult to achieve the desired surface coverage. The use of star-shaped PEG enables to overcome these difficulties. The additive forms highly cross-linked networks with high surface coverage around the PLGA fibers and suppresses protein adsorption in that way [235].

We have shown before that sP(EO-*stat*-PO)/PLGA fibers on glass substrates have protein-repellent properties [171]. The aim of this study was to analyze whether free-standing sP(EO-*stat*-PO)/PLGA membranes also suppress protein adsorption and whether the protein-repellent properties remained stable over long-term storage. Therefore, BSA coupled with tetramethylrhodamine as a model protein was incubated on sP(EO-*stat*-PO)/PLGA and PLGA membranes which were stored for up to one year before protein measurements. Compared to uncoated PLGA meshes, sP(EO-*stat*-PO) coated membranes revealed significant higher resistance against protein adsorption. PLGA membranes showed strong fluorescence, whereas the absence of any fluorescence intensity on the sP(EO-*stat*-PO)/PLGA membranes indicated the lack of adsorbed proteins. Protein adsorption did not change on membranes prepared and stored in sealed centrifuge tubes for up to one year prior to protein adsorption measurements, which argued for the long-term stability of the cross-linked star-polymer surfaces. The suppression of BSA tetramethylrhodamine conjugate adsorption is an indicator for a hydrogel-like, non-fouling surface of the membrane. The measured protein adsorption for functionalized membranes is in general agreement with the protein adsorption studies which were conducted with functionalized fibers on glass substrates. To evaluate the exact amount of adsorbed proteins to the membrane and possible changes out of storage, further investigations should include the quantification of surface-adsorbed BSA. Moreover, future studies remain to be performed to clarify if, for instance, sterilization, which is indispensable for cell culture experiments, has an influence on protein adsorption. It would also be interesting to investigate, to which extent the protein-repellent properties are influenced by incubating the membrane for longer times in buffer or

medium. Cell-culture experiments with fibroblasts and HaCaT cells demonstrated that sP(EO-*stat*-PO)/PLGA membranes retained their cell-repellent properties, and thus probably their protein-repellent properties over a culture period of 10 days. However, to use the functionalized membrane as support structure for the development of tissue models, far longer protein-repellent stabilities are required.

Altogether, the study demonstrated, that the combination of bioresorbable PLGA and NCO-sP(EO-*stat*-PO) leads to stable electrospun membranes with protein-repellent properties. The minimized protein adsorption on the fibers surfaces can be attributed to the presence of PEG chains. The hydrophilic nature of these polymers prevents hydrophobic interactions between the fiber surface and proteins.

5.3.2 Cell adhesion and proliferation on functionalized membranes

The requirements for biomaterials continue to become more and more specific and complex. While two decades ago, characteristics such as mechanical stability and biodegradability were considered acceptable, today functions such as the activation of specific cell-material interactions are essential. Several approaches have been used in biological and therapeutic applications to promote selective cell adhesion. Peptides were grafted on polymers before electrospinning or modified with bioactive molecules after electrospinning [236]. Thereby, every functionalization method has its strengths and weaknesses. Cell-adhesion-mediating peptide sequences were so far either physically adsorbed [167] or covalently attached [168, 169] to the surface of the fibers. However, the methods were often time-consuming and involved several activation and coupling steps [237, 238]. Kim *et al.* produced nanofiber meshes to mimic the ECM structure. They used a blend mixture of PLGA and PLGA-*b*-PEG-NH_2 di-block copolymer and grafted GRGDY onto the aminated surface of the electrospun mesh under hydrating conditions [239]. Synthesizing block copolymers, using them for electrospinning, and afterward modifying them with peptide sequences is a complex procedure.

In contrast, combining PLGA with NCO-sP(EO-*stat*-PO) and peptide sequences allows the simple and time-saving one-step preparation of functionalized fibers. In

this way, cell-adhesive peptides derived from fibronectin and collagen IV were bound to fibers immobilized on glass substrates to allow the straightforward microscopical analysis. Integrin receptors recognize the peptide sequences and mediate interaction of the cells with the embedded biologically active peptide sequences [240]. The functionalized glass substrates revealed specific adhesion of HaCaT cells, as well as fibroblasts to the fibers depending on the peptide sequence [235].

To exploit this spinning technology and to develop biomimetic artificial basement membranes, we used NCO-sP(EO-*stat*-PO) as reactive additive for the electrospinning of PLGA to generate free-standing biodegradable meshes. In the context of the intended application as basement membrane towards skin and oral mucosa tissue engineering, we considered the ability to support fibroblast adhesion and infiltration, as well as the capacity for keratinocyte adhesion, proliferation, and differentiation as the most important properties. To investigate which peptide combinations are favorable for fibroblasts and HaCaT cells, spontaneously immortalized human keratinocytes derived from human abdominal skin [241], membranes with peptides derived from major functional binding sequences of the basement membrane were electrospun, and cell proliferation of fibroblasts and HaCaT cells was studied on these membranes.

Fibroblasts and HaCaT cells attached to all bioactivated fibers, flattened and spread their plasma membranes over the substrate, indicating a high number of binding sites on the material [242, 243]. Comparison of fibroblast and HaCaT adhesion revealed that both cells types grew to confluence on membranes functionalized with fibronectin and fibronectin/laminin/collagen IV derived peptide sequences, whereas on membranes functionalized with laminin/collagen IV derived peptides, HaCaT showed higher proliferation rates than fibroblasts indicating a minor effect of collagen IV and laminin peptide sequences on fibroblasts. The finding that fibronectin promotes fibroblast adhesion and growth, while laminin and collagen type IV are favorable for HaCaT cells are in accordance with the situation in the natural environment. While fibronectin is an important constituent of the reticular

lamina facing the dermis, collagen type IV and laminin play a major role in the basal lamina attached to the epidermis [244, 245].

Previous work did not propose the strong adhesion and proliferation of HaCaT cells on membranes functionalized with the fibronectin derived binding sequence. We reported of significantly lower adhesion of HaCaT cells on the fibronectin derived peptide CGRGDS than on the collagen IV derived peptide sequence CGEFYFDLRLKGDK, albeit both peptides had synergistic effects on cell adhesion [18]. This difference can, however, be resolved by the reduced porosity and increased ligand density of the free-standing electrospun membranes in comparison to the flat substrates with single functionalized fibers which have been used before [246].

Culturing membranes over a prolonged period of 10 days confirmed that fibroblasts and HaCaT cells proliferated well on the functionalized membranes. Cell numbers increased over the investigated period so that it can be assumed that degradation of PLGA had no negative effect on cell growth. The cell suppressive characteristics of sP(EO-*stat*-PO)/PLGA were stable with a marginal number of cells attaching to the substrate.

SEM micrographs of HaCaT cells and fibroblasts revealed that cells favor the structures of the electrospun membrane and maintain a physiological shape, suggesting that the cells function biologically on the membrane. Some cells showed a spherical morphology; this is most likely due to the paraformaldehyde fixing/ethanol dehydration and CO_2 critical point drying steps, rendering the cell culture environment unfavorable and causing the cells to retract their micro-extensions [247].

In summary, this study demonstrates that the functionalized electrospun membranes prevent protein adsorption. Selective cell adhesion of fibroblasts and HaCaT cells could be realized by means of non-adhesive coatings that are functionalized with binding sequences of the major functional components of the basement membrane. From these experimental data, it could be supposed that the combination of minimized nonspecific protein adsorption with immobilization of active molecules as well as the simplicity of the production of these free-standing

3D fibrous membranes is a unique and promising feature for the construction of artificial basement membranes.

5.4 Functionalized membranes for skin tissue engineering

If keratinocytes and fibroblasts are cultured separately on a collagen or fibrin gel, they can form a basement membrane by themselves, although it is mechanically weak and takes a long time to develop [248]. However, few studies have addressed the establishment of artificial basement membranes due to its complex structure. Electrospun membranes are considered to be promising candidates due to their high porosities, flexibility in polymer choice, and their morphological, as well as topographical characteristics bearing resemblance to the collagen fibrils in natural basement membranes. Natural polymers such as laminin [249] and animal tumor derived matrix extract, known as matrigel [250], have been used for electrospinning. However, natural polymers are difficult to isolate and yields are typically low. Moreover, cross-linking is required to increase mechanical properties, materials could be immunogenic, batch-to-batch variations occur and modifications are hard to realize. Electrospinning of collagen resulted in meshes with structures more like a film after hydration [249]. Natural proteins undergo significant swelling and therefore change surface structure from nano- to microscale. Maintenance of the nanoscale fiber diameter is, however, essential to preserve the biomimetic topography of the basement membrane. Crosslinking often destroys the porosity of the mesh and causes flattening of the fibers. The molecular structure of native proteins can also be changed by solvents needed for solution electrospinning. While combining electrospinning of natural polymers with synthetic polymers [251, 252] may be sufficient to improve the mechanical characteristics, some parameters can nevertheless not be controlled.

Electrospinning of synthetic polymers provides greater control upon material and membrane properties. Since synthetic biomaterials lack biological binding sites, they are equipped with molecular cues mimicking certain aspects of natural basement membranes. While larger peptide sequences result in variations in behavior and cleavage, undesired effects could be eliminated to a great extent by

using short peptide sequences [253, 254]. Hozumi *et al.* conjugated peptide sequences to chitosan and investigated the biological activities of the resulting matrices as artificial basement membrane [97]. However, to our knowledge, a completely synthetic, biocompatible, biofunctional, and biomimetic membrane representing sufficient cues to promote cell adhesion, proliferation and extracellular matrix remodeling in a co-culture system has to be established to date.

5.4.1 Isotropic membranes for skin tissue engineering

In the natural environment, collagen type IV, fibronectin, and laminin are major functional components of basement membranes. Thereby, collagen type IV is responsible for the network structure; laminin and fibronectin contribute to the biological functions and play an essential role for tissue development and regeneration. Mono-culture experiments with HaCaT cells and fibroblasts have shown that synthetic matrices composed of sP(EO-*stat*-PO)/PLGA modified with cell-adhesion-mediating peptide sequences from exactly these proteins appear to be an ideal starting product to fully control material properties and cell-matrix interactions and to act as a bioactive and degradable membrane and surrogate of basement membranes.

Thus, biologically active peptide binding sequences derived from fibronectin, laminin and collagen type IV were involved in the electrospinning approach. Two other critical components of the basement membrane, perlecan and nidogen were not included in the artificial basement membrane, because they crosslink collagen and the laminin network [255] and therefore, they are not essential in artificial membranes. sP(EO-*stat*-PO)/PLGA fibers modified with peptide sequences revealed fiber diameters of 300 $\pm$ 34 nm. By comparison, the fibrils of epithelial basement membranes are in the range of 22-92 nm [256]. Hence, an important question for further research would be to determine whether it is possible to decrease the fiber diameter of sP(EO-*stat*-PO)/PLGA membranes to more closely resemble the diameter of the fibrils in natural basement membranes.

Fibroblasts were seeded on the functionalized membranes, and after 7 days, HaCaT cells were added on the other side of the membrane. Models were cultured 7 days

under submerged conditions and 14 days at air-liquid interface. The air-liquid interface culture is known to improve tissue development and differentiation in certain tissues [257]. Histological analysis confirmed that it was possible to build up a co-culture model of HaCaT cells and fibroblasts with both cell types organizing spatially in the membrane. Unlike Guimareas *et al* [258], in the present study, fibroblasts migrated into the membrane, while HaCaT cells formed a well attached continuous barrier layer on the upper surface of the membrane. Cells produced the typical extracellular matrix proteins collagen type I, III, IV, as well as fibronectin and laminin V, hence, started to remodel the matrix. These results illustrate that the functionalized electrospun membrane supports cellular ingrowth, provides stimuli that cause polarization, and permits a crosstalk between two cell types, a sign of functional tissue-specific behavior.

5.4.2 Bipolar membranes for skin tissue engineering

Although the electrospun matrix showed promising results as artificial basement membrane, several aspects might still be missing. In order to resemble physiologic conditions, it has to be taken into account that *in vivo* the basement membrane is a fusion of two laminae: the basal lamina with an increased content of collagen type IV and laminin and the reticular lamina with higher amounts of fibronectin. Hence, in order to develop a physiological membrane, a bi-layered membrane was prepared. A solution containing the fibronectin derived peptide sequence CGRGDS was electrospun on a rotating collector as basal lamina with subsequent spinning of a solution containing collagen type IV and laminin derived peptide sequences CGYIGSR, CGIKVAV, CGEFYFDLRLKGDK on top of the first mesh as reticular lamina. This approach enables the layered construction of membranes for co-culture systems. The side containing fibronectin derived peptides served for fibroblasts, the side containing collagen type IV and laminin derived peptides for HaCaT cells.

The bi-layered membrane enabled the culturing of cells separately in two distinct layers. Keratinocytes formed a well attached continuous layer on the upper surface of the membrane and achieved spatial organization expressing cytokeratin 10 and cytokeratin 14. Fibroblasts were positively stained for vimentin. Histological cross-sections reveal that collagen type I, III, and fibronectin is produced by HaCaT

cells and fibroblasts, collagen IV is mainly synthesized by fibroblasts. Laminin V is expressed on the border between epithelial cells and electrospun matrix and is therefore of epithelial origin. The expression of the extracellular matrix proteins is consistent with that of native human skin and in accordance with the literature [259]. To ensure that the antibodies did not stain the peptide sequences incorporated into the membrane, electrospun fibers without cells were stained with the same antibodies as negative controls. No staining could be observed for these membranes.

The synthesis of extracellular matrix proteins is an indication that cells start to remodel their microenvironment. The ability to investigate extracellular matrix remodeling and new tissue formation on synthetic membranes, which can be modified with different bioactive substances, enables the systematic investigation of tissue remodeling and provides the framework for future studies to analyze the influence of various extracellular matrix proteins, of mono- and co-culture, and of cell lines, primary cells, or a combination of both on extracellular matrix remodeling and new tissue formation.

A limiting factor of electrospinning is that membranes consist of tightly packed nanofiber-layers that do not provide pores large enough for cell infiltration and growth and represent a 2D, rather than a 3D cell culture substrate. Histological cross-sections of the peptide modified sP(EO-*stat*-PO)/PLGA membranes illustrated that fibroblasts infiltrate the membrane. Localization of vimentin, a typical marker for fibroblasts and collagen type IV expression confirmed that the cells migrate in the membrane and it is not an artefact originating from cryo-sectioning. Thus, the membrane provides a 3D microenvironment for the cells rather than a flat substrate. Comparison of isotropic and bipolar membranes showed that fibroblasts are able to colonize the entire thickness of the isotropic membrane whereas on the bi-layered membrane, fibroblasts migrated into the part of the bi-layered membrane containing fibronectin derived peptide sequences and did not further migrate into the part of the membrane containing collagen and laminin derived sequences. These results generally correspond to the observations seen on the membrane in mono-culture experiments, where fibroblasts proliferated much stronger on CGRGDS, the

fibronectin derived binding sequence, in comparison to membranes modified with laminin and collagen derived peptide sequences. However, the effects were much more pronounced in the bipolar mesh. In mono-culture, the cells are only in contact with one substrate without an alternative, so that the fibroblasts adhere also to the less favored substrates. When the fibroblasts reach the contact point between the two meshes in the bipolar construct, they show a very clear preferential adhesion and migration. Another evidence for the fibroblast migration into the basolateral mesh containing fibronectin derived peptide sequences is the selective contraction of this part of the bipolar mesh. After co-culture, this part appears much thinner in comparison to the membrane functionalized with laminin and collagen IV derived peptide sequence, although the membranes were prepared from the same volume. Human fibroblasts are known to produce contractile forces up to 2.65 µN/cell [260], which can result in scaffold contraction as observed here.

Several different biomaterials have been developed to mimic the bi-layered structure of the basement membrane in the skin. One of the most widely used and commercially available skin substitutes is Integra®, an bipolar membrane composed of silicone as upper layer and a collagen-glycosaminoglycan porous sub-layer [261]. Bi-layered chitosan-gelatin porous membranes [262], gelatin chondroitin-6-sulphate-hyaluronic acid membranes [263], and a dense chitosan film with a porous chitosan sponge [264] were developed as membranes for skin tissue engineering. Yannas *et al.* combined a dense silicone film which acted as an obstacle to prevent bacterial infection and to control the loss of body fluid with a porous collagen sponge [265]. All the described bi-layered membranes have in common that they are composed of a dense surface layer and a sub-layer of a porous or sponge-like structure. However, only a few papers have been published producing bi-layered porous membranes as support structure for tissue engineering applications. In 2013, Arnal-Pastor *et al.* combined the non-adhering properties of hyaluronic acid with PLLA as cell adherent face [266]. In another study, Pan *et al.* developed a bi-layered membrane by electrospinning of poly(e-caprolactone-co-lactide)/poloxamer (PLCL/poloxamer) and a dextran/gelatin hydrogel [267]. An aligned fiber layer which provides mechanical strength and a random fiber layer with higher porosities and larger pores for cell

infiltration and vascularization were electrospun both from PLA [268]. However, all approaches include different materials which all have the problems related to the lack of homogeneity in the structure with comparable mechanical characteristics and degradation patterns. Moreover, none of the described membranes was applied in co-culture experiments.

The system presented here enables the production of bi-layered membranes from one polymer that do not separate and swell comparably, indicating that during mesh preparation, remaining isocyanate groups on the second spinning procedure covalently reacted with amine groups on the underlying mesh, resulting in a coherent structure. Based on this and on the identical sP(EO-*stat*-PO)/PLGA base material, we conclude that the degradation pattern and mechanical stability is comparable for the bi-layered structure and the isotropically functionalized membrane.

The results of the co-culture with fibroblasts and HaCaT cells are encouraging and should be investigated in further detail. Nevertheless, cross-sections of HaCaT/fibroblast models revealed some alterations in the tissue architecture compared to native skin. The epidermal layers of HaCaT cells on the isotropic membranes and on the bipolar membranes appeared to be thinner than in native skin. The density of the cells was lower and the cells seemed to be larger compared to primary human keratinocytes. It seems also that the stratum corneum-like layers were not ideally formed. Also other research groups have reported on the lack of terminal differentiation in HaCaT cells [269, 270]. Efforts to improve growth and differentiation of HaCaT cells, including the addition of growth factors as EGF and TGF-α to the media, did not markedly influence terminal differentiation [17, 258]. Boelsma *et al.* confirmed differences in tissue architecture of HaCaT cell models compared to normal human keratinocytes and native epidermis and the presence of rounded cells with abnormally shaped nuclei [271]. Other research groups have reported on the absence of clear granular and cornified layers [241]. One reason for that might be that the ultimate steps of terminal differentiation, the generation of a mature cornified epithelium, do not occur. Furthermore, HaCaT cells seem to have an impaired capacity to synthesize lipids as ceramides and triglycerides that are

necessary for a proper barrier formation [269]. This is another hint indicating certain defects in the regulatory mechanism of terminal differentiation. On the contrary, as soon as HaCaT cells have been cultured *in vivo*, they form an orderly structured and differentiated epidermal tissue indicating a differentiation capacity close to native human keratinocytes [269, 272]. Due to these limitations, the next part of the work will focus on the development of co-culture skin models with primary keratinocytes.

Altogether, synthetic membranes are widely applied for tissue engineering applications, providing a surface for cells and a support structure for developing tissues. However, often the membranes do not closely emulate the structure and composition of natural membranes. Herein, the potential of free-standing biocompatible, biofunctional, and biomimetic isotropic and bipolar functionalized polyester membranes modified with NCO-sP(EO-*stat*-PO), and bioactive peptides derived from major components of the basement membrane was evaluated as temporary artificial basement membrane to build up a co-culture of skin cells. The membrane provided cues for adequate cell behavior, supported desired cell functions, and maintained specific phenotypic activities on both sides. The developed artificial basement membrane with different behaviors on each of its faces may comprehensively recapitulate matrix remodeling and new tissue formation in pendency of influential parameters such as membrane composition, fiber diameter, co-culture, and external parameter as dynamic cell culture conditions.

5.5 Functionalized membranes for primary skin cells

Until now, skin models developed on the functionalized membranes are based on primary fibroblasts and HaCaT cells. The use of the human keratinocyte cell line allows unlimited access by passaging and cryopreservation. Moreover, reproducibility and consistency of the skin equivalents are guaranteed, thereby allowing specific pathways or variables to be identified and assessed.

5.5.1 Functionalized membranes for epithelial skin models

Development of a co-culture model based on HaCaT cells and fibroblasts demonstrated differences in tissue architecture of HaCaT cells compared to primary keratinocytes. Thus, the next step was to engineer tissue models based on primary keratinocytes. To this aim, keratinocytes were seeded on fixed electrospun membranes, cultured for 24 hours under submerged conditions and afterward for 3, 7, 10, 15, and 19 days under air-liquid interface. As a control, models on commercially available polycarbonate membranes were prepared. Polycarbonate membranes are widely used for the development of epidermal skin models. Keratinocytes grew to 10-12 viable cell layers of polarized epithelium on the polycarbonate membranes, whereas keratinocytes on the electrospun matrices displayed a diffuse epithelium after 19 days. This was contrary to our expectations, because on day 3, 1-2 homogeneous layers of keratinocytes were detectable on the electrospun matrix. SEM images of primary keratinocytes on fibers affirmed that cells adhered and spread on the fibers after 24 hours. Cells adopted a flattened, polygonal-shape with filopodia- and lamellipodia-like extensions. There were some round, non-spreading cells which might have occurred due to the paraformaldehyde fixing or dehydration and CO_2 critical point drying steps. The models appeared comparable to the insert models. However, the thickness and structure of the epithelium on the electrospun membrane did deteriorate over time. After 7 days, 2-3 cell layers were visible with the development of some holes. These holes may have resulted from cryo-sectioning because they also occurred on the cryo-sectioned insert models. The paraffin embedded tissue models, in contrast, revealed a homogeneous structure. After 10 days, keratinocytes started to dissolve from the electrospun membrane. After 19 days, only a few keratinocytes were left on the electrospun membranes. These results were confirmed by MTT assay and TEER measurements. The viability of insert models and electrical resistance increased over culture time, whereas the viability of electrospun models stayed constant or decreased. A change in electrical resistance could not be detected on models based on electrospun membranes. Different techniques to fix the membranes for cell culture experiments were studied, as it seemed that cells fell through the membrane. If the cell density is too low to mediate cell-cell interactions,

tissue development is hindered. However, changing cell crowns and cell densities did not improve keratinocyte proliferation.

5.5.2 Functionalized membranes for co-culture skin models

The interference of fibroblasts and keratinocytes appears to be crucial for the development of skin equivalents. Fibroblasts secrete ECM proteins and regulate keratinocyte proliferation, migration, and differentiation. Keratinocytes, in turn, stimulate fibroblasts to produce growth factors and cytokines, such as keratinocyte growth factor (KGF), fibroblast growth factor (FGF7), IL-6 and GM-CSF [273]. Boehnke *et al*. determined the minimum amount of fibroblasts required to form a skin equivalent. Complete absence of dermal cells resulted in atrophic epithelia. Cell densities of 5×10^4 cells/cm^2 fibroblasts allowed to form a well-developed epithelium [274]. To provide the stimuli of the fibroblasts to the keratinocytes, a co-culture model of primary keratinocytes and fibroblasts was developed.

The models were constructed as already described for HaCaT/fibroblast co-culture models. After 7 days of fibroblast culture on the membranes, keratinocytes were added, cultured for further 7 days under submerged conditions and then, 14 days under air-liquid interface. H&E stained cross-sections of the obtained co-culture models revealed that the models appeared comparable to the mono-culture models. However, in comparison to mono-culture models, the epidermis did not dissolve after several days in culture from the matrix. Models revealed to be similar in histology after 3 days and 19 days in culture. Changing culture conditions to only 1 day submerged conditions after adding keratinocytes instead of 7 days and increasing the seeding density of keratinocytes did not promote the formation of an epithelial layer. To stimulate fibroblast proliferation and production of ECM proteins, fibroblasts were pre-cultured in normal DMEM medium supplemented with ascorbic acid phosphate, which triggers fibroblast proliferation. However, the higher amount of fibroblasts did not enhance the proliferation of keratinocytes. The inadequate tissue formation of primary keratinocytes might be explained by two different approaches. One explanation would be that the functionalized membranes do not mimic sufficiently the structure and biochemical composition of the natural basement membrane, and thus lead to discrepancies in cell attachment, migration

or differentiation of primary keratinocytes. The discrepancies may also be attributed to differences in cell morphology and receptor expressing of primary keratinocytes and HaCaT cells.

A vast majority of biomaterials fosters cell adhesion by adsorbing proteins for example from blood or media. For biomaterials with protein-suppressing properties, as for sP(EO-*stat*-PO)/PLGA membranes, all biological information must be engineered on the surface of the biomaterial. The results of the keratinocyte experiments support the assumption that the cues presented on the electrospun matrix are not potent enough for the attachment of primary keratinocytes. Integrin-mediated signaling mechanisms, induced by native RGD-containing matrix proteins, cannot be completely remodeled by the synthesized RGD motif. Native integrin-binding proteins have a 1000-fold higher potency to stimulate integrin signaling than isolated RGD domain [275]. This is probably caused by additional domains that are involved in the activation of integrin-dependent signaling in native proteins. Keratinocytes migrate on immobilized RGD sequences; however, maximum migration levels on RGD were never as high as those achieved on whole fibronectin [276].

Another argument might be that the fibronectin, laminin, and collagen type IV derived binding motifs included in the electrospun membrane are not the ones which are essential for keratinocyte attachment, proliferation, and migration. Whereas the fibronectin derived binding sequence RGD is well studied and extensively used in the literature [277], it is very little known so far about the laminin and collagen type IV derived sequences used for modification. It might be that keratinocytes interact with other binding motifs of laminin and collagen type IV than the ones attached to the electrospun membrane.

Moreover, it should be considered that, although keratinocytes produce extracellular matrix proteins, they do not attach to the protein-repellent surface of the sP(EO-*stat*-PO)/PLGA membranes so that they are available for keratinocytes. The non-fouling properties of the functionalized fibers could also explain why the co-culture did not ameliorate the development of the epithelium. The fibers do not interact and bind the extracellular matrix proteins produced by the fibroblasts and

therefore do not provide keratinocytes with adequate stimulation for proliferation and differentiation. In contrast, the widely used polycarbonate membranes for skin tissue engineering are hydrophobic. Proteins and growth factors adsorb to the surface and stimulate adhesion and proliferation of keratinocytes. Growth factors are known to cooperate with integrin receptors in the regulation of adhesion related signaling networks [278].

At first glance, it was surprising to see that primary keratinocytes attached to the fibers but then seem to dissolve after several days instead of forming a polarized epithelium as seen when cultured on polycarbonate membranes. The time dependent response of the primary keratinocytes to the matrix could be due to the fact that keratinocytes degrade the peptide sequences. In another publication, it was demonstrated that keratinocytes have the potential to degrade collagen type IV in the basement membrane [279]. Amano *et al.* investigated that inhibitors of MMPs 1, 2, 3, and 9, markedly augmented the deposition of laminin 5 and collagen type IV and VII collagens at the dermal-epidermal junction, resulting in the formation of a continuous epidermal basement membrane [280]. Hence, the time dependent change in keratinocyte adhesion on the electrospun matrix could be explained by the fact that keratinocytes degrade the peptide sequences included in the electrospun membrane. After several days, the peptide sequences are so far degraded so that keratinocytes cannot properly migrate and proliferate on the membrane.

The time dependent decrease of attaching keratinocytes to the functionalized membranes could also be explained by the fact that cells attach, but do not migrate and proliferate. Cell migration is, however, indispensable for sustained growth and requires both cell-cell and cell-substratum contacts [281, 282]. The mean pore size, which is an essential aspect for tissue-engineered membranes, may not promote migration of keratinocytes. It has been shown that the cell migration potential decreases with increasing the pore size [283]. If pores are too small, cell infiltration is hindered, while nutrition and waste exchange are limited. If pores are too large, there is a reduced ligand density for cell migration. Depending on the size of the cells and the receptor density, various pore sizes might be favorable. For fibroblasts, it

was published that that the largest distance that fibroblasts could bridge was approximately 200 µm [284]. It was observed that keratinocytes do not span between fibers by adopting stretched or elongated phenotype as observed for human fibroblasts [285]. Moreover, keratinocytes are much smaller in diameter and are therefore able to bridge only smaller gaps. An indication that pore size plays a tremendous role in keratinocyte proliferation and differentiation is that primary keratinocytes developed on polycarbonate inserts with pore sizes of 0.4 µm forming 10-12 viable cell layers, but on inserts with 4 µm, only 1-2 cell layers of diffused epithelium were formed. The fact that the pore size of electrospun fibers is too large for primary keratinocytes might be the reason why other groups also had problems culturing keratinocytes on electrospun membranes. Oral mucosa epithelial cells were seeded on electrospun PLGA membranes to recreate a tissue-engineered oral mucosa. A thin layer of epithelial cells was formed. However, the epithelium is not of the quality of that achieved using membranes based on cadaveric dermis [286]. Franco *et al.* fabricated a bi-layered membrane for skin tissue engineering. Testing cytocompatibility of electrospun PCL/PLGA with human keratinocyte cells showed no statistically significant proliferation [287].

Our data rules out that, in contrast to primary keratinocytes, HaCaT cells were able to form an epithelium consisting of several cell layers on the functionalized membranes. Thus, comparing differences of HaCaT cells and primary keratinocytes may lead to an answer why cells behaved differently on the functionalized fibers. As soon as primary keratinocytes have divided one to five times, all their progenies undergo terminal differentiation with the loss of the ability to adhere to the matrix. In contrast, HaCaT have the potential to divide substantially more often due to mutation. If the initial cell density of primary keratinocytes is too low to form cell-cell contacts and promote normal cell growth, the cells do not have the potential to divide as often as HaCaT cells to close the gaps and develop normal epithelial structures.

Cells interact with the membrane through cell surface receptors called integrins. Integrins constitute a large family of cell surface molecules involved in cell-cell and cell-matrix interactions. They consist of α and β subunits and affect cellular behavior

by transmitting extracellular signals to the intracellular compartment. One tissue in which integrins are believed to play an important role in determining the spatial organization of the cells is the epidermis [288]. A different integrin expression profile can be found on HaCaT cells compared to primary keratinocytes. HaCaT cells constitutively express the integrins $\alpha_5\beta_1$ and $\alpha_5\beta_6$ which seem to participate in cell spreading and lateral migration. In contrast, $\alpha_5\beta_1$ and $\alpha_5\beta_6$ receptors are not present in normal primary keratinocytes, but are induced during wound healing. In primary keratinocytes, $\alpha_2\beta_1$ is involved in adhesion to collagen type IV and also functions synergistically with $\alpha_3\beta_1$ in the adhesion to laminin; in non-differentiating keratinocytes, $\alpha_2\beta_1$ appears to be involved in adhesion to laminin, the major collagen receptor might be instead the $\alpha_1\beta_1$ integrin receptor. Migration of primary keratinocytes on fibronectin is mediated by $\alpha_5\beta_1$ integrins, whereas the main fibronectin receptor of HaCaT cells is the $\alpha_5\beta_6$ receptor [289, 290]. The differences in integrin receptor expression might be a possible explanation for the diverse cell behavior of HaCaT cells on the functionalized electrospun fibers. The different integrin composition might allow HaCaT cells to migrate and proliferate on the membrane, but primary keratinocytes not.

Beside the different integrin expression pattern, investigations of Adams and Watt have shown that non-differentiating keratinocytes express integrins at higher levels [291]. Both primary keratinocytes and non-differentiating keratinocytes adhered to collagen type IV, laminin and fibronectin, but non-differentiating keratinocytes adhered more rapidly. Whereas maximal adhesion for non-differentiating keratinocytes was obtained after 1 hour of incubation, primary keratinocyte adhesion occurred only after 3-4 hours. 75-90 % of non-differentiating keratinocytes adhered to all substrates, but only 60-65 % of primary keratinocytes to fibronectin, 40-45 % to collagen type I and type IV and 33 % to laminin. Moreover, non-differentiating keratinocytes adhered at lower coating concentrations compared to primary keratinocytes [290, 291]. These data indicate that non-differentiating cells are less demanding in extracellular matrix composition and reduced amounts of adhesion proteins are sufficient for fast cell adhesion. In contrast, keratinocytes are much more concerned on sufficient extracellular matrix concentration and on extracellular matrix proteins presented to the cells.

Despite tremendous progress in the last years, the understanding of cellular processes and interactions at the interface towards biomaterials is still not fully understood. Further research is needed to elucidate the impact of different surface characteristics on cellular behavior. HaCaT cells and primary fibroblasts adhered to the functionalized electrospun fibers. However, primary keratinocytes in mono-culture and in co-culture with primary fibroblasts failed to form a multilayered, well stratified and keratinized epidermal layer. Thus, non-differentiating keratinocytes have a number of characteristics that distinguish them from human primary keratinocytes, which might be decisive for adhesion, migration and proliferation on the functionalized electrospun fibers. To our knowledge, although an immense amount of papers was published on electrospinning, there is nothing published describing the development of a skin model based on electrospun fibers and primary keratinocytes with comparable structure and functionality as described for insert models, collagen gels or cadaveric dermis.

Finally, it is important to realize that the ideal cell source for tissue-engineered models depends on the intended application. Although for clinical applications a robust tissue-engineered model based on primary cells is desirable, for *in vitro* applications, characteristics as reproducibility and the lack of batch-to-batch variability are of more importance.

5.6 Functionalized membranes for oral mucosa tissue engineering

Due to ethical concerns for animal welfare, as well as to the limited relevancy of animal models to predict human responses, the personal care and pharmaceutical industry increasingly relies upon reconstructed tissues to evaluate the safety of their products. Since monolayer cell culture models lack differentiated cells and the barrier properties of cells found *in vivo*, the obtained results may not be applied to native tissue. It was reported that alcohol-containing mouthwashes may cause severe toxicity. However, the results were based on 2D cell culture. In 2D cell culture, all cells are exposed to alcohol at the same time and are instantly affected by its toxic effects. In 3D cell cultures, only the superficial cells are exposed to test

substances. The cells in the deeper layers are protected by the upper layers [292]. Comparing monolayer culture systems with 3D oral mucosa models, the first showed an exaggerated response. Sun *et al.* reported similar results. When experiments are moved to 3D, there is often a cytoprotective effect detected [293]. Moreover, cytokine and growth factor release from 3D models differs from those in 2D cell culture [294]. Currently, only two companies, SkinEthic and MatTek, sell oral mucosa models, partly based on primary cells and partly based on a transformed human keratinocytes cell line (TR 146) obtained from squamous cell carcinoma.

Models that are used for research and development and not commercially available are also often based on the human keratinocyte cell line TR146. However, the cells do not form a fully differentiated oral epithelium [295]. Cell lines may not always reflect the responses of primary epithelial cells. Notably, primary cells harbor some advantages over cell lines. They are not genetically altered to survive in cell culture; thus their proliferation potential is limited. Nevertheless, the genome of primary cells, and possibly their transcriptome and proteome, are much closer to the *in vivo* situation, although the latter two are highly dependent on the environment and might be lost during primary culture as well [296].

The aim of the study was to develop a tissue-engineered epithelial oral mucosa model based on primary cells. In a first step, the isolation procedure of cells from oral mucosa biopsies was optimized. Fibroblasts showed a typical elongated morphology on plastic surfaces and expressed vimentin, a marker for cells with mesenchymal origin. Keratinocytes grew in cobblestone morphology and expressed cytokeratin 14, a marker for basal keratinocytes. Cytokeratin 10 was weakly expressed, which proves the basal state of the cells. For the experiments, keratinocytes were not used after passage 2 to ensure non-differentiated state of the cells. Fibroblasts were employed until passage 3.

Two different membranes, electrospun sP(EO-*stat*-PO)/PLGA membranes modified with fibronectin, laminin, and collagen type IV derived peptide sequences and polycarbonate membranes were tested for their suitability as supporting structure. The fact that the functionalized electrospun PLGA fibers are biocompatible and biodegradable makes them to appropriate candidates for reconstructing the oral

mucosa. Epithelial oral mucosa equivalents with primary oral mucosa keratinocytes and co-culture experiments with oral fibroblasts and primary keratinocytes revealed that keratinocytes formed 1-2 confluent layers on the upper surface of the electrospun matrix. Interestingly, there were no differences detectable between mono-culture and co-culture experiments. However, the cells failed to develop a multilayered epithelium close to the *in vivo* situation. The results are comparable with these obtained for the skin models based on electrospun membranes. As described for human epithelial keratinocytes, electrospun membranes might have pores which are too big for adequate keratinocyte adhesion, proliferation, and differentiation. Another explanation may be that the cell-adhesion-mediating peptide sequences attached to the surface of the membrane are not sufficient or the wrong ones for appropriate cellular behavior. Experiments of Moharamzadeh *et al*. confirmed the difficulties of developing oral mucosa models on electrospun membranes [297]. They used electrospun PLLA membranes and found that epithelial oral mucosa cells did not form a well-developed epithelium. Laminating the membranes enabled the formation of 1-2 cell layers of keratinocytes.

For clinical applications, biodegradability of a membrane is desirable, as it facilitates the replacement by the host tissue, whereas a non-degradable membrane could induce a foreign body reaction. However, the main focus of the work was the use of the membrane for *in vitro* test models. Polycarbonate membranes are well established and widely used for *in vitro* skin tissue engineering. Hence, they were applied as a support structure for the construction of oral epithelial models instead of functionalized electrospun PLGA membranes.

Histological analysis revealed that epithelial cells grown on polycarbonate inserts for 24 hours under submerged conditions and for 14 days under air-liquid interface show a characteristic epidermal structure including stratum basale, stratum spinosum, stratum granulosum, and stratum corneum. The stratum corneum is relatively thin, which is typical for oral mucosa in comparison to reconstructed skin equivalents. The morphology of the oral mucosa models resembled the commercially available EpiOral™ and EpiGingival™ oral mucosal models of MatTek Corporation. Immunohistochemical characterization showed that the cytokeratin

expression profile was similar to the native oral mucosa. The high amount of Ki 67 positive cells showed that after 14 days in culture the cells were still able to proliferate to that the epithelium is still able to self-renew.

An important function of the oral epithelium is the protection of the underlying tissue from toxins and microorganism. Therefore, the oral mucosa models were evaluated for their barrier function and integrity by measuring TEER, as well as FITC-dextran and carboxyfluorescein permeation. All three methods are non-invasive and allow to monitor the development of oral mucosa models during the whole culture period so that after different points in time the same model can be investigated. The amount of FITC-dextran and carboxyfluorescein that passes the models can be easy evaluated spectrometrically. TEER values of oral mucosa models increased over culture time. At day 14, a value of 3623 Ω cm^2 was measured after subtraction of the TEER values of the inserts without cells. Compared to the literature, these TEER values are relatively high. Kimura *et al.* measured TEER values of human oral mucosa models on insert membranes of 130-140 Ω cm^2 [298] and MatTek`s EpiOral™ and EpiGingival™ tissue showed an average TEER value of 413 Ω cm^2 and 516 Ω cm^2, respectively [299]. In comparison, TEER values of commercially available EpiDerm™ skin models are in the range of 5100 Ω cm^2. To our knowledge, nothing is published about reference values of native human oral mucosa, probably because it is not possible to gain biopsies in adequate sizes to allow the measurement of the electrical resistance.

FITC-dextran is a commonly used substance to analyze the barrier function of *in vitro* models, mainly intestinal models. Yet, other tissue-engineered models are also tested with the substance. A marginal amount of FITC-dextran passed the oral mucosa models, though inserts without cells allowed to permeate also a minor amount of 12.4 % FITC-dextran solution. Consequently, FITC-dextran with a molecular weight of 4 kDa might be not suitable for the studies, because the molecular weight is too high to permeate the tight barrier of the oral mucosa models. Therefore, carboxyfluorescein measurements were performed. With a molecular weight of 376 Da, carboxyfluorescein seemed to be more suitable. Permeation studies confirmed these results. Whereas 6.5 % carboxyfluorescein could permeate

through the models after 3 days in culture, the oral mucosa equivalents formed a tight barrier after 7 days in culture. In comparison, 60 % carboxyfluorescein permeated the inserts without cells over the entire investigated time period. To evaluate how long models can resist carboxyfluorescein permeation, models were incubated for up to 360 minutes with the substance. Comparison with skin models revealed that oral mucosa models became leaky after 120 minutes of carboxyfluorescein incubation, whereas skin models did not allow carboxyfluorescein permeation over the investigated time period. These results are in general agreement with values published in the literature. It is estimated that the permeability of the oral mucosa is 4-4000 greater than that of the skin [300] depending on the region of the oral cavity.

The ET-50 assay is another assay, which was applied to determine the barrier function of the oral mucosa models. Triton X-100 is applied to the apical compartment to determine the exposure time that reduces the viability to 50 % (ET-50). It permeates the tissue and damages the basal cell layers, thereby the permeation rate is dependent on the barrier of the models. Thus, the assay measures the barrier function of a tissue indirectly. Triton X-100 was incubated for eight different exposure times. MTT was used to measure the viability of the models after treatment. After 114 minutes of Triton X-100 exposure, the viability of our oral mucosa models was reduced to 50 %. Commercially available EpiOral™ model from the MatTek Corporation show ET-50 values of 61 minutes [301]. As a comparison, ET-50 values of epidermal skin equivalents are in the range of 5-8 hours. A reason for the increased TEER and ET-50 values of the models in comparison to the MatTek model might be the fact that the cells isolated for the models derive from different parts in the oral cavity. Whereas it is known that the cells for the EpiOral™ model derive from the buccal tissue which is not stratified, the origin of our tissue biopsies is unknown. Biopsies were obtained from the dental clinic, where a lot of gingiva reconstructions are performed. It is probable that the biopsies derive from the gingiva, which is more stratified. TEER values support this assumption. Due to data protection rules it was not possible to obtain detailed information on the origin of the biopsies. Beside the determination of the barrier function, the ET-50 value measurement was employed to test the intra-lot and inter-lot reproducibility of the

tissue models. The intra-lot variability was very low. For further experiments and to minimize inter-lot reproducibility, the origin of the biopsy material should, however, be regarded.

A potential application of the oral mucosa models is the assessment of biological effects of dental materials [302, 303] and oral health care products [72]. Irritation studies of two commercially oral health care products, chlorhexamed® and salviathymol® showed that the oral mucosa equivalents are able to determine the irritation potential of these products. Chlorhexamed®, which is commercially available as an antimicrobial mouth rinse containing chlorhexidine, and salviathymol®, an antiseptic solution based on several medical plants, did not decrease the viability of the oral mucosa equivalents, if applied in the recommended dilution. The negative control PBS revealed likewise no reduction in viability. Applying a 100 times increased concentration of salviathymol® reduced the viability of oral mucosa models to 2 % and was comparable with the effects of SDS treatment which was applied as positive control. Irritant materials are identified by their ability to decrease cell viability below 50 % [304]. Hence, it can be concluded that chlorhexamed® and salviathymol® do not have an irritative potential on the oral mucosa models if applied properly. The findings of the irritation study are promising and should be explored with other substances and materials applied in the oral cavity. Another important question for future studies is to determine the effects of corrosive and sensitizing substances on the oral mucosa models.

At the present time, most of the *in vitro* studies examining irritation potential and drug transport across the oral mucosa are performed in animals. However, their reliability is doubted, because of species differences. Moreover, ethical doubts on animal based studies arise. Additionally, using animal tissues surgically removed from the oral cavity results in the question, how well the dissected tissue is preserved which in turn will directly affect the permeation observed. The oral mucosa models based on primary oral keratinocytes represented important features of the human oral mucosa. Thus, the model provides a highly reproducible and inexpensive system and can be used as drug delivery system. Moreover, it is possible to investigate interactions of restorative dental materials, pharmaceuticals,

and oral health care products applied in the mouth cavity before clinical trials with the system. The equivalents may be of value for toxicological studies and to investigate the inflammatory or tissue damaging effects of dentifrices, mouthwashes, anesthetic pastes. The effects of various agents on epithelial morphogenesis or wound healing can be studied.

5.7 Future perspectives

There is a high demand of artificial basement membranes which promote cell adhesion, migration, proliferation and allow the crosstalk between different cell types and matrix remodeling. Therefore, new membranes need to be developed for tissue engineering and 3D cell culture, which reflect the *in vivo* situation of basement membranes more precisely. This work investigated the applicability of electrospun meshes, based on the synthetic polymer PLGA, modified with NCO-sP(EO-*stat*-PO) and bioactive peptide sequences as artificial basement membranes towards skin and oral mucosa tissue engineering. It was demonstrated that both the isotropic and bipolar membranes are suitable in order to establish a skin model with important features of human skin. The electrospun membrane was able to induce cell adhesion and proliferation, provided cues to guide cells to apical-basolateral polarization and enabled the invasion of fibroblasts. Consequently, this model might be applicable for studying 3D cell adhesion and matrix remodeling processes, as well as for gaining deeper knowledge of the fundamental processes in skin tissue formation.

As a next step, it might be of interest whether the membrane could be modified in a way that primary keratinocytes can be employed instead of the HaCaT cell line. HaCaT cells reveal a different integrin expression pattern than primary keratinocytes, so that adapting peptide composition and concentration, as well as membrane appearance would evoke the possibility of rebuilding a skin model with only primary cells. It might be interesting to investigate what cues are necessary to promote keratinocyte adhesion and proliferation. Studies may include different peptide sequences, growth factors, different fiber morphology and stability, since all these factors may have an influence on cellular behavior. In might also be compelling

to see if inclusion of other cells than keratinocytes and fibroblasts has an impact on cell proliferation.

In this work, a basement membrane was developed towards skin tissue engineering. However, the membrane could also be modified for the needs of different tissues due to the easily adaptable system. The degradation profile and mechanical properties of the isotropic and bipolar membranes can be adapted conveniently to different needs by changing the polymer or the ratio of lactide and glycolide in PLGA. The biological activity can be modified by including different peptides, as well as growth factors.

The bipolar membrane with different behavior on each of its faces could be very interesting also for other advanced tissue engineering fields. The membrane could find a variety of applications in which different behavior on each face of a single construct are desirable in terms of hydrophobicity, biodegradation rate or cell attachment. The hydrophilic, non-adhering face with sP(EO-*stat*-PO)/PLGA membranes could be used to prevent post-surgical adherences, a major issue in surgery and as a protective layer to avoid intrusion of bacteria or protein adsorption. On the other side, sP(EO-*stat*-PO)/PLGA membranes modified with bioactive peptide sequences can be applied to promote cell attachment and spreading.

In a next step, a membrane can be developed which is able to induce apical-basolateral polarization and to guide the different cell types to their respective compartments. For this purpose, different peptide sequences, as well as growth factors could be included and the fiber morphology could be adapted to the requirements of the different cell types. The membrane could be incubated in a mixture of two or more different cells and the cues of the membrane are able to guide the cells to their compartment.

The static culture conditions might not be sufficient to reflect the *in vivo* situation completely, as physiologic stimuli, such as appropriate air humidity and shear stress, cannot be mimicked. In order to provide more physiological conditions, membranes could be cultured in flow-bioreactor. In such a setup, the upper side of the membrane could be exposed to air with appropriate temperature and air

humidity while stromal or endothelial cells on the other side are supplied with medium.

The established protocol of the oral mucosa models could be optimized by isolating epidermal progenitor or stem cells to increase the proliferation capacity of the cells. For further experiments and to determine the inter-lot reproducibility, it is necessary to include the origin of the biopsy to characterize the tissue more specifically. To reflect the *in vivo* situation more accurately, fibroblastic cells should be included in the models. Fibroblasts are important to promote growth and differentiation of keratinocytes. Inclusion of immune cells such as lymphocytes, monocytes, and Langerhans cells would enable to study the pathogenesis of infectious diseases.

In conclusion, this work provides the basics for a further establishment of artificial basement membranes, which might have a great impact on fundamental research studies. Mimicking the physical fibrillary structure by electrospinning and in addition incorporating ECM components to mimic the composition could offer a safe and promising way building up also other basement membranes for different tissue engineering applications.

6 References

[1] O'Brien FJ. Biomaterials & scaffolds for tissue engineering. Mater Today. 2011;14:88-95.

[2] Cao Y, Vacanti JP, Paige KT, Upton J, Vacanti CA. Transplantation of chondrocytes utilizing a polymer-cell construct to produce tissue-engineered cartilage in the shape of a human ear. Plast Reconstr Surg. 1997;100:297-302.

[3] Meyer U, Meyer T, Handschel J, Wiesmann HP. Fundamentals of Tissue Engineering and Regenerative Medicine: Springer Berlin Heidelberg; 2009.

[4] Tabata Y. Biomaterial technology for tissue engineering applications. J R Soc Interface. 2009;6 Suppl 3:S311-24.

[5] Persidis A. Tissue engineering. Nat Biotech. 1999;17:508-10.

[6] Watson CJE, Dark JH. Organ transplantation: historical perspective and current practice. Br J Anaesth. 2012;108:i29-i42.

[7] Eurotransplant. Organ Facts and Figures. 26. November 2014, Brussels.

[8] Groeber F, Holeiter M, Hampel M, Hinderer S, Schenke-Layland K. Skin tissue engineering--in vivo and in vitro applications. Adv Drug Deliv Rev. 2011;63:352-66.

[9] Place ES, Evans ND, Stevens MM. Complexity in biomaterials for tissue engineering. Nat Mater. 2009;8:457-70.

[10] van der Worp HB, Howells DW, Sena ES, Porritt MJ, Rewell S, O'Collins V, et al. Can animal models of disease reliably inform human studies? PLoS Med. 2010;7:e1000245.

[11] Hartung T. Food for thought look back in anger–What clinical studies tell us about preclinical work. Altex. 2013;30:275.

[12] Berthiaume F, Maguire TJ, Yarmush ML. Tissue engineering and regenerative medicine: history, progress, and challenges. Annual review of chemical and biomolecular engineering. 2011;2:403-30.

[13] Skalak R, Fox CF. Tissue engineering: proceedings of a workshop, held at Granlibakken, Lake Tahoe, California, February 26-29, 1988: Alan R. Liss; 1988.

[14] Lutolf M, Hubbell J. Synthetic biomaterials as instructive extracellular microenvironments for morphogenesis in tissue engineering. Nat Biotechnol. 2005;23:47-55.

[15] Badylak SF, Weiss DJ, Caplan A, Macchiarini P. Engineered whole organs and complex tissues. The Lancet.379:943-52.

[16] Bell E, Ehrlich HP, Buttle DJ, Nakatsuji T. Living tissue formed in vitro and accepted as skin-equivalent tissue of full thickness. Science. 1981;211:1052-4.

[17] Pruniéras M, Régnier M, Woodley D. Methods for cultivation of keratinocytes with an air-liquid interface. J Invest Dermatol. 1983;81:28s-33s.

[18] Kadhim M, Salomaa S, Wright E, Hildebrandt G, Belyakov OV, Prise KM, et al. Non-targeted effects of ionizing radiation–implications for low dose risk. Mutat Res. 2013;752:84-98.

[19] Agache PG, Agache P, Humbert P, Maibach H. Measuring the skin: Springer Science & Business Media; 2004.

[20] Wagner H, Zghoul N, Lehr C-M, Schäfer UF. Human skin and skin equivalents to study dermal penetration and permeation. Cell culture models of biological barriers: in vitro test systems for drug absorption and delivery. 2002:289.

[21] Yamaguchi Y, Hearing VJ. Physiological factors that regulate skin pigmentation. BioFactors. 2009;35:193-9.

[22] Raj D, Brash DE, Grossman D. Keratinocyte apoptosis in epidermal development and disease. J Invest Dermatol. 2006;126:243-57.

[23] Paus R, Cotsarelis G. The biology of hair follicles. N Engl J Med. 1999;341:491-7.

[24] Elias PM. Stratum corneum defensive functions: an integrated view. J Invest Dermatol. 2005;125:183-200.

[25] Boulais N, Misery L. The epidermis: a sensory tissue. Eur J Dermatol. 2008;18:119-27.

[26] Johnston LJ, Halliday GM, King NJ. Langerhans cells migrate to local lymph nodes following cutaneous infection with an arbovirus. J Invest Dermatol. 2000;114:560-8.

[27] Encyclopædia Britannica Online J, from <http://www.britannica.com/science/epidermis-anatomy/images-videos/Section-through-human-skin-and-underlying-structures/2027 > (20.01.2016)

[28] Fuchs E. Scratching the surface of skin development. Nature. 2007;445:834-42.

[29] Zhang Z, Michniak-Kohn BB. Tissue engineered human skin equivalents. Pharmaceutics. 2012;4:26-41.

[30] van Smeden J, Janssens M, Gooris GS, Bouwstra JA. The important role of stratum corneum lipids for the cutaneous barrier function. Biochim Biophys Acta. 2014;1841:295-313.

[31] Scheuplein RJ, Blank IH. Permeability of the skin. Physiol Rev. 1971;51:702-47.

[32] MacNeil S. Progress and opportunities for tissue-engineered skin. Nature. 2007;445:874-80.

[33] Schoellhammer CM, Blankschtein D, Langer R. Skin Permeabilization for Transdermal Drug Delivery: Recent Advances and Future Prospects. Expert opinion on drug delivery. 2014;11:393-407.

[34] Brohem CA, da Silva Cardeal LB, Tiago M, Soengas MS, de Moraes Barros SB, Maria-Engler SS. Artificial Skin in Perspective: Concepts and Applications. Pigment cell & melanoma research. 2011;24:35-50.

[35] El Ghalbzouri A, Commandeur S, Rietveld MH, Mulder AA, Willemze R. Replacement of animal-derived collagen matrix by human fibroblast-derived dermal matrix for human skin equivalent products. Biomaterials. 2009;30:71-8.

[36] Metcalfe AD, Ferguson MW. Bioengineering skin using mechanisms of regeneration and repair. Biomaterials. 2007;28:5100-13.

[37] Teubl BJ, Absenger M, Fröhlich E, Leitinger G, Zimmer A, Roblegg E. The oral cavity as a biological barrier system: Design of an advanced buccal in vitro permeability model. Eur J Pharm Biopharm. 2013;84:386-93.

[38] Harris D, Robinson JR. Drug delivery via the mucous membranes of the oral cavity. J Pharm Sci. 1992;81:1-10.

[39] Walker D. Oral mucosal immunology: an overview. ANNALS-ACADEMY OF MEDICINE SINGAPORE. 2004;33:27-30.

[40] Liu J, Bian Z, Kuijpers-Jagtman A, Von den Hoff J. Skin and oral mucosa equivalents: construction and performance. Orthod Craniofac Res. 2010;13:11-20.

[41] MacNeil S. Biomaterials for tissue engineering of skin. Mater Today. 2008;11:26-35.

[42] Augustine R, Kalarikkal N, Thomas S. Advancement of wound care from grafts to bioengineered smart skin substitutes. Progress in Biomaterials. 2014;3:103-13.

[43] Priya SG, Jungvid H, Kumar A. Skin tissue engineering for tissue repair and regeneration. Tissue engineering Part B, Reviews. 2008;14:105-18.

[44] Sun BK, Siprashvili Z, Khavari PA. Advances in skin grafting and treatment of cutaneous wounds. Science. 2014;346:941-5.

[45] Carsin H, Ainaud P, Le Bever H, Rives J, Lakhel A, Stephanazzi J, et al. Cultured epithelial autografts in extensive burn coverage of severely traumatized patients: a five year single-center experience with 30 patients. Burns. 2000;26:379-87.

[46] Chant H, Woodrow T, Manley J. Autologous skin cells: a new technique for skin regeneration in diabetic and vascular ulcers. J Wound Care. 2013;22:S10-5.

[47] Burke JF, Yannas IV, Quinby WC, Bondoc CC, Jung WK. Successful use of a physiologically acceptable artificial skin in the treatment of extensive burn injury. Ann Surg. 1981;194:413-28.

[48] Hart CE, Loewen-Rodriguez A, Lessem J. Dermagraft: Use in the Treatment of Chronic Wounds. Adv Wound Care. 2012;1:138-41.

[49] Noordenbos J, Dore C, Hansbrough JF. Safety and efficacy of TransCyte for the treatment of partial-thickness burns. J Burn Care Rehabil. 1999;20:275-81.

[50] Streit M, Braathen LR. Apligraf--a living human skin equivalent for the treatment of chronic wounds. Int J Artif Organs. 2000;23:831-3.

[51] Bello YM, Falabella AF, Eaglstein WH. Tissue-engineered skin. Am J Clin Dermatol. 2001;2:305-13.

[52] Portes P, Grandidier M-H, Cohen C, Roguet R. Refinement of the Episkin® protocol for the assessment of acute skin irritation of chemicals: follow-up to the ECVAM prevalidation study. Toxicol In Vitro. 2002;16:765-70.

[53] Andriani F, Margulis A, Lin N, Griffey S, Garlick JA. Analysis of microenvironmental factors contributing to basement membrane assembly and normalized epidermal phenotype. J Invest Dermatol. 2003;120:923-31.

[54] Parenteau NL, Bilbo P, Nolte CJ, Mason VS, Rosenberg M. The organotypic culture of human skin keratinocytes and fibroblasts to achieve form and function. Cytotechnology. 1992;9:163-71.

[55] Stark HJ, Boehnke K, Mirancea N, Willhauck MJ, Pavesio A, Fusenig NE, et al. Epidermal homeostasis in long-term scaffold-enforced skin equivalents. J Investig Dermatol Symp Proc. 2006;11:93-105.

[56] Sahuc F, Nakazawa K, Berthod F, Collombel C, Damour O. Mesenchymal-epithelial interactions regulate gene expression of type VII collagen and kalinin in keratinocytes and dermal-epidermal junction formation in a skin equivalent model. Wound Repair Regen. 1996;4:93-102.

[57] Lindberg K, Badylak SF. Porcine small intestinal submucosa (SIS): a bioscaffold supporting in vitro primary human epidermal cell differentiation and synthesis of basement membrane proteins. Burns. 2001;27:254-66.

[58] Ng KW, Hutmacher DW. Reduced contraction of skin equivalent engineered using cell sheets cultured in 3D matrices. Biomaterials. 2006;27:4591-8.

[59] Bruin P, Smedinga J, Pennings AJ, Jonkman MF. Biodegradable lysine diisocyanate-based poly(glycolide-co-epsilon-caprolactone)-urethane network in artificial skin. Biomaterials. 1990;11:291-5.

[60] Ng KW, Khor HL, Hutmacher DW. In vitro characterization of natural and synthetic dermal matrices cultured with human dermal fibroblasts. Biomaterials. 2004;25:2807-18.

[61] Mohammadi M, Mofid R, Shokrgozar MA. Peri-implant soft tissue management through use of cultured gingival graft: a case report. Acta Med Iran. 2011;49:319-24.

[62] Luitaud C, Laflamme C, Semlali A, Saidi S, Grenier G, Zakrzewski A, et al. Development of an engineering autologous palatal mucosa-like tissue for potential clinical applications. J Biomed Mater Res B Appl Biomater. 2007;83:554-61.

[63] Izumi K, Neiva RF, Feinberg SE. Intraoral grafting of tissue-engineered human oral mucosa. Int J Oral Maxillofac Implants. 2013;28:e295-303.

[64] Hüsing B, Bührlen B, Gaisser S. Human Tissue Engineered Products: Today's Markets and Future Prospects2003.

[65] MacNeil S, Shepherd J, Smith L. Production of tissue-engineered skin and oral mucosa for clinical and experimental use. Methods Mol Biol. 2011;695:129-53.

[66] Nielsen HM, Rassing MR. TR146 cells grown on filters as a model of human buccal epithelium: IV. Permeability of water, mannitol, testosterone and beta-adrenoceptor antagonists. Comparison to human, monkey and porcine buccal mucosa. Int J Pharm. 2000;194:155-67.

[67] Evaluation of an oral care product safety screening program utilizing the in vitro skinethic human gingival epithelium (RHG) and oral buccal (RHO) models URL<http://www.episkin.com/iso_album/re_v05mar11.pdf> (08.10.2015).

[68] Schaller M, Zakikhany K, Naglik JR, Weindl G, Hube B. Models of oral and vaginal candidiasis based on in vitro reconstituted human epithelia. Nat Protocols. 2006;1:2767-73.

[69] Whiley RA, Cruchley AT, Gore C, Hagi-Pavli E. Candida albicans strain-dependent modulation of pro-inflammatory cytokine release by in vitro oral and vaginal mucosal models. Cytokine. 2012;57:89-97.

[70] Lundqvist C, Thornhill M, Williams D, Smith S, Cruchley A. The effect of sodium lauryl sulphate on epithelial homeostasis. J Dent Res. 2002;81:3054.

[71] Moharamzadeh K, Brook IM, Van Noort R, Scutt AM, Smith KG, Thornhill MH. Development, optimization and characterization of a full-thickness tissue engineered human oral mucosal model for biological assessment of dental biomaterials. J Mater Sci Mater Med. 2008;19:1793-801.

[72] Koschier F, Kostrubsky V, Toole C, Gallo MA. In vitro effects of ethanol and mouthrinse on permeability in an oral buccal mucosal tissue construct. Food Chem Toxicol. 2011;49:2524-9.

[73] Schlage WK, Iskandar AR, Kostadinova R, Xiang Y, Sewer A, Majeed S, et al. In vitro systems toxicology approach to investigate the effects of repeated cigarette smoke exposure on human buccal and gingival organotypic epithelial tissue cultures. Toxicol Mech Methods. 2014;24:470-87.

[74] Odioso LL, Doyle MJ, Quinn KW, Bartel RL, Zimber MP, Stevens-Burns D. Development and characterization of an in vitro gingival epithelial model. J Periodontal Res. 1995;30:210-9.

[75] Izumi K, Takacs G, Terashi H, Feinberg SE. Ex vivo development of a composite human oral mucosal equivalent. J Oral Maxillofac Surg. 1999;57:571-7.

[76] Cho KH, Ahn HT, Park KC, Chung JH, Kim SW, Sung MW, et al. Reconstruction of human hard-palate mucosal epithelium on de-epidermized dermis. J Dermatol Sci. 2000;22:117-24.

[77] Mostefaoui Y, Claveau I, Ross G, Rouabhia M. Tissue structure, and IL-1beta, IL-8, and TNF-alpha secretions after contact by engineered human oral mucosa with dentifrices. J Clin Periodontol. 2002;29:1035-41.

[78] Schmalz G, Arenholt-Bindslev D, Hiller KA, Schweikl H. Epithelium-fibroblast co-culture for assessing mucosal irritancy of metals used in dentistry. Eur J Oral Sci. 1997;105:86-91.

[79] Yadev NP, Murdoch C, Saville SP, Thornhill MH. Evaluation of tissue engineered models of the oral mucosa to investigate oral candidiasis. Microb Pathog. 2011;50:278-85.

[80] Nittayananta W, Hladik F, Klausner M, Harb S, Dale BA, Coombs RW. HIV type 1 fails to trigger innate immune factor synthesis in differentiated oral epithelium. AIDS Res Hum Retroviruses. 2009;25:1013-21.

[81] Hai R, Chu A, Li H, Umamoto S, Rider P, Liu F. Infection of human cytomegalovirus in cultured human gingival tissue. Virol J. 2006;3:84.

[82] Duong HS, Le AD, Zhang Q, Messadi DV. A novel 3-dimensional culture system as an in vitro model for studying oral cancer cell invasion. Int J Exp Pathol. 2005;86:365-74.

[83] Vracko R. Basal lamina scaffold-anatomy and significance for maintenance of orderly tissue structure. Am J Pathol. 1974;77:314-46.

[84] Paulsson M. Basement membrane proteins: structure, assembly, and cellular interactions. Crit Rev Biochem Mol Biol. 1992;27:93-127.

[85] Kalluri R. Basement membranes: structure, assembly and role in tumour angiogenesis. Nat Rev Cancer. 2003;3:422-33.

[86] Khoshnoodi J, Pedchenko V, Hudson BG. Mammalian collagen IV. Microsc Res Tech. 2008;71:357-70.

[87] Royce PM, Steinmann B. Connective Tissue and Its Heritable Disorders: Molecular, Genetic, and Medical Aspects: Wiley; 2003.

[88] Smola H, Stark HJ, Thiekotter G, Mirancea N, Krieg T, Fusenig NE. Dynamics of basement membrane formation by keratinocyte-fibroblast interactions in organotypic skin culture. Exp Cell Res. 1998;239:399-410.

[89] Erickson AC, Couchman JR. Still more complexity in mammalian basement membranes. Journal of Histochemistry & Cytochemistry. 2000;48:1291-306.

[90] Timpl R, Brown JC. Supramolecular assembly of basement membranes. Bioessays. 1996;18:123-32.

[91] LeBleu VS, Macdonald B, Kalluri R. Structure and function of basement membranes. Exp Biol Med (Maywood). 2007;232:1121-9.

[92] Kalluri R. Basement membranes: structure, assembly and role in tumour angiogenesis. Nature reviews Cancer. 2003;3:422-33.

[93] Bohnert A, Hornung J, Mackenzie IC, Fusenig NE. Epithelial-mesenchymal interactions control basement membrane production and differentiation in cultured and transplanted mouse keratinocytes. Cell Tissue Res. 1986;244:413-29.

[94] Woodley DT, Stanley JR, Reese MJ, O'Keefe EJ. Human dermal fibroblasts synthesize laminin. J Invest Dermatol. 1988;90:679-83.

[95] Marinkovich MP, Keene DR, Rimberg CS, Burgeson RE. Cellular origin of the dermal-epidermal basement membrane. Dev Dyn. 1993;197:255-67.

[96] Smyth N, Vatansever HS, Murray P, Meyer M, Frie C, Paulsson M, et al. Absence of basement membranes after targeting the LAMC1 gene results in embryonic lethality due to failure of endoderm differentiation. J Cell Biol. 1999;144:151-60.

[97] Hozumi K, Kumai J, Yamada Y, Nomizu M. Active Peptide-Conjugated Chitosan Matrices as an Artificial Basement Membrane. Polymers. 2015;7:281-97.

[98] Santoro MM, Gaudino G. Cellular and molecular facets of keratinocyte reepithelization during wound healing. Exp Cell Res. 2005;304:274-86.

[99] Iozzo RV. Basement membrane proteoglycans: from cellar to ceiling. Nature Reviews Molecular Cell Biology. 2005;6:646-56.

[100] Zeng ZS, Cohen AM, Guillem JG. Loss of basement membrane type IV collagen is associated with increased expression of metalloproteinases 2 and 9 (MMP-2 and MMP-9) during human colorectal tumorigenesis. Carcinogenesis. 1999;20:749-55.

[101] Yamada KM, Cukierman E. Modeling Tissue Morphogenesis and Cancer in 3D. Cell. 2007;130:601-10.

[102] Griffith LG, Swartz MA. Capturing complex 3D tissue physiology in vitro. Nat Rev Mol Cell Biol. 2006;7:211-24.

[103] Doshi J, Reneker DH. Electrospinning process and applications of electrospun fibers. Industry Applications Society Annual Meeting, 1993, Conference Record of the 1993 IEEE1993. p. 1698-703 vol.3.

[104] Han D, Gouma P-I. Electrospun bioscaffolds that mimic the topology of extracellular matrix. Nanomed Nanotechnol Biol Med. 2006;2:37-41.

[105] Anton F. Process and apparatus for preparing artificial threads. Google Patents; 1934.

[106] Bhardwaj N, Kundu SC. Electrospinning: A fascinating fiber fabrication technique. Biotechnol Adv. 2010;28:325-47.

[107] Baker BM, Gee AO, Sheth NP, Huffman GR, Sennett BJ, Schaer TP, et al. Meniscus tissue engineering on the nanoscale. J Knee Surg. 2009;22:45-59.

[108] Bonzani IC, George JH, Stevens MM. Novel materials for bone and cartilage regeneration. Curr Opin Chem Biol. 2006;10:568-75.

[109] Jang J-H, Castano O, Kim H-W. Electrospun materials as potential platforms for bone tissue engineering. Adv Drug Del Rev. 2009;61:1065-83.

[110] Seidlits SK, Lee JY, Schmidt CE. Nanostructured scaffolds for neural applications. 2008.

[111] Cao H, Liu T, Chew SY. The application of nanofibrous scaffolds in neural tissue engineering. Adv Drug Del Rev. 2009;61:1055-64.

[112] Zahedi P, Rezaeian I, Ranaei-Siadat SO, Jafari SH, Supaphol P. A review on wound dressings with an emphasis on electrospun nanofibrous polymeric bandages. Polym Adv Technol. 2010;21:77-95.

[113] Kumbar S, James R, Nukavarapu S, Laurencin C. Electrospun nanofiber scaffolds: engineering soft tissues. Biomedical Materials. 2008;3:034002.

[114] Wray LS, Orwin EJ. Recreating the microenvironment of the native cornea for tissue engineering applications. Tissue Engineering Part A. 2009;15:1463-72.

[115] Sell SA, McClure MJ, Garg K, Wolfe PS, Bowlin GL. Electrospinning of collagen/biopolymers for regenerative medicine and cardiovascular tissue engineering. Adv Drug Del Rev. 2009;61:1007-19.

[116] Chen J, Xu J, Wang A, Zheng M. Scaffolds for tendon and ligament repair: review of the efficacy of commercial products. Expert Rev Med Devices. 2009;6:61-73.

[117] Lim SH, Mao H-Q. Electrospun scaffolds for stem cell engineering. Adv Drug Del Rev. 2009;61:1084-96.

[118] Doshi J, Reneker DH. Electrospinning process and applications of electrospun fibers. J Electrostatics. 1995;35:151-60.

[119] Shearer H, Ellis MJ, Perera SP, Chaudhuri JB. Effects of common sterilization methods on the structure and properties of poly(D,L lactic-co-glycolic acid) scaffolds. Tissue Eng. 2006;12:2717-27.

[120] Lee KH, Kim HY, Bang HJ, Jung YH, Lee SG. The change of bead morphology formed on electrospun polystyrene fibers. Polymer. 2003;44:4029-34.

[121] Fong H, Chun I, Reneker DH. Beaded nanofibers formed during electrospinning. Polymer. 1999;40:4585-92.

[122] Yang Q, Li Z, Hong Y, Zhao Y, Qiu S, Wang C, et al. Influence of solvents on the formation of ultrathin uniform poly(vinyl pyrrolidone) nanofibers with electrospinning. J Polym Sci, Part B: Polym Phys. 2004;42:3721-6.

[123] Tao J, Shivkumar S. Molecular weight dependent structural regimes during the electrospinning of PVA. Mater Lett. 2007;61:2325-8.

[124] Huang C, Chen S, Lai C, Reneker DH, Qiu H, Ye Y, et al. Electrospun polymer nanofibres with small diameters. Nanotechnology. 2006;17:1558.

[125] Liu H, Hsieh Y-L. Ultrafine fibrous cellulose membranes from electrospinning of cellulose acetate. Journal of Polymer Science Part B: Polymer Physics. 2002;40:2119-29.

[126] Zong X, Kim K, Fang D, Ran S, Hsiao BS, Chu B. Structure and process relationship of electrospun bioabsorbable nanofiber membranes. Polymer. 2002;43:4403-12.

[127] Yuan X, Zhang Y, Dong C, Sheng J. Morphology of ultrafine polysulfone fibers prepared by electrospinning. Polym Int. 2004;53:1704-10.

[128] Megelski S, Stephens JS, Chase DB, Rabolt JF. Micro- and Nanostructured Surface Morphology on Electrospun Polymer Fibers. Macromolecules. 2002;35:8456-66.

[129] Casper CL, Stephens JS, Tassi NG, Chase DB, Rabolt JF. Controlling Surface Morphology of Electrospun Polystyrene Fibers: Effect of Humidity and Molecular Weight in the Electrospinning Process. Macromolecules. 2003;37:573-8.

[130] Mit-uppatham C, Nithitanakul M, Supaphol P. Ultrafine Electrospun Polyamide-6 Fibers: Effect of Solution Conditions on Morphology and Average Fiber Diameter. Macromol Chem Phys. 2004;205:2327-38.

[131] Huang Z-M, Zhang YZ, Kotaki M, Ramakrishna S. A review on polymer nanofibers by electrospinning and their applications in nanocomposites. Composites Sci Technol. 2003;63:2223-53.

[132] Sell SA, Wolfe PS, Garg K, McCool JM, Rodriguez IA, Bowlin GL. The use of natural polymers in tissue engineering: a focus on electrospun extracellular matrix analogues. Polymers. 2010;2:522-53.

[133] Greiner A, Wendorff JH. Electrospinning: a fascinating method for the preparation of ultrathin fibers. Angew Chem Int Ed. 2007;46:5670-703.

[134] Norouzi M, Boroujeni SM, Omidvarkordshouli N, Soleimani M. Advances in Skin Regeneration: Application of Electrospun Scaffolds. Advanced Healthcare Materials. 2015;4:1114-33.

[135] Demir MM, Yilgor I, Yilgor E, Erman B. Electrospinning of polyurethane fibers. Polymer. 2002;43:3303-9.

[136] Khil MS, Cha DI, Kim HY, Kim IS, Bhattarai N. Electrospun nanofibrous polyurethane membrane as wound dressing. Journal of Biomedical Materials Research Part B: Applied Biomaterials. 2003;67:675-9.

[137] Lee K, Kim H, Khil M, Ra Y, Lee D. Characterization of nano-structured poly (ε-caprolactone) nonwoven mats via electrospinning. Polymer. 2003;44:1287-94.

[138] Zhang Y, Ouyang H, Lim CT, Ramakrishna S, Huang ZM. Electrospinning of gelatin fibers and gelatin/PCL composite fibrous scaffolds. Journal of Biomedical Materials Research Part B: Applied Biomaterials. 2005;72:156-65.

[139] Son WK, Youk JH, Lee TS, Park WH. The effects of solution properties and polyelectrolyte on electrospinning of ultrafine poly (ethylene oxide) fibers. Polymer. 2004;45:2959-66.

[140] Pakravan M, Heuzey M-C, Ajji A. A fundamental study of chitosan/PEO electrospinning. Polymer. 2011;52:4813-24.

[141] Srinivasan G, Reneker DH. Structure and morphology of small diameter electrospun aramid fibers. Polym Int. 1995;36:195-201.

[142] Ma PX, Choi JW. Biodegradable polymer scaffolds with well-defined interconnected spherical pore network. Tissue Eng. 2001;7:23-33.

[143] Lu L, Peter SJ, Lyman MD, Lai HL, Leite SM, Tamada JA, et al. In vitro and in vivo degradation of porous poly(DL-lactic-co-glycolic acid) foams. Biomaterials. 2000;21:1837-45.

[144] Wu L, Ding J. In vitro degradation of three-dimensional porous poly(D,L-lactide-co-glycolide) scaffolds for tissue engineering. Biomaterials. 2004;25:5821-30.

[145] Blackwood KA, McKean R, Canton I, Freeman CO, Franklin KL, Cole D, et al. Development of biodegradable electrospun scaffolds for dermal replacement. Biomaterials. 2008;29:3091-104.

[146] Makadia HK, Siegel SJ. Poly Lactic-co-Glycolic Acid (PLGA) as Biodegradable Controlled Drug Delivery Carrier. Polymers (Basel). 2011;3:1377-97.

[147] Pham QP, Sharma U, Mikos AG. Electrospinning of polymeric nanofibers for tissue engineering applications: a review. Tissue Eng. 2006;12:1197-211.

[148] Hollister SJ. Porous scaffold design for tissue engineering. Nature materials. 2005;4:518-24.

[149] Thull R. Surface functionalization of materials to initiate auto-biocompatibilization in vivo. Materialwiss Werkstofftech. 2001;32:949-52.

[150] Halperin A. Polymer Brushes that Resist Adsorption of Model Proteins: Design Parameters. Langmuir. 1999;15:2525-33.

[151] Latour RA. Biomaterials: protein-surface interactions. Encyclopedia of biomaterials and biomedical engineering. 2005;28:1-15.

[152] Calvet JL, Grafahrend D, Klee D, Möller M. Sterilization effects on starPEG coated polymer surfaces: characterization and cell viability. J Mater Sci Mater Med. 2008;19:1631-6.

[153] Milton H, Zalipsky S. Poly (ethylenglycol) chemistry and biological applications. ACS Symp Ser1997.

[154] Offenhausser A, Bocker-Meffert S, Decker T, Helpenstein R, Gasteier P, Groll J, et al. Microcontact printing of proteins for neuronal cell guidance. Soft Matter. 2007;3:290-8.

[155] Prime KL, Whitesides GM. Adsorption of proteins onto surfaces containing end-attached oligo(ethylene oxide): a model system using self-assembled monolayers. J Am Chem Soc. 1993;115:10714-21.

[156] Ostuni E, Chapman RG, Holmlin RE, Takayama S, Whitesides GM. A survey of structure-property relationships of surfaces that resist the adsorption of protein. Langmuir. 2001;17:5605-20.

[157] Li L, Chen S, Zheng J, Ratner BD, Jiang S. Protein adsorption on oligo (ethylene glycol)-terminated alkanethiolate self-assembled monolayers: the molecular basis for nonfouling behavior. The Journal of Physical Chemistry B. 2005;109:2934-41.

[158] Herrwerth S, Eck W, Reinhardt S, Grunze M. Factors that determine the protein resistance of oligoether self-assembled monolayers-internal hydrophilicity, terminal hydrophilicity, and lateral packing density. J Am Chem Soc. 2003;125:9359-66.

[159] Yang Z, Galloway JA, Yu H. Protein interactions with poly (ethylene glycol) self-assembled monolayers on glass substrates: diffusion and adsorption. Langmuir. 1999;15:8405-11.

[160] Lee S-W, Laibinis PE. Protein-resistant coatings for glass and metal oxide surfaces derived from oligo (ethylene glycol)-terminated alkyltrichlorosilanes. Biomaterials. 1998;19:1669-75.

[161] McPherson T, Kidane A, Szleifer I, Park K. Prevention of Protein Adsorption by Tethered Poly(ethylene oxide) Layers: Experiments and Single-Chain Mean-Field Analysis. Langmuir. 1998;14:176-86.

[162] Unsworth LD, Tun Z, Sheardown H, Brash JL. In situ neutron reflectometry investigation of gold-chemisorbed PEO layers of varying chain density: relationship of layer structure to protein resistance. J Colloid Interface Sci. 2006;296:520-6.

[163] Gasteier P, Reska A, Schulte P, Salber J, Offenhausser A, Moeller M, et al. Surface grafting of PEO-based star-shaped molecules for bioanalytical and biomedical applications. Macromol Biosci. 2007;7:1010-23.

[164] Groll J, Ademovic Z, Ameringer T, Klee D, Moeller M. Comparison of Coatings from Reactive Star Shaped PEG-s tat-PPG Prepolymers and Grafted Linear PEG for Biological and Medical Applications. Biomacromolecules. 2005;6:956-62.

[165] Dankers PYW, Harmsen MC, Brouwer LA, Van Luyn MJA, Meijer EW. A modular and supramolecular approach to bioactive scaffolds for tissue engineering. Nat Mater. 2005;4:568-74.

[166] Dean 3rd J, Culbertson KC, D'Angelo AM. Fibronectin and laminin enhance gingival cell attachment to dental implant surfaces in vitro. The International journal of oral & maxillofacial implants. 1994;10:721-8.

[167] Ma Z, Gao C, Ji J, Shen J. Protein immobilization on the surface of poly-L-lactic acid films for improvement of cellular interactions. Eur Polym J. 2002;38:2279-84.

[168] Steffens GC, Nothdurft L, Buse G, Thissen H, Hocker H, Klee D. High density binding of proteins and peptides to poly(D,L-lactide) grafted with polyacrylic acid. Biomaterials. 2002;23:3523-31.

[169] Ma Z, Gao C, Yuan J, Ji J, Gong Y, Shen J. Surface modification of poly-L-lactide by photografting of hydrophilic polymers towards improving its hydrophilicity. J Appl Polym Sci. 2002;85:2163-71.

[170] Yoo HS, Kim TG, Park TG. Surface-functionalized electrospun nanofibers for tissue engineering and drug delivery. Adv Drug Del Rev. 2009;61:1033-42.

[171] Grafahrend D, Heffels K-H, Beer MV, Gasteier P, Möller M, Boehm G, et al. Degradable polyester scaffolds with controlled surface chemistry combining minimal protein adsorption with specific bioactivation. Nat Mater. 2011;10:67-73.

[172] Perlin L, MacNeil S, Rimmer S. Production and performance of biomaterials containing RGD peptides. Soft matter. 2008;4:2331-49.

[173] Ruoslahti E, Pierschbacher MD. New perspectives in cell adhesion: RGD and integrins. Science. 1987;238:491-7.

[174] Cook AD, Hrkach JS, Gao NN, Johnson IM, Pajvani UB, Cannizzaro SM, et al. Characterization and development of RGD-peptide-modified poly (lactic acid-co-lysine) as an interactive, resorbable biomaterial. J Biomed Mater Res. 1997;35:513-23.

[175] Gümüşderelioğlu M, Türkoğlu H. Biomodification of non-woven polyester fabrics by insulin and RGD for use in serum-free cultivation of tissue cells. Biomaterials. 2002;23:3927-35.

[176] Aumailley M, Bruckner-Tuderman L, Carter WG, Deutzmann R, Edgar D, Ekblom P, et al. A simplified laminin nomenclature. Matrix Biol. 2005;24:326-32.

[177] Graf J, Ogle RC, Robey FA, Sasaki M, Martin GR, Yamada Y, et al. A pentapeptide from the laminin B1 chain mediates cell adhesion and binds the 67,000 laminin receptor. Biochemistry. 1987;26:6896-900.

[178] Iwamoto Y, Robey FA, Graf J, Sasaki M, Kleinman HK, Yamada Y, et al. YIGSR, a synthetic laminin pentapeptide, inhibits experimental metastasis formation. Science. 1987;238:1132-4.

[179] Graf J, Ogle RC, Robey FA, Sasaki M, Martin GR, Yamada Y, et al. A pentapeptide from the laminin B1 chain mediates cell adhesion and binds to 67000 laminin receptor. Biochemistry. 1987;26:6896-900.

[180] Bushkin-Harav I, Littauer U. Involvement of the YIGSR sequence of laminin in protein tyrosine phosphorylation. FEBS Lett. 1998;424:243-7.

[181] Jun H-W, West JL. Endothelialization of microporous YIGSR/PEG-modified polyurethaneurea. Tissue Eng. 2005;11:1133-40.

[182] Tashiro K-i, Sephel G, Weeks B, Sasaki M, Martin G, Kleinman HK, et al. A synthetic peptide containing the IKVAV sequence from the A chain of laminin mediates cell attachment, migration, and neurite outgrowth. J Biol Chem. 1989;264:16174-82.

[183] Edwards WB, Anderson CJ, Fields GB, Welch MJ. Evaluation of radiolabeled type IV collagen fragments as potential tumor imaging agents. Bioconj Chem. 2001;12:1057-65.

[184] Grafahrend D, Heffels KH, Moller M, Klee D, Groll J. Electrospun, biofunctionalized fibers as tailored in vitro substrates for keratinocyte cell culture. Macromol Biosci. 2010;10:1022-7.

[185] Salber J, Gräter S, Harwardt M, Hofmann M, Klee D, Dujic J, et al. Influence of Different ECM Mimetic Peptide Sequences Embedded in a Nonfouling Environment on the Specific Adhesion of Human-Skin Keratinocytes and Fibroblasts on Deformable Substrates. Small. 2007;3:1023-31.

[186] Choi B-H, Choi YS, Kang DG, Kim BJ, Song YH, Cha HJ. Cell behavior on extracellular matrix mimic materials based on mussel adhesive protein fused with functional peptides. Biomaterials. 2010;31:8980-8.

[187] Massia SP, Hubbell JA. An RGD spacing of 440 nm is sufficient for integrin alpha V beta 3-mediated fibroblast spreading and 140 nm for focal contact and stress fiber formation. The Journal of cell biology. 1991;114:1089-100.

[188] Neff JA, Tresco P, Caldwell K. Surface modification for controlled studies of cell–ligand interactions. Biomaterials. 1999;20:2377-93.

[189] Megelski S, Stephens JS, Chase DB, Rabolt JF. Micro-and nanostructured surface morphology on electrospun polymer fibers. Macromolecules. 2002;35:8456-66.

[190] Kingshott P, McArthur S, Thissen H, Castner DG, Griesser HJ. Ultrasensitive probing of the protein resistance of PEG surfaces by secondary ion mass spectrometry. Biomaterials. 2002;23:4775-85.

[191] Wagner MS, McArthur SL, Shen M, Horbett TA, Castner DG. Limits of detection for time of flight secondary ion mass spectrometry (ToF-SIMS) and X-ray photoelectron spectroscopy (XPS): detection of low amounts of adsorbed protein. J Biomater Sci Polym Ed. 2002;13:407-28.

[192] Krithica N, Natarajan V, Madhan B, Sehgal PK, Mandal AB. Type I collagen immobilized poly (caprolactone) nanofibers: Characterization of surface modification and growth of fibroblasts. Adv Eng Mater. 2012;14:B149-B54.

[193] El-Amin S, Lu H, Khan Y, Burems J, Mitchell J, Tuan R, et al. Extracellular matrix production by human osteoblasts cultured on biodegradable polymers applicable for tissue engineering. Biomaterials. 2003;24:1213-21.

[194] Renaudin A, Chabot V, Grondin E, Aimez V, Charette PG. Integrated active mixing and biosensing using surface acoustic waves (SAW) and surface plasmon resonance (SPR) on a common substrate. Lab on a Chip. 2010;10:111-5.

[195] Takeichi M, Okada T. Roles of magnesium and calcium ions in cell-to-substrate adhesion. Exp Cell Res. 1972;74:51-60.

[196] Tennant JR. Evaluation of the trypan blue technique for determination of cell viability. Transplantation. 1964;2:685-94.

[197] Mosmann T. Rapid colorimetric assay for cellular growth and survival: application to proliferation and cytotoxicity assays. J Immunol Methods. 1983;65:55-63.

[198] Zong X, Ran S, Kim K-S, Fang D, Hsiao BS, Chu B. Structure and Morphology Changes during in Vitro Degradation of Electrospun Poly(glycolide-co-lactide) Nanofiber Membrane. Biomacromolecules. 2003;4:416-23.

[199] Baker BM, Gee AO, Metter RB, Nathan AS, Marklein RA, Burdick JA, et al. The potential to improve cell infiltration in composite fiber-aligned electrospun scaffolds by the selective removal of sacrificial fibers. Biomaterials. 2008;29:2348-58.

[200] Whited BM, Whitney JR, Hofmann MC, Xu Y, Rylander MN. Pre-osteoblast infiltration and differentiation in highly porous apatite-coated PLLA electrospun scaffolds. Biomaterials. 2011;32:2294-304.

[201] Milleret V, Simona B, Neuenschwander P, Hall H. Tuning electrospinning parameters for production of 3D-fiber-fleeces with increased porosity for soft tissue engineering applications. Eur Cell Mater. 2011;21:286-303.

[202] Mikos AG, McIntire LV, Anderson JM, Babensee JE. Host response to tissue engineered devices. Adv Drug Deliv Rev. 1998;33:111-39.

[203] Holy CE, Dang SM, Davies JE, Shoichet MS. In vitro degradation of a novel poly (lactide-co-glycolide) 75/25 foam. Biomaterials. 1999;20:1177-85.

[204] Wu L, Zhang J, Jing D, Ding J. “Wet-state” mechanical properties of three-dimensional polyester porous scaffolds. Journal of Biomedical Materials Research Part A. 2006;76:264-71.

[205] Li S. Hydrolytic degradation characteristics of aliphatic polyesters derived from lactic and glycolic acids. J Biomed Mater Res. 1999;48:342-53.

[206] Therin M, Christel P, Li S, Garreau H, Vert M. In vivo degradation of massive poly (α-hydroxy acids): validation of in vitro findings. Biomaterials. 1992;13:594-600.

[207] Cui W, Li X, Zhou S, Weng J. Degradation patterns and surface wettability of electrospun fibrous mats. Polym Degradation Stab. 2008;93:731-8.

[208] Kim K, Yu M, Zong X, Chiu J, Fang D, Seo Y-S, et al. Control of degradation rate and hydrophilicity in electrospun non-woven poly (D, L-lactide) nanofiber scaffolds for biomedical applications. Biomaterials. 2003;24:4977-85.

[209] Powell HM, Boyce ST. Fiber density of electrospun gelatin scaffolds regulates morphogenesis of dermal-epidermal skin substitutes. J Biomed Mater Res A. 2008;84:1078-86.

[210] Holy CE, Cheng C, Davies JE, Shoichet MS. Optimizing the sterilization of PLGA scaffolds for use in tissue engineering. Biomaterials. 2000;22:25-31.

[211] Holy CE, Cheng C, Davies JE, Shoichet MS. Optimizing the sterilization of PLGA scaffolds for use in tissue engineering. Biomaterials. 2001;22:25-31.

[212] Edwards C, Marks R. Evaluation of biomechanical properties of human skin. Clin Dermatol. 1995;13:375-80.

[213] Duan B, Yuan X, Zhu Y, Zhang Y, Li X, Zhang Y, et al. A nanofibrous composite membrane of PLGA–chitosan/PVA prepared by electrospinning. Eur Polym J. 2006;42:2013-22.

[214] Bürck J, Heissler S, Geckle U, Ardakani MF, Schneider R, Ulrich AS, et al. Resemblance of Electrospun Collagen Nanofibers to Their Native Structure. Langmuir. 2013;29:1562-72.

[215] Jassal M, Sengupta S, Warner SB, Bhowmick S. Quantitative characterization of functionally modified micron–submicron fibers for tissue regeneration: a review. Textile Research Journal. 2013:0040517513481870.

[216] Goddard JM, Hotchkiss JH. Polymer surface modification for the attachment of bioactive compounds. Prog Polym Sci. 2007;32:698-725.

[217] Grassetti DR, Murray JF. Determination of sulfhydryl groups with 2,2'- or 4,4'-dithiodipyridine. Arch Biochem Biophys. 1967;119:41-9.

[218] van Wachem PB, Vreriks CM, Beugeling T, Feijen J, Bantjes A, Detmers JP, et al. The influence of protein adsorption on interactions of cultured human endothelial cells with polymers. J Biomed Mater Res. 1987;21:701-18.

[219] Miller BF, O´Toole MT. Miller-Keane Encyclopedia and Dictionary of Medicine, Nursing, and Allied Health, Seventh Edition. 2006.

[220] Williams D. Revisiting the definition of biocompatibility. Med Device Technol. 2003;14:10-3.

[221] Kingshott P, Griesser HJ. Surfaces that resist bioadhesion. Curr Opin Solid State Mater Sci. 1999;4:403-12.

[222] Hench LL, Polak JM. Third-Generation Biomedical Materials. Science. 2002;295:1014-7.

[223] Cheung H-Y, Lau K-T, Lu T-P, Hui D. A critical review on polymer-based bio-engineered materials for scaffold development. Composites Part B: Engineering. 2007;38:291-300.

[224] Ratner BD, Hoffman AS, Schoen FJ, Lemons JE. Biomaterials science: an introduction to materials in medicine: Academic press; 2004.

[225] Hutmacher D, Goh J, Teoh S. An introduction to biodegradable materials for tissue engineering applications. Ann Acad Med Singapore. 2001;30:183-91.

[226] Roach P, Farrar D, Perry CC. Interpretation of Protein Adsorption: Surface-Induced Conformational Changes. J Am Chem Soc. 2005;127:8168-73.

[227] Lee JH, Lee HB, Andrade JD. Blood compatibility of polyethylene oxide surfaces. Prog Polym Sci. 1995;20:1043-79.

[228] Fick J, Steitz R, Leiner V, Tokumitsu S, Himmelhaus M, Grunze M. Swelling Behavior of Self-Assembled Monolayers of Alkanethiol-Terminated Poly(ethylene glycol): A Neutron Reflectometry Study. Langmuir. 2004;20:3848-53.

[229] Tokumitsu S, Liebich A, Herrwerth S, Eck W, Himmelhaus M, Grunze M. Grafting of Alkanethiol-Terminated Poly(ethylene glycol) on Gold. Langmuir. 2002;18:8862-70.

[230] Mougin K, Lawrence MB, Fernandez EJ, Hillier AC. Construction of cell-resistant surfaces by immobilization of poly(ethylene glycol) on gold. Langmuir. 2004;20:4302-5.

[231] Piehler J, Brecht A, Valiokas R, Liedberg B, Gauglitz G. A high-density poly(ethylene glycol) polymer brush for immobilization on glass-type surfaces. Biosens Bioelectron. 2000;15:473-81.

[232] Huang N-P, Michel R, Voros J, Textor M, Hofer R, Rossi A, et al. Poly(l-lysine)-g-poly(ethylene glycol) Layers on Metal Oxide Surfaces: Surface-Analytical Characterization and Resistance to Serum and Fibrinogen Adsorption. Langmuir. 2001;17:489-98.

[233] Groll J, Ademovic Z, Ameringer T, Klee D, Moeller M. Comparison of coatings from reactive star shaped PEG-stat-PPG prepolymers and grafted linear PEG for biological and medical applications. Biomacromolecules. 2005;6:956-62.

[234] Amirgoulova EV, Groll J, Heyes CD, Ameringer T, Rocker C, Moller M, et al. Biofunctionalized polymer surfaces exhibiting minimal interaction towards immobilized proteins. Chemphyschem. 2004;5:552-5.

[235] Grafahrend D, Heffels KH, Beer MV, Gasteier P, Moller M, Boehm G, et al. Degradable polyester scaffolds with controlled surface chemistry combining minimal protein adsorption with specific bioactivation. Nat Mater. 2011;10:67-73.

[236] Agarwal S, Wendorff JH, Greiner A. Use of electrospinning technique for biomedical applications. Polymer. 2008;49:5603-21.

[237] Patel S, Kurpinski K, Quigley R, Gao H, Hsiao BS, Poo MM, et al. Bioactive nanofibers: synergistic effects of nanotopography and chemical signaling on cell guidance. Nano Lett. 2007;7:2122-8.

[238] Kim TG, Park TG. Surface functionalized electrospun biodegradable nanofibers for immobilization of bioactive molecules. Biotechnol Prog. 2006;22:1108-13.

[239] Kim TG, Park TG. Biomimicking extracellular matrix: cell adhesive RGD peptide modified electrospun poly(D,L-lactic-co-glycolic acid) nanofiber mesh. Tissue Eng. 2006;12:221-33.

[240] Hynes RO. Integrins: Versatility, modulation, and signaling in cell adhesion. Cell. 1992;69:11-25.

[241] Boukamp P, Petrussevska RT, Breitkreutz D, Hornung J, Markham A, Fusenig NE. Normal keratinization in a spontaneously immortalized aneuploid human keratinocyte cell line. J Cell Biol. 1988;106:761-71.

[242] LeBaron RG, Athanasiou KA. Extracellular matrix cell adhesion peptides: functional applications in orthopedic materials. Tissue Eng. 2000;6:85-103.

[243] Rezania A, Thomas CH, Branger AB, Waters CM, Healy KE. The detachment strength and morphology of bone cells contacting materials modified with a peptide sequence found within bone sialoprotein. J Biomed Mater Res. 1997;37:9-19.

[244] Courtoy PJ, Timpl R, Farquhar MG. Comparative distribution of laminin, type IV collagen, and fibronectin in the rat glomerulus. J Histochem Cytochem. 1982;30:874-86.

[245] Madri JA, Roll FJ, Furthmayr H, Foidart JM. Ultrastructural localization of fibronectin and laminin in the basement membranes of the murine kidney. J Cell Biol. 1980;86:682-7.

[246] Roessler S, Born R, Scharnweber D, Worch H, Sewing A, Dard M. Biomimetic coatings functionalized with adhesion peptides for dental implants. J Mater Sci Mater Med. 2001;12:871-7.

[247] Nakamura F. Biochemical, electron microscopic and immunohistological observations of cationic detergent-extracted cells: detection and improved preservation of microextensions and ultramicroextensions. BMC Cell Biol. 2001;2:10.

[248] El Ghalbzouri A, Jonkman MF, Dijkman R, Ponec M. Basement membrane reconstruction in human skin equivalents is regulated by fibroblasts and/or exogenously activated keratinocytes. Journal of investigative dermatology. 2005;124:79-86.

[249] Neal RA, McClugage SG, Link MC, Sefcik LS, Ogle RC, Botchwey EA. Laminin nanofiber meshes that mimic morphological properties and bioactivity of basement membranes. Tissue Eng Part C Methods. 2009;15:11-21.

[250] de Guzman RC, Loeb JA, VandeVord PJ. Electrospinning of matrigel to deposit a basal lamina-like nanofiber surface. J Biomater Sci Polym Ed. 2010;21:1081-101.

[251] Neal RA, Lenz SM, Wang T, Abebayehu D, Brooks BP, Ogle RC, et al. Laminin-and basement membranepolycaprolactone blend nanofibers as a scaffold for regenerative medicine. Nanomater Environ. 2014;2.

[252] Lv J, Chen L, Zhu Y, Hou L, Liu Y. Promoting epithelium regeneration for esophageal tissue engineering through basement membrane reconstitution. ACS Appl Mater Interfaces. 2014;6:4954-64.

[253] de Guzman RC, Loeb JA, VandeVord PJ. Electrospinning of matrigel to deposit a basal lamina-like nanofiber surface. Journal of Biomaterials Science, Polymer Edition. 2010;21:1081-101.

[254] Drumheller PD, Hubbell JA. Polymer networks with grafted cell adhesion peptides for highly biospecific cell adhesive substrates. Anal Biochem. 1994;222:380-8.

[255] Yamada Y, Hozumi K, Nomizu M. Construction and Activity of a Synthetic Basement Membrane with Active Laminin Peptides and Polysaccharides. Chemistry – A European Journal. 2011;17:10500-8.

[256] Abrams GA, Schaus SS, Goodman SL, Nealey PF, Murphy CJ. Nanoscale topography of the corneal epithelial basement membrane and Descemet's membrane of the human. Cornea. 2000;19:57-64.

[257] Rosdy M, Clauss LC. Terminal epidermal differentiation of human keratinocytes grown in chemically defined medium on inert filter substrates at the air-liquid interface. J Invest Dermatol. 1990;95:409-14.

[258] Guimaraes A, Martins A, Pinho ED, Faria S, Reis RL, Neves NM. Solving cell infiltration limitations of electrospun nanofiber meshes for tissue engineering applications. Nanomedicine (Lond). 2010;5:539-54.

[259] Werner S, Krieg T, Smola H. Keratinocyte–fibroblast interactions in wound healing. J Invest Dermatol. 2007;127:998-1008.

[260] Fray TR, Molloy JE, Armitage MP, Sparrow JC. Quantification of single human dermal fibroblast contraction. Tissue Eng. 1998;4:281-91.

[261] Heimbach DM, Warden GD, Luterman A, Jordan MH, Ozobia N, Ryan CM, et al. Multicenter postapproval clinical trial of Integra dermal regeneration template for burn treatment. J Burn Care Rehabil. 2003;24:42-8.

[262] Mao JS, Zhao LG, Yin YJ, Yao KD. Structure and properties of bilayer chitosan–gelatin scaffolds. Biomaterials. 2003;24:1067-74.

[263] Wang TW, Sun JS, Wu HC, Huang YC, Lin FH. Evaluation and biological characterization of bilayer gelatin/chondroitin-6-sulphate/hyaluronic acid membrane. J Biomed Mater Res B Appl Biomater. 2007;82:390-9.

[264] Ma J, Wang H, He B, Chen J. A preliminary in vitro study on the fabrication and tissue engineering applications of a novel chitosan bilayer material as a scaffold of human neofetal dermal fibroblasts. Biomaterials. 2001;22:331-6.

[265] Yannas IV, Burke JF, Orgill DP, Skrabut EM. Wound tissue can utilize a polymeric template to synthesize a functional extension of skin. Science. 1982;215:174-6.

[266] Arnal-Pastor M, Martinez Ramos C, Perez Garnes M, Monleon Pradas M, Valles Lluch A. Electrospun adherent-antiadherent bilayered membranes based on cross-linked hyaluronic

acid for advanced tissue engineering applications. Mater Sci Eng C Mater Biol Appl. 2013;33:4086-93.

[267] Pan J-f, Liu N-h, Sun H, Xu F. Preparation and Characterization of Electrospun PLCL/Poloxamer Nanofibers and Dextran/Gelatin Hydrogels for Skin Tissue Engineering. PLoS One. 2014;9:e112885.

[268] Pu J, Yuan F, Li S, Komvopoulos K. Electrospun bilayer fibrous scaffolds for enhanced cell infiltration and vascularization in vivo. Acta Biomater. 2015;13:131-41.

[269] Boelsma E, Verhoeven MC, Ponec M. Reconstruction of a human skin equivalent using a spontaneously transformed keratinocyte cell line (HaCaT). J Invest Dermatol. 1999;112:489-98.

[270] Maas-Szabowski N, Starker A, Fusenig NE. Epidermal tissue regeneration and stromal interaction in HaCaT cells is initiated by TGF-alpha. J Cell Sci. 2003;116:2937-48.

[271] Prunieras M, Regnier M, Woodley D. Methods for cultivation of keratinocytes with an air-liquid interface. J Invest Dermatol. 1983;81:28s-33s.

[272] Rosdy M, Clauss L-C. Terminal epidermal differentiation of human keratinocytes grown in chemically defined medium on inert filter substrates at the air-liquid interface. J Invest Dermatol. 1990;95:409-14.

[273] Smola H, Thiekötter G, Fusenig NE. Mutual induction of growth factor gene expression by epidermal-dermal cell interaction. The Journal of cell biology. 1993;122:417-29.

[274] Boehnke K, Mirancea N, Pavesio A, Fusenig NE, Boukamp P, Stark H-J. Effects of fibroblasts and microenvironment on epidermal regeneration and tissue function in long-term skin equivalents. Eur J Cell Biol. 2007;86:731-46.

[275] Hautanen A, Gailit J, Mann DM, Ruoslahti E. Effects of modifications of the RGD sequence and its context on recognition by the fibronectin receptor. J Biol Chem. 1989;264:1437-42.

[276] Kim JP, Zhang K, Chen JD, Wynn KC, Kramer RH, Woodley DT. Mechanism of human keratinocyte migration on fibronectin: unique roles of RGD site and integrins. J Cell Physiol. 1992;151:443-50.

[277] Ruoslahti E. RGD and other recognition sequences for integrins. Annu Rev Cell Dev Biol. 1996;12:697-715.

[278] Tran KT, Griffith L, Wells A. Extracellular matrix signaling through growth factor receptors during wound healing. Wound Repair Regen. 2004;12:262-8.

[279] Woodley DT, Kalebec T, Banes AJ, Link W, Prunieras M, Liotta L. Adult human keratinocytes migrating over nonviable dermal collagen produce collagenolytic enzymes that degrade type I and type IV collagen. J Invest Dermatol. 1986;86:418-23.

[280] Amano S, Akutsu N, Matsunaga Y, Nishiyama T, Champliaud MF, Burgeson RE, et al. Importance of balance between extracellular matrix synthesis and degradation in basement membrane formation. Exp Cell Res. 2001;271:249-62.

[281] Dalby M, Riehle M, Johnstone H, Affrossman S, Curtis A. In vitro reaction of endothelial cells to polymer demixed nanotopography. Biomaterials. 2002;23:2945-54.

[282] Andersson AS, Olsson P, Lidberg U, Sutherland D. The effects of continuous and discontinuous groove edges on cell shape and alignment. Exp Cell Res. 2003;288:177-88.

[283] Murphy CM, Haugh MG, O'Brien FJ. The effect of mean pore size on cell attachment, proliferation and migration in collagen–glycosaminoglycan scaffolds for bone tissue engineering. Biomaterials. 2010;31:461-6.

[284] Sun T, Donoghue PS, Higginson JR, Gadegaard N, Barnett SC, Riehle MO. The interactions of astrocytes and fibroblasts with defined pore structures in static and perfusion cultures. Biomaterials. 2011;32:2021-31.

[285] Sun T, Norton D, Ryan AJ, MacNeil S, Haycock JW. Investigation of fibroblast and keratinocyte cell-scaffold interactions using a novel 3D cell culture system. J Mater Sci Mater Med. 2007;18:321-8.

[286] Selim M, Bullock AJ, Blackwood KA, Chapple CR, MacNeil S. Developing biodegradable scaffolds for tissue engineering of the urethra. BJU Int. 2011;107:296-302.

[287] Franco RA, Min YK, Yang HM, Lee BT. Fabrication and biocompatibility of novel bilayer scaffold for skin tissue engineering applications. J Biomater Appl. 2013;27:605-15.

[288] Rippa AL, Vorotelyak EA, Vasiliev AV, Terskikh VV. The role of integrins in the development and homeostasis of the epidermis and skin appendages. Acta naturae. 2013;5:22-33.

[289] Koivisto L, Larjava K, Hakkinen L, Uitto VJ, Heino J, Larjava H. Different integrins mediate cell spreading, haptotaxis and lateral migration of HaCaT keratinocytes on fibronectin. Cell Adhes Commun. 1999;7:245-57.

[290] Adams JC, Watt FM. Changes in keratinocyte adhesion during terminal differentiation: Reduction in fibronectin binding precedes α5β1 integrin loss from the cell surface. Cell. 1990;63:425-35.

[291] Adams JC, Watt FM. Expression of beta 1, beta 3, beta 4, and beta 5 integrins by human epidermal keratinocytes and non-differentiating keratinocytes. J Cell Biol. 1991;115:829-41.

[292] Moharamzadeh K, Franklin KL, Brook IM, van Noort R. Biologic assessment of antiseptic mouthwashes using a three-dimensional human oral mucosal model. J Periodontol. 2009;80:769-75.

[293] Sun T, Jackson S, Haycock JW, MacNeil S. Culture of skin cells in 3D rather than 2D improves their ability to survive exposure to cytotoxic agents. J Biotechnol. 2006;122:372-81.

[294] Xu Q, Izumi K, Tobita T, Nakanishi Y, Feinberg SE. Constitutive release of cytokines by human oral keratinocytes in an organotypic culture. J Oral Maxillofac Surg. 2009;67:1256-64.

[295] Yadev NP, Murdoch C, Saville SP, Thornhill MH. Evaluation of tissue engineered models of the oral mucosa to investigate oral candidiasis. Microb Pathog. 2011;50:278-85.

[296] Pan C, Kumar C, Bohl S, Klingmueller U, Mann M. Comparative Proteomic Phenotyping of Cell Lines and Primary Cells to Assess Preservation of Cell Type-specific Functions. Molecular & Cellular Proteomics : MCP. 2009;8:443-50.

[297] Moharamzadeh K, Brook IM, Van Noort R, Scutt AM, Smith KG, Thornhill MH. Development, optimization and characterization of a full-thickness tissue engineered human oral mucosal model for biological assessment of dental biomaterials. Journal of materials science Materials in medicine. 2008;19:1793-801.

[298] Kimura T, Yamano H, Tanaka A, Matsumura T, Ueda M, Ogawara K, et al. Transport of D-glucose across cultured stratified cell layer of human oral mucosal cells. J Pharm Pharmacol. 2002;54:213-9.

[299] Kubilus J, Ayehunie S, Breyfogle B, Dale D, Kimball J, Wertz P, et al. Characterization and testing of new buccal and gingival tissue models. Amer Assoc Dent Res Meet, Abstract. 2006;399.

[300] Galey WR, Lonsdale HK, Nacht S. The in vitro permeability of skin and buccal mucosa to selected drugs and tritiated water. J Invest Dermatol. 1976;67:713-7.

[301] Klausner M, Ayehunie S, Breyfogle BA, Wertz PW, Bacca L, Kubilus J. Organotypic human oral tissue models for toxicological studies. Toxicol In Vitro. 2007;21:938-49.

[302] Trombetta D, Mondello MR, Cimino F, Cristani M, Pergolizzi S, Saija A. Toxic effect of nickel in an in vitro model of human oral epithelium. Toxicol Lett. 2005;159:219-25.

[303] Vande Vannet BM, Hanssens JL. Cytotoxicity of two bonding adhesives assessed by three-dimensional cell culture. Angle Orthod. 2007;77:716-22.

[304] No OT. 439.(2010). vitro skin irritation: reconstructed Human epidermis test method, OECD guidelines for the testing of chemicals.1:1-18.

7 Appendix

7.1 Standard Operating Procedure Protocols

7.1.1 Collagen type I isolation from rate tale

7.1.2 Sterile working station

7.1.3 Isolation dermal keratinocytes

7.1.4 Isolation dermal fibroblasts

7.1.5 Passaging of cells

7.1.6 Cell number and viability

7.1.7 Freezing and thawing of cells

7.1.8 Cells on chamberslides

7.1.9 Cells on cytospots

7.1.10 Full thickness skin equivalents

7.1.11 Live/Dead staining with FDA/PI

7.1.12 MTT viability assay

7.1.13 FITC-dextran

7.1.14 PFA fixation

7.1.15 Paraffin embedding

7.1.16 Haematoxylin & Eosin staining

7.1.17 Immunohistochemical staining with HRP-based detection system

-

7.2 Publications and conference contributions

Articles

Rossi A., Wistlich L., Heffels K.H., Walles H., Groll J., Isotropic versus bipolar functionalized biomimetic artificial basement membranes and their evaluation in long term human cell co-culture. Advanced Healthcare Materials (2016).

Lotz C., Schmid F.F., **Rossi A.**, Kurdyn S., Kampik D., Wever B., Walles H., Groeber F., Alternative methods for the replacement of eye irritation testing. Altex (2016).

Simon-Yarza T., **Rossi A.**, Heffels K.H., Prosper F., Groll J., Blanco-Prieto MJ., Polymeric electrospun scaffolds: Neuregulin encapsulation and biocompatibility studies in a model of myocardial ischemia. Tissue Engineering Part A (2015).

Rossi A.*, Appelt-Menzel A.*, Kurdyn S., Walles H., Groeber F., Generation of a Three-dimensional Full Thickness Skin Equivalent and Automated Wounding. Journal of Visualized Experiments (JoVE) (2015).

Rossi A., Fecher D., Dandekar G., Schweinlin M., Steinke M., Humane 3D-in vitro-Testsysteme für die präklinische Forschung. Biospektrum (2014).

Rossi A., Cornea Testsystem basierend auf einem Organmodell. Jahresbericht 13/14 Fraunhofer Institut für Grenzflächen- und Bioverfahrenstechnik IGB Stuttgart. (2013).

Patent

Rossi A., Schwarz T., Hansmann J., Groeber F., Walles H., Verfahren zur Langzeitstabilisierung von Korneagewebe (102014222547.7).

Oral presentations

3D Cell Culture 2016: How close to 'in vivo' can we get? Models, applications & translation, Freiburg (Germany), 19 to 21 April, 2016: Functionalized electrospun nanofibers for the development of a three-dimensional skin model.

4th International Conference Strategies in Tissue Engineering, Würzburg (Germany), 10 to 12 June, 2015: Functionalized electrospun nanofibers for the development of a three-dimensional skin model.

9th World Congress on Alternatives and Animal Use in the Life Sciences, Prague (Czech Republic), 24 to 28 August, 2014: Development of 3D basement membranes.

9th World Congress on Alternatives and Animal Use in the Life Sciences, Prague (Czech Republic), 24 to 28 August, 2014: Organ-like three-dimensional test systems.

9th Biological Barriers, Saarbrücken (Germany), 16 to 21 February, 2014: Development of 3D Basement membranes.

World Conference on Regenerative Medicine, Leipzig (Germany), 23 to 25 October, 2013: Functionalized electrospun nanofibers for the development of a basement membrane.

Posters

3D Cell Culture 2016: How close to 'in vivo' can we get? Models, applications & translation, Freiburg (Germany), 19 to 21 April, 2016: Development and characterization of an epithelial- and co-culture tissue-engineered human oral mucosa model.

"Be there or die? The role of the microenvironment in B-cell behavior in health and disease", San Feliu de Guixols (Spain), 16 to 21 May, 2015: Functionalized electrospun nanofibers for the development of a three-dimensional skin model.

54th Annual Meeting and ToxExpo, San Diego (CA, United States), 22 to 26 March, 2015: Functionalized electrospun nanofibers for the development of a three-dimensional skin model.

4th Galenus Workshop “Drug Delivery to Human Skin”, Saarbrücken (Germany), 25 to 27 February, 2015: Development of 3D Basement membranes.

3D Cell Culture, Freiburg (Germany), 25 to 27 June, 2014: Development of 3D Basement membranes.

25th European Conference on Biomaterials, Madrid (Spain), 8 to 12 September, 2013: Functionalized electrospun nanofibers for the development of a basement membrane.

7.3 Curriculum vitae

7.4 Acknowledgment

Ich möchte mich an dieser Stelle herzlichst bei allen bedanken, die mich in den vergangenen Jahren im Rahmen dieser Arbeit begleitet und unterstützt haben.

Mein ganz besonderer Dank gilt Frau Prof. Dr. Heike Walles und Herrn Prof. Dr. Jürgen Groll für die intensive Betreuung und Unterstützung. Die vielen Ideen und Anregungen zu Experimenten, sowie viele Gespräche und Diskussionen haben sehr zum Gelingen dieser Arbeit beigetragen. Auch möchte ich mich für die Möglichkeit zur Teilnahme an zahlreichen wissenschaftlichen Konferenzen und Symposien, und den lehrreichen Erfahrungen, die ich dadurch sammeln konnte, bedanken. Außerdem danke ich ganz herzlich Herrn Prof. Dr. Dr. Lorenz Meinel, der mich als weiterer Betreuer in meinem Promotionskomitee mit Anregungen und Ratschlägen unterstützt hat.

Darüber hinaus danke ich für die Übernahme des Prüfungsvorsitzes Frau Prof. Dr. Ulrike Holzgrabe.

Für die Finanzierung meiner Arbeit danke ich dem Bayern Fit Programm (Kap.1340 tit 686 63).

Bei Sabine Adam, Özlem Elbert und Tesda Barthel möchte ich mich sehr herzlich für die geduldige organisatorische Zusammenarbeit, sowie die gute Atmosphäre im Sekretariat bedanken.

Ich bedanke mich außerdem bei allen Arbeitskollegen des Lehrstuhls für Tissue Engineering und Regenerative Medizin und des Lehrstuhl für Funktionswerkstoffe in der Medizin und Zahnmedizin, die mir bei sämtlichen Fragen und neuen Methoden immer hilfsbereit zur Seite standen und ein angenehmes Arbeiten ermöglichten.

Bedanken möchte ich mich auch bei Dr. Dirk Grafahrend und Dr. Karl-Heinz Heffels, die viele der ursprünglichen Daten, welche Grundlage dieser Arbeit waren, generiert haben.

Darüber hinaus bedanke ich mich bei Sabine Willhelm, die mir im Labor stets mit Rat und Tat zur Seite stand.

Mein Dank gilt auch Herr Dr. Dr. Linz aus der Zahnklinik der Universität Würzburg für die Bereitstellung der Biopsien der Mundschleimhaut.

Bei Herrn Prof. Krohne möchte ich mich für die kompetente Hilfe bei der SEM-Analyse bedanken.

Daniela Zdzieblo, Jodie Haigh, Florian Groeber und Christina Schneider, danke ich für die hilfreichen Ratschläge bei der Korrektur meiner Dissertation.

Besonderer Dank gilt meiner Familie, die mich mein ganzes Leben unterstützt und stets an mich glaubt. Danke, dass es euch gibt!

Abschließend möchte ich meinem Freund Daniel danke sagen für die Geduld, Unterstützung, sein Verständnis in sämtlichen Lebenssituationen und dass ich mich immer auf ihn verlassen kann.

7.5 Affidavit

I hereby confirm that my thesis entitled “Development of functionalized electrospun fibers as biomimetic artificial basement membranes” is the result of my own work. I did not receive any help or support from commercial consultants. All sources and/or materials applied are listed and specified in the thesis.

Furthermore, I confirm that this thesis has not yet been submitted as part of another examination process neither in identical nor in similar form.

…… ……

Place, Date Signature

7.6 Eidesstattliche Erklärung

Hiermit erkläre ich an Eides statt, die Dissertation „Entwicklung funktionalisierter elektrogesponnener Fasern als biomimetische künstliche Basalmembranen“ eigenständig, d.h. insbesondere selbständig und ohne Hilfe eines kommerziellen Promotionsberaters, angefertigt und keine anderen als die von mir angegebenen Quellen und Hilfsmittel verwendet zu haben.

Ich erkläre außerdem, dass die Dissertation weder in gleicher noch in ähnlicher Form bereits in einem anderen Prüfungsverfahren vorgelegen hat.

…… ……

Ort, Datum Unterschrift